LUND UNIVERSITY

Network Synchronization and Control Based on Inverse Optimality

A Study of Inverter-Based Power Generation

Jouini, Taouba

2021

[Link to publication](#)

Network Synchronization and Control Based on Inverse Optimality

A Study of Inverter-Based Power Generation

TAOUBA JOUINI
DEPARTMENT OF AUTOMATIC CONTROL | LUND UNIVERSITY

LUND

UNIVERSITY

Network Synchronization and Control Based on Inverse Optimality

A Study of Inverter-Based Power Generation

Taouba Jouini
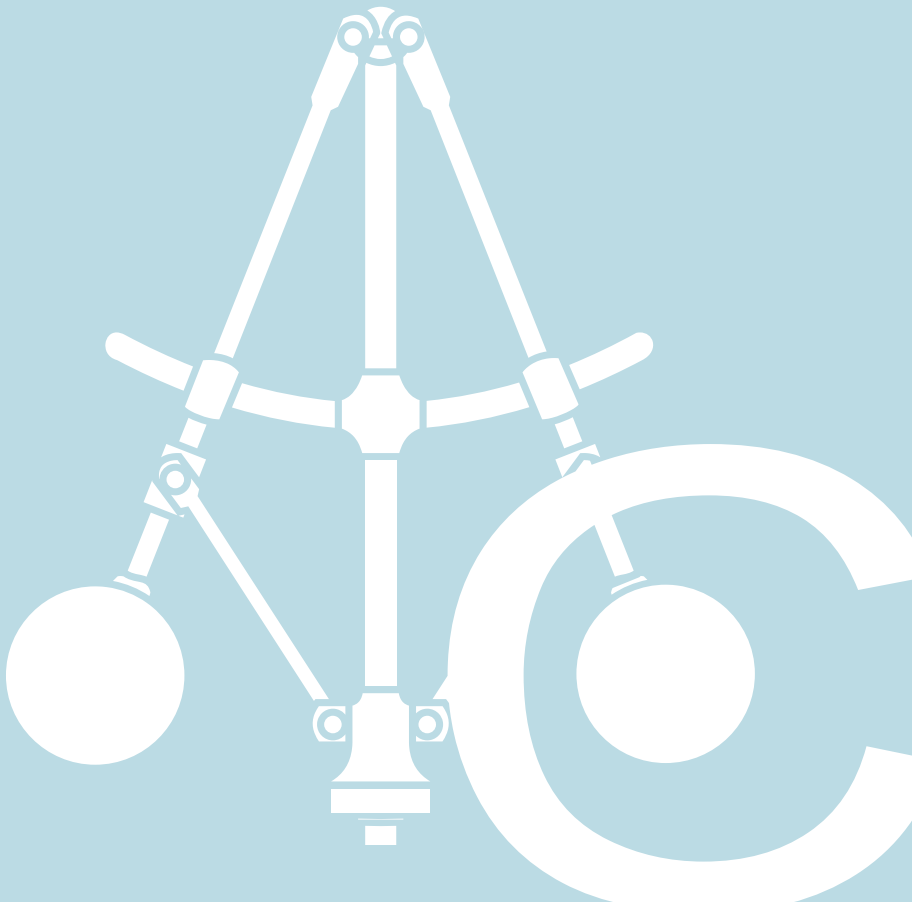
LUND
UNIVERSITY

Department of Automatic Control

To Kaouther — my Mom,
and All Tunisian Women, the Granddaughters of Dihiya Tadmut.

Acknowledgements

Hereby, I acknowledge *chronologically* the group of people that contributed to the existence of this thesis work.

First and foremost, my warmest and deepest thank goes to my mother Kaouther, who has always been a source of motivation and inspiration for me. She fiercely believed in me and what I can become one day, when no one else did, and genuinely guided my first steps towards the woman I am today. This thesis is an ode to her, for her tremendous and uncountable efforts to put me early on, on the road of excellence in education.

Second, I would like to sincerely thank the talented engineer, Amira Sinini for opening my eyes early on, on the studies of Cybernetics engineering (Technische Kybernetik) and explaining systems and control to my younger self, in a simple, yet compelling way. Without the appetizing presentation she held during my first year as a German course student back in early 2010, systems and control engineering wouldn't have been brought to my attention or even crossed my mind. Thank you Amira. You are an inspiration to anyone who knows you.

Third, it goes without saying that my studies at the university of Stuttgart and in particular the encounter with Prof. Frank Allgöwer has only grown and shaped my interest in systems and control theory over the years. His excitement about control is contagious and his passion about the field is unparalleled. Sitting in many of his control courses, as a bachelor and later master student, was a purely entertaining experience with numerous stories that taught me a lot beyond the course material. I would like to also thank all staff and members of the Institute of Systems Theory and Control (IST) at the university of Stuttgart for their dedication and the high-quality of their teaching and research. Many of them guided my baby steps in control over the years; only to name a few: Dr. Georg S. Seyboth, Dr. Matthias Bürger, Dr. Daniella Schittler, Prof. Nicole Radde and Prof. Christian Ebenbauer.

Fourth, I would like to thank Prof. Florian Dörfler for introducing me to the world of coupled oscillator synchronization and control of power systems, opening my eyes on many of the challenges awaiting control theorists

Financial Support

Abstract

This thesis dwells upon the synthesis of system-theoretical tools to understand and control the behavior of nonlinear networked systems. This work is at the crossroads of three topics: synchronization in coupled high-order oscillators, inverse optimal control and the application of inverter-based power systems. The control and stability of power systems leverages the theoretical results obtained for synchronization in coupled high-order oscillators and inverse optimal control.

First, we study the dynamics of coupled high-order nonlinear oscillators. These are characterized by their rotational invariance, meaning that their dynamics remain unchanged following a static shift of their angles. We provide sufficient conditions for local frequency synchronization based on both direct, indirect Lyapunov methods and center manifold theory.

Second, we study inverse optimal control problems, embedded in networked settings. In this framework, we depart from a given stabilizing control law, with an associated control Lyapunov function and reverse engineer the cost functional to guarantee the optimality of the controller. In this way, inverse optimal control generates a whole family of optimal controllers corresponding to different cost functions. This provides analytically explicit and numerically feasible solutions in closed-form. This approach circumvents the complexity of solving partial differential equations descending from dynamic programming and Bellman's principle of optimality. We show this to be the case also in the presence of disturbances in the dynamics and the cost. In networks, the controller obtained from inverse optimal control has a topological structure (e.g., it is distributed) and thus feasible for implementation. The tuning is analogous to that of linear quadratic regulators.

Third, motivated by the pressing changes witnessed by the electrical grid toward renewable energy generation, we consider power system stability and control as the main application of this thesis. In particular, we apply our theoretical findings to study a network of power electronic inverters. We first propose a controller we term *the matching controller*, a control strategy that, based on DC voltage measurements, endows the inverters with an oscillatory

behavior at a common desired frequency. In closed-loop with the matching control, inverters can be considered as nonlinear oscillators. Our study of the dynamics of nonlinear oscillator network provides feasible physical conditions that ask for damping on DC- and AC-side of each converter, that are sufficient for system-wide frequency synchronization. Furthermore, we showcase the usefulness of inverse optimal control for inverter-based generation at two different settings to synthesize robust *angle controllers* with respect to common disturbances in the grid and provable stability guarantees. All the controllers proposed in this thesis, provide the electrical grid with important services, namely power support whenever needed, as well as power sharing among all inverters.

Sammanfattning

Denna avhandling handlar om att ta fram systemteoretiska verktyg för att förstå och styra beteendet i olinjära system med nätverksstruktur. Arbetet görs i ett område som gränsar till tre olika ämnen: synkronisering av kopplade högre ordningens oscillatorer, inversoptimal reglering och kraftsystemtillämpningar med frekvensomriktare. Reglering och stabilisering av kraftsystem görs med hjälp av teoretiska resultat för oscillatorsynkronisering och inversoptimal reglering.

För det första studerar vi dynamiken i kopplade högre ordningens oscillatorer med rotatationsinvarians. Invariansen betyder att dynamiken inte påverkas av ett gemensamt fasskifte i alla noder. Vi ger tillräckliga villkor för frekvenssynkronisering baserat på indirekta och direkta Lyapunovmetoder, liksom på centrala mångfaldssatsen.

För det andra studerar vi inversoptimala styrproblem med nätverksstruktur. I detta ramverk utgår vi från en given stabiliserande styrlag med tillhörande Lyapunovfunktion och härleder en målfunktion för vilken regulatorn är optimal. Från den givna regulatorn genererar inversoptimal styrteori sedan en hel familj av regulatorer som alla är optimala med avseende på tillhörande målfunktioner. Detta ger analytiskt explicita och numeriskt lösbara villkor i sluten form. Tillvägagångssättet undviker svårigheten med att lösa de partiella differentialekvationer som normalt uppstår i samband med dynamisk programmering och Bellmans optimalitetsprincip. Idén utvidgas även till fallet med störningar i dynamik och målfunktion. För problem med nätverksstruktur leder metoden till distribuerade styrlagar, vilket förenklar deras implementering i nätverket. Metoden har tydliga analogier med klassisk linjärkvadratisk reglering.

För det tredje, motiverade av behovet att hantera förnyelsebar elproduktion, studerar vi dynamik och reglering av kraftsystem som huvudtillämpning i denna avhandling. Särskilt tar vi hjälp av våra nya teoretiska resultat för att studera nätverkskopplade frekvensomriktare. Först inför vi en reglerstrategi som ger omriktarna baserat på DC-spänningsmätningar ett oscillatorbeteende med ett gemensamt referensvärde på frekvensen. Detta gör

att omriktarna beter sig som olinjära oscillatorer och vår teori ger tillräckliga villkor på AC- och DC-sidorna i omriktarna för att garantera frekvenssynkronisering. Dessutom visar vi hur inversoptimal reglering kan användas för att ställa in omriktarvinkelregulatorer med garantier för stabilitet och robusthet i nätverket. Alla de föreslagna regulatorerna förser nätet med de viktiga tjänsterna att styra och fördela effekt i elnätet.

Deutsche Kurzfassung

In dieser Arbeit werden systemtheoretische Werkzeuge zur Regleranalyse und -synthese von nichtlinearen vernetzten Systemen behandelt. Das liegt an der Schnittstelle von drei verschiedenen Themen: Synchronisierung von gekoppelten hoch-dimensionalen Oszillatoren, inverse optimale Regelung und Energiesysteme mit hohem Anteil wechselrichterbasierter Anlagen. Die Stabilitätsbetrachtung von Energiesystemen hat die theoretischen Ergebnisse der Synchronisierung gekoppelter hoch-dimensionaler Oszillatoren sowie die inverse optimale Regelung genutzt.

Zuerst untersuchen wir die Dynamik von gekoppelten nichtlinearen hoch-dimensionalen Oszillatoren, die durch ihre Rotationsinvarianz gekennzeichnet sind. Dass heisst, dass die Systemdynamik nach statischer Verschiebung ihrer Winkel unverändert bleibt. Wir liefern hinreichende Stabilitätsbedingungen basierend sowohl auf direkten sowie indirekten Lyapunov Methoden und dem Zentrumsmannigfaltigkeits-Theorem, damit die Oszillatoren auf eine gemeinsame Frequenz synchronisieren.

Zweitens untersuchen wir die inverse optimale Regelung, eingebettet in Netzwerken. In diesem Rahmen gehen wir von einem gegebenen stabilisierenden Regler mit einer zugehörigen Lyapunov Funktion aus, und entwickeln das Kostenfunktional zurück, um die Optimalität des Reglers zu gewährleisten. Auf diese Weise erzeugt die inverse optimale Regelung, eine ganze Familie von optimalen Reglern, die Kostenfunktionen entsprechen. Dies liefert analytisch explizite und numerisch zulässige Lösungen in geschlossener Form. Dieser Ansatz umgeht die Komplexität der Lösung partieller Differentialgleichungen, die von der dynamischen Programmierung und dem Optimalitätsprinzip von Bellman abstammen. Das gilt auch, wenn die Dynamik und die Kosten unter dem Einfluss von Störungen sind, d.h. im Rahmen der robusten optimalen Regelung. Der Regler, der durch die inverse optimale Regelung in Netzwerken erhalten wird, hat eine topologische Struktur, (er ist z. B. verteilt) und ist damit praktisch anwendbar. Das Tuning von inverse optimalen Reglern ist analog zu linear quadratischen Reglern.

Drittens betrachten wir, motiviert von dringenden Veränderungen des Stromnetzes zu erneuerbaren Energieerzeugung, die Stabilität und Regelung von Energiesystemen als die Hauptanwendung dieser Arbeit. Insbesondere wenden wir unsere theoretischen Ergebnisse an, um ein Netzwerk von Wechselrichtern zu untersuchen. Wir schlagen den *Matching Regler* vor. Das ist eine Regelstrategie, die, basierend auf die gemessene DC spannungen, den Wechselrichtern ein oszillierendes Verhalten bei einer gewünschten Frequenz verleiht. Sobald die Wechselrichter im geschlossenen Regelkreis sind, können sie als nichtlineare Oszillatoren betrachtet werden. Unsere Untersuchung der Dynamik nichtlinearer Oszillatornetzwerke liefert hinreichende, praktisch anwendbare und physikalisch interpretierbare Bedingungen, die Dämpfung auf der DC- sowie AC-Seite von jedem Wechselrichter, verlangen um die Frequenzsynchronizierung zu gewährleisten. Andererseits demonstrieren wir die Nützlichkeit der inversen optimalen Regelung für die wechselrichterbasierte Energieerzeugung unter verschiedenen hinreichenden Bedingungen, um robuste *Winkelregler* in Bezug auf übliche Störungen im Netz mit nachweisbaren Stabilitätsgarantien, zu entwerfen. Alle in dieser Arbeit vorgeschlagenen Regler stellen dem Stromnetz wichtige Dienste zur Verfügung, nämlich Leistungsunterstützung und Leistungsaufteilung zwischen allen Wechselrichtern.

List of Acronyms

AC	Alternating Current
CLF	Control Lyapunov Function
DC	Direct Current
EU	European Union
HJB	Hamilton-Jacobi-Bellman
HJI	Hamilton-Jacobi-Isaacs
IDA	Interconnection and Damping Assignment
LQR	Linear Quadratic Regulator
MIGRATE	Massive InteGRATion of power Electronic devices
MPC	Model Predictive Control
PBC	Passivity-Based Control
PI	Proportional and Integral
PID	Proportional, Integral and Derivative
PH	Port-Hamiltonian
PLL	Phase-Locked-Loop
RES	Renewable Energy Sources
RL	Resistive and Inductive
SM	Synchronous Machines
USA	United States of America
VOC	Virtual Oscillator Control
VSC	Voltage Source Converter
VSM	Virtual Synchronous Machine

List of symbols

$\mathbb{R}$	space of real numbers
$\mathbb{R}_{\geq 0}$	space of non-negative real numbers
$\mathbb{C}$	space of complex numbers
$\mathbb{N}$	space of non-negative integers
$\mathbb{S}^1$	unit circle
$\mathbb{T}^n = \overbrace{\mathbb{S}^1 \times \cdots \times \mathbb{S}^1}^{n-\text{times}}$	$n-$dimensional unit torus
$\mathcal{L}_2[0, \infty)$	space of $\mathcal{L}_2$ bounded functions $f : [0, \infty) \to \mathbb{R}^n$, i.e., $\sqrt{\int_0^\infty f^\top(s)f(s)\,\mathrm{d}s} < \infty$
$\dot{x}(t)$	$\frac{\mathrm{d}x}{\mathrm{d}t}$: time-derivative of $x(t)$
$\nabla_x V(x)$	$\frac{\mathrm{d}V}{\mathrm{d}x}$: gradient (a column vector) of a function $V : \mathbb{R}^n \to \mathbb{R}$ with respect to x
$\mathcal{V} = \{v_1, \ldots v_n\}$	set of nodes
$\mathcal{E} = \{e_1, \ldots e_m\}$	set of edges
$\{a_e\}_{\{e \in \mathcal{E}\}}$	set of edge weights
$G = (V, \mathcal{E}, \{a_e\}_{\{e \in \mathcal{E}\}})$	network graph
t	time
W	Watts (active power unit)
KW	Kilowatts
MW	Megawatts
var or VAR	VARS (reactive power unit)
Kvar or KVAR	Kilovars
Mvar or MVAR	Megavars
$\mathrm{Re}(\lambda)$	real part of a complex number $\lambda \in \mathbb{C}$
$||v||$	$2-$norm of a vector $v \in \mathbb{R}^n$
$I_n,\ n \in \mathbb{N}$	$n-$dimensional identity matrix: $\begin{bmatrix} 1 & \cdots & 0 \\ & \ddots & \\ 0 & \cdots & 1 \end{bmatrix}$

Contents

Contents

1

Introduction

The omnipresence of networked systems in a multitude of fields ranging from economic, social to biological applications is striking. Real life examples abound of network interactions: the ebb and flow of generating units in power systems steadily responding to changes in the electrical grid, transportation systems, in which traffic jam and bottleneck situations are ubiquitous, or gene regulators, which decide upon gene expression and hence the future of cell types. The local interaction between several units or subsystems via virtual (e.g., communication) or physical (e.g., transmission lines) links, described by a certain network topology, dictates a global behavior for the whole group [Zampieri, 2008].

Networked systems are modeled as graphs. A graph is a collection of nodes or vertices, and edges. Formally, we consider networks as weighted directed (i.e., oriented) graphs represented by a triplet $G = (\mathcal{V}, \mathcal{E}, \{a_e\}_{\{e \in \mathcal{E}\}})$. The pair $(\mathcal{V}, \mathcal{E})$ is the set of nodes $\mathcal{V} = \{v_1, \dots v_n\}$, the edge set $\mathcal{E}$ given by an unordered pairs of vertices (i, j) with $i, j \in \mathcal{V}$ and $\{a_e\}_{\{e \in \mathcal{E}\}}$ is a collection of strictly positive weights for the edges. The neighborhood of a vertex is defined by the set of nodes directly connected to it. A directed graph is defined by a unidirectional orientation of the connections between the nodes. An undirected graph is given by a bidirectionally oriented edges [Godsil and Royle, 2001].

Our setup hinges on the modeling of the individual dynamical subsystems or agents (e.g., power generators, cities) as vertices and the links interconnecting them as edges (e.g., transmission lines, traffic routes) associated with edge weights (line admittances, traveling times). The edges can be directed or bidirectionally oriented. Fig. 1.1 depicts an important example of networked systems consisting of a simplified version of the power network of Western System Coordinating Council (WSCC), which promotes the bulk electric system reliability for the entire western interconnection system in the USA [Delavari et al., 2018]. It is comprised of three generators, all represented by synchronous machines, and connected to three load buses via transmission lines. Another example of networked systems, is given by a traffic system in
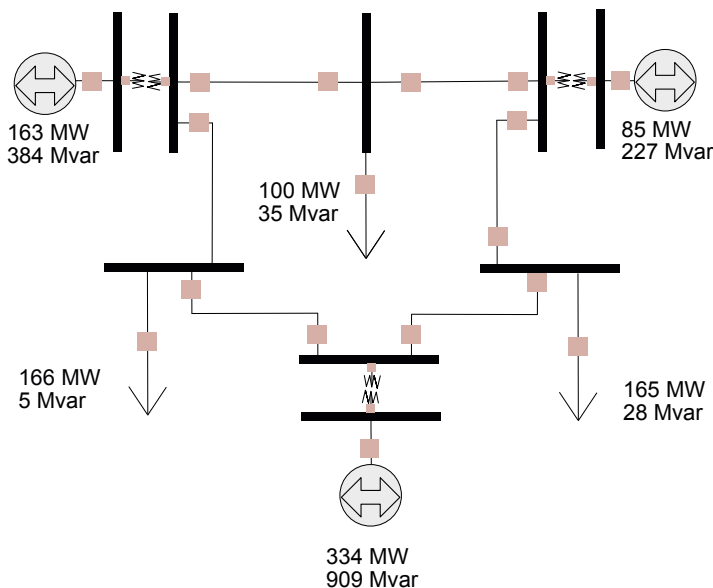
Figure 1.1   A simplified diagram of WSCC 9-bus test case that represents a simple approximation of the Western System Coordinating Council. It is equivalent to a power system with nine buses comprising three synchronous machines represented by the circular gray nodes and three load buses represented by arrows pointing downwards [Delavari et al., 2018].

Fig. 1.2. It illustrates the flow on a highway network in Los Angeles. The different cities represent graph nodes and the directed arrows depict inter-city traffic flow connections [Como and Fagnani, 2021]. Throughout this thesis, we consider weighted undirected (i.e., all edges are bidirectionally oriented) graphs and power networks as the main application of this thesis, in the example of the network depicted in Fig. 1.1.

Next, we introduce three topics that are central to the thesis and which are summarized in Fig. 1.3. First, synchronization in coupled oscillators is introduced, where we discuss Kuramoto oscillator dynamics and different notions of synchronization. Second, we study optimal feedback control with special emphasis dedicated to the importance of cost design in optimal control. This leads to the study of so-called *inverse optimal control* problems. Third and last, stability and control in power systems are presented as the main application under consideration, where the control requirements for transitioning to inverter-based generation in today's electrical grid are underlined.

The link between these three topics can be established as follows: The understanding of coupled oscillator dynamics provides the theoretical foundation to study power systems' trajectories, where each generator is consid-

Figure 1.2   An example of a traffic flow as a networked system from [Como and Fagnani, 2021]. The real highway network in Los Angeles is depicted in **A)**. The traffic flow on some possible paths from Santa Monica (given by node ①) to Santa Ana (given by node ⑰) is shown in **B)**. The links are represented by directed arrows.

ered as an oscillator and the transmission lines play the role of the coupling between all generators in the network. In inverse optimal control, stabilizing controllers are designed and shown to be optimal with respect to an *a posteriori* defined cost. This leads, in the context of power systems and coupled oscillator dynamics, to system-wide frequency synchronization with optimality guarantees.

1.1   Synchronization in coupled oscillators

Our main focus is in characterizing synchronization in a network of coupled oscillators. Intuitively, *oscillations* are defined by a behavior that does not approach any definite constant value as time goes on and keeps changing. The simplest kind of example is harmonic oscillations, where their sinusoidal motion changes *periodically*. Their dynamics are given by,

$$\theta(t) = A\sin(\omega\,t + \phi), \tag{1.1}$$

where $A > 0$ is the amplitude of the harmonic oscillation, $\omega \in \mathbb{R}$ is the frequency and $\phi \in \mathbb{S}^1$ is the initial phase angle.

Moreover, the term *synchronization* itself derives from Latin referring to individuals sharing a common notion of time and achieving *temporal coincidence* of some events. Hence, *self-organized* dynamics emerge [Wieland, 2010]. Historically speaking, the problem of synchronization was first addressed by
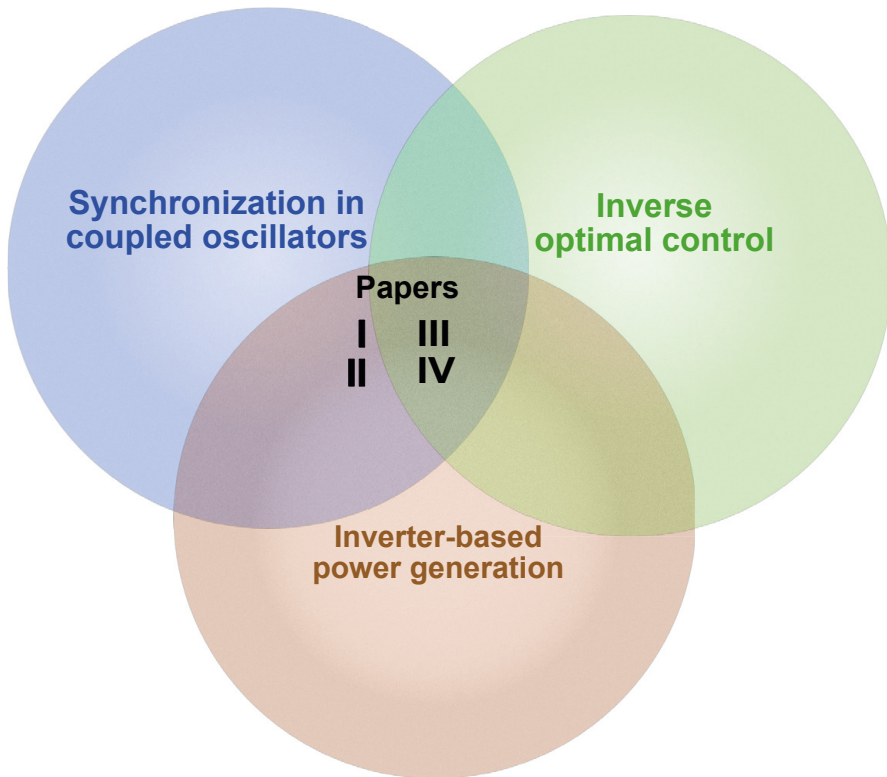
Figure 1.3 Summary of the four papers included in this thesis. Papers I and II lie at the intersection of coupled oscillator synchronization and inverter-based power generation, whereas Papers III and IV extend inverse optimal control theory while dealing with oscillator synchronization in the context of the control of power networks.

Huygens. Huygens had invented the pendulum clock in 1657. He, subsequently, had demonstrated mathematically that a pendulum would follow an isochronous path, i.e., a path such that a point mass traveling along it without friction, has a periodic motion and the period of which is independent of the initial position [Bennett et al., 2002].

Given a vector $\theta = [\theta_1, \ldots, \theta_n]^\top \in \mathbb{T}^n$, the angle $\theta_i \in \mathbb{S}^1$ refers to the $i-$th component of θ and $\dot{\theta}_i$ is its time derivative. We differentiate between three notions of synchronization in the following definitions [Bullo, 2021].

- *Frequency synchrony*: A phase angle vector $\theta : \mathbb{R}_{\geq 0} \to \mathbb{T}^n$ is frequency synchronized if $\dot{\theta}_i(t) = \dot{\theta}_j(t)$ for all times t, for all $i \neq j$ with $i, j \in \mathcal{V}$.

- *Phase synchrony*: A phase angle vector $\theta : \mathbb{R}_{\geq 0} \to \mathbb{T}^n$ is phase synchro-
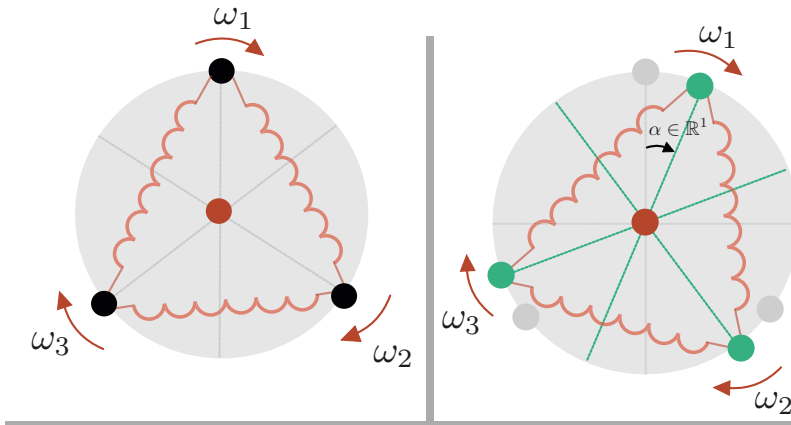
Figure 1.4 *Left side*: Representation of three Kuramoto oscillators (1.2) with angles $\theta_i \in \mathbb{S}^1, i = 1, 2, 3$, rotating on the unit circle according to their natural frequencies $\omega_i \in \mathbb{R}^1, i = 1, 2, 3$. The edge weights are identical and correspond to identical red springs. They couple every two neighboring oscillators with a uniform (across all oscillators) strength k/n, see e.g., [Dörfler et al., 2013; Bullo, 2021]. *Right side*: A shift of the phase angles of the Kuramoto model (1.2) by the same value $\alpha \in \mathbb{R}^1$ results in no change in their dynamics. The new angular positions are colored in green. This is referred to as *rotational invariance*.

nized if $\theta_i(t) = \theta_j(t)$ for all times t and for all $i \neq j$ with $i, j \in \mathcal{V}$.

- *Asymptotic synchronization*: We define phase angle vectors that asymptotically achieve synchronization properties. A vector $\theta(t)$ achieves for example frequency synchronization if $\lim_{t\to\infty} |\dot{\theta}_i(t) - \dot{\theta}_j(t)| = 0$, for all $i \neq j$ with $i, j \in \mathcal{V}$.

EXAMPLE 1.1—KURAMOTO OSCILLATOR [KURAMOTO, 1975]
Given a graph $G = (\mathcal{V}, \mathcal{E}, \{a_e\}_{e\in\mathcal{E}})$. One of the most celebrated oscillators in physics and control is the Kuramoto coupled oscillator model [Kuramoto, 1975] described by the following equation,

$$\dot{\theta}_i = \omega_i - \frac{k}{n} \sum_{j=1}^n \sin(\theta_i - \theta_j), \quad i \in \mathcal{V}, \tag{1.2}$$

where $\theta_i \in \mathbb{S}^1$ is the $i-$th oscillator phase angle, $\omega_i \in \mathbb{R}$ is the natural rotational frequency, $k > 0$ is the coupling strength and the weights associated to an edge $(i, j) \in \mathcal{E}$ are identical and set to the value $a_{ij} = k/n$. In fact, each oscillator's angle is represented in Fig. 1.4 by a phase angle $\theta_i \in \mathbb{S}^1$ on the circle, that is rotating with a natural frequency $\omega_i \in \mathbb{R}, i = 1, \ldots, n$ and linked

$t \geq 0$
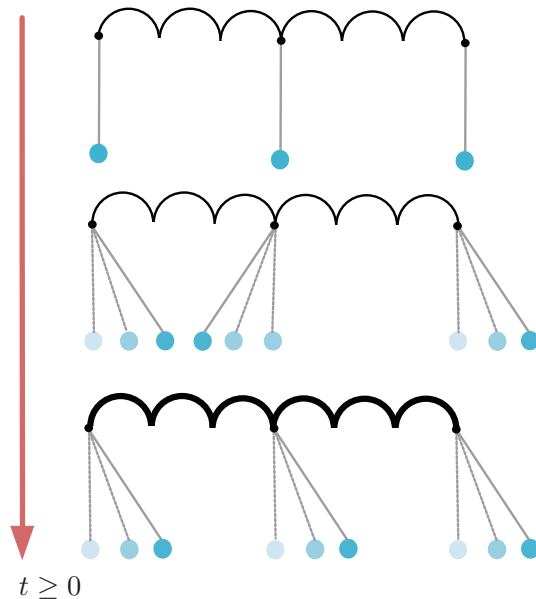
Figure 1.5 Phase synchronization of a system of three coupled pendula is analogous to frequency synchronization of coupled oscillators. The coupling is setup through the common spring. Phase synchronization is achieved if there is sufficiently strong coupling between the pendula [Witthaut et al., 2017].

to neighboring oscillators' angles via a uniform (among all neighboring oscillators) coupling k/n. Similar to the pendulum system shown in Fig. 1.5, if the coupling (represented by a string) between oscillators (represented by the pendula) is weak, then the motion of the oscillators is incoherent. A strong coupling induces frequency synchronization: all oscillators move at the same velocity.

Once each Kuramoto oscillator is represented by a phase angle evolving on the circle, it is known that their angle dynamics given by (1.2) are invariant under an arbitrary shift of *all* angles. This is referred to as *rotational invariance* explained in Fig. 1.4. In this thesis, we will study the stability of high-order oscillator models, where each oscillator is represented, not only by their phase angles, but also by other internal state dynamics, such as the ones arising in the study of inverter-based generation. These converter systems are also characterized by their rotational invariance, following a static shift of their angles. ∎

Next, we introduce the second topic that is encountered in this thesis.

Oscillator synchronization deals mainly with stability in coupled oscillator networks. Stability comes in many settings as a byproduct of solving optimization problems by finding optimal solutions that are shown later to be stabilizing for the system dynamics. What if we flip the order and start instead from a stabilizing controller to later recover optimality? How should optimality be understood in this case? i.e., with respect to which cost? The next section aims to give the preliminaries for this important research direction.

1.2   Inverse optimal control

Optimality is a universal principle, where many physical and chemical processes in nature are governed by solutions to optimization problems. Given a cost functional representing a measure of performance, optimal control amounts to choosing the *best path* among all paths feasible to a given dynamical system that minimizes the cost.

1.2.1   Direct optimal control

Chronologically speaking, optimal control stems from the *calculus of variation*, a branch of mathematics dealing with path optimization in a static, i.e., non-dynamic setting [Kot, 2014]. The modern treatment of optimal control started from the late 1950s, when two mathematical breakthroughs were made [Boltyanskiy et al., 1962; Vinter, 2010; Liberzon, 2011]. On the one hand, the maximum principle provided a set of necessary conditions for a control function to be optimal [Liberzon, 2011]. On the other hand, dynamic programming provided necessary and sufficient conditions for optimality by solving the *Hamilton-Jacobi-Bellman (HJB)* equation [Vinter, 2010]. From an engineering point of view, many examples of optimal control problems arise spontaneously, every time a new quantity (e.g., product, accuracy of information) is synthesized while a performance index is taken into account: information theory, sales and marketing, production of goods etc. For example, in the moon lander problem proposed by [Miele, 1962], the aim is to answer the following question: how should we land safely a spacecraft on the moon's surface with the least possible amount of fuel consumption? The moon lander problem was subsequently solved by [Meditch, 1964] and [Gazzola and Marchini, 2021] based on optimal control theory.

1.2.2   Cost design in optimal control: the LQR problem

In many optimal control problems, the cost functional can be regarded as a tuning knob that trades off control effort with error decay rate. We illustrate this simple yet useful idea through the linear quadratic regulator (LQR) problem. LQR aims to design a linear controller, so as to minimize the integral

of a quadratic function along trajectories of the system. It has gained broad and unfaded research interest since the rigorous mathematical exposition of the paper [Kalman, 1960].

In the following, we consider the optimal control of a linear time-invariant system with respect to quadratic performance criteria over an infinite time interval formulated as follows.

$$I(x_0, u(\cdot)) := \underset{u}{\text{minimize}} \quad \int_0^\infty \left(x^\top(\tau) Q x(\tau) + u^\top(\tau) R u(\tau) \right) \mathrm{d}\tau \qquad (1.3\text{a})$$

$$\text{subject to} \quad \dot{x} = Ax + Bu, \qquad (1.3\text{b})$$

$$x(0) = x_0 \,. $$

The value of the performance index $I(\cdot, \cdot)$ is determined on one side by the initial condition $x(0) = x_0$ and on the other side by choice of the input $u \in \mathbb{R}^m$. The state $x \in \mathbb{R}^n$ is uniquely given by the linear dynamics (1.3b) starting at x_0. In the formulation (1.3a), there is a compromise between decay transients (via the term $x^\top Q x$) and input energy (via the term $u^\top R u$). For this, we assume the following,

$$\begin{aligned} Q = Q^\top &\geq 0 \,, \\ R = R^\top &> 0. \end{aligned} \qquad (1.4)$$

Given a symmetric and positive semi-definite matrix $Q = M^\top M$, a symmetric positive definite matrix R, and if the pair (A, B) is controllable and (A, M) is observable, then, the optimal feedback law is given by

$$u^*(x) = -R^{-1} B^\top P x, \qquad (1.5)$$

where P is the unique, positive definite solution of the algebraic Riccati equation,

$$PA + A^\top P + Q - PBR^{-1}B^\top P = 0. \qquad (1.6)$$

The closed-loop system (i.e., (1.3b) together with (1.5)) is asymptotically stable for any admissible (i.e., satisfying (1.4)) Q and R matrices; see [Kalman, 1960; Willems, 1971]. We make the following observations in regards of the LQR problem (1.3).

- The optimal control law (1.5) can be tuned as a function of the input matrix R.

- The cost of (1.3) is quadratic in the state x and in the input u. It has degrees of freedom in both performance and control design via the matrices Q and R in (1.4), penalizing deviation from the origin
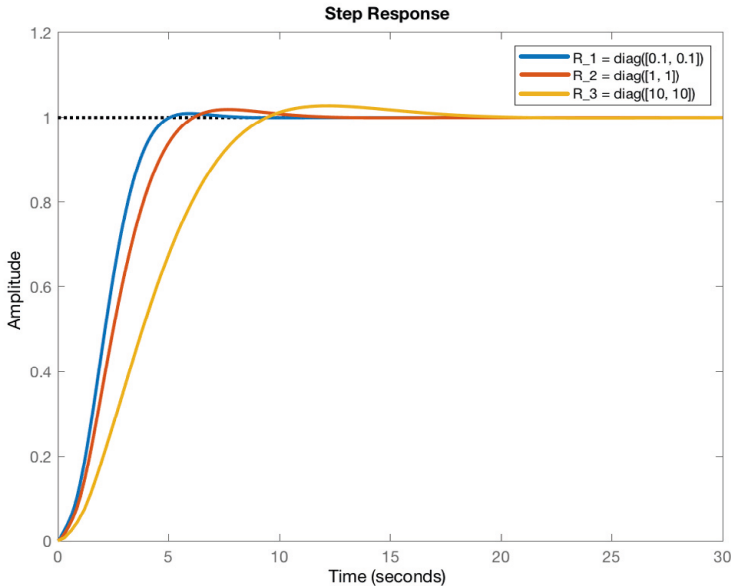
Figure 1.6   Optimal control solution to Example 1.2. Three different choices of the input weighting matrices R_1, R_2, R_3, where closed-loop trajectories, in blue are resulting from $R_1 = 0.1 \cdot I_2$, in red from $R_2 = I_2$, and in yellow from $R_3 = 10 \cdot I_2$, where I_2 is the identity matrix in $\mathbb{R}^2$. With a decreasing control effort (corresponding to higher penalty on the diagonal entries of the matrix R), the system trajectories take a longer time to settle to the desired amplitude value.

and the permissible control effort, respectively. The choice of matrices Q and R is not unique and depends on the engineering application at hand, while preserving closed-loop stability [Murray, 2009]. This freedom can be exploited to improve the controller implementation. See later Example 1.2.

- Recall also that, for a diagonal input matrix R, the LQR controller (1.5) comes with natural robustness margins as a result of its optimality (namely 60° phase margin and infinite gain margin) [Zhang and Fu, 1996].

EXAMPLE 1.2—LQR TUNING: A TRADE-OFF
The ducted fan is an indoor flying, tethered representation of the longi-

Figure 1.7   An example of a ducted fan from [Murray, 2009].

tudinal dynamics of an aircraft. Fig. 1.7 shows an example of the ducted fan. The experiment has been designed in Caltech to study rapid transition between hover, forward flight and reverse flight, as well as other aggressive flight maneuvers [Murray, 2009]. Upon system linearization, we derive an LQR controller to regulate the amplitude of the linearized dynamics to a reference value. We plot the resulting closed-loop step responses while looking at different input weightings depicted in Fig. 1.6. Note how a decreasing control effort (corresponding to higher penalty on the diagonal entries of the matrix R), implies a slower error decay rate of the system amplitude and vice versa.   ∎

It is important to keep these ideas in mind, as we move towards cost design in optimal control problems subject to general nonlinear dynamics that will be investigated later in this thesis. In particular, the non-unique choice of the quadratic cost in (1.3), leads naturally to the study of different choices of the cost functional, embedded in the framework of so-called *inverse optimal* control. This is the key for understanding future developments in this thesis.

1.3   Inverter-based power generation

In this section, we introduce the third topic of this thesis. We now study the main application of our work: the control and stability of inverter-based power systems. The system-theoretic understanding of power networks infers results obtained from canonical coupled oscillator models (e.g., the Kuramoto oscillator) due to the similarity between their respective dynamics. Inverse optimal control relies on starting from an existing stabilizing controller (e.g., suggested by power system experts) to design a performance metric that makes the suggested controller optimal. In summary, we leverage the link to these topics for the control and stability of power networks.

1.3.1 Societal context of a transforming power system

Electricity is the most important form of energy used in industrially developed societies [Kundur et al., 1994]. Due to the exceedingly complex nature of power systems, they present various challenges to engineers. From planning and construction to operation, every day power system theorists and practitioners are faced with a new problem that might impede a successful power delivery. An example of a power system is the Swedish grid depicted in Fig. 1.8. The Swedish transmission grid for electricity consists of about 17,000 km power lines, over 200 transformer and switching substations as well as AC and HVDC interconnectors. The electricity generation is dominated by hydro power plants (squares) interconnected via high voltage transmission lines (in red).

Today's electrical grid is imperatively transforming as the global energy demand grows explosively, and the environmental concerns about climate change resulting from greenhouse gas emission, carbon footprint etc., are increasingly emphasized. Additionally, social, technological and behavioral changes will have a significant impact on energy systems. Old infrastructure and equipment also affect the grid operation. For example, Sweden has one of the world's oldest national grids. Many of the transmission lines and stations are approaching the end of their technical lifetime and must soon be renewed. According to Svenska Kraftnät (the Swedish transmission system operator), the line connecting Storfinnforsen and Midskog is the world's oldest 400 kV line. It entered service in 1952 and now needs to be replaced with a modern line to be able to receive new wind power planned in the same area.

Moving forward, the European Union is committed to reducing greenhouse gas emissions to 80–95% below 1990 levels by 2050 in the context of necessary reductions by developed countries [European Commission, 2012]. The analysis of the ramifications of decarbonization shows that energy transition is possible and will be less costly in the long run than current policies. All scenarios show that electricity will have to play a much greater role than now (almost doubling its share in final energy demand to 36–39% in 2050). The EU energy transition scenarios are depicted in Fig. 1.9. A particularly strong focus is put on renewable resources (wind, solar, photovoltaics) and is expected to take the lion's share in the final energy consumption (75% in 2050) accompanied by a low nuclear providing only 32% of total power generation. To achieve this, the power system would have to undergo fundamental changes and achieve a significant level of decarbonisation already in 2030 (57–65% in 2030 and 96–99% in 2050).

In the United States, wind energy grew at a record pace in 2020, representing the largest source of new additions to the USA electric-generating capacity. The USA installed a record 17 GW of new wind capacity in 2020 bringing the total cumulative to 122 GW, with a significant expansion of the
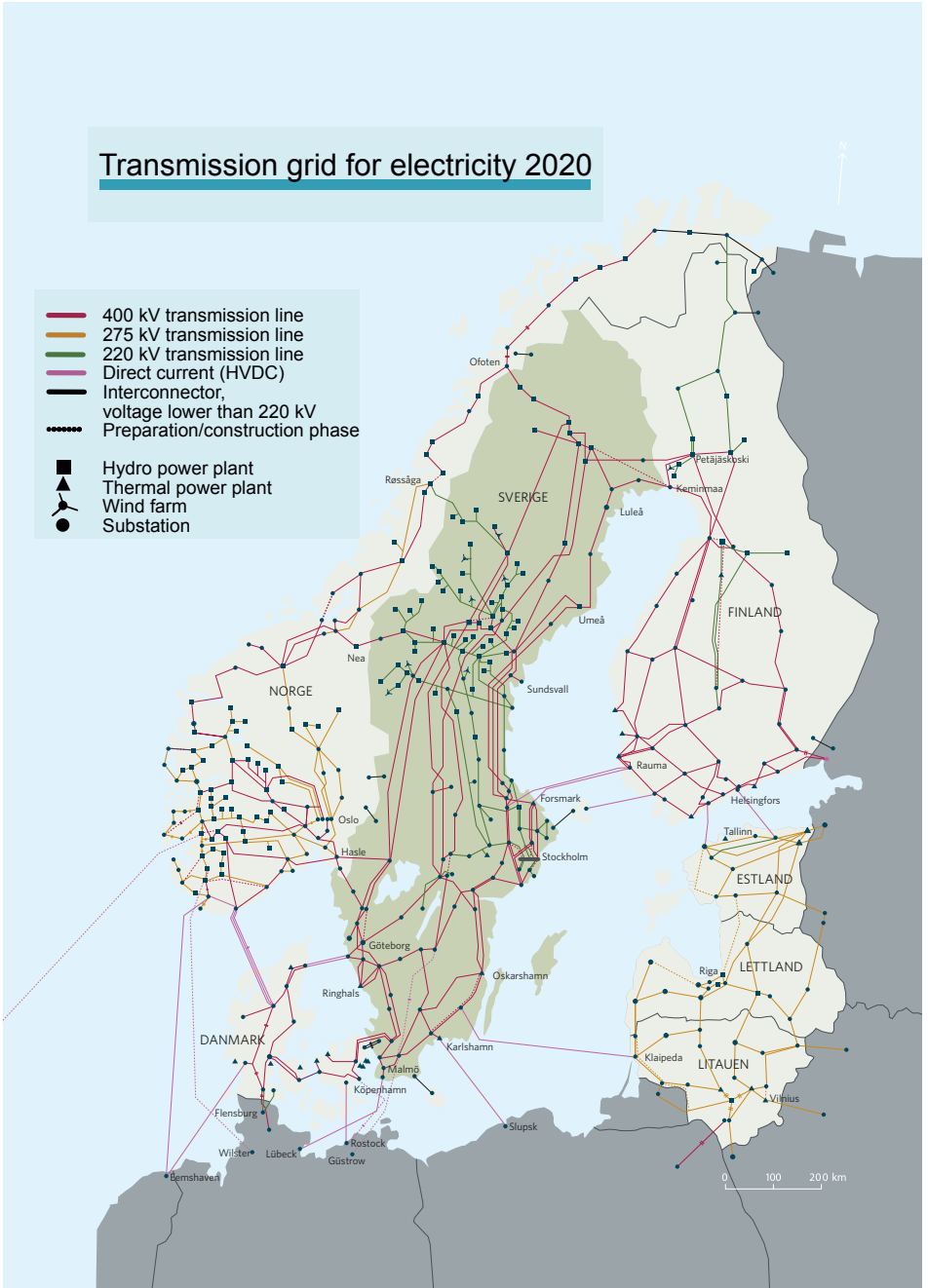
Figure 1.8   Transmission system of the Swedish national grid in 2020 [Svenska Kraftnät, 2020].
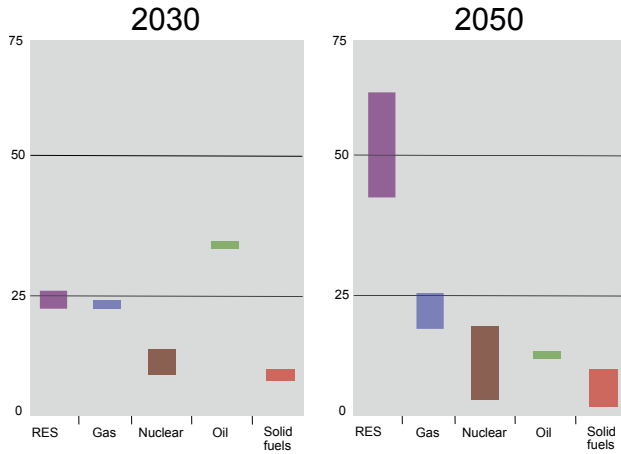
Figure 1.9 Evolution of the share of fuel and renewable energy resources in primary energy consumption from 2030 to 2050 according to EU decarbonization scenarios [European Commission, 2012]. Renewable Energy Sources (RES) will dominate the share by 2050 by more than 50%, accompanied by a strong decline in fuels (oil, nuclear, solid fuels) to less than 20%.
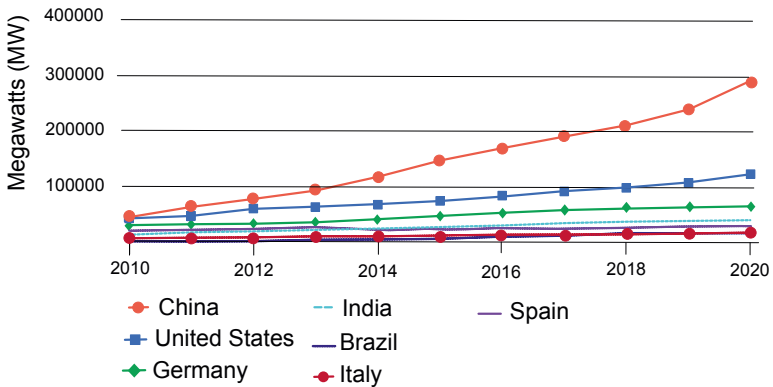
Figure 1.10 Chart data compiled from the wind technologies market report 2010-2020. China, USA and Germany have the greatest total of installed wind power capacity. Source: ["Land-Based Wind Market Report: 2021 Edition" 2021].

pipeline for offshore wind projects. The cost of wind energy generation con-

tinued to decline – laying the groundwork for significant future gains and a rapid acceleration of renewable energy deployment in a 100% clean electricity by 2035 ["Land-Based Wind Market Report: 2021 Edition" 2021]. Fig. 1.10 depicts the evolution of international wind power capacity (in megawatts) among leading countries. China, USA and Germany have the greatest total of installed wind power capacity with China leading the charts with around 300 000 MW as of 2020.

For the energy transition to succeed, reliable electrical power service must be put into place. This means, ideally, that loads are fed at constant frequency and voltage at all times. This implies that both frequency and voltage are kept within close tolerances to their desired values. One of the first requirements for reliable service, in the presence of renewable energy resources, is to keep the generation units running in parallel with adequate capacity to respond to the load demand. A loss of synchronism among generators leads to significant voltage and frequency fluctuations that may activate the protection schemes in power system by automatically tripping the transmission lines [Anderson and Fouad, 2008]. Power system stability is thus concerned with the evolution of their dynamics following a perturbation. If the perturbation does not involve any net change in the power, the generation units will return to their original state. If power imbalance occurs, a new operating state is necessary. In any of these states, all interconnected units should remain synchronized in frequency, i.e., the power system is stable. That being said, all units are operating in parallel and at the same speed. Formally, we define the stability, transient and small-signal stability of a power system from [Kundur et al., 1994; Kundur et al., 2004] as follows,

DEFINITION 1.1—POWER SYSTEM AND TRANSIENT STABILITY
If the oscillatory response of a power system during the transient period following a disturbance is damped and the system settles in a finite time to a new steady operating condition, we say that the power system is stable. If the power system is not stable, it is considered unstable.

Moreover, *transient stability* is particularly concerned with frequency stability, that is the ability to maintain synchronism in frequency during the first swing with a period of study of up to 10s under large disturbances. If the disturbances are small, we refer to the frequency stability as *small-signal* stability. ∎

Transient and small-signal stability given in Definition 1.1 will be treated throughout this thesis.

1.3.2 Transitioning from synchronous machines to power converters

In this section, we illustrate the properties of two control devices that interface the grid. We start with synchronous machines, whose dynamics
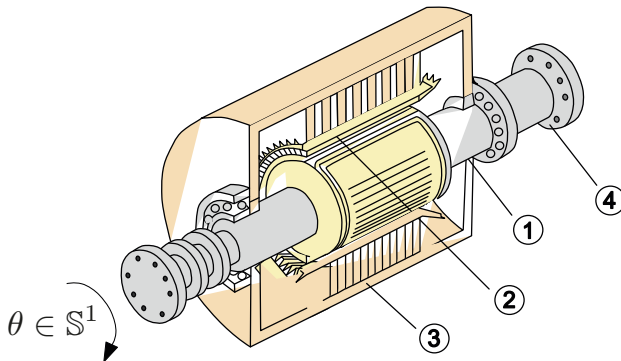
Figure 1.11   Simplified scheme of a synchronous machine. ① represents the rotor, the rotating (mechanical) element of the machine at a rotor phase angle $\theta \in \mathbb{S}^1$, ② depicts the armature windings wrapped around the rotor and belong to the electrical part of the machine and put together in a stator case given by ③. The armature windings carry current across the field and generate an electromotive force (EMF). Finally, ④ depicts a coupling element. A synchronous machine is coupled, on one side, to a prime mover, e.g., a steam turbine, and on the other side, to a load bus or power transmission system [Gülen, 2019]. See also Fig. 1.1 for a network of synchronous machines.

have dominated the power system operation for decades and then introduce DC/AC power converters or inverters that play a central role in the integration of renewable energy to achieve 100% clean electricity. We illustrate their differences to understand how a transition to converter-based generation is possible.

An example of a synchronous machine with its mechanical (rotor) and electrical components (stator) is represented in Fig. 1.11. Traditionally, synchronous machines rarely loose frequency synchronism or fall out of step, due to their large rotational masses that maintain them in synchronism. In fact, the acceleration or deceleration of the machine is governed by,

$$\dot{\theta}(t) = \omega(t) \qquad (1.7)$$
$$M\,\dot{\omega}(t) = -D(\omega(t) - \omega^*) + P_e^* - P_e(t),$$

where $\theta(t)$ is the rotor angle, $\omega(t)$ is the frequency and ω^* is the desired frequency, $M > 0$ is inertia mass, $D > 0$ is the damping coefficient, $P_e(t)$ is the active power injected into/extracted from the grid and P_e^* is its nominal or reference value. By investigating the electrical power expression $P_e(t)$ which depends on diffusive coupling between phase angles of neighboring machines, it becomes apparent that Eq. (1.7), or the so-called *swing equation* encapsulates coupled second-order oscillator dynamics. Note that the oscil-
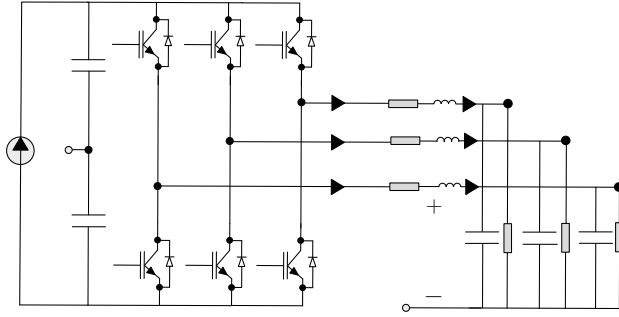
Figure 1.12 Representation of two-level three-phase inverter with an RLC output filter [Yazdani and Iravani, 2010]. The inverter topology was originally proposed by Nabae et al. in 1981 [Nabae et al., 1981]. An inverter draws active power from a DC source (e.g., battery), that is transformed into AC power, through the switching behavior and interface the electrical grid to respond to load demand. The output voltage is at desired frequency and amplitude. This is achieved via appropriate design of controllers for the switching positions.

latory behavior arises naturally in power systems as a consequence of the dynamics (1.7).

On the other hand, DC/AC converters or inverters are power electronics designed from simple circuitry. Their importance stems from being at the interface between power generation (primary energy source), on one side and the electrical grid, on the other side, where they convert DC into AC power. An efficient power transfer relies eminently on the control of these electrical circuits. A typical circuit of a two-level three-phase inverter with an RLC output filter is represented in Fig. 1.12. The switching block consists of bipolar transistors (IGBTs) and anti-parallel diodes. The DC circuit consists of a current source, set in parallel with DC capacitor and DC conductance accounting for losses on the DC-side. On the AC-side lies an output filter consisting of a resistor, placed in series with an inductance and connected to a shunt capacitance and a constant impedance load. Power conversion follows from the high switching behavior of the converters through a modulation signal, representing the main control input to the converter. Commonly, the system is assumed to be averaged, i.e., all AC quantities are averaged over a switching period and balanced and all phases sum up to zero. In this thesis, the models will not account for the losses due to the switching behavior [Yazdani and Iravani, 2010].

All in all, converters are known for their nonlinear switching dynamics, simple circuitry, fast control capabilities, their small size and light weight, which makes them amenable for transportation and deployment for large
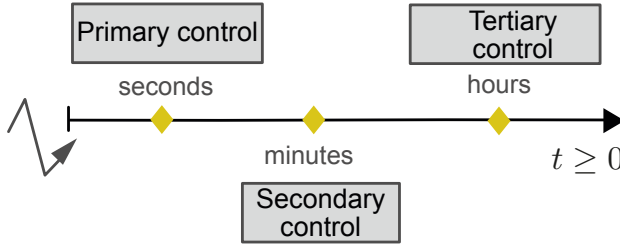
Figure 1.13   Summary of time scale separation for frequency control in the presence of synchronous machines following a disturbance at time $t = 0$. Primary control keeps the frequency within acceptable tolerance intervals and acts in a matter of seconds. The secondary control restores the frequency to nominal and the tertiary control updates within hours the power set points of the generations units in the network.

scale penetration. Due to the absence of large rotational inertia in converters, power systems are commonly referred to as *low-inertia*, as opposed to classical high-inertia power systems based on the dominant presence of synchronous machines. One ramification of their inherently different design and operation is that, converter control presents numerous challenges and bonus features.

Time-scale separation refers to three different time scales, within which each control layer intervenes to regulate the frequency, following a disturbance. The classical control hierarchy strictly delimits *primary* frequency control, keeping the system frequency within acceptable ranges and taking place in a matter of seconds, *secondary* control, aiming to restore the frequency to nominal and based on automatic generation control [Simpson-Porco, 2020] from tens of seconds to minutes, and *tertiary* control that dispatches updated power references based on optimization routines and operates in every 5-15 min [Kundur et al., 2004]. Primary and secondary control remain as our main focus in this thesis. A summary of the time scale separation is presented in Fig. 1.13. In this sense, time scale separation, that is commonly assumed in control of machines due to the slow dynamics of governor control (e.g., steam turbines), may not hold, since the synchronous machines will be retired from the grid and thus their dynamics and controls (1.7) do not hold anymore. The instantaneous response of converters suggests that this timeline might be broken and a rethinking of the different time scales for control is mandatory. In fact, a too fast response of converter control can excite oscillations in the transmission grid that destabilize the entire system [Jouini et al., 2018]. Also, measurement and communication delays can destabilize a power converter network.

Moreover, the control of converters remains fragile given their small size with no inertia, compared to the resilient control of machines that relies pri-
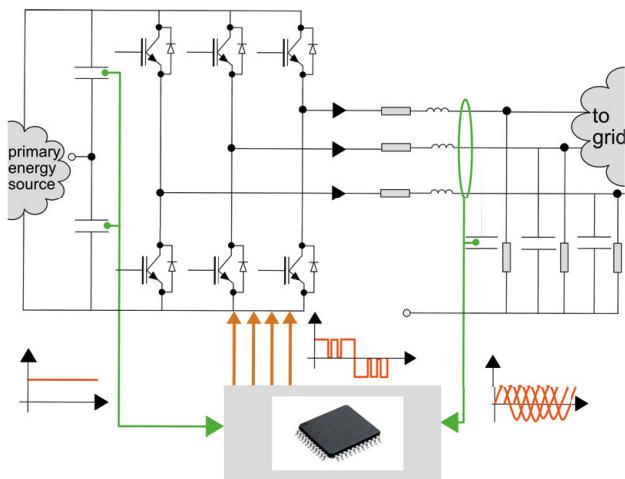
Figure 1.14 Control structure of three-phase DC/AC converter [Lin et al., 2020]. Based on DC and AC grid measurements, the control algorithm is implemented digitally on an embedded micro-controller and acts on the converter power stage by adjusting its modulation input according to the changes in the grid.

marily on their physics but also on the accumulated knowledge of decades of their control and operation. In fact, there is no established body of experience for operating hybrid or power systems with significant amounts of inverter-based resources [Lin et al., 2020]. Another difference between the control of machines and converters, lies in the intermittent generation of renewable energy resources (solar, wind) in converter-based generation, compared to dispatchable and thus well-known power generation based on synchronous machines. Finally, the centralized bulk generation is gradually being replaced by more distributed and fully decentralized converter controllers, which makes the overall network less prone to computational errors and communication delays.

Even though many of the classical power system stability notions described in [Kundur et al., 1994] (e.g., frequency stability) include definitions that are rather coherent with the electro-mechanical nature of synchronous machines, the structural similarities between a machine's rotor angle and a converter's digital angle implemented via a control algorithm, suggest that the definition of power systems and transient stability (see Definition 1.1) can be applied to power networks dominated by converters [Lin et al., 2020].
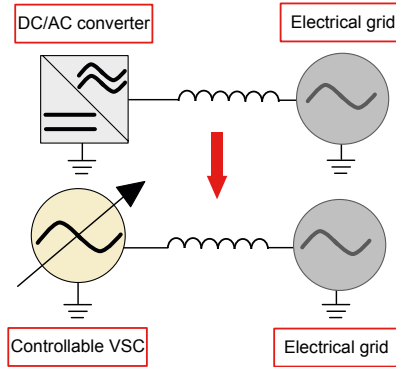
Figure 1.15 Modeling of the converter in Fig. 1.12 as a controllable ideal voltage source (VSC) connected to the electrical grid through an impedance.

1.3.3 Control requirements for inverter-based power generation

The general structure of a DC/AC converter with closed-loop control scheme is shown in Fig. 1.14. The control requirements for the massive integration of power converters can be summarized as follows.

The ability of synchronous machines to respond to the grid frequency change through an adjustment in its power output by enforcing a given amplitude and voltage to be formed at the point of common coupling is referred to as *grid-forming* [Rocabert et al., 2012]. A behavior that emulates the electromechanical interaction of synchronous machines with the grid and provides functionalities that are traditionally provided by synchronous machines is thus required, when designing future converter controls [Denis, 2017]. Grid-forming control algorithms endow the grid with autonomous primary control and therefore the capability of counteracting common grid disturbances by keeping the frequency within acceptable ranges. As shown in Fig. 1.15, the converter is regarded as an ideal voltage source with an output impedance and can co-exist with other grid-forming inverters, synchronous machines and grid devices on the same system.

Key requirements are *plug and play properties*. These are decentralized stability and robustness certificates that are independent of the number and type of the devices connected to the grid and are thus important in both high- and low-inertia systems [Jouini et al., 2016]. This term encapsulates system-wide frequency synchronization, thus transient stability as well as other important services namely load supply and power sharing among multiple inverters guaranteed by droop behavior [Dörfler et al., 2015] trading off active and reactive power injections with the voltage amplitude and frequency. Moreover, it is desired to induce a *droop behavior* as depicted in Fig. 1.16 at steady state, exhibiting a linear trade-off between frequency ver-
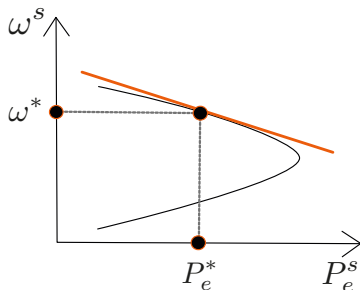
Figure 1.16 A typical nose curve for power to frequency droop: a variation in active power at steady state $P_e^s := \lim_{t\to\infty} P_e(t)$ results in a frequency deviation at steady state $\omega^s := \lim_{t\to\infty} \omega(t)$. Upon a linearization around nominal values, droop behavior is characterized by a linear trade off (via a droop slope) between the steady state of active power and frequency.

sus active power, as well as power sharing, where each unit provides power in proportion to its capacity (or its programmable droop slope) [Dörfler et al., 2015]. It is also important to endow grid-forming converters with black-start capabilities. This means that a converter can start the power network following a complete blackout and the system operation can be restored as well as virtual inertia to reduce to rate of change of frequency (RoCoF), after a sudden loss of load or generation. Finally, it is necessary that all grid resources including controlled inverters showcase *interoperability*, i.e., compatibility in their operation and interactions with the remainder of the electrical components, encompassing the hybrid operation with synchronous machines [Lin et al., 2020].

1.4   Research questions

In the following discussion, we provide a brief account of the open research questions that underpin the topics of this thesis.

① From a system-theoretic perspective, how can we understand and predict frequency synchronization in a network of coupled oscillators, where each oscillator is represented by high-order dynamics, and provide control strategies with provable stability guarantees that achieve desired waveforms? We address this first question in Papers I and II.

② How can we exploit cost design for the setting, where the cost, in addition to the system dynamics, is affected by bounded disturbances, to circumvent numerical and computational complexity, resulting from solving partial differential equations? In networks, how can we derive

optimal control laws that inherit topological structure, i.e., that are feasible for implementation, in an explicit and closed-form? We investigate this second question in Papers III and IV.

③ Bearing the two previous questions in mind and given a power system network dominated by inverter-based generation interconnected via transmission lines, how can we derive primary (and possibly secondary) frequency controllers with a feasible structure, i.e., whose implementation is possible, while also guaranteeing transient or small-signal stability? Under which mild physical conditions can this be achieved? Can we also guarantee plug and play properties and improve upon existing control schemes? We answer this third question in all papers.

2

Systems and control preliminaries

In this chapter, we introduce the reader to important system-theoretical and control notions, revolving around passivity, Lyapunov stability, center manifold theory and optimal control. These will be necessary for the understanding of many concepts treated in the remainder of this thesis.

2.1 Passivity

Consider the following nonlinear system Σ with input $u \in \mathbb{R}^m$ and output $y \in \mathbb{R}^m$,

$$\Sigma: \quad \begin{cases} \dot{x} & = f(x, u), \\ y & = h(x, u), \end{cases} \tag{2.1}$$

with $x \in \mathbb{R}^n$. Assume that $f : \mathbb{R}^n \times \mathbb{R}^m \mapsto \mathbb{R}^n$ is continuous and locally Lipschitz and $h : \mathbb{R}^n \times \mathbb{R}^m \mapsto \mathbb{R}^m$ is continuous. Let the equilibrium be at the origin, that is,

$$f(0, 0) = 0, \; h(0, 0) = 0.$$

The passivity of Σ can be defined, according to [Sepulchre et al., 2012, Ch.2], as follows.

DEFINITION 2.1—PASSIVITY
The system Σ is said to be *passive* relative to (u, y) if there exists a function $S : \mathbb{R}^n \to \mathbb{R}$ with $S(0) = 0$, such that for all $x \in \mathbb{R}^n$,

$$S(x) \geq 0, \tag{2.2}$$

$$S(x(T)) - S(x(0)) \leq \int_0^T u^\top(t)\, y(t) \, \mathrm{d}t,$$
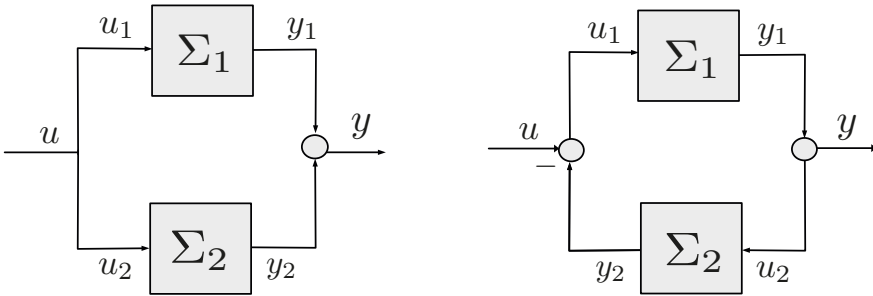
Figure 2.1 Representation of two systems Σ_1 and Σ_2 under parallel (*left*) and feedback (*right*) interconnections.

for all $u \in \mathbb{R}^m$ and $T \geq 0$. The function S is called a *storage function*. If the storage function $S(x)$ is differentiable, we can write (2.2) as,

$$\dot{S}(x) \leq u^\top y. \qquad \blacksquare$$

Intuitively, the system Σ is passive relative to (u, y) if the increase in its energy during the interval $[0, T]$ is not bigger, than the energy supplied to the system during the same interval [Sepulchre et al., 2012, Ch.2].

Interconnection of passive systems Given that two nonlinear systems Σ_1 and Σ_2, both in the form (2.1), are passive relative to (u_1, y_1) and (u_2, y_2), respectively, our goal is to ensure the interconnection is also passive and of the form (2.1) and is thus well-posed. The interconnections considered thus far, are either in parallel or in feedback as illustrated in Fig. 2.1. Following [Sepulchre et al., 2012, Ch.2], we have the result below on interconnected passive systems.

> THEOREM 1—INTERCONNECTIONS PRESERVING PASSIVITY
> Suppose that Σ_1 and Σ_2 are passive systems relative to (u_1, y_1) and (u_2, y_2), respectively. Then the two systems, one obtained by the parallel interconnection, and the other obtained by the feedback interconnection, are both passive relative to (u, y).

Thus, the passivity property is preserved under parallel and feedback interconnection of passive systems. This is illustrated using the following example in power systems from [Schaft, 2000, Ch.4].

EXAMPLE 2.1—FEEDBACK INTERCONNECTION IN POWER SYSTEMS
Consider a power system of synchronous machines, interconnected by a network described by a graph $G = (\mathcal{V}, \mathcal{E}, \{\gamma_e\}_{\{e \in \mathcal{E}\}})$ of purely inductive transmission lines modeling the synchronous machines by swing equations. Let

$|\mathcal{V}| = n$ and $|\mathcal{E}| = m$. Assuming that all voltage and current signals are sinusoidal of the same frequency and all voltages have constant amplitude, we arrive at the following model. Associated to the $n-$vertices, each $i-$th synchronous machine is described by the passive system

$$\dot{p}_i = -D_i \, M_i^{-1} p_i + u_i,$$
$$y_i = M_i^{-1} p_i,$$

where $i = 1, \ldots, n$, $p_i = M_i \omega_i$ is the momentum deviation and $\omega_i \in \mathbb{R}$ is the frequency deviation from nominal frequency ω^* (e.g., 50 Hz) with $M_i > 0$ the inertia and $D_i > 0$ the damping constant of the synchronous machine, and u_i is the incoming power. Let $\mathcal{B}$ denote the $n \times m$ incidence matrix of the associated graph G. Since q_j denotes the phase differences across the $j-$th line, the dynamics of the $j-$th line, associated to the $j-$th edge of the graph, is given by the passive system,

$$\dot{q}_j = v_j,$$
$$z_j = \gamma_j \sin(q_j),$$

where $j = 1, \ldots, m$. The constant $\gamma_j > 0$ is determined by the susceptance of the line and the voltage amplitude at the adjacent vertices. Here z_j equals the active power through the $j-$th line. Denoting $p = (p_1, \ldots, p_n)^T$, $\omega = (\omega_1, \ldots, \omega_n)^T$, and $q = (q_1, \ldots, q_m)^T$, the final system resulting from the interconnection

$$u = -\mathcal{B}\, z, \quad v = \mathcal{B}^\top y,$$

is given as,

$$\begin{bmatrix} \dot{q} \\ \dot{p} \end{bmatrix} = \begin{bmatrix} 0 & \mathcal{B}^\top \\ -\mathcal{B} & -D \end{bmatrix} \begin{bmatrix} \gamma \, \underline{\sin}(q) \\ M^{-1} p \end{bmatrix} + \begin{bmatrix} 0 \\ u \end{bmatrix}, \tag{2.3}$$
$$y = M^{-1} p,$$

with $p = M\omega$. Let D and M denote, respectively, the diagonal matrices with elements $D_i, M_i > 0$, $i = 1, \ldots, n$ and γ the diagonal matrix with elements γ_j, $j = 1, \ldots, m$. Furthermore $\underline{\sin} : \mathbb{R}^m \to \mathbb{R}^m$ denotes the element-wise sine function, i.e., $\underline{\sin}(q) = (\sin(q_1), \ldots, \sin(q_m))^\top$. Finally, the input u denotes the vector of generated/consumed power and the output y the vector of frequency deviations, both associated to the vertices. The resulting system (2.3) is passive relative to (u, y) and the storage function

$$S(q, p) = \frac{1}{2} p^\top M^{-1} p - \sum_{j=1}^{m} \gamma_j \cos(q_j). \qquad \blacksquare$$

Incremental passivity We study passivity properties of nonlinear systems described in error coordinates with respect to a desired non-zero steady state. In these settings, it becomes crucial to extend passivity from Definition 2.1 to accommodate the shifted system dynamics (with respect to a non-zero steady state). For this purpose, we state the definition of incremental passivity, adapted from [Schaft, 2000, Ch.4].

DEFINITION 2.2—INCREMENTAL PASSIVITY
Consider a nonlinear system Σ as given in (2.1), with input and output spaces $\mathbb{R}^m$ and state space $\mathbb{R}^n$, respectively. The system (2.1) is called *incrementally passive* if there exists a function, called the *incremental storage function*,

$$S : \mathbb{R}^n \times \mathbb{R}^n \to \mathbb{R}_+,$$

such that,

$$S(x_1(T), x_2(T)) \leq S(x_1(0), x_2(0)) + \int_0^T (u_1(t) - u_2(t))^\top (y_1(t) - y_2(t)) \, \mathrm{d}t \,, \tag{2.4}$$

for all $T \geq 0$, and for all pairs of input functions $u_1, u_2 : [0, T] \to \mathbb{R}^m$ and all pairs of initial conditions $(x_1(0), x_2(0))$ with resulting pairs of state and output trajectories $x_1, x_2 : [0, T] \to \mathbb{R}^n$ and $y_1, y_2 : [0, T] \to \mathbb{R}^m$. ∎

The differential version of the incremental passivity inequality (2.4) takes the form

$$\frac{\mathrm{d}S}{\mathrm{d}x_1} f(x_1, u_1) + \frac{\mathrm{d}S}{\mathrm{d}x_2} f(x_2, u_2) \leq (u_1 - u_2)^\top (y_1 - y_2).$$

Port-Hamiltonian systems Port-Hamiltonian systems are defined in terms of a *Hamiltonian function* together with two geometric structures corresponding, respectively, to power-conserving interconnection and energy dissipation. The Hamiltonian is equal to the *total stored energy* of the system that is shaped via the system's geometric structures. The Hamiltonian function automatically satisfies the passivity inequality (2.2). The following definition is taken from [Schaft, 2000, Ch.6].

DEFINITION 2.3—INPUT-STATE-OUTPUT PORT-HAMILTONIAN SYSTEM
An input-state-output port-Hamiltonian system with $n-$dimensional state space $\mathbb{R}^n$, input and output spaces $\mathbb{R}^m$, and Hamiltonian $H : \mathbb{R}^n \to \mathbb{R}$, is given by

$$\dot{x} = [J(x) - R(x)] \frac{\mathrm{d}H}{\mathrm{d}x}(x) + G(x)\,u$$

$$y = G^\top(x) \frac{\mathrm{d}H}{\mathrm{d}x}(x) \,,$$

where $G(x)$ is the $m \times n$ input matrix and the $n \times n$ matrices $J(x)$ and $R(x)$ satisfy $J(x) = -J^\top(x)$ and $R(x) = R^\top(x) \geq 0$. ∎

Note that the internal interconnection structure is described by the matrix $J(x)$, which by skew-symmetry is power-conserving, and a resistive structure given by the matrix $R(x)$, which by its non-negativity is responsible for the internal dissipation of energy [Schaft, 2000, Ch.6].

2.2 Lyapunov method

Stability theory is a cornerstone in systems theory and control engineering. Lyapunov theorems give sufficient conditions for system stability. In the remainder, we consider the autonomous system

$$\dot{x} = f(x), \quad x(0) = x_0. \tag{2.5}$$

Given a set $\mathcal{D} \subseteq \mathbb{R}^n$, we assume that $f : \mathcal{D} \to \mathbb{R}^n$ is continuous and locally Lipschitz.

2.2.1 Point stability

In this section, we are concerned with stability of equilibrium points. Assume that $\mathcal{D}$ contains the origin and $f(0) = 0$. That is, the origin is an equilibrium of (2.5).

Direct Lyapunov method   We define point stability following [Khalil, 2002, Ch.4].

DEFINITION 2.4—POINT STABILITY
The equilibrium point $x = 0$ of (2.5) is

- stable if, for each $\epsilon > 0$, there is $\delta = \delta(\epsilon) > 0$ such that,

$$\|x(0)\| < \delta \Rightarrow \|x(t)\| < \epsilon, \quad t \geq 0, \tag{2.6}$$

- unstable if it is not stable,

- asymptotically stable if it is stable and δ can be chosen that,

$$\|x(0)\| < \delta \Rightarrow \lim_{t \to \infty} \|x(t)\| = 0. \tag{2.7}$$

∎

Next, we state Lyapunov's stability theorem, also known as *direct Lyapunov method*.

THEOREM 2—DIRECT LYAPUNOV METHOD

Let $x = 0$ be an equilibrium point for (2.5) and $\mathcal{D} \subseteq \mathbb{R}^n$ be a domain containing $x = 0$. Let $V : \mathcal{D} \to \mathbb{R}$ be a continuously differentiable function such that, $V(0) = 0$ and

$$V(x) > 0, \quad x \in \mathcal{D} \setminus \{0\}. \tag{2.8a}$$

If $\dot{V}(x) \leq 0$ in $\mathcal{D}$, then $x = 0$ is stable. Moreover, if

$$\dot{V}(x) < 0, \tag{2.9a}$$

in $\mathcal{D} \setminus \{0\}$, then $x = 0$ is asymptotically stable.

A function V that satisfies the conditions of Theorem 2 is called a *Lyapunov function* for the nonlinear system (2.5). If it additionally holds that,

$$\|x\| \to \infty \Rightarrow V(x) \to \infty,$$

then V is called a *radially unbounded* Lyapunov function. If $\mathcal{D} = \mathbb{R}^n$ and V is a radially unbounded Lyapunov function, then the origin is *globally asymptotically stable*

If a Lyapunov candidate fails to satisfy the asymptotic stability condition because $\dot{V}(x)$ is only negative semidefinite (i.e., $\dot{V} \leq 0$), we can use LaSalle's theorem to study the stability of the equilibrium.

THEOREM 3—LASALLE'S THEOREM

Let $\Omega \subset \mathcal{D}$ be a compact set that is positively invariant with respect to (2.5). Let $V : \mathcal{D} \to \mathbb{R}$ be a continuously differentiable function such that $\dot{V}(x) \leq 0$ in Ω. Let E be the set of all points in Ω where $\dot{V}(x) = 0$. Let N be the largest invariant set in E. Then every solution starting in Ω approaches N as $t \to \infty$.

Indirect Lyapunov method   The next theorem gives conditions, under which we can draw conclusions about the stability of the origin for the nonlinear system (2.5) by investigating the stability of a *linear* system. This is known as *Lyapunov's indirect method*. Further assumptions are taken in regards of the vector field f in the following theorem from [Khalil, 2002, Ch.4].

THEOREM 4—LYAPUNOV'S INDIRECT METHOD

Let $x = 0$ be an equilibrium point for the nonlinear system (2.5), where f is continuously differentiable and $\mathcal{D}$ is a neighborhood of the origin. Let

$$A = \left. \frac{\mathrm{d}f}{\mathrm{d}x}(x) \right|_{x=0}. \tag{2.10}$$

Then,

1. The origin is asymptotically stable if $\text{Re}(\lambda_i) < 0$ for all eigenvalues of A.

2. The origin is unstable if $\text{Re}(\lambda_i) > 0$ for one or more of the eigenvalues of A.

Note that Theorem 4 does not say anything about the case when $\text{Re}(\lambda_i) \leq 0$, for all i, with $\text{Re}(\lambda_i) = 0$ for some i. In this case the linearization fails to determine the stability of the equilibrium point.

2.2.2 Set stability

Here, we are concerned with stability of a given closed and invariant set $\mathcal{M} \subseteq \mathbb{R}^n$ for the system (2.5) following [Lin et al., 1996; Angeli, 2004]. Let

$$\|x\|_{\mathcal{M}} = \inf_{a \in \mathcal{M}} \|x - a\|,$$

denote the distance from a point x to the set $\mathcal{M}$. Stability and asymptotic stability with respect to $\mathcal{M}$ are defined as follows.

DEFINITION 2.5—SET STABILITY
 If

$$\forall \epsilon > 0 \,, \exists \, \delta > 0 : \quad \|x(0)\|_{\mathcal{M}} < \delta \quad \Rightarrow \quad \|x(t)\|_{\mathcal{M}} < \epsilon, \quad t \geq 0, \qquad (2.11)$$

then, $\mathcal{M}$ is stable. Additionally, let $\mathcal{D} \subseteq \mathbb{R}^n$ be a set in the neighborhood of $\mathcal{M}$ with

$$\mathcal{M} \subseteq \mathcal{D} \subseteq \mathbb{R}^n.$$

If $\forall x(0) \in \mathcal{D} \subseteq \mathbb{R}^n$,

$$\lim_{t \to \infty} \|x(t)\|_{\mathcal{M}} \to 0, \qquad (2.12)$$

then, $\mathcal{M}$ is asymptotically stable. If $\mathcal{D} = \mathbb{R}^n$, then $\mathcal{M}$ is globally asymptotically stable. ∎

Let $\mathcal{D} = \mathbb{R}^n$. In the following, we extend the definition of a Lyapunov function for the system (2.5) to study the stability of $\mathcal{M}$ with respect to trajectories of (2.5).

DEFINITION 2.6—LYAPUNOV FUNCTION WITH RESPECT TO A SET
 A Lyapunov function for the system (2.5) with respect to a non-empty, closed, invariant set $\mathcal{M} \subseteq \mathbb{R}^n$ is a function $V : \mathbb{R}^n \to \mathbb{R}$ such that V is smooth (i.e., infinitely differentiable) on $\mathbb{R}^n \setminus \mathcal{M}$ and satisfies,

1. there exist two $\mathcal{K}_\infty$[1] functions α_1 and α_2 such that for any $x \in \mathbb{R}^n$,

$$\alpha_1(\|x\|_{\mathcal{M}}) \leq V(x) \leq \alpha_2(\|x\|_{\mathcal{M}}),$$

2. there exists a continuous, positive definite function α_3 such that for any $x \in \mathbb{R}^n \setminus \mathcal{M}$,

$$\nabla_x^\top V(x)\, f(x) \leq -\alpha_3(\|x\|_{\mathcal{M}}).$$

To formally characterize set stability using the direct Lyapunov method, we use the following result from [Lin et al., 1996].

> THEOREM 5—LYAPUNOV STABILITY WITH RESPECT TO A SET
> Let $\mathcal{M} \subseteq \mathbb{R}^n$ be a nonempty, closed, invariant subset for the nonlinear system (2.5). Then, (2.5) is globally asymptotically stable with respect to $\mathcal{M}$ if and only if there exists a smooth Lyapunov function V (in the sense of Definition 2.6) with respect to $\mathcal{M}$.

2.3   Center manifold theory

This section is about center manifolds with respect to stability of the equilibria of autonomous vector fields following [Wiggins, 1990, Ch.18] and [Khalil, 2002, Ch.8]. Based on Definition 2.5, center manifold theory can be extended to study set stability, see e.g., [Krick et al., 2009].

We start with the following system dynamics,

$$\dot{x} = Ax + g_1(x, w), \tag{2.13}$$
$$\dot{w} = Bw + g_2(x, w),$$

where the matrices $A \in \mathbb{R}^{c \times c}$ and $B \in \mathbb{R}^{s \times s}$ have the following properties:

1. A is a matrix of real numbers having eigenvalues with zero real parts.

2. B is a matrix of real numbers having eigenvalues with negative real parts,

and g_1, g_2 are nonlinear twice continuously differentiable functions with the following properties:

$$g_i(0, 0) = 0, \quad \frac{\mathrm{d}g_i}{\mathrm{d}x}(0, 0) = 0, \quad \frac{\mathrm{d}g_i}{\mathrm{d}w}(0, 0) = 0, \quad i = 1, 2. \tag{2.14}$$

---

[1] A continuous function $\alpha : [0, a) \to [0, \infty)$ is said to belong to class $\mathcal{K}$ if it is strictly increasing and $\alpha(0) = 0$. It is said to belong to class $\mathcal{K}_\infty$ if $a = \infty$ and $\alpha(r) \to \infty$ as $r \to \infty$, [Khalil, 2002, Ch.4].

In this setup $(x, w) = (0, 0)$ is an equilibrium point for (2.13) and we are interested in studying its stability properties. The linearization of (2.13) about the equilibrium is given by:

$$\dot{x} = Ax,$$
$$\dot{w} = Bw.$$

The origin point is non-hyperbolic (due to the zero real-part of the eigenvalues of the matrix A). It has a $c-$dimensional invariant center subspace and an $s-$dimensional invariant stable subspace given by:

$$E^c = \{(x, w) \in \mathbb{R}^{c \times s} \,|\, w = 0\}, \tag{2.15}$$
$$E^s = \{(x, w) \in \mathbb{R}^{c \times s} \,|\, x = 0\}. \tag{2.16}$$

There is a $c-$dimensional, local center manifold that passes through the origin and is tangent to E^c at the origin. The existence of the center manifold is given by the following theorem in [Khalil, 2002, Ch.8].

> THEOREM 6—EXISTENCE OF THE CENTER MANIFOLD
> If g_1 and g_2 are twice continuously differentiable and satisfy (2.14), all eigenvalues of A have zero real parts, and all eigenvalues of B have negative real parts, then there exists a constant $\delta > 0$ and a continuously differentiable function h, defined for all $\|x\| < \delta$, such that $w = h(x)$ is a center manifold for (2.13).

In particular, if $w = h(x)$ is an invariant manifold for (2.13) and h is smooth, i.e., infinitely differentiable, then it is called a *center manifold* and it can be written as,

$$W^c(0) = \{(x, w) \in \mathbb{R}^c \times \mathbb{R}^s \,|\, w = h(x), h(0) = 0, \frac{\mathrm{d}h}{\mathrm{d}x}(0) = 0\}, \tag{2.17}$$

which is valid in a neighborhood of the origin, i.e., for $\|x\|$ sufficiently small. The application of the center manifold theory for analyzing the behavior of the trajectories of (2.13) near the origin is based on two theorems describing:

- the dynamics restricted to the center manifold,

- the stability of the origin restricted to the center manifold and its relation to the stability of the origin of the full system (2.13).

> THEOREM 7—DYNAMICS ON THE CENTER MANIFOLD
> The dynamics of (2.13) restricted to the center manifold is given by:
>
> $$\dot{\xi} = A\xi + g_1(\xi, h(\xi)), \quad \xi \in \mathbb{R}^c, \tag{2.18}$$
>
> for $\|\xi\|$ sufficiently small.

We refer to (2.18) as the *reduced system*. We use the variable ξ instead of x to avoid confusing a point ξ on the center manifold with a point x on the coordinate axis and this, in view of the comparison between the trajectories of the full system (2.13) and the reduced system (2.18). See later Theorem 8.

The next theorem says that the stability properties of the origin of the reduced system imply the same stability properties of the origin of the full system (2.13). Additionally, it gives precise results for the case that the origin is (asymptotically) stable. It says that trajectories starting at initial conditions sufficiently close to the origin asymptotically approach a trajectory in the center manifold. This is the main result of center manifold theory called *the reduction principle*, see [Wiggins, 1990, Ch.18].

THEOREM 8—REDUCTION PRINCIPLE

- Suppose that the origin of (2.18) is stable (asymptotically stable) (unstable), then the origin of (2.13) is also stable (asymptotically stable) (unstable).

- Suppose that the origin of (2.18) is stable. Then if $(x(t), w(t))$ is a solution of (2.13) with $(x(0), w(0))$ sufficiently small, then there is a solution $\xi(t)$ of (2.18) such that as $t \to \infty$,

$$x(t) = \xi(t) + r_1(t),$$
$$w(t) = h(\xi(t)) + r_2(t),$$

where $\gamma_i, c_i > 0$ is a constant and $\|r_i(t)\| < c_i e^{-\gamma_i t}$, $i = 1, 2$.

2.4 Optimal control

In this section, we will consider cost functionals of the form,

$$J(u) = \int_{t_0}^{t_f} L(t, x(t), u(t)) \, \mathrm{d}t. \tag{2.19}$$

and aim to solve the following optimization problem,

$$\begin{aligned} \underset{u \in \mathbb{R}^m}{\text{minimize}} \quad & J(u) & (2.20) \\ \text{subject to} \quad & \dot{x}(t) = f(t, x(t), u(t)), & (2.21) \\ & x(t_0) = x_0, \end{aligned}$$

Here $L : \mathbb{R} \times \mathbb{R}^n \times \mathbb{R}^m \to \mathbb{R}$ is the running cost (or Lagrangian). Since the cost depends on the initial data, as well as on the control, it would be

more accurate to write $J(t_0, x_0, u)$, but we write $J(u)$ for simplicity and to reflect the fact that the cost is being minimized over the space of control functions [Liberzon, 2011, Ch.5].

Dynamic programming Dynamic programming leads to necessary as well as sufficient conditions for optimality expressed as a function of the Hamilton-Jacobi-Bellman (HJB) partial differential equation for the optimal cost [Liberzon, 2011, Ch.5]. The basic idea of dynamic programming is to consider, instead of the problem of minimizing $J(t_0, x_0, u)$ in (2.19) for given t_0 and x_0, the *family* of minimization problems associated with this cost functionals. This relies on *the principle of optimality* defined below. See [Liberzon, 2011, Ch.5] .

DEFINITION 2.7—PRINCIPLE OF OPTIMALITY
For every $(t, x) \in [t_0, t_f] \times \mathbb{R}^n$ and every $\delta t \in (0, t_f - t]$, the value function V defined by

$$V(t, x) := \inf_{u_{[t, t_f]}} J(u)$$

where $u_{[t, t_f]}$ is the control restricted to the interval $[t, t_f]$ satisfies the relation

$$V(t, x) = \inf_{u_{[t, t+\delta t]}} \int_t^{t+\delta t} L(t, x(s), u(s)) \, \mathrm{d}s + V(t + \delta t, x(t + \delta t)), \quad (2.22)$$

where $x(t)$ on the right-hand side is the state trajectory corresponding to the control $u[t, t + \delta t]$ and satisfying $x(t) = x$. ∎

We have the following remarks.

- Note that the existence of an optimal controller and hence of the optimal cost is not actually assumed. This is why $V(t, x)$ is defined with an infinimum and not with a minimum. When an optimal control u^* exists, then it is replaced by the minimum, achieved when $u = u^*$.

- The optimality principle conveys that we can search over a small time interval for a control that minimizes the cost over this interval plus the subsequent optimal cost-to-go, $V(t + \delta t, x(t + \delta t))$. Thus the minimization problem on the interval $[t, t_f]$ is split into two intervals, one on $[t, t + \delta t]$ and the other on $[t + \delta t, t_f]$.

- Eq. (2.22) describes a dynamic relationship among the optimal values of the cost for different t and x.

We define the equation,

$$-\frac{\mathrm{d}V(t, x)}{\mathrm{d}t} = \inf_{u \in \mathbb{R}^m} \left\{ L(t, x, u) + \left(\frac{\mathrm{d}V(t, x)}{\mathrm{d}x} \right)^\top f(t, x, u) \right\}. \quad (2.23)$$

Eq. (2.23) must hold for all $t \in [t_0, t_f)$ and all $x \in \mathbb{R}^n$. This equation for the value function V is called *the Hamilton-Jacobi-Bellman* (HJB) equation. It is a PDE since it contains partial derivatives of V with respect to t and x. The boundary condition that accompanies Eq. (2.23) is $V(t_f, x) = 0$.

For *infinite horizon* problems, the cost functional (2.19) becomes

$$J(u) = \int_0^\infty L(x(t), u(t)) \, \mathrm{d}t \,, \tag{2.24}$$

and the HJB equation in (2.23) becomes

$$0 = \inf_{u \in \mathbb{R}^m} \left\{ L(x, u) + (\nabla_x V(x))^\top f(x, u) \right\}.$$

Robust optimal control Let us now assume that the system dynamics are affected by disturbances and given by,

$$\dot{x} = f(x, u, w), \tag{2.25}$$

where, for all $t \geq 0$, $w(t) \in \mathcal{W}$ is the disturbance input taking values in a bounded disturbance set $\mathcal{W} \subseteq \mathbb{R}^n$, e.g., $w(t) \in \mathcal{L}_2[0, \infty)$. A generalization of the HJB partial differential equation is given by [Başar and Bernhard, 2008, Ch.2],

$$-\frac{\mathrm{d}V(t, x)}{\mathrm{d}t} = \inf_{u \in \mathbb{R}^m} \sup_{w \in \mathcal{W}} \left[L(t, x, u) + \left(\frac{\mathrm{d}V(t, x)}{\mathrm{d}x} \right)^\top f(t, x, u, w) \right]. \tag{2.26}$$

The counterpart of (2.23) is now the continuous-time Isaacs (or, Hamilton-Jacobi-Isaacs) (HJI) equation given in (2.26), which is a generalization of the HJB partial differential equation. In the infinite horizons case, i.e., with the cost functional defined in (2.24), the HJI equation becomes

$$0 = \inf_{u \in \mathbb{R}^m} \sup_{w \in \mathcal{W}} \left[L(x, u) + (\nabla_x V(x))^\top f(x, u, w) \right].$$

3

Literature synopsis

This thesis work lies at the intersection of three main topics: synchronization in coupled oscillators, inverse optimal control in networked settings, and the application to inverter-based power systems. This chapter conveys an overview picture of the state-of-the-art literature. It covers each topic individually and highlights the different gaps and limitations that this thesis aims to fill.

3.1 Oscillator synchronization problems

3.1.1 Synchronization in scientific research

Consider a system of finite number of oscillators with a given interaction topology, where the dynamics at the $i-$th oscillator are described using the phase angle $\theta_i \in \mathbb{S}^1$. One of the widely used models is the Kuramoto coupled oscillator model (1.2) that represents a canonical model and a prototype that is naturally encountered in different applications [Dörfler and Bullo, 2014]. For instance, many biological and neural systems can be seen as networks of interacting periodic processes. In this context, the study of oscillations is pervasive, due to their presence e.g., across brain regions, where the understanding of neural oscillations is a starting key element towards understanding of the brain activity and its malfunction [Bick et al., 2020]. Another example is deep brain stimulation, known to be an effective treatment for a variety of neurological disorders, including Parkinson's disease, using coupled oscillator dynamics to describe how the brain oscillations should change, when stimulation is applied at a particular state of the system [Weerasinghe et al., 2019]. Moreover, oscillating chemical reactions in living systems are vital for regulating circadian rhythms, metabolic processes, the transcription of DNA and other crucial biological functions [Shklyaev et al., 2020]. Kuramoto's model has been also generalized to other large systems of biological oscillators, such as chorusing frogs, and even human concert audiences clapping in unison [O'Keeffe et al., 2017]. Other applications include planar

collective motion of particles [Sepulchre et al., 2007]. Finally, the study of frequency synchronization in power systems [Dörfler and Bullo, 2012b; Dörfler and Bullo, 2014] is the main application considered in this thesis.

Conditions for frequency synchronization   Control theorists have shown an increasing interest in complex networks of coupled oscillators and have recently contributed to many novel approaches and results, where a finite number of oscillators has been taken under the loupe.

A vast body of literature deals with frequency synchronization of Kuramoto models, mostly for *unweighted* graphs (i.e., if the weight has the value one, then the corresponding edge is called unweighted) with *special* topologies. The works of [Aeyels and Rogge, 2004; Mirollo and Strogatz, 2005] consider all-to-all connection between Kuramoto oscillators and rigorously characterize the spectrum and the associated eigenvectors of the linearized system model, for a finite number of oscillators. This allows to derive bounds on the critical coupling, i.e., the smallest coupling coefficient, for which a global phase-locked state can exist, and is characterized via the bisection algorithm [Verwoerd and Mason, 2008].

A graph, whose vertices can be divided into two disjoint sets U and V with the property that every edge connects a vertex in U to one in V, is called *a bipartite* graph. A *complete bipartite* graph is a bipartite graph in which every vertex of U is connected with every vertex of V. A cycle is a directed path that starts and ends at the same vertex. A graph with no cycle is called *acyclic*.

Complete bipartite graphs have been considered in [Verwoerd and Mason, 2009], where the critical coupling coefficient can be found using an efficient algorithm. For acyclic graphs, [Jadbabaie et al., 2004] and [Dörfler et al., 2013] derive necessary and sufficient conditions in closed-form as a function of the network topology and parameters, or equivalently in terms of an intuitive, linear, and static auxiliary system. Even though necessary conditions can be derived for some special topologies [Chopra and Spong, 2009; Dörfler et al., 2013], only sufficient conditions are prevalent in the analysis of oscillator synchronization with *arbitrary* topologies [Jadbabaie et al., 2004; Dörfler and Bullo, 2012b]. It is known that a strongly coupled and sufficiently homogeneous network synchronizes but the characterization of the threshold from incoherence to synchrony is the ultimate goal of many of these works [Dörfler et al., 2013]. Intuitively, these conditions read as follows: if the dissimilarities between natural frequencies in some metric norm (e.g., Euclidean or 2-norm [Jadbabaie et al., 2004], worst-case or ∞-norm [Dörfler et al., 2013]) are dominated by the coupling strength, then Kuramoto oscillators will synchronize in frequency.

To arrive at these synchronization conditions, numerous system-

theoretical and control tools are deployed to grasp the phenomena governing coupled oscillators. In this context, Lyapunov methods are widely used to study the stability of synchronized solutions such as linear quadratic [Chopra and Spong, 2009] or sinusoidal quadratic functions of neighboring angle differences [Franci et al., 2010]. Additionally, contraction analysis allows the study of nonlinear trajectories by looking at their virtual displacement dynamics and measuring well-defined distances between these via integration. Lyapunov functions founded on contraction analysis have led to an improved understanding of systems with symmetry (e.g., possessing a rotational invariance) and the generalization of synchronization results confined to an arc [Dörfler and Bullo, 2012b] into the full circle based on an almost global stability analysis [Forni and Sepulchre, 2013]. Another Lyapunov candidate, given by the maximum angle difference between any two oscillators, is continuous but non-differentiable, generally appearing also in the study of positive systems (a class of systems with the property that its state variables are never negative, given a positive initial state), as in [Rantzer and Valcher, 2018].

Common control-theoretic tools for the stability analysis of nonlinear systems include passivity [Willems, 2007] and port-Hamiltonian formulations [Schaft and Jeltsema, 2014], input-to-state and set stability. These have been the subject of many theoretical investigations [Dörfler and Bullo, 2014]. Finally, algebraic graph theory relying on the properties of the Laplacian matrix and its pseudo-inverse and the Brouwer-Fixed Point theorem (stating that, a continuous function that maps a non-empty compact, convex set into itself has at least one fixed point) have led to concrete and elegant synchronization conditions [Jadbabaie et al., 2004; Jafarpour and Bullo, 2018] that are ingeniously improved upon existing literature.

Beyond Kuramoto oscillator   Extensions of the Kuramoto oscillator model include the study of higher-order oscillatory behaviors. The first-order model in (1.2) can be replaced by the dynamics of the second order following the swing dynamics presented in (1.7), naturally appearing e.g., in the study of physical systems such as power systems [Acebrón et al., 2005]. Furthermore, other extended studies include heterogeneously delayed systems embedded in a directed graph with fixed topology [Schmidt et al., 2012], switched topology [Papachristodoulou et al., 2010], generalized coupling with interaction dynamics [Izhikevich, Kuramoto, et al., 2006] and the analysis of random graphs based on numerical computations and analytical estimates on the synchronization capability of the network [Nishikawa et al., 2003; Moreno and Pacheco, 2004] .

3.1.2   Limitations and remedies

- The studies listed above give intuitive insights into the sensitivities affecting frequency synchronization in first-order Kuramoto (1.2) or second-order oscillator models (1.7) such as network topology and critical coupling, but fail to explain stability behavior for high-order systems with rotational invariance. These arise, e.g., in power system dynamics after a static shift in all generators' angles. This motivates the extension of many existing results to the study of frequency synchronization on high-order manifolds for systems with this property. High-order coupled oscillator dynamics are treated in Paper II of this thesis.

- Many of the frequency synchronization conditions derived from the literature are implicit, i.e., involve solving a program to certify stability, see e.g., [Vu and Turitsyn, 2015; Schiffer et al., 2019]. In many cases, these programs might not have a solution and thus can be infeasible. Even if feasible, the conditions are not explicitly given in a closed-form, which makes it hard to find a valid mapping from the space of oscillators and network parameters to the stability condition and hence develop an intuition on how to satisfy them. This motivates the search for explicit, closed-form conditions for frequency synchronization in coupled oscillators. This will be shown in Paper II of this thesis.

We also refer the reader to Sections 4.2 stating our contributions of Paper II.

3.2   Inverse optimal control

3.2.1   Cost design in optimal control

In optimal control, it is ubiquitous to start from an *a priori* defined cost functional subject to (possibly) nonlinear system dynamics with the goal to find an unknown optimal control law that represents a solution to an optimization problem. Consider for example the following continuous-time infinite-horizon optimal control problem given by,

$$
\begin{aligned}
\underset{u \,\in\, \mathbb{R}^m}{\text{minimize}} \quad & \int_0^\infty \left[q(x(s)) + \kappa(u(s)) \right] \, \mathrm{d}s \\
\text{subject to} \quad & \dot{x}(t) = f(x(t), u(t)), \\
& x(0) = x_0,
\end{aligned}
\tag{3.1}
$$

where $x \in \mathbb{R}^n$ denotes the state vector, $x(0) = x_0$ is the initial state. The input is represented by the vector $u \in \mathbb{R}^m$. The mapping $f : \mathbb{R}^n \times \mathbb{R}^m \to \mathbb{R}^n$ is a nonlinear vector field assumed to be continuous and locally Lipschitz

with $f(0,0) = 0$. Thus, without loss of generality, the zero state or the origin is a steady state, when no inputs are applied. Additionally, the mappings $\kappa : \mathbb{R}^m \to \mathbb{R}_{>0}$ is given by $\kappa(u) = u^\top R u$, where $R = R^\top > 0$ and $q : \mathbb{R}^n \to \mathbb{R}_{>0}$ with $q(0) = 0$ is assumed to be continuous.

Most often the ingredients of the optimal control problem (3.1) are set up as follows: the vector field f is a model built from first-order principles, while q and κ represent together the running cost and play the role of tuning knobs to shape the dynamics of the closed-loop trajectories. Concretely, to make the input signal u less aggressive, one increases the penalty on u via tuning of the input matrix R. Similarly, to improve the disturbance attenuation, we increase the penalty on u in the input matrix R. The resulting closed loop is always stable, irrespective of the cost integrands, $q(x)$ and $\kappa(u)$. This follows from the observation that every *value function* defined by,

$$V(x_0) := \inf_{u \in \mathbb{R}^m} \int_0^\infty [q(x(s)) + \kappa(u(s))] \, \mathrm{d}s, \tag{3.2}$$

is a Lyapunov function candidate.

Limitations of direct optimal control   The optimization problem (3.1) is generally very hard to solve and non-feasible in most settings either analytically or numerically, except in simplified linear settings such as LQR problems. Analytically, finding a concise, closed-form controller is generally hard because it involves solving a partial differential equations. Numerically, this approach suffers from *the curse of dimensionality*, so named by Bellman. As the dimension of the system grows larger and larger, the number of samples needed to discretize the partial differential equations equation often grows exponentially. For systems with dimensions higher than two, there are no practical ways to solve this partial differential equation. Even the mere existence of a solution in this case cannot be guaranteed *a priori*. Most approximate methods yield only results valid in a region, whose size must be estimated by numerical computations [Lincoln and Rantzer, 2006]. These difficulties are more pronounced in the study of solutions to (3.1) subject to bounded disturbances that involves solving the Hamilton-Jacobi-Isaacs partial differential equations [Ba sar and Bernhard, 2008].

Furthermore, how to choose a cost function which accurately reflects the functional objectives of the system and at the same time yields an optimal control law that is simple, concise and in closed-form is a cumbersome task. It mainly requires a trade off between complexity of the physical structures to implement and minimal (e.g., monetary) budget and input effort. All the above have motivated a change of perspective in the formulation of optimal control by asking the following question:

Given a particular feedback control law, what is the family of criterion functions, for which this law is optimal? [Kalman, 1964]

The inverse optimal control problem aims to find an answer to this question.

3.2.2   Inverse optimal control: main idea and properties

In the sequel, consider the input-affine nonlinear system dynamics that is subject to disturbances,

$$\dot{x}(t) = f(x(t)) + G^\top u(x(t)) + G_w^\top w(t), \quad t > 0 \tag{3.3}$$
$$x(0) = x_0,$$

where $G \in \mathbb{R}^{m \times n}, G_w \in \mathbb{R}^{w \times n}$ are input matrices, $w \in \mathbb{R}^w$ is the system disturbance that lies in $\mathcal{L}_2[0, \infty)$, i.e., satisfying,

$$\int_0^\infty w^\top(t)\, w(t)\, \mathrm{d}t < \infty.$$

Instead of asking for a control law $u(x)$ corresponding to a given performance criterion, we seek to determine *all* performance criteria (if any) for which a given control law is optimal [Kalman, 1964]. In particular, we start from a known and stabilizing control law $u^*(x)$, associated with a (robust) control Lyapunov function V, i.e., a continuously differentiable function that satisfies

$$\nabla_x^\top V (f(x) + G^\top u^*(x) + G_w^\top w) < 0. \tag{3.4}$$

Then, we can retrieve the running cost functional $q(x)$ *a posteriori*. In other words, we reverse engineer the cost for which the given controller is optimal. In this sense, the problem is called *inverse* because $q(x)$ is determined *after* a feedback controller has been designed [Haddad and Chellaboina, 2011; Sepulchre et al., 2012]. This motivates the following definition from [Sepulchre et al., 2012].

DEFINITION 3.1—INVERSE OPTIMAL ROBUST STABILIZING CONTROL
 Let $w = 0$. A control law $u^*(x)$ is inverse optimal stabilizing for the system (3.3) if

- it achieves asymptotic stability of the origin of (3.3).

- it is of the following form,

$$u^*(x) = -\frac{1}{2} R^{-1} G \nabla_x V, \tag{3.5}$$

  where $R = R^\top > 0$ and $V : \mathbb{R}^n \to \mathbb{R}_{>0}$ is a control Lyapunov function of (3.3).

For $w \neq 0$, a control law $u^*(x)$ is *inverse optimal robust stabilizing* for the system (3.3), if it is inverse optimal stabilizing for all disturbances $w \in \mathcal{L}_2[0, \infty]$. ∎

Evolving the idea of inverse optimal control   The first inverse optimal control problem has been posed and solved by R.E. Kalman in 1964 for linear systems with quadratic cost [Kalman, 1964]. Later, [Moylan and Anderson, 1973; Casti, 1974] and others studied more general forms of the cost functional for which the variational problem has nontrivial solution, e.g., involving a strictly convex integrand in the state or input and subject to general nonlinear systems. For the disturbance-free setting, it has been shown that, if the control law is of the form (3.5), then there exists an *a posteriori* defined cost functional, so that the proposed controller is optimal, i.e., that the control Lyapunov function V satisfies the HJB equation. For the control problem (3.1), the cost functional is given by,

$$q(x) = \nabla_x^\top V(f(x) + G^\top u^*(x)) - \kappa(u^*).$$

This result has been later generalized by Freeman [Freeman and Kokotovic, 1996] and also by [Haddad and Chellaboina, 2011] to disturbance attenuation problems, where the disturbance is explicitly incorporated into the system dynamics, e.g., as given in (3.3), leading to the study of HJI partial differential equation.

The converse link established by inverse optimal control, namely that, *every Lyapunov function is a meaningful value function*, has a handful of implications on the study of nonlinear control synthesis. First, compared to other control approaches such as feedback linearization that have no stability margin (that is, with a slightly perturbed feedback, the closed-loop system trajectories tend to infinity), inverse optimal stabilizing controllers are robust against disturbances and use the nonlinearity to enhance the rate of decrease of the Lyapunov function [Sepulchre et al., 2012]. Furthermore, by restricting the class of cost functionals to include a real penalty on both the state via $q(x)$ and the input via $\kappa(u)$, the optimal closed-loop system inherits the nonlinear analog of desirable phase and gain margins, similar to multivariable LQR controllers known to possess (for a diagonal input matrix R, see [Lehtomaki et al., 1981]) an *infinite* gain margin and 60° phase margin. In the example of nonlinear control problems, the optimal controller (3.5) is robust against an infinite increase in gain, also called *high-gain* control [Glad, 1987; Sepulchre et al., 2012]. A summarizing overview of direct and inverse optimal control approaches is given in Fig. 3.1.

Properties of inverse optimal control   One can interpret the control law (3.5) as a damping control for unforced asymptotically stable systems, following [Sepulchre et al., 2012], where the derivative of V can be made more negative. This can be inferred from the control gain matrix $K = \frac{1}{2}R^{-1}$ in (3.5) that plays the role of an additional damping for energy dissipation of V. This establishes a link to the powerful theory of dissipativity [Willems,
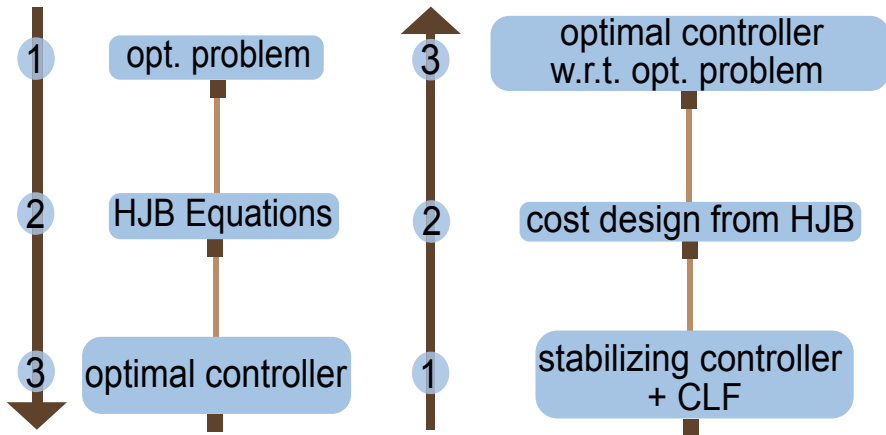
Figure 3.1 A summary of the direct optimal control approach (*left*) and inverse optimal control (*right*).

1972a; Willems, 1972b] and motivates the study of inverse optimal control for passive systems, where (3.5) amounts to choosing,

$$u = -K\,y, \quad K = \frac{1}{2}R^{-1} > 0,$$

with the output $y = \nabla_x^\top V G$. This is the so-called *damping injection* with the matrix K being the so-called *damping injection gain* [Ortega et al., 2002] and agrees with the idea of damping control for stable systems. In this way, we extract or dissipate energy from the system and therefore increase the rate of convergence of the energy function towards an equilibrium. Finally, the link between the powerful theory of dissipativity and inverse optimality [Sepulchre et al., 2012] makes the latter an indirect approach to derive a controller that renders the closed-loop system passive without explicitly requiring, *a priori*, a certain passivity structure e.g., that the dynamics follow a port-Hamiltonian system, which might be restrictive.

3.2.3 Engineering applications and beyond

Thanks to the structural properties encoded by the control law (3.5), inverse optimal control has led to the synthesis of useful optimal controllers in numerous engineering applications, from the stabilization of a rigid [Krstic and Tsiotras, 1999] and under-actuated spacecraft [Geng et al., 2016] in aerospace engineering, output voltage regulation of DC/DC power converter circuits [Vega and Alzate, 2014], neutral networks in stochastic nonlinear systems [Cao et al., 2019] to flexible joint robot manipulator [Ha et al., 2007], output trajectory tracking [Ornelas et al., 2010], non-cooperative differential

games [Molloy et al., 2019] and even glycemic control in patients [Sanchez and Ornelas-Tellez, 2017] and neuroscience [Berret and Jean, 2016].

More recent applications of inverse optimal problems have been more pronounced at the interface of data-driven control and reinforcement learning [Self et al., 2020; Ab Azar et al., 2020] via so-called *cost learning* [Finn et al., 2016] e.g., to establish a model of human overall locomotion path generation to given target positions and orientations, based on newly collected motion data [Mombaur et al., 2010], or in application to multi-agent systems [Jin and Mou, 2021]. The aim in these works is to determine, for a given dynamical process and an observed solution of the optimal trajectories, the optimization criterion that has produced the solution, and this, for example, by inferring the parameters that define the cost function [Zhang et al., 2019; Zhang, 2019]. Recent research involves not only the learning of the cost but also the identification of the state and input constraints that are part of the optimal control problem [Menner et al., 2021].

3.2.4   Limitations and remedies

- The generalization to disturbance attenuation problems in [Freeman and Kokotovic, 1996], although considering general non-linear dynamics, does not take the disturbance into account in the integrand of the cost to minimize. Oftentimes, the explicit expression of the cost hard to guess, where the dependence on system parameters and control gains is not visible. This can be remedied by compromising the generality of both system dynamics and cost functionals, e.g., by opting for input-affine dynamics with a cost that is quadratic in input and disturbance. This leads to an explicit expression for the cost, in the disturbed case, that can be interpreted and implemented directly. This will be discussed in Paper III.

- In networked settings, inverse optimal control makes optimal feedback solutions more intuitive and accessible, i.e., without computational burden, and endows control synthesis with topological structure. The structure of the controller descends from the gradient of the control Lyapunov function, that results, in many cases, in *a distributed* control law. This allows for a feasible control implementation. Despite this important aspect of inverse optimal control, it has not been highlighted in the literature. Our work in Papers III and IV aims to bridge this gap.

We also refer the reader to Sections 4.3 and 4.4 of this thesis stating our contributions of Papers III and IV.

3.3   Stability and control in power systems

3.3.1   Modeling and control of multi-machine systems

Multi-machine models are obtained after a series of restrictive assumptions on the system at hand. As in [Kundur et al., 1994; Sauer et al., 2017], prevalent modeling assumptions relate to the operation in *quasi-stationary* mode, i.e., around a given steady state. The transmission lines are modeled as impedances and the loads are either modeled as impedances or constant current and power sources. After Kron reduction [Dörfler and Bullo, 2012a], the electrical network is represented only by generators interconnected via transmission lines with negligible conductances. In most of the cases, the mathematical model obtained from these procedures, can be cast as first- or second-order coupled oscillator dynamics. It is fundamentally instructive to understand the transient stability of multi-machines by inferring results from the accumulated knowledge of synchronization of coupled oscillators in physics and control engineering. This seems to give satisfactory and intuitive answers for multi-machines systems, e.g., under the assumption of highly damped generators [Dörfler and Bullo, 2012b] and purely inductive (lossless) lines [Pai, 1981; Kundur et al., 1994].

As soon as we stray away from these special assumptions in cases, where, e.g., due to common disturbances in the grid, power systems are operated far from steady state conditions and the transmission lines are lossy (with non trivial conductance), a myriad of challenges start to surface in the stability analysis of multi-machines. In real world scenarios, large swings are common. Due to a burst of winter weather, Texas suffered an outage of two weeks and three days, in the period between February 10–27 of 2021, likely to be the worst on record in US history. More than 10 million people were without power for days [Busby et al., 2021; Najmabadi and Martinez, 2021]. Another example is when the large frequency swings became a principal means by which a blackout on 14th of August 2003 spread across a wide region in Canada and the Northeast of the United States [Kamel and Glotfelty, 2003]. This massive power outage affected approximately 50 million people in the Midwest and Northeast United States and Ontario, Canada.

Transient stability in multi-machine systems   The power system models, including linearized power system models, are only valid when the generator velocities are very close to the synchronous velocity, or in quasi-stationary mode [Schiffer et al., 2016]. Neglecting the transmission line conductances stems from the finding in [Chiang, 1989] concluding that there is no general energy function for multi-machine power systems with losses. Furthermore, it has been shown in [Ortega et al., 2005] that the obtained asymptotic stability conditions and hence the region of attraction cannot be generalized from

lossless to lossy links (with non-trivial conductance), since a different (than that of the lossless case) Lyapunov candidate needs to be designed. This emphasizes that the invalidity of certain model assumptions has significant ramifications on the study of power system stability. Despite considerable efforts made to find Lyapunov functions for power systems with lossy transmission lines [Pai and Murthy, 1973; Skar, 1980; Tsolas et al., 1985; Caliskan and Tabuada, 2014], this has remained an open problem within the power system community for decades.

It is noteworthy that numerous studies on the investigated transient stability, rely on a setup composed of a single machine connected to an infinite bus [Kundur et al., 1994; Leonov, 2006; Barabanov et al., 2016], where the angle of the infinite bus is embedded in the model representation. Extending the corresponding Lyapunov analysis to general multi-machine power systems is non-trivial. This is largely due to the inherent difference in the topology between the state space of one-dimensional angle dynamics or angle dynamics higher than two [Skar, 1980]. Considerable efforts have been invested in this generalization [Shaik et al., 2012; Caliskan and Tabuada, 2014], where the main difficulty remains in constructing error coordinates compatible with the topological space of the $n-$dimensional torus.

Depending on the initial conditions, it is possible to show almost global stability results, i.e., up to initial conditions of a measure zero set, all trajectories converge to a desired steady state [Barabanov et al., 2016; Schiffer et al., 2019; Colombino et al., 2019]. Finally, the accuracy of the Lyapunov-based methods is evaluated based on comparison of the provided region of attraction to that of other existing methods, like the closest unstable equilibrium method [Chang et al., 1995]. It can be estimated by borrowing ideas from optimization-based algorithms, as in gradient-like methods [De Persis and Monshizadeh, 2017], while also considering additional operational and reserve constraints [Vu and Turitsyn, 2015].

EXAMPLE 3.1—ROLE OF SYSTEM PARAMETERS IN GLOBAL STABILITY [LEONOV, 2006]
To illustrate the role of the system parametric choice in inducing and sustaining globally stable oscillations, let us consider the following simple yet insightful example modeling a synchronous electrical motor. Consider

$$\dot{\theta} = \eta \qquad\qquad (3.6)$$
$$\dot{\eta} = -\alpha\eta - \sin(\theta) + \gamma,$$

where $\alpha, \gamma > 0$. The stability of (3.6) can be readily studied using the direct method of Lyapunov.

Note that for $0 < \gamma < 1$, there exists a steady state θ^s (modulo 2π) to (3.6) that is asymptotically stable, where $\cos(\theta^s) > 0$ and another one

A) $\alpha > \alpha_{cri}$

B) $\alpha = \alpha_{cri}$

C) $\alpha < \alpha_{cri}$
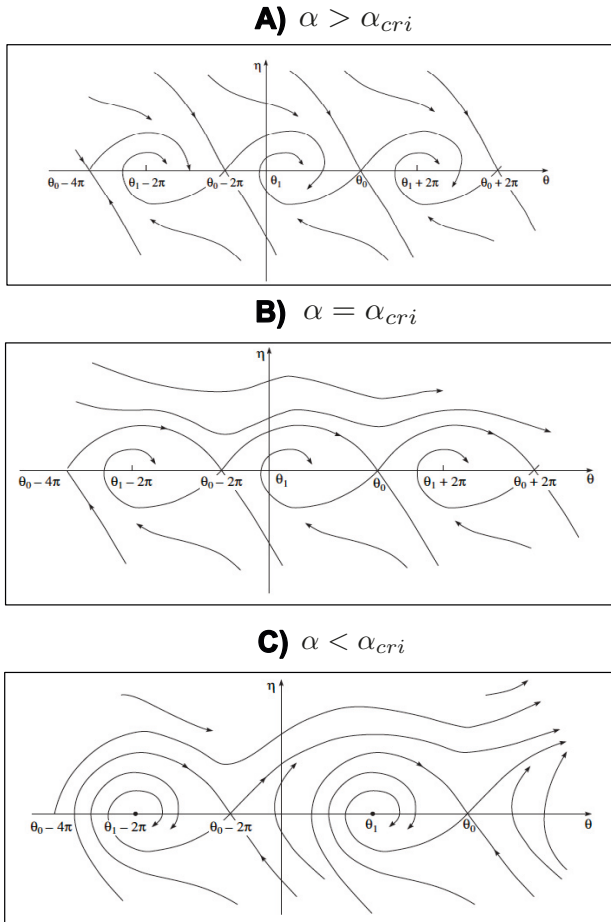
Figure 3.2   Three different arrangements of the trajectories in the phase space of system dynamics (3.6) depending on the parameter $\alpha > 0$.

θ^u (modulo 2π) that is a (unstable) saddle with $\cos(\theta^u) < 0$. Depending on the operating range of the damping α, three operating regimes that are illustrated in Fig. 3.2 may appear. First, for a sufficiently damped system $\alpha > \alpha_{cri}$, global stability is assured in **A)**, where the separatrices tend to the saddle equilibria of system θ^u and are the boundaries of the attraction domains of the asymptotically stable states θ^s. The entire phase space is decomposed into such attraction domains. Second, for a critically damped system $\alpha = \alpha_{cri}$, the attraction domains of the stable equilibrium states are also bounded by such separatrices in **B)**. However, these domains do not fill the entire phase space anymore. Third, for $\alpha < \alpha_{cri}$, **C)** depicts instability

corridors appear between the separatrices and the space is decomposed into such corridors and the region of attraction of asymptotically stable steady states. ■

Similar to the physical world, where the laws governing interactions in a set of particles are invariant with respect to static translations and rotations of the whole rigid body [Sarlette, 2009], the dynamics of the power system trajectories are invariant under a static shift in their angles, or said to possess a *rotational invariance*. The symmetry of the vector field describing the power system dynamics, indicates the existence of a continuum of steady states for the multi-machine dynamics. In particular, the rotational invariance is the topological consequence of the absence of a reference frame or absolute angle in power systems and regarded thus far as an obstacle for defining suitable error coordinates for the stability analysis. If the steady state set is a linear subspace [Schiffer et al., 2019], a common approach, to alleviate this, is to perform transformations into the quotient space either resulting from projecting into the orthogonal complement, or grounding a node [Tegling et al., 2015], where classical tools of proving stability with respect to a point can be deployed.

3.3.2 Nonlinear control of multi-converter systems

In the remainder, we go through the most important control strategies developed for frequency regulation of DC/AC converters-based generation.

Droop control Inspired by the dynamics governing synchronous machines and the analogy drawn to synchronization in coupled oscillator dynamics, droop control is the most well-established grid-forming method, first proposed by [Chandorkar et al., 1993]. It has since been extensively studied in the literature both in control theory and in practice. Droop control presumes that the inverter represented in Fig. 1.12 can be cast as controllable voltage source and thus acts on *phasor* quantities, i.e., a representation of each inverter by a (fixed) amplitude and a controllable phase angle on the circle. This presumes an operation that is close to a nominal operating point. In a network of inverters with inductive lines, the voltage magnitude is set to a constant (one per unit) and the electrical phase angle is chosen to follow the swing dynamics of synchronous machines (1.7). This translates to,

$$\dot{\theta}_i = \omega_i \tag{3.7}$$
$$M_i \dot{\omega}_i = -D_i \, \omega_i + \sum_{j \in \mathcal{N}_i} (\sin(\theta_{ij}) - \sin(\theta_{ij}^*)),$$

where $\omega_i \in \mathbb{R}$ is the frequency (with respect to a nominal value ω^* at the i−th inverter). If the set $\mathcal{N}_i$ denotes the neighborhood of the i−th inverter, then

$\theta_{ij} = \theta_i - \theta_j$ and $\theta_{ij}^* = \theta_i^* - \theta_j^*$ are the angle difference between neighboring inverters' angles and at the prescribed steady state. The coefficients $M_i > 0$ and $D_i > 0$ denote the inertia mass and damping, which are the parametric tuning gains of the $i-th$ droop control. At steady state, droop control (3.7) exhibits droop behavior as the $(P - \omega)$ law shown in Fig. 1.16. Droop control ensures system-wide synchronization and power sharing among converters as delineated in [Dörfler and Bullo, 2012b; Simpson-Porco et al., 2013].

In comparison to the conventional bulk power plants, in which the synchronous machines dominate, the generator units have either very small or no rotating mass and damping property. In this sense, the parameters $M_i, D_i > 0$ are understood as *virtual* quantities (to emphasize the fact that droop control is digitally implemented) representing inertia and damping, respectively. The question of proper tuning of these parameters has attracted attention with considerable efforts to find an optimal value for control gains e.g., by solving optimization problems that minimize important metrics of performance, for example $\mathcal{H}_2$ system norm measuring the coherency in a linear network-reduced power system model [Poolla et al., 2017]. The plug and play properties of the droop control, resulting from power to frequency droop, depicted by the nose curve in Fig. 1.16, allow, e.g., power sharing among converters [Dörfler et al., 2015] and accommodate scenarios, where the exact steady state value of the power generation is uncertain or unknown. All these advantageous properties make the control via emulation of synchronous machine amenable for large scale control of converter-based power systems and compatible with existing components of the electrical system, and thereby an attractive solution for distributed renewable energy generation.

The dynamics of synchronous machines remain a source of inspiration for a multitude of other converter control strategies that mimic their behavior, such as virtual synchronous machines [Bevrani et al., 2014] and synchroverters [Zhong and Weiss, 2010]. One particular controller that relies on *exact* model matching of high-order dynamics of three-phase synchronous machines with three-phase balanced and averaged DC/AC converters derived from first-order principles (with dynamics following the diagram depicted in Fig. 1.12) is the *matching control* introduced in [Jouini et al., 2016; Jouini, 2016]. The particularity of this controller relies on easily measured DC-side voltage, and representing an indicator of power imbalance in the grid *without* prior assumptions on quasi-stationary steady state and the operation on phasor quantities. A study of the properties of the matching control will be discussed in this thesis.

Virtual oscillator control   A control strategy that attempts to overcome the restrictive assumptions of droop control (quasi-stationary steady state, operation with phasor quantities), is the *virtual oscillator control* (VOC) which is

an electrical realization of Van der Pol Oscillator [Khalil, 2002]. The virtual oscillator controller emulates the dynamics of nonlinear oscillators and globally stabilizes arbitrary initial conditions to a sinusoidal steady state. It can be implemented on a digital micro-controller, while acting on the converter's input. The Van der Pol oscillator is composed of a parallel RLC circuit and a nonlinear voltage-dependent current source. Leveraging Kirchoff's circuit equations, the dynamics of the oscillator can be written as,

$$L \frac{\mathrm{d}i_L}{\mathrm{d}t} = v, \qquad\qquad\qquad (3.8)$$

$$C \frac{\mathrm{d}v}{\mathrm{d}t} = \sigma v - k v^3 - \frac{v}{R_{voc}} - i_L + \epsilon\, u(t),$$

where v denotes the converter terminal voltage, $u(t)$ is the current input to the Van der Pol oscillator and k, σ, ϵ are positive constants. The resistor $R_{voc} > 0$, is set in parallel with the inductance $L > 0$ and the capacitor $C > 0$, where i_L is the current flowing through the inductance. Even though virtual oscillator control has provable droop properties [Sinha et al., 2015], the control gains are hard to tune due to a lack of physical intuition on how to choose their values. It was also not possible to track active and reactive power reference in the original formulation of VOC, see [Johnson et al., 2013].

These limitations have motivated a variant of VOC suggested in [Colombino et al., 2019] that allows active and reactive power to be dispatched, hence the name *dispatchable Virtual Oscillator Control* (d-VOC). The d-VOC is a combination of a synchronizing feedback term, together with a decentralized magnitude control law and allows for global stabilization of the angles and voltage magnitudes at their desired values, corresponding to a pre-specified solution of the AC power-flow equations. The controller exhibits a droop behavior around the standard operating point, which makes it backward compatible with the existing power system operation.

Passivity-based control   Other converter control strategies rely on energy-based modeling and control [Schaft, 2000; Schaft and Jeltsema, 2014] descending from the theory of passivity and the observation that a typical power network dynamics can be formulated as a port-Hamiltonian system [Shaik et al., 2012; Schiffer et al., 2016] and is thus a passive system. Namely, the main idea is that passive interconnections *preserve* and passive damping *dissipates* energy and thus shapes the total system energy. This has led to the development of the theory of interconnection and damping assignment [Ortega et al., 2002] and passivity-based control [Zonetti, 2016; Zonetti et al., 2021], applied to the control of converters in power systems.

Inverse optimal control for power systems   Even though direct optimal control and dynamic programming have been widely used for optimization in

power networks [Lu et al., 2008; Sanchez-Sanchez et al., 2019], inverse optimal control formulations have gained only limited attention in the DC/AC converter control literature. The applications of inverse optimal control in converter control are mainly concerned with the voltage regulation of DC/DC boost power converters [Vega and Alzate, 2014; Liu et al., 2014; Zhang et al., 2013; Ornelas-Tellez et al., 2012; Pahlevaninezhad et al., 2012] and other electrical components such as an induction wind generator [Ruiz-Cruz et al., 2018].

3.3.3   Limitations and remedies

- The frequency/angle controllers proposed in the literature, rely mainly only AC measurements to achieve synchronization in converter-based generation, assuming full control of the DC side [Bevrani et al., 2014], which is often an unrealistic assumption. Therefore, DC-side modeling is often neglected and many of the proposed controllers miss out on the utility of DC capacitor voltage for converter control. On the other hand, DC-side circuitry reflects the power imbalance in the grid through the DC-side capacitor voltage. This motivates *the matching control*, a novel controller that uses DC-side measurements to achieve frequency synchronization in converter-based generation that will be discussed in Papers I and II.

- Droop control assumes quasi-stationarity, which is a strong assumption, given the fluctuating nature of the electrical grid, where the operation is commonly far away from a desired steady state. Moreover, virtual oscillator control is hard to tune with many parameters affecting the control performance and its droop behavior, and is not straightforward how to assign dispatched active and reactive power set-points. This motivates the design of DC/AC converter controls that overcome the limitations of being at the vicinity of some steady states and that are easy to tune. This is achieved by the matching control that will be discussed in Papers I and II.

- As conveyed by the literature review, inverse optimal control has not been applied to control of DC/AC converters. Given the numerous advantages of inverse optimal control, this motivates the novelty of our work discussed in Papers III and IV.

We also refer the reader to Chapter 4 of this thesis stating our contributions of all Papers.

4

Contributions

In this chapter, we review the content of this thesis work by highlighting the contributions and novelty of each of the selected four papers.

4.1 Paper I: Grid-forming control for power converters based on matching of synchronous machines

Summary   With preliminary results in [Jouini et al., 2016; Jouini, 2016], we consider in [Arghir et al., 2018] the problem of grid-forming control of power converters in low-inertia systems. We start from an averaged and balanced DC/AC power converter in Fig. 1.12 and a synchronous machine model that retain basic first-order model principles and derive a grid-forming controller that we term *the matching controller*. This is achieved by coupling the DC and AC circuits that measure the DC bus voltage, which is viewed as an indicator of frequency imbalance. We transform the dynamics into the rotating coordinates to decouple the dynamics of the augmented state from the DC/AC converter variables, analyze the system stability by means of the Lyapunov method and find sufficient conditions for strict passivity with respect to incremented DC and AC ports, global asymptotic stability as well as droop behavior in steady-state. Furthermore, we establish cross-links to recently adopted control approaches (virtual oscillator control, passivity-based control). We analyze and implement outer control loops fulfilling AC frequency regulation via PID control. We ensure AC voltage amplitude tracking by means of asymptotic disturbance decoupling via feed-forward and passive PI control under the assumption relying on available measurements of the load current. To alleviate this realizable yet impeding assumption, we also implement a droop controller that trades off between power output and amplitude of the AC filter capacitor. Stability analysis is then conducted for each control approach using Lyapunov theory. Our simulations are presented for demonstration in a single converter as well as a two-converter case study.
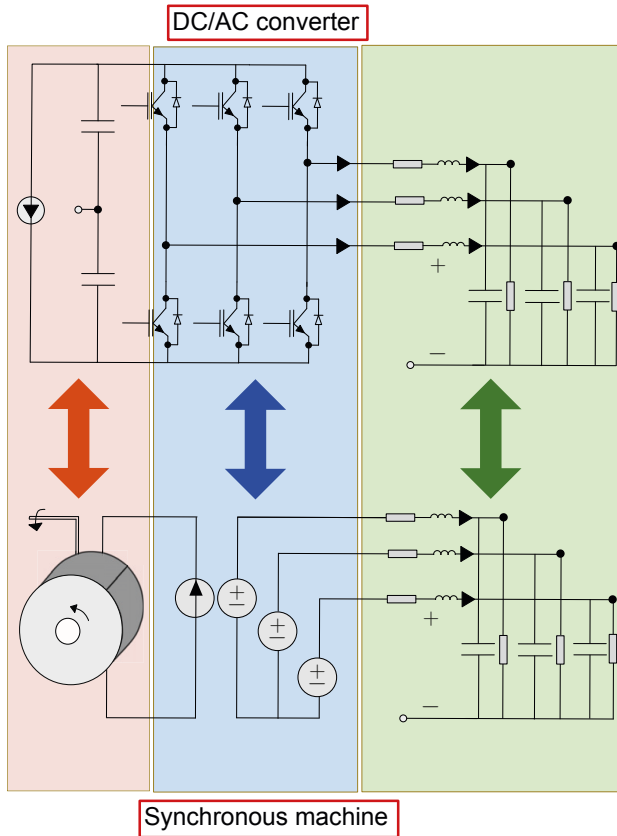
Figure 4.1 Structural similarities between a three-phase high-order a DC/AC converter (top) and synchronous machine (bottom) model. The colors red, blue and green highlight the analogies between different components of the machine and converter; DC circuit and the machine's rotor, the switching block and back electromotive force voltage as well as the machine's and converter's output AC filters.

Contribution 1: matching control design   Our fully decentralized control approach is inspired by identifying the structural similarities between the two models depicted in Fig. 4.1 and matching these via state feedback control. In other words, through a proper choice of the input, we explicitly match the two models, so that they become structurally equivalent. This is the motivation behind the name, *matching control*. Our control strategy can be allied to a multitude of ideas rooted in nonlinear control, e.g., the matching of general nonlinear systems via state feedback [Di Benedetto and Isidori, 1986]. The controller is a nonlinear function representing an integrator that
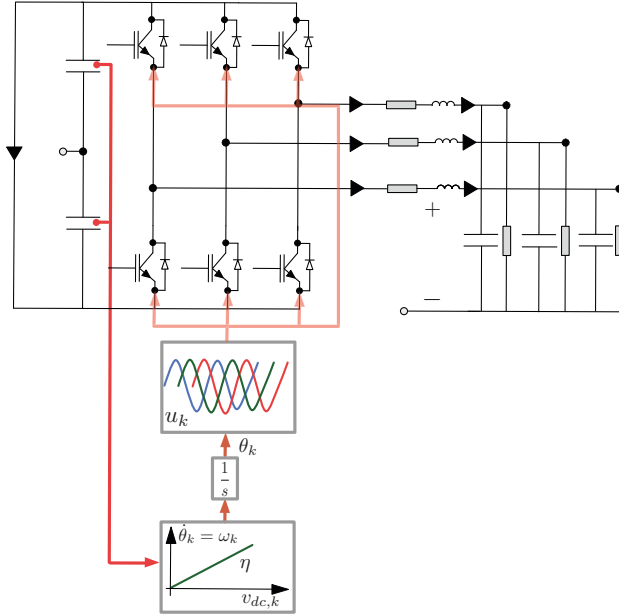
Figure 4.2 A diagram illustrating the basic idea of the matching control. The matching control acts on the modulation signal considered as the main input to the converter's switching block.

uses the measurement of the DC-side voltage. It can be understood as an embedding of a virtual angle in $\mathbb{R}^2$, whose dynamics are linearly dependent on the DC voltage and fed as input to the DC/AC converter. The key idea of the matching control is summarized in Fig. 4.2.

Contribution 2: closed-loop stability Our stability analysis relies eminently on the analogy drawn between DC/AC converter model and synchronous machines. The Lyapunov method adopted in [Caliskan and Tabuada, 2014] for a single machine infinite bus scenario is applied to our closed-loop system and extended to incremental passivity as a key requirement for stability under interconnection. This allows to derive a sufficient condition for incremental passivity and global stability upon transformation into a rotating coordinate frame. Our stability condition depends on the steady-state under consideration and converter parameters and can be satisfied upon appropriate tuning of the control gains. It asks for sufficient damping on the DC and AC sides of the converter.

Contribution 3: outer loops for frequency and voltage regulation   Additionally, we extend the matching control with outer loops that strengthen the coupling between DC and AC components, while preserving passivity. We deploy a passivity-based control approach, which lends itself useful for frequency and voltage regulation inspired by ideas from [Khalil, 2002; Zonetti et al., 2014]. For frequency regulation, we increment the matching control with a PID controller by considering the DC current source as an input. We later prove that the proposed control scheme achieves exact regulation of the frequency to a given prescribed value with *zero* error at steady-state. Additionally, we exploit the degree of freedom in the modulation (i.e., the main input to the converter) amplitude to propose three control schemes that stabilize the output voltage amplitude to a constant value.

Under the assumption on load current measurement, a feed-forward controller is first proposed for amplitude regulation and proven to converge to the desired value at steady-state, if the admissible load current is below a certain bound. Second, PI-passivity based control is proposed which designs a passive output to ensure a strict decrease of the storage function to a well-defined steady-state value. The incremented converter model is proven to guarantee exact tracking of the desired reference. The two previously discussed controllers achieve exact tracking but under the assumption of exact knowledge of the disturbance and the admission of integral action. Even though, we consider a single converter setup, integral action can be detrimental in a network setting due to conflicting objectives between the controllers. This motivates our third approach based on droop control. Similar to voltage droop in resistive power networks, we introduce a droop behavior between converter output power and the modulation magnitude. This results in a proportional action that does not necessarily achieve the desired steady-state but allows for better coordination between the converters in view of a network setup. The proposed control strategies for frequency and voltage regulation are summarized in Fig. 4.3.

4.2   Paper II: Frequency synchronization of a high-order multi-converter system

Summary   This work generalizes the transient stability results of a single converter in closed-loop with the matching control in Paper I into a more fundamental analysis of a network consisting of DC/AC converters. The dynamics of each converter are defined on a high-order manifold. Based on the rotational invariance of the resulting vector field, we first identify the steady-state set, whose feasibility defines a mapping from the steady-state angles into DC power input as a function of the network topology and converter parameters. Second, we study local asymptotic stability with respect to the
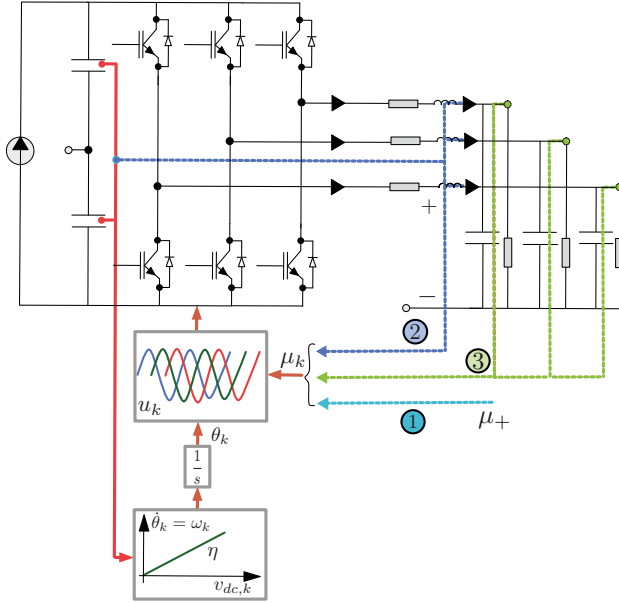
Figure 4.3 Outer loops for frequency and voltage regulation. The control strategy ① relies on feed-forward control, assuming full knowledge of the disturbance, ② is derived from passivity-based control using DC voltage and AC current measurements and ③ is based on droop control by measuring the power output.

steady-state set by deploying the center manifold theorem. This is devised under the premise that the Jacobian of the linearized dynamics of the multi-converter system has only one eigenvalue at zero and the real-parts of all remaining eigenvalues are in the open-left half-plane. We provide an example approach on how to find a sufficient condition that satisfies this assumption and contextualize our finding by providing intuitive physical interpretations. We validate our results in simulations on a three-converter system.

Contribution 1: steady-state characterization By considering high-order system dynamics, we characterize the steady-state set of the multi-sourced converter system. The vector field has a rotational invariance, under a static shift of all angles by the same value and the rotation of AC signals. This rotational invariance is preserved at steady-state and as a consequence the steady-state set defines a continuum of equilibria. Its feasibility is determined by a mapping from the nominal steady-state angles, network topology and converter parameters into the DC power inputs to the converters. The steady-state set is distinguished by a synchronous frequency at steady-state
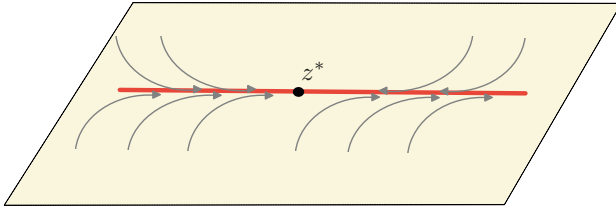
Figure 4.4   Evolution of the linearized trajectories of the multi-converter system on the tangent space at z^* represented in Fig. 4.5 under the Jacobian eigenvalue condition, namely that only one eigenvalue is at zero (associated with a zero eigenspace direction) and the real-parts of all other eigenvalues are in the open-left half-plane.

corresponding to a nominal value, stationary angles and stationary AC quantities (inductor current, capacitor voltage, line current). This is shown after transformation into $dq-$frame with an angle rotating at nominal frequency.

Contribution 2: local synchronization using center manifold theory   We study local asymptotic stability of the characterized steady-state set by applying the center manifold theory. In other words, in a neighborhood of the steady-state set, we seek to find (mild) assumptions, under which asymptotic stability of the nominal steady-state can be guaranteed. For this, we depart from the following eigenvalue condition. Given a matrix with one zero eigenvalue, the goal is to guarantee that the remainder of the modes are confined to the open-left half-plane. As a consequence, the one-dimensional zero eigenspace is asymptotically stable. A summary of the eigenvalue condition is depicted in Fig. 4.4. We provide *one* approach on how to satisfy this condition.

Under the assumption of the system Jacobian's eigenvalues, we decompose the nonlinear dynamics into two subsystems, whose dynamics are zero and Hurwitz respectively, we can apply the center manifold theory, where the reduction principle revolves around the following idea [Wiggins, 1990, Ch.18]. By bringing the multi-converter system into the decomposed dynamical form, we prove local asymptotic stability of the steady-state. Physically, our sufficient stability conditions specify an upper bound on the power factor at each converter that can be satisfied with sufficient AC damping as well as a lower bound on the DC damping gain, which makes them explicit and feasible to verify individually at each converter. An overall summary of the contributions is found in Fig. 4.5.
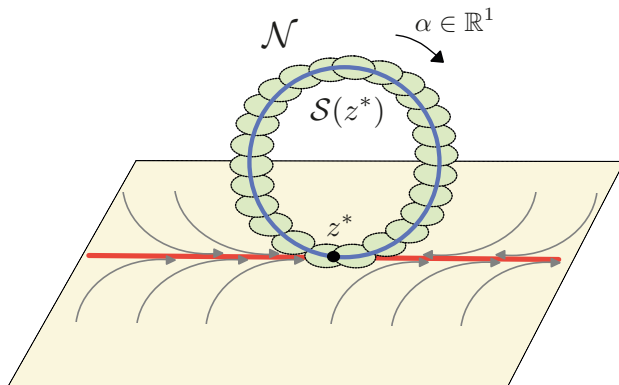
Figure 4.5 A summary of local synchronization of the multi-converter system. The blue circle represents the steady-state set $\mathcal{S}(z^*)$, resulting from a static shift $\alpha \in \mathbb{R}$ of all converters' angles, and the green area depicts a neighborhood $\mathcal{N}$ thereof. Trajectories initialized on $\mathcal{N}$, converge to a point on the steady-state set $\mathcal{S}(z^*)$.

4.3 Paper III: On cost design in applications of optimal control

Summary In this work, we extend inverse optimal control to a setting, where the nonlinear cost functionals together with the system dynamics are subject to bounded disturbances. We illustrate the usefulness of inverse optimal control in networked settings for designing controllers with topological structure, through diverse examples in linear and nonlinear systems. We demonstrate the utility of control synthesis via inverse optimal control to find a distributed and thus feasible optimal controller for coupled oscillator dynamics. We validate our results in simulations on a three-oscillator system. A summary of the ideas presented in this paper is depicted in Fig. 4.6.

Contribution 1: cost functional with a disturbance term Our min-max problem formulation is an extension of the min-max formulation presented in [Freeman and Kokotovic, 1996] to a class of cost functional, where the disturbance enters through a quadratic term in the cost subject to input-affine system dynamics. This allows for the explicit calculation of the worst-case disturbance and thus the explicit derivation of a cost functional *a posterior*.

Contribution 2: tuning aspect in inverse optimal control Our work puts emphasis on the tuning aspect of inverse optimal stabilizing controllers along the lines of other works [Haddad and Chellaboina, 2011; Sepulchre et al., 2012]. We illustrate through different remarks, examples, and also numerically, that the input gain matrix represents a tuning knob that can be used to
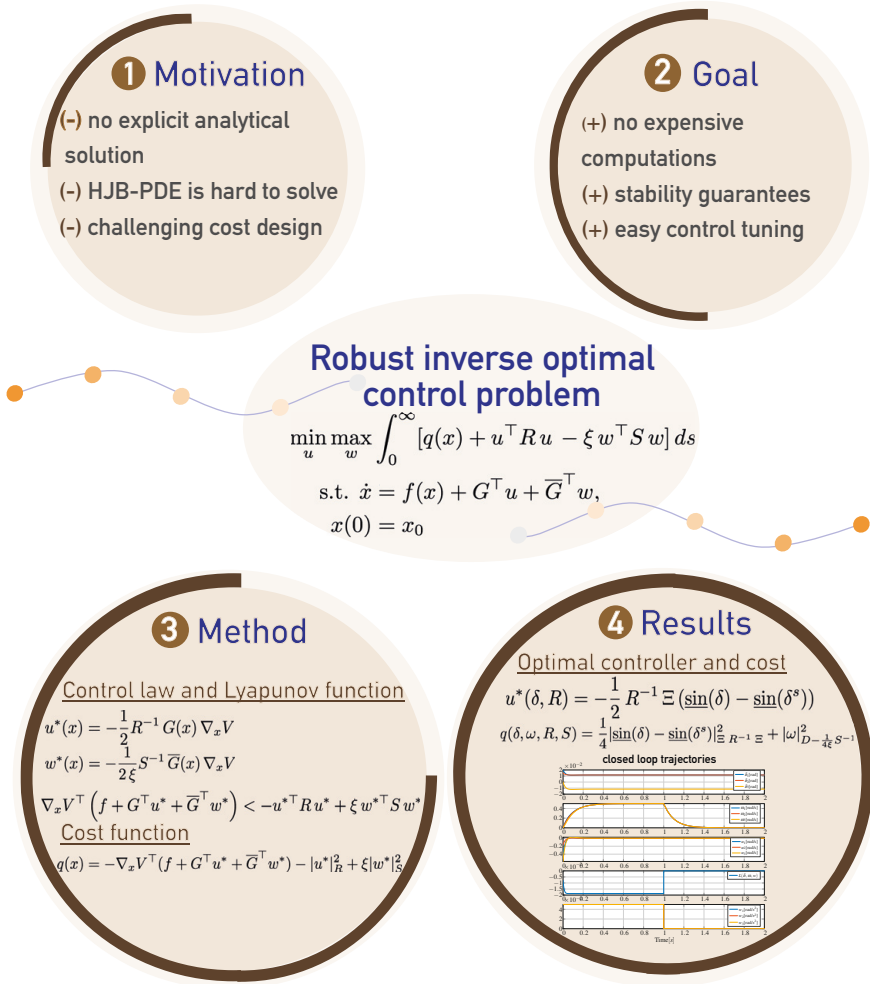
Figure 4.6   Summary of the content of Paper III

improve the error decay rate or minimize the control effort, while keeping the same value function. This analogously applies for the robust setting, where the disturbance input gain matrix is an tuned to penalize the disturbance deviations.

Contribution 3: robust inverse angle stabilization in coupled oscillators   We apply inverse optimal control in networked systems to design a controller with

topological structure, e.g., a distributed controller. The resulting network structure of the controller descends from the gradient of the chosen control Lyapunov function and is useful for feasible implementations.

Our main application of inverse optimal control is intended for angle stabilization in coupled oscillators. The goal is to improve the error decay rate of the angle transients, while converging to an induced steady-state in second-order coupled oscillators, that can represent, e.g., droop-controlled inverters, and this, by using direct angle control as in [Zhang and Xie, 2015; Zhang and Xie, 2016; Arghir and Dörfler, 2019; Tayyebi et al., 2020]. We take into account the generation and the grid-side volatility represented by a disturbance that acts on the frequency dynamics. Under mild assumptions on the neighboring steady-state angle differences, we arrive at a distributed control law, that stabilizes the angles at an induced steady-state. A decrease in the input gain matrix improves the error decay rate in angle transients significantly, and the convergence to the induced steady-state is faster, which corroborates our results.

4.4   Paper IV: Inverse optimal control for angle stabilization in converter-based generation

Summary   We demonstrate the usefulness of inverse optimal control for power networks. We suggest an optimal control law that stabilizes the phase angles of voltage source controllers converters to an induced steady-state, characterized by a zero frequency error. The control law is inverse optimal stabilizing for the converter dynamics, i.e., it is the unique solution of an optimal control problem, where the cost is defined *a posteriori*. We show that the implementation of the angular droop control is feasible. In fact, it is possible to be implemented in a decentralized manner using only power measurements. We showcase our results on simulations of a network of high-order DC/AC converters, each represented by the model from Paper I. A summary of the ideas presented in this paper are depicted in Fig. 4.7.

Contribution 1: inverse optimal control for power networks   To the best of our knowledge, there has not been research linking inverse optimal control to the control of inverters in power systems and thus there is room for contributions in this direction. The objective is to design an inverse optimally stabilizing controller design (in the sense of Definition 3.1), that utilizes the grid measurement, while minimizing a performance metric that meets the requirements of a desired power system operation.

Contribution 2: angle stabilization with zero frequency error   The angular droop control linearly trades active power with angle deviation at steady-

Figure 4.7 Summary of the content of Paper IV
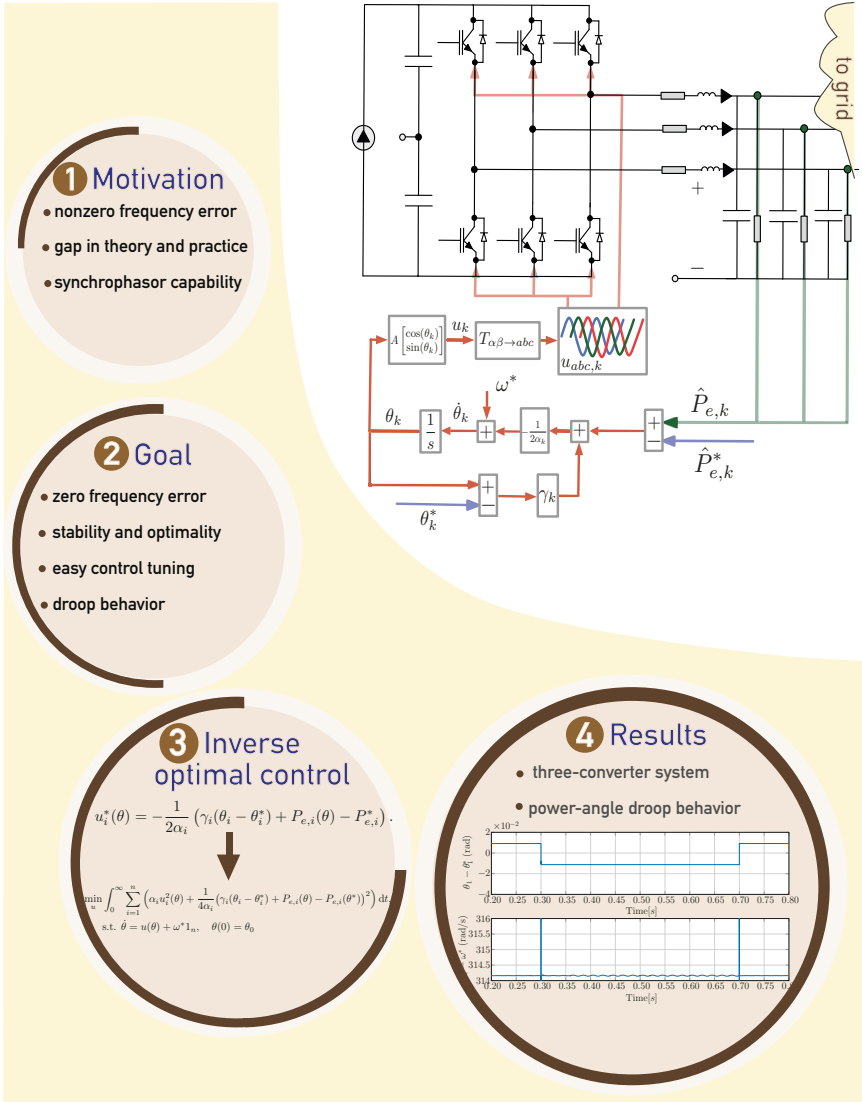
state and thus achieves exact frequency regulation with no stringent separation between primary and secondary frequency control. This implies that the

controller compresses the time scale separation, commonly assumed in conventional, machine-dominated power systems. Therefore, we substitute two control layers with a single one that achieves the same objective of restoring the system frequency to nominal. Thereby, the converter phase angles are stabilized to an induced steady-state, where the convergence rate is traded with the allowed control effort.

Contribution 3: bridge a gap between control and power system community
We reversely engineer the angular droop control suggested in [Zhang and Xie, 2015; Zhang and Xie, 2016] and show that this idea can be backed up by inverse optimal control theory. In an attempt to bridge a gap between theory and practice, our work explains the benefits of angular droop control from a system-theoretic point of view by stabilizing the converter dynamics, while guaranteeing optimality, and demonstrates its effectiveness on realistic simulation scenarios.

4.5   Statement of contributions

This thesis was drafted and written by Taouba Jouini at the Department of Automatic Control, LTH - Lund University, during the time period from August 2019 to January 2022 as a partial fulfillment of the requirements for obtaining a PhD degree. The first part of the results presented in this thesis were conducted during the stay of Taouba Jouini as a research assistant at the Laboratory of Automatic Control (IfA), ETH - Zürich from December 2016 to January 2019 under the supervision of Prof. Florian Dörfler. The second part of the results were obtained under the supervision of Prof. Anders Rantzer and Dr. Emma Tegling at the Department of Automatic Control at LTH, Lund University. The thesis includes the following four main papers.

Paper I

Arghir, C., T. Jouini, and F. Dörfler (2018). "Grid-forming control for power converters based on matching of synchronous machines". *Automatica* **95**, pp. 273–282. DOI: `10.1016/j.automatica.2018.05.037`.

The first two authors contributed equally. This paper entails partial results from the second author's master's thesis. The matching control had been suggested by the co-supervisor Catalin Arghir. Almost all ideas are contributions resulting from discussions between the first and second author and have been derived under the supervision of the third author.

Paper II

Jouini, T. and Z. Sun (2021). "Frequency synchronization of a high-order multi-converter system". *ArXiv:2007.14064, to appear in IEEE Transactions on Control of Network Systems.* DOI: `10.1109/TCNS.2021.3128493`.

The ideas of this work build on the results obtained in the following paper:

Jouini, T. and F. Dörfler (2019). "Local synchronization of two DC/AC converters via matching control". In: *2019 18th European Control Conference (ECC)*. IEEE, pp. 2996–3001. DOI: `10.23919/ECC.2019.8795908`.

The first author came up with most of the extensions and discussed these with the second author. Prof. Anders Rantzer suggested the center manifold theorem to prove local asymptotic stability. The rest is entirely the first author's contribution. The paper was written by the first and revised by the second author.

Paper III

Jouini, T. and A. Rantzer (2021). "On cost design in applications of optimal control". *IEEE Control Systems Letters*, pp. 1–1. DOI: `10.1109/LCSYS.2021.3079642`.

The first author came up with the idea of cost design in inverse optimal control. The second author pointed out the powerful potential of this idea. The first author provided (numerical) examples and discussed these with the second author. The paper was first written by the first and then revised by the second author.

Paper IV

Jouini, T., A. Rantzer, and E. Tegling (2021). "Inverse optimal control for angle stabilization in converter-based generation". *ArXiv:2101.11141, submitted to American Control Conference (ACC).*

The third author drew the attention of the first author to existing angular droop control law in the power system literature. The first author suggested to find a connection to optimal control and discussed these with the second and third authors. The paper was written by the first and then revised by the second and third authors.

Other publications   In addition to the publications included in this thesis, the author has been part of the following publications that are not included.

Jouini, T. and F. Dörfler (2019). "Local synchronization of two DC/AC converters via matching control". In: *2019 18th European Control Conference (ECC)*. IEEE, pp. 2996–3001. DOI: `10.23919/ECC.2019.8795908`.

Jouini, T. and Z. Sun (2020). "Fully decentralized conditions for local convergence of DC/AC converter network based on matching control". In: *2020 59th IEEE Conference on Decision and Control (CDC)*, pp. 836–841. DOI: `10.1109/CDC42340.2020.9304344`.

Jouini, T. and Z. Sun (2020). "Performance analysis and optimization of power systems with spatially correlated noise". *IEEE Control Systems Letters* **5**:1, pp. 361–366. DOI: `10.1109/LCSYS.2020.3002219`.

Jouini, T. and Z. Sun (2021). "Distributed learning for optimal allocation of synchronous and converter-based generation". In: *2021 29th Mediterranean Conference on Control and Automation (MED)*. IEEE, pp. 386–391.

Jouini, T., U. Markovic, and D. Gross (2018). "WP3-Control and Operation of a Grid with 100% converter-based devices". *Final deliverables of Migrate project.* URL: `https://www.h2020-migrate.eu`.

Paper I

Grid-forming control for power converters based on matching of synchronous machines

Catalin Arghir   Taouba Jouini   Florian Dörfler

Abstract

We consider the problem of grid-forming control of power converters in low-inertia power systems. Starting from an average-switch three-phase power converter model, we draw parallels to a synchronous machine (SM) model and propose a novel converter control strategy which dwells upon the main characteristic of a SM: the presence of an internal rotating magnetic field. In particular, we augment the converter system with a virtual oscillator whose frequency is driven by the DC-side voltage measurement and which sets the converter pulse-width-modulation signal, thereby achieving exact matching between the converter in closed-loop and the SM dynamics. We then provide a sufficient condition asserting existence, uniqueness, and global asymptotic stability of a shifted equilibrium, all in a rotating coordinate frame attached to the virtual oscillator angle. By actuating the DC-side input of the converter we are able to enforce this condition and provide additional inertia and damping. In this framework, we illustrate strict incremental passivity, droop, and power-sharing properties which are compatible with conventional power system operation requirements.We subsequently adopt disturbance-decoupling and droop techniques to design additional control loops that regulate the DC-side voltage, as well as AC-side frequency and amplitude, while in the end evaluating them with numerical experiments.

1. Introduction

The electrical power system is currently undergoing significant changes in its structure and mode of operation due to a major shift in generation technology from synchronous machines (SMs) to power electronics-based DC/AC converters, or simply *inverters*. As opposed to SMs, which store kinetic energy in their rotor moment of inertia, these devices are on the one hand designed with little or no built-in energy storage capacity, while on the other hand actuated at much faster time scales. SMs with their large rotational inertia, self-synchronizing physics, and associated controls, act as safeguards against faults and disturbances – all of which are absent in *low-inertia systems* with a dominant share of distributed and variable renewable sources interfaced through inverters. Hence, the proper control of inverters is regarded as one of the key challenges when massively integrating renewable energy sources [Denis et al., 2015; Kroposki et al., 2017; Taylor et al., 2016].

Converter control strategies are classified into two groups. While there is no universally accepted definition, inverters are usually termed *grid-following* if their controls are designed for a stiff grid, and they deliver power at the stiff AC grid frequency usually measured through a phase-locked loop (PLL). Otherwise, these converters are termed *grid-forming* when they are assigned to interact with a non-stiff grid similarly as SMs do by balancing kinetic and electrical energy in such a way that a frequency consensus is achieved. A low-inertia system cannot be operated with only grid-following units. With this in mind, we review the literature on grid-forming control.

The inherent self-synchronizing property of SMs has inspired controllers such as *droop* and *virtual synchronous machines* (VSMs) [Chen et al., 2011; D'Arco and Suul, 2013; Karapanos et al., 2011; Torres and Lopes, 2013; Van Wesenbeeck et al., 2009; Zhong and Weiss, 2010]. These controllers are designed to emulate the behavior of SM models of various degrees of fidelity and are based on measurements of AC quantities such as injected power, frequency, and amplitude. For example, *inverse droop* and related VSM control strategies measure the AC frequency through a PLL and accordingly adapt the converter power injection based on a simple SM swing equation model. The latter is encoded in a micro-controller whose outputs are tracked by the converter modulation signal typically through a cascaded control architecture. For these, and other VSM implementations, the time delays resulting from measuring and processing of AC quantities render control often ineffective [Bevrani et al., 2014; Denis et al., 2015; ENTSO-E, 2016].

Droop control can also be implemented by measuring the injected power and by adapting accordingly the converter frequency [Guerrero et al., 2012], but its applicability is limited to inductive grids and with a possibly narrow region of attraction [De Persis and Monshizadeh, 2017; Dörfler et al., 2015; Sinha et al., 2015b]. Additionally, the inverter's DC-side storage element is

often not included in the model, nor in the control design, which, in our view, misses a key insight: namely, the DC bus voltage can reflect the power imbalance and serve as valuable feedback signal. Finally, alternative control strategies employ *nonlinear virtual oscillators* fed by AC current measurements [Colombino et al., 2017; Johnson et al., 2014; Sinha et al., 2015a]. For these strategies global stability certificates are known, but their design and analysis is quite involved (as a result, no controllers for regulation of amplitudes and frequency are known thus far) and their compatibility with SMs is unclear to this date. Another set of literature relevant to our methodology is *passivity-based control* (PBC) [Schaft, 2000] and *interconnection and damping assignment* (IDA) [Ortega and Garcia-Canseco, 2004]. Their application to DC/DC converters [Escobar et al., 1999; Zonetti et al., 2014], AC/DC converters [Perez et al., 2004], and power systems in general [Caliskan and Tabuada, 2014; Fiaz et al., 2013] suggests a physically insightful analysis based on shaping the energy and dissipation functions. As we will further see, our analysis relies also on a characterization of the power system steady-state specification [Groß et al., 2016; Groß and Dörfler, 2017] which restricts the class of admissible controllers.

Our main contributions are three-fold. First, we propose a novel grid-forming control strategy that matches the electromechanical energy exchange pattern in SMs. This is achieved by augmenting the converter dynamics with an internal model of a harmonic oscillator whose frequency tracks the value of the DC-side voltage measurement. This voltage-driven oscillator is then assigned to drive the converter's pulse-width-modulation cycle, thereby assuring that the closed-loop converter dynamics exactly *match* the SM dynamics, whereas the DC voltage serves as the key control and imbalance signal akin to the SM's angular velocity [Jouini et al., 2016]. Based on a Lyapunov approach we provide a sufficient condition certifying existence, uniqueness, and global asymptotic stability of driven equilibria, in a coordinate frame attached to the virtual oscillator angle. By actuating the DC-side input current we are able to satisfy this condition. We also preserve strict incremental passivity, droop, and power-sharing properties of the closed-loop system. Our approach is grounded in foundational control methods, while being systematically extensible to PBC and IDA designs. Additionally, the key DC voltage signal is readily available while all other approaches rely on extensive processing of the AC measurements. Second, building on the proposed matching controller, we further design overarching control loops that regulate the DC voltage, AC frequency, and AC amplitude. This is done by pursuing an approach based on disturbance decoupling, which performs asymptotic output voltage amplitude tracking, while rejecting the load current seen as a measurable disturbance. We then suggest extensions based on employing PBC and voltage-power droop control strategies, which have been previously investigated in various settings. Third and finally, we evaluate the performance

and robustness of our designs by comparing them in numerical experiments of single and multi-converter scenarios.

The remainder of the paper is organized as follows. Section 2 introduces the models and the control objectives. Section 3 proposes the matching controller and derives its properties. Section 4 designs the regulation and disturbance-decoupling controllers. Section 5 presents a numerical case study, and Section 6 concludes the paper.

2. The three-phase converter model, synchronous machine model, & their analogies

2.1 Preliminaries and coordinate transformations

In this paper

$$\boldsymbol{I} = \begin{bmatrix} 1 & 0 \\ 0 & 1 \end{bmatrix},$$

denotes the identity and

$$\boldsymbol{J} = \begin{bmatrix} 0 & -1 \\ 1 & 0 \end{bmatrix},$$

denotes the rotation by $\pi/2$ in $\mathbb{R}^2$, while

$$\mathbf{e}_2 = \begin{bmatrix} 0 \\ 1 \end{bmatrix},$$

is a natural basis vector in $\mathbb{R}^2$. We denote by $\|\cdot\|$ the standard Euclidean norm for vectors or the induced norm for matrices.

The three-phase AC system is assumed to be symmetrical namely all passive elements have equal values for each phase element. Due to this symmetry, any three-phase quantity $z_{abc} \in \mathbb{R}^3$ is assumed to satisfy

$$\begin{bmatrix} 1 & 1 & 1 \end{bmatrix} z_{abc} = 0;$$

see Remark 1. We consider a coordinate transformation to distinguish between the component along the span of the vector

$$\begin{bmatrix} 1 & 1 & 1 \end{bmatrix}^\top \in \mathbb{R}^3,$$

which we denote by $z_\gamma \in \mathbb{R}$ and the other two components $z_{\alpha\beta} \in \mathbb{R}^2$ lying on the associated orthogonal complement called the $\alpha\beta-$frame:

$$\begin{bmatrix} z_{\alpha\beta} \\ z_\gamma \end{bmatrix} = \sqrt{2/3} \begin{bmatrix} 1 & -\frac{1}{2} & -\frac{1}{2} \\ 0 & \frac{\sqrt{3}}{2} & -\frac{\sqrt{3}}{2} \\ \frac{1}{\sqrt{2}} & \frac{1}{\sqrt{2}} & \frac{1}{\sqrt{2}} \end{bmatrix} z_{abc}. \tag{1}$$
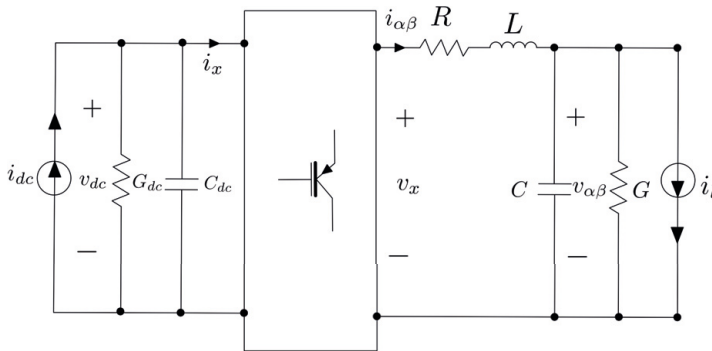
Figure 1.   Circuit diagram of a 3−phase DC/AC converter.

Given a reduced three-phase quantity $z_{\alpha\beta}$ and an angle $\theta \in \mathbb{S}^1$, we define the $dq-$coordinate transformation $(z_{\alpha\beta}, \theta) \mapsto z_{dq} \in \mathbb{R}^2$, via

$$\mathbf{R}_\theta = \begin{bmatrix} \cos(\theta) & -\sin(\theta) \\ \sin(\theta) & \cos(\theta) \end{bmatrix},$$

as,

$$z_{dq} = \mathbf{R}_\theta^\top z_{\alpha\beta}. \tag{2}$$

Consequently, we have that a sinusoidal steady state solution of the form $\dot{z}_{\alpha\beta}^\star = \omega^\star I z_{\alpha\beta}^\star$, with associated frequency $\omega^\star$, is mapped to an equilibrium $\dot{z}_{dq}^\star = 0$ in the $dq-$frame whose transformation angle satisfies $\dot{\theta}^\star = \omega^\star$. Throughout this article, a variable denoted $z_{dq}^\star$ or $z_{\alpha\beta}^\star$ is used to represent a steady state solution induced by exogenous inputs, e.g., load parameters or set-points.

2.2   Three-Phase DC/AC Converter Model

We start by reviewing the standard average-switch[1] model of a three-phase, two level, voltage source inverter in $\alpha\beta-$coordinates. See [Tabesh and Iravani, 2008] for a comprehensive study. The model is described by a continuous-time system whose main feature is the nonlinearity captured by the modulation (switching) block, as depicted in Fig. 1.

The DC circuit consists of a controllable current source $i_{dc} \in \mathbb{R}$ in parallel with a capacitance $C_{dc} > 0$ and a conductance $G_{dc} > 0$. The DC-side switching current is denoted by $i_x \in \mathbb{R}$, while $v_{dc} \in \mathbb{R}$ represents the voltage across the DC capacitance. The AC circuit contains at each phase an inductance

---

[1] For the time scales of interest, we assume a sufficiently high switching frequency that allows us to discard the PWM carrier harmonics and use continuous-time dynamics.

$L > 0$ in series with a resistance $R > 0$ connected to a shunt capacitance $C > 0$ and shunt conductance $G > 0$. Here $v_{\alpha\beta} \in \mathbb{R}^2$ denotes the AC voltage across the output capacitor.

The dissipative elements G_{dc}, G and R model the parasitic losses in the converter. Furthermore, $i_{\alpha\beta} \in \mathbb{R}^2$ denotes the AC current in the inductors and $v_x \in \mathbb{R}^2$ the average AC voltage at the switching node. The inverter model is terminated at its AC-ports with a load current i_l drawn by a weak AC grid, which will be made more specific in Assumption 1.

The switching block is defined as the average-switch model of a 6-switch 2-level inverter with an associated complementary pulse-width-modulation (PWM) carrier and a modulation signal $m_{\alpha\beta} \in \{x \in \mathbb{R}^2 : \|x\| \leq 1\}$. To preserve energy conservation, the switching block is assumed to be lossless, i.e., it satisfies the identities,

$$i_x = \frac{1}{2} m_{\alpha\beta}^\top i_{\alpha\beta} \ , \ v_x = \frac{1}{2} m_{\alpha\beta} v_{dc}.$$

By putting it all together, the inverter model can be written as the following bilinear system:

$$C_{dc}\dot{v}_{dc} = -G_{dc}v_{dc} + i_{dc} - \frac{1}{2}i_{\alpha\beta}^\top m_{\alpha\beta} \tag{3a}$$

$$L\dot{i}_{\alpha\beta} = -Ri_{\alpha\beta} - v_{\alpha\beta} + \frac{1}{2}v_{dc}m_{\alpha\beta} \tag{3b}$$

$$C\dot{v}_{\alpha\beta} = -Gv_{\alpha\beta} + i_{\alpha\beta} - i_l . \tag{3c}$$

REMARK 1—ZERO SEQUENCE

We will construct the three-phase modulation signal $m_{abc} = 0$ in such a way that $m_\gamma = 0$ which implies that $v_{x,\gamma} = 0$. For a balanced load, it also holds that $i_{l,\gamma} = 0$. We are left with the following dynamics for the $\gamma-$subsystem:

$$L\dot{i}_\gamma = -Ri_\gamma - v_\gamma \tag{4a}$$

$$C\dot{v}_\gamma = -Gv_\gamma + i_\gamma . \tag{4b}$$

Since (4) is an asymptotically stable linear system, the omission of the $\gamma-$component is well justified. ∎

2.3 Control objectives

In this section, we map out the control objectives to be achieved via the two main actuation inputs, the modulation signal $m_{\alpha\beta}$ and the DC-side current injection i_{dc}. Broadly speaking we require the following:

(i) Grid-forming: The objective of *grid-forming control* is best defined by mimicking the electromechanical interaction of a SM with the grid rather

than prescribing the converter's frequency to track the grid frequency, e.g., via a PLL. The synchronization properties of SMs rely on a particular kinetic to electrical energy exchange pattern. This can be induced in the DC/AC converter by exactly matching the SM's dynamics.

(ii) Voltage and amplitude regulation: We intend to exactly regulate v_{dc} and $v_{\alpha\beta}$ to prescribed references, possibly requiring knowledge of system parameters and full state measurements. If the load current measurements are uncertain or unknown, we aim instead to achieve a linear *droop* characteristic between the converter modulation frequency and its power output. Such a local droop behavior is known to guarantee power sharing and compatibility with other droop-like controllers in a power system [Dörfler et al., 2015; Sinha et al., 2015a].

(iii) Strict incremental passivity: We aim to preserve strict incremental passivity [Schaft, 2000] with respect to the AC and DC ports, $u = (i_{dc}, -i_l)$ and $y = (v_{dc}, v_{dq})$, and relative to a desired steady-state solution $x^* = (v_{dc}^*, i_{dq}^*, v_{dq}^*)$. More precisely, we seek a positive definite storage function that is decreasing along system trajectories, where the system remains strictly incrementally passive after implementing the controller.

In the sequel, we further specify these objectives, in more suitable coordinates, and also consider alternative objectives such as voltage amplitude droop control.

2.4 The synchronous machine model

In what follows, we consider a SM model which lends itself useful in designing the matching controller. We consider a single-pole-pair, non-salient rotor SM under constant excitation, defined in $\alpha\beta-$frame as in [Caliskan and Tabuada, 2014], together with a capacitor at its AC terminal, and described by the state-space model

$$\dot{\theta} = \omega \tag{5a}$$

$$M\dot{\omega} = -D\omega + \tau_m + L_m i_f \begin{bmatrix} -\sin(\theta) \\ \cos(\theta) \end{bmatrix}^\top i_{\alpha\beta} \tag{5b}$$

$$L_s \dot{i}_{\alpha\beta} = -R_s i_{\alpha\beta} - v_{\alpha\beta} - L_m i_f \begin{bmatrix} -\sin(\theta) \\ \cos(\theta) \end{bmatrix} \omega \tag{5c}$$

$$C\dot{v}_{\alpha\beta} = -Gv_{\alpha\beta} + i_{\alpha\beta} - i_l. \tag{5d}$$

Here, $M > 0$ and $D > 0$ are the rotor inertia and damping coefficients, τ_m is the driving mechanical torque, $L_m > 0$ is the stator-to-rotor mutual inductance, $L_s > 0$ the stator inductance. We denote the rotor angle by $\theta \in \mathbb{S}^1$, its angular velocity by $\omega \in \mathbb{R}$, the current in the stator winding by $i_{\alpha\beta} \in \mathbb{R}^2$, and the stator resistance by $R_s > 0$. At its terminals the SM is interfaced to the grid through a shunt capacitor with capacitance $C > 0$ and

capacitor voltage $v_{\alpha\beta} \in \mathbb{R}^2$, a constant load conductance $G > 0$, and the load current extraction denoted by $i_l \in \mathbb{R}^2$. The strength of the rotating magnetic field inside the SM (5) is given by the rotor current i_f which is assumed to be regulated to a constant value (here, negative), as in [Aghir et al., 2016] and [Caliskan and Tabuada, 2014].

Observe the similarities between the inverter model (3) and the SM model (5). The DC capacitor is analogous to the rotor moment of inertia, while the electrical torque and the electromotive force (EMF) (the rightern-most terms in (5b) and (5c)) play the same role as i_x and v_x. The self-synchronizing properties of a multi-machine power system are attributed to the exchange of kinetic and electrical energy through electrical torque and the EMF pair. In the following section, we will assign this very mechanism for the inverter dynamics (3).

3. Grid-forming SM matching control

From [Groß and Dörfler, 2017], we know that every converter modulation controller inducing a synchronous, balanced, and sinusoidal steady state must necessarily include an *internal model* of an oscillator of the form $\dot{m}^{\star}_{\alpha\beta} = \omega^* \boldsymbol{J} m^{\star}_{\alpha\beta}$. Thus, the first step in our design is to assign a sinusoidal modulation scheme parameterized in polar coordinates as in [Jouini et al., 2016]

$$m_{\alpha\beta} = \mu \begin{bmatrix} -\sin(\theta) \\ \cos(\theta) \end{bmatrix} , \tag{6a}$$

where $\theta \in \mathbb{S}^1$ and $\mu \in [0,1]$ are the modulation's signal magnitude and angle, as controls to be specified. In the next step, we design a grid-forming modulation controller by *matching* the converter dynamics (3), augmented with the internal model (6a), to the SM dynamics (5). Upon visual inspection we observe that this is achieved by dynamic feedback

$$\dot{\theta} = \eta \cdot v_{dc}, \tag{6b}$$

where the constant $\eta = \omega_0/v_{dc,ref} > 0$ encodes the ratio between the nominal AC frequency ω_0 and the DC voltage reference $v_{dc,ref}$. All subsequent developments will be based on the matching control (6).

REMARK 2—EQUIVALENT SM INTERPRETATION
By defining the equivalent angular velocity as $\omega = \eta v_{dc}$ and by picking the

modulation amplitude as $\mu = -2\eta L_m i_f$, we can rewrite i_x and v_x as

$$i_x = -\eta L_m i_f \begin{bmatrix} -\sin(\theta) \\ \cos(\theta) \end{bmatrix}^\top i_{\alpha\beta}\,, \tag{7}$$

$$v_x = -L_m i_f \begin{bmatrix} -\sin(\theta) \\ \cos(\theta) \end{bmatrix} \omega\,. \tag{8}$$

We identify the AC-side switch voltage v_x with the equivalent EMF voltage and the DC-side current i_x/η with the equivalent electrical torque in the machine. Finally, we rewrite the closed loop (3), (6) as the equivalent SM,

$$\dot{\theta} = \omega\,, \tag{9a}$$

$$\frac{C_{dc}}{\eta^2}\dot{\omega} = -\frac{G_{dc}}{\eta^2}\omega + \frac{i_{dc}}{\eta} - \frac{1}{\eta}m_{\alpha\beta}(\theta)^\top i_{\alpha\beta}\,, \tag{9b}$$

$$L\dot{i}_{\alpha\beta} = -Ri_{\alpha\beta} - v_{\alpha\beta} + \frac{1}{2\eta}\omega m_{\alpha\beta}(\theta)\omega\,, \tag{9c}$$

$$C\dot{v}_{\alpha\beta} = -Gv_{\alpha\beta} + i_{\alpha\beta} - i_l\,, \tag{9d}$$

where we identify C_{dc}/η^2, G_{dc}/η^2, and i_{dc}/η with the equivalent mechanical inertia, damping, and mechanical driving torque, respectively. ∎

3.1   Closed-loop incremental passivity

In this section, we show how the matching controller (6) can achieve desirable stability and passivity properties in an appropriate $dq-$frame, while formulating them with respect to an induced operating point. Consider the closed-loop inverter dynamics (3), (6). By applying the $dq-$coordinate transformation with angle θ to $i_{\alpha\beta}$ and $v_{\alpha\beta}$, we arrive at the following subsystem, which is independent of the angle state variable

$$C_{dc}\dot{v}_{dc} = -G_{dc}v_{dc} + i_{dc} - \frac{\mu}{2}\mathbf{e}_2^\top i_{dq}\,, \tag{10a}$$

$$L\dot{i}_{dq} = -Ri_{dq} + v_{dc}\eta L\mathbf{J}i_{dq} + \frac{\mu}{2}\mathbf{e}_2 v_{dc} - v_{dq}\,, \tag{10b}$$

$$C\dot{v}_{dq} = -Gv_{dq} + v_{dc}\eta C\mathbf{J}v_{dq} - i_{l,dq} + i_{dq}\,. \tag{10c}$$

The following result characterizes the strict incremental passivity of the $dq-$frame inverter system (10), with respect to a steady state solution, as per Definition 1 in [Trip et al., 2018].

> THEOREM 1—STRICT PASSIVITY IN $dq-$FRAME
> Consider the model-matched system (10) and assume that, for a given constant input $u^* = (i_{dc}^*, i_{l,dq}^*)$, there exists an equilibrium $x^* = (v_{dc}^*, i_{dq}^*, v_{dq}^*)$

that satisfies

$$\frac{C^2\|v_{dq}^*\|^2}{4G} + \frac{L^2\|i_{dq}^*\|^2}{4R} < \frac{G_{dc}}{\eta^2}. \tag{11}$$

Then, system (10) with input $u = (i_{dc}, -i_{l,dq})$ and output $y = (v_{dc}, v_{dq})$ is strictly passive relative to the pair (x^*, u^*).

Proof. Our proof is inspired by [Caliskan and Tabuada, 2014]. Starting from the assumptions of the theorem, we define the error coordinates $\tilde{v}_{dc} = v_{dc} - v_{dc}^*$, $\tilde{i}_{dq} = i_{dq} - i_{dq}^*$, $\tilde{v}_{dq} = v_{dq} - v_{dq}^*$, $\tilde{i}_{l,dq} = i_{l,dq} - i_{l,dq}^*$, $\tilde{i}_{dc} = i_{dc} - i_{dc}^*$ as well as $\omega^* = \eta v_{dc}^*$, such that the associated transient dynamics are expressed as

$$\begin{aligned}
C_{dc}\dot{\tilde{v}}_{dc} &= -G_{dc}\tilde{v}_{dc} + \tilde{i}_{dc} - \frac{\mu}{2}\mathbf{e}_2^\top\tilde{i}_{dq} \\
L\dot{\tilde{i}}_{dq} &= -\left(R\mathbf{I} + v_{dc}^*\eta L\mathbf{J} + \tilde{v}_{dc}\eta L\mathbf{J}\right)\tilde{i}_{dq} \\
&\quad + \frac{\mu}{2}\mathbf{e}_2\tilde{v}_{dc} - \tilde{v}_{dc}\eta L\mathbf{J}i_{dq}^* - \tilde{v}_{dq} \\
C\dot{\tilde{v}}_{dq} &= -(G\mathbf{I} + v_{dc}^*\eta C\mathbf{J} + \tilde{v}_{dc}\eta C\mathbf{J})\tilde{v}_{dq} - \tilde{i}_{l,dq} - \tilde{v}_{dc}\eta C\mathbf{J}v_{dq}^* + \tilde{i}_{dq}.
\end{aligned} \tag{12}$$

By considering the physical storage of the circuit elements, we define the incremental positive definite and differentiable storage function $\mathcal{V}_1 : \mathbb{R}^5 \to \mathbb{R}_{>0}$ as

$$\mathcal{V}_1 = \frac{1}{2}C_{dc}\tilde{v}_{dc}^2 + \frac{1}{2}\tilde{i}_{dq}^\top L\tilde{i}_{dq} + \frac{1}{2}\tilde{v}_{dq}^\top C\tilde{v}_{dq}. \tag{13}$$

Due to the skew symmetry of $\mathbf{J}$, the derivative of $\mathcal{V}_1$ along the trajectories of the error system (12) reads as

$$\dot{\mathcal{V}}_1 = -\begin{bmatrix}\tilde{v}_{dc} & \tilde{i}_{dq}^\top & \tilde{v}_{dq}^\top\end{bmatrix}\mathcal{Q}\begin{bmatrix}\tilde{v}_{dc} & \tilde{i}_{dq}^\top & \tilde{v}_{dq}^\top\end{bmatrix}^\top - \tilde{v}_{dq}^\top\tilde{i}_{l,dq} + \tilde{i}_{dc}\tilde{v}_{dc},$$

where the symmetric matrix $\mathcal{Q} \in \mathbb{R}^{5\times5}$ is given by

$$\mathcal{Q} = \begin{bmatrix} G_{dc} & \frac{1}{2}(\eta L\mathbf{J}i_{dq}^*)^\top & \frac{1}{2}(\eta C\mathbf{J}v_{dq}^*)^\top \\ \frac{1}{2}(\eta L\mathbf{J}i_{dq}^*) & R\mathbf{I} & 0 \\ \frac{1}{2}(\eta C\mathbf{J}v_{dq}^*) & 0 & G\mathbf{I} \end{bmatrix} \tag{14}$$

By evaluating all leading principal minors of $\mathcal{Q}$ we see that under condition (11), $\mathcal{Q}$ is positive definite. Hence, system (12) is strictly passive with input $(\tilde{i}_{dc}, -\tilde{i}_{l,dq})$ and output $(\tilde{v}_{dc}, \tilde{v}_{dq})$. $\qquad\square$

The importance of this result is that, when the load current $i_{l,dq}$ and the source current i_{dc} are constant, the origin of (12) is rendered asymptotically stable via Lyapunov's direct method. Since $\mathcal{V}_1$ is radially unbounded, we obtain global asymptotic stability as well as the abscence of any other type of equilibrium. We shall further pursue this analysis after closing the passive ports of the inverter via a suitable DC actuation and an AC load current.

3.2   Closed-loop incremental stability

The strict passivity condition (11) requires sufficiently large damping in the AC and DC components of the converter. However, the parasitic resistances R and G_{dc} can be arbitrarily small in practice. To alleviate this shortage of stabilizing dissipation, we implement a DC-side actuation akin to governor speed droop control for generators to enforce condition (11). We propose the current source i_{dc} to implement the proportional (P) controller

$$i_{dc} = i_{dc,ref} - K_p(v_{dc} - v_{dc,ref}),\qquad(15)$$

with gain $K_p > 0$ and set-points $i_{dc,ref} > 0$ and $v_{dc,ref} > 0$ for the DC-side current injection and the DC-side voltage, respectively.

   We are now ready to introduce the load model which we find best representative for the grid-forming application. Assume that the load consists of a constant shunt impedance $\mathcal{Y}_l = G_l\mathbf{I} + B_l\mathbf{J}$ accounting for passive devices (e.g., RLC circuits) connected to the converter. In parallel with this impedance, consider a sinusoidal current source with state s_l having, for all time, the same frequency ω as the converter and otherwise constant amplitude. The latter can model a weak grid without grid-forming units, i.e., without any generator or inverter that regulates frequency and voltage, but possibly containing grid-following units equipped with PLLs which (instantaneously) synchronize to the frequency ω.

ASSUMPTION 1
The load current i_l is given by the following system driven by the input $(\omega, v_{\alpha\beta})$,

$$\begin{aligned}\dot{s}_l &= \omega\mathbf{J}s_l\\ i_l &= (G_l\mathbf{I} + B_l\mathbf{J})v_{\alpha\beta} + s_l,\end{aligned}\qquad(16)$$

where $G_l, B_l > 0$ are constant parameters, and $s_l \in \mathbb{R}^2$ is the state of an internal oscillator.

   Notice that the internal state s_l of this load model, when represented in the converter-angle $dq-$coordinates, becomes a constant. All devices in the network can now be studied with respect to a single $dq-$frame angle, namely that the virtual oscillator. In this scenario, we arrive at the following corollary.

COROLLARY 2—CLOSED-LOOP STABILITY WITH DC-SIDE P-CONTROL
Consider the inverter in system (10) together with P-controller (15) on the DC-side and load (16) on the AC-side. Assume there exists a steady

state $x^* = (v_{dc}^*, i_{dq}^*, v_{dq}^*, i_{dc}^*, i_{l,dq}^*)$ satisfying

$$\frac{C^2\|v_{dq}^*\|^2}{4G} + \frac{L^2\|i_{dq}^*\|^2}{4R} < \frac{G_{dc} + K_p}{\eta^2}. \tag{17}$$

Then, for stationary loads $s_{dq} = s_{l,dq}^*$, the steady state x^* is unique and globally asymptotically stable.

Observe that condition (17) can be met by suitable choice of gain K_p and that the condition is worst at no load, i.e., when $G_l = 0$. Furthermore, at this point, we cannot necessarily guarantee exact regulation of v_{dc} to a particular $v_{dc,ref}$ without having access to the load measurement. This discussion will be addressed later, in Section 4.

Finally, the incremental passivity property highlighted in Theorem 1 and Corollary 2 is regarded as a key requirement for stability under interconnection, see [Caliskan and Tabuada, 2014; Fiaz et al., 2013], however this requires a single coordinate frame analysis for the networked scenario. Since in our work we use a $dq-$coordinate frame attached to a particular converter angle, the analysis does not pertain to a setup containing multiple (grid-forming) inverters. Nevertheless, this property is preserved in all our subsequent developments. In what follows, we investigate the steady-state droop behavior of the closed loop (10), (15).

3.3   Droop properties of matching control

An important aspect of *plug-and-play* operation in power systems is steady-state power sharing amongst multiple inverters by means of a droop characteristic. This is typically achieved via a trade-off between power injection and voltage amplitude or frequency [Dörfler et al., 2015]. We now investigate these steady state properties which arise naturally in the closed-loop system (3), (6), (15).

Let $r_x^* = \frac{1}{2}\mu v_{dc}^*$ and $\omega_x = \eta v_{dc}^*$ denote the switching node voltage amplitude and frequecy at steady state. Let $P_x = v_x^{\star\top} i_{\alpha\beta}^\star$ and $Q_x = v_x^{\star\top} \mathbf{J}^\top i_{\alpha\beta}^\star$ denote the active and reactive powers flowing from the switching node, at steady state, as per the convention in [Akagi et al., 1983], and assume that they are constant.

Two converters indexed by i, j are said to achieve *proportional power sharing* at a pre-defined ratio $\rho > 0$ if $P_{x,i}^*/P_{x,j}^* = \rho$. Furthermore, the linear sensitivity factors relating steady state active power injection P_x to voltage amplitude r_x and frequency ω_x, are defined here as the *droop coefficients* $d_r = \partial P_x/\partial r_x$ and $d_\omega = \partial P_x/\partial \omega_x$. Their relationship is given in the proposition that follows.

PROPOSITION 3—DROOP SLOPES

Consider system (3), together with matching controller (6) and the DC-side controller (15). Denote $\omega_x = \omega^*$, and define the constant $i_0 = i_{dc,ref} + K_p v_{dc,ref}$. The following statements hold at equilibrium:

1. Nose curves: the switching voltage amplitude r_x has the following expression as a function of i_0 and P_x

$$r_x^* = \frac{\mu}{4(G_{dc} + K_p)}\left(i_0 \pm \sqrt{i_0^2 - 4(G_{dc} + K_p)P_x}\right),$$

with a similar expression for the virtual frequency $\omega_x = \frac{2\eta}{\mu}r_x$. Moreover, the reactive power Q_x and the quantities r_x, ω_x are not related.

2. Droop behavior: around the operating point ω_x, the expression for the frequency droop is given by:

$$d_\omega = -\frac{2(G_{dc} + K_p)}{\eta^2}\omega_x^* + \frac{i_0}{\eta}. \qquad (18a)$$

with an analogous expression for the switching node voltage amplitude droop d_r, since $r_x = \frac{\mu}{2/eta}\omega_x$.

3. Power sharing: Consider a pair of converters i and j, $\{i, j\} \subset \mathbb{N}$ with identical values of DC conductance $G_{dc} = 0$, identical DC-side voltage references $v_{dc,ref} > 0$ and control gain $\eta > 0$. The converters achieve proportional power sharing at ratio $\rho = P_{x,i}^*/P_{x,j}^*$ if

$$K_{p,i} = \rho K_{p,j} , \quad i_{dc,ref,i} = \rho\, i_{dc,ref,j} , \qquad (19)$$

or equivalently if $d_{\omega,i} = \rho\, d_{\omega,j}$ with $P_{dc} = v_{dc,ref} \cdot i_{dc,ref}$.

Proof. To prove statement (1), consider the DC-side dynamics (3a) at steady state

$$0 = -(G_{dc} + K_p)v_{dc}^* + i_0 - i_x^*. \qquad (20)$$

We multiply (20) by v_{dc}^* to obtain quadratic expression relating $P_x = i_x^{*\top} v_{dc}^*$ and v_{dc}^*, at steady state:

$$v_{dc}^* = \frac{i_0 \pm \sqrt{i_0^2 - 4(G_{dc} + K_p)P_x^*}}{2(G_{dc} + K_p)}. \qquad (21)$$

The claimed nose curves follow directly. Consider now

$$P_x^* = \frac{-4(G_{dc} + K_p)}{\mu^2}r_x^{*2} + \frac{2i_0 r_x^*}{\mu} = \frac{-(G_{dc} + K_p)}{\eta^2}\omega_x^{*2} + \frac{i_0}{\eta}\omega_x^*. \qquad (22)$$
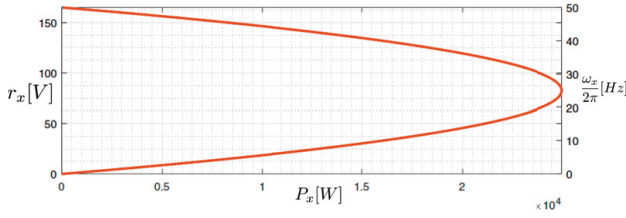
Figure 2.   Steady state profiles (r_x, P_x) and (ω_x, P_x) for the set of converter parameters described in Section 5.

By linearizing the above equations around the steady state operating point ω_x, we find the droop slopes in (18). Finally, the proportional power sharing ratio $\rho > 0$ between two converters i and j is given by setting $G_{dc} = 0$ in (22)

$$\rho = \frac{P^*_{x,i}}{P^*_{x,j}} = \frac{\dfrac{K_{p,i}}{\eta^2}\omega^*_x - \dfrac{i_{0,i}}{\eta}}{\dfrac{K_{p,j}}{\eta^2}\omega^*_x - \dfrac{i_{0,j}}{\eta}}. \tag{23}$$

The latter equality is satisfied if (19) holds. □

The following remarks can now be drawn: Statement (1) gives two solutions[2] for the voltage amplitude r_x. Among these two, the so-called *high-voltage solution* (with the plus sign) is the practically relevant operating point as depicted in Fig.3.3. From statement (1), we can also deduce that the maximal active power which can be delivered at the switching node, $P_{max} = i_0^2 / (4(G_{dc} + K_p))$, is marked by the right tip of the nose curve. No stationary solutions exist beyond this bifurcation point. To the best of our knowledge, a typical inverter design will have, by design, its operating region away from the tip of the nose curve, where the linear sensitivity factors are a good approximation and parametric bifurcations of no practical concern.

Regarding statement (3), the power sharing conditions (19) are perfectly analogous to the ones in conventional droop control [Dörfler et al., 2015]: the droop slopes and the power set-points must be related by same ratio ρ. Finally, we remark that similar expressions as in (19) can be obtained for a non-zero DC-side damping and heterogeneous converter parameters.

---

[2] For the rest of this paper, our system is not subject to constant power loads and admits a unique induced equilibrium.

3.4 Relation to other converter control strategies

Our matching control can be understood from the viewpoint of PBC by writing the inverter (3) as the port-Hamiltonian system [Schaft, 2000]

$$\dot{z} = [\mathcal{J}(m) - \mathcal{D}]\,\nabla H(z) + \mathcal{G}u\,,$$

where $z = (C_{dc}v_{dc}, Li_{\alpha\beta}, Cv_{\alpha\beta})^\top$ is the state, m is the modulation, $u = (i_{dc}, -i_l)^\top$ is an exogenous input, $H(z) = \frac{1}{2}C_{dc}^{-1}v_{dc}^2 + \frac{1}{2}i_{\alpha\beta}^\top L^{-1}i_{\alpha\beta} + \frac{1}{2}v_{\alpha\beta}^\top C^{-1}v_{\alpha\beta}$ is the physical energy, as in (13), and $\mathcal{J}(m)$ is a skew-symmetric interconnection matrix, depending on the modulation signal m, $\mathcal{D}$ and $\mathcal{G}$ are positive definite damping and input matrices. The port-Hamiltonian structure is preserved upon augmenting the inverter with the internal model (6a). On this ground, we can link our approach to that of PBC and IDA-based matching control [Ortega and Garcia-Canseco, 2004]. In particular, matching controller (6) together with P-controller (15) can be understood as IDA reshaping the $\mathcal{J}$ and $\mathcal{D}$ matrices.

Our control strategy can also be associated with oscillator-based controller methods. By defining $m \in \mathbb{R}^2$ as the controller state, we can rewrite (6) as

$$\dot{m} = \omega \boldsymbol{J} m\,,$$

i.e., the matching control (6) is an oscillator with constant amplitude $\|m(0)\| = \mu$ and state-dependent frequency $\omega = \eta v_{dc}$ as feedback for the converter dynamics (3). This control strategy resembles the classic *proportional resonant control* [Teodorescu et al., 2006] with the difference that the frequency of the oscillator (3.4) adapts to the DC voltage which again reflects the grid state. Another related control strategy is *virtual oscillator control* encoding the inverter terminal dynamics as a nonlinear limit cycle oscillator adapting to the grid state [Johnson et al., 2014; Sinha et al., 2015a].

4. Voltage and frequency regulation

Starting from the model-matching controller (6), we now look to design outer control loops for the current source i_{dc} as well as the modulation amplitude μ with the aim of tracking a given constant reference initially for the DC capacitor voltage and then also for the AC capacitor voltage amplitude.

4.1 Exact frequency regulation via integral control

In some scenarios, e.g., in islanded microgrids, it is desirable that inverters also contribute to frequency regulation (usually called secondary control) rather than mere droop control. Inspired by frequency regulation of SMs via governor control, i.e., controlling the torque in (5) as a function of the frequency, we propose a frequency regulation strategy by pairing the passive

inputs and outputs, $\tilde{i}_{dc} = i_{dc} - i_{dc,ref}$ and $\tilde{v}_{dc} = v_{dc} - v_{dc,ref}$, respectively, in the inverter model (10), in aim of tracking a reference frequency $\omega_{ref} = \eta v_{dc,ref}$. We propose the PID controller

$$i_{dc} = i_{dc,ref} - K_p \tilde{v}_{dc} - K_i \int_0^t \tilde{v}_{dc}(\tau)\, d\tau - K_d \dot{\tilde{v}}_{dc}\,, \tag{24}$$

where $i_{dc,ref} > 0$ is a user-defined parameter, and K_p, K_i, K_d are positive control gains.

Before proceeding to the stability result, we put together system (10), controller (24), and load model (16), and express the closed-loop in error coordinates formulated relative to an induced equilibrium. To account for the newly introduced integral term, we define the state variable $\xi \in \mathbb{R}$ and denote its steady state value by ξ^* such that $\tilde{\xi} = \xi - \xi^*$.

$$\dot{\tilde{\xi}} = \tilde{v}_{dc}$$

$$(C_{dc} + K_p)\dot{\tilde{v}}_{dc} = -(G_{dc} + K_p)\tilde{v}_{dc} - K_i\tilde{\xi} - \frac{\mu}{2}\mathbf{e}_2^\top \tilde{i}_{dq}$$

$$L\dot{\tilde{i}}_{dq} = -\left(\mathcal{Z} + \tilde{\omega}\,L\mathbf{J}\right)\tilde{i}_{dq} - \tilde{\omega}L\mathbf{J}i_{dq}^* \tag{25}$$

$$+ \frac{\mu}{2}\begin{bmatrix} 0 \\ 1 \end{bmatrix}\tilde{v}_{dc} - \tilde{v}_{dq}$$

$$C\dot{\tilde{v}}_{dq} = -\left(\mathcal{Y} + \tilde{\omega}\,C\mathbf{J}\right)\tilde{v}_{dq} - \tilde{\omega}C\mathbf{J}v_{dq}^* + \tilde{i}_{dq}\,.$$

where $\mathcal{Z} = R\mathbf{I} + \omega^*L\mathbf{J}$ and $\mathcal{Y} = G\mathbf{I} + \omega^*C\mathbf{J}$ are the impedance of the AC-side inductor and the admittance of the AC-side capacitor, respectively. Since PID control of the DC-voltage (24) is common practice in DC/AC converters, we will see that pairing it with the matching control (6) yields exact AC frequency regulation.

The following result addresses existence, uniqueness, and stability of a desired steady state of the closed-loop system (25) satisfying $v_{dc}^* = v_{dc,ref}$ and $\omega^* = \omega_0$. Typically, in such systems, ω_0 can be seen as the grid nominal frequency, while $v_{dc,ref}$ the reference voltage of the converter's DC-link capacitor. By appropriately choosing the gain $\eta = \omega_0/v_{dc,ref}$, we are able to achieve both specifications.

> THEOREM 4—EXACT FREQUENCY REGULATION
> Consider the closed-loop system (25) and a given set-point $\omega_0 > 0$. The following two statements hold:
>
> 1. There exists a unique steady state at the origin with $\omega^* = \omega_0$ as system frequency.
>
> 2. Assuming condition (17) is satisfied, the zero-equilibrium of (25) is globally asymptotically stable.

Proof. A steady-state of the closed loop (25) is characterized by $\tilde{v}_{dc} = 0$ and a linear set of equations $A \begin{bmatrix} \tilde{\xi} & \tilde{i}_{dq}^\top & \tilde{v}_{dq}^\top \end{bmatrix}^\top = 0$, where $A \in \mathbb{R}^{5 \times 5}$ is given by

$$
A = \begin{bmatrix}
-K_i & -\frac{\mu}{2}\mathbf{e}_2^\top & 0 \\
0 & -\mathcal{Z} & \mathbf{I} \\
0 & -\mathbf{I} & -(\mathcal{Y} + \mathcal{Y}_l)
\end{bmatrix} \in \mathbb{R}^{5 \times 5}. \tag{26}
$$

It follows that

$$
\det(A) = -K_i \| \mathcal{Z}(\mathcal{Y} + \mathcal{Y}_l) + \mathbf{I} \|^2,
$$

such that the positivity of the converter and load parameters assures invertibility of A, and hence

$$
\begin{bmatrix} \tilde{\xi} & \tilde{i}_{dq}^\top & \tilde{v}_{dq}^\top \end{bmatrix}^\top = 0.
$$

Thus, there is a unique zero steady-state for this error subsystem. The stability proof of this steady state is analogous to the proof of Corollary 2 after replacing the original storage function $\mathcal{V}_1$ with $\mathcal{V}_2 = \mathcal{V}_1 + \frac{1}{2}K_i\tilde{\xi}^2 + \frac{1}{2}K_d\tilde{v}_{dc}^2$, to account for $\tilde{\xi}$ and the gain K_d. With these modifications the derivative of the storage function $\mathcal{V}_2$ becomes

$$
\dot{\mathcal{V}}_2 = - \begin{bmatrix} \tilde{v}_{dc} & \tilde{i}_{dq}^\top & \tilde{v}_{dq}^\top \end{bmatrix} \mathcal{Q} \begin{bmatrix} \tilde{v}_{dc} & \tilde{i}_{dq}^\top & \tilde{v}_{dq}^\top \end{bmatrix}^\top \leq 0,
$$

where $\mathcal{Q}$ is as in (14) with G_{dc} and G replaced by $G_{dc} + K_p$ and $G + G_l$ respectively. Finally a LaSalle-type argument accounting for the state $\tilde{\xi}$ together with radial unboundedness of $\mathcal{V}_2$ guarantees global asymptotic stability. □

Notice that the P-control on the DC voltage enhances the overall system stability, as discussed before. Furthermore, by comparing systems (10) and (25), we observe that the effect of the PID gains is to provide additional inertia and damping to the DC circuit. Lastly, from a conventional power system perspective, it is instructive to write the frequency error dynamics, whereby $\tilde{\omega} = \eta \tilde{v}_{dc}$

$$
\frac{(C_{dc} + K_d)}{\eta^2} \dot{\tilde{\omega}} = -\frac{(G_{dc} + K_p)}{\eta^2} \tilde{\omega} - \frac{K_i}{\eta} \int \tilde{\omega} - \frac{1}{\eta} i_x,
$$

which for $K_i = 0$ resemble the standard classic swing equations with synthetic droop and inertia induced by K_p and K_d.

We conclude that for secondary frequency regulation – independently of the particular modulation strategy – a sufficiently large equivalent DC energy storage is required to cope with a given power imbalance. If the task of frequency regulation is to be shouldered by multiple inverters, then the

decentralized integral control in (24) can be easily adapted to broadcast AGC-like or consensus-based distributed integral control schemes [De Persis and Monshizadeh, 2017; Dörfler and Grammatico, 2017; Dörfler et al., 2015], which assure robust power sharing.

4.2 Amplitude regulation by disturbance feedback

This section investigates a series of controllers designed to regulate the AC-side voltage amplitude $\|v_{\alpha\beta}\|$ to a desired set-pint $r_{ref} > 0$—Throughout this section, we assume that the load in Assumption 1 has zero shunt impedance, namely that $\mathcal{Y}_l = 0$, i.e., the load is purely of constant- (in dq−frame) current nature, so that $i_{l,dq} = s_{l,dq}$. This modeling choice is not merely done for simplicity of exposition (the load impedance can always be absorbed in the filter conductance G) but mainly due to the fact that all amplitude controllers (most importantly, droop control) explicitly or implicitly rely on a measurement of the load current which is considered to be exogenous signal.

4.2.1 Feasibility and feedforward control. We now consider as actuation input, the modulation amplitude μ, analogously to standard practice in SM excitation current. Formally, our control objective is the achieve $\|v_{dq}\| = r_{ref}$, at steady state. Let us first characterize the feasibility of this task in terms of the system parameters.

THEOREM 5—EXISTENCE OF LOAD INDUCED EQUILIBRIA
Consider the closed-loop inverter model (25) with $\mathcal{Y}_l = 0$. For given set-points $r_{ref} > 0$, $v_{dc,ref} > 0$ and constant load current $s_{l,dq} \in \mathbb{R}^2$, define the quantity

$$\psi = r_{ref}^2 \|\mathcal{Z}\mathcal{Y} + \boldsymbol{I}\|^2 - \|\mathcal{Z}s_{l,dq}\|^2. \tag{27}$$

Then, the following statements are equivalent:

1. There exists a unique steady state $(\xi^*, v_{dc}^*, i_{dq}^{*\top}, v_{dq}^{*\top})^\top$ that satisfies $\|v_{dq}^*\| = r_{ref}$ and $\mu > 0$; and

2. $\psi > 0$.

Proof. We formulate the equilibria of system (25), together with the require-

ment that $\|v_{dq}^*\| = r_{ref}$, as

$$0 = v_{dc}^* - v_{dc,ref} \tag{28a}$$

$$0 = -(G_{dc} + K_p)v_{dc}^* - K_i\xi^* - \frac{\mu}{2}\mathbf{e}_2^\top i_{dq}^* \tag{28b}$$

$$0 = -(R\mathbf{I} + v_{dc}^*\eta L\mathbf{J})i_{dq}^* + \frac{\mu}{2}\mathbf{e}_2 v_{dc}^* - v_{dq}^* \tag{28c}$$

$$0 = -(G\mathbf{I} + v_{dc}^*\eta C\mathbf{J})v_{dq}^* - i_{l,dq} + i_{dq}^* \tag{28d}$$

$$0 = v_{dq}^{*\top} v_{dq}^* - r_{ref}^2, \tag{28e}$$

By subsequent elimination of variables, we can solve Eqs.(28) for μ in terms of input $s_{l,dq}$ and set-point $v_{dc,ref}$. We arrive at the quadratic equation

$$0 = \mu^2 - b\,\mu + \frac{4}{v_{dc,ref}^2}p\,,$$

where $b = \frac{4}{v_{dc,ref}}\mathbf{e}_2^\top \mathcal{Z}^\top s_{l,dq}$ is the sum of the two solutions $\mu_\pm$ of the quadratic equation. These solutions

$$\mu_\pm = \frac{b}{2} \pm \sqrt{\left(\frac{b}{2}\right)^2 + \frac{4\psi}{v_{dc,ref}}} \tag{30}$$

are real valued and have opposite signs $\mu_+ > 0$, $\mu_- < 0$ if and only if $\psi > 0$. In what follows, we restrict ourselves to the unique positive solution $\mu_+ > 0$. Notice from (28a) that $v_{dc}^* = v_{dc,ref}$. After replacing $\mu_\pm$ into (28b), (28c), (28d), the remaining equations are linear $A\begin{bmatrix}\tilde{\xi} & \tilde{i}_{dq}^\top & \tilde{v}_{dq}^\top\end{bmatrix}^\top = 0$ with A is nonsingular, as in the proof of Theorem 4. These equations can be solved uniquely for $(\xi^*, i_{dq}^{*\top}, v_{dq}^{*\top})^\top$ which is consistent with (28e) by choice of $\mu > 0$.   □

The condition $\psi > 0$ can be interpreted as an upper bound for the admissible constant load current $s_{l,dq}$ as a function of the given set-point r_{ref}, since otherwise there would be no real-valued solution for μ. Observe that the constraint $\mu_\pm \leq 1$ can be enforced by adjusting the converter parameters and by further limiting the maximum allowable load.

4.2.2 Disturbance decoupling control. Starting from the insights given by Theorem 5, we are able to construct a disturbance-feedback, asymptotic output tracking controller which relies on measurement of the load current $s_{l,dq}$ to produce the modulation input μ according to (30). This approach can be regarded as a system inversion of the transfer path from $i_{l,dq}$ to the regulated voltage output $\|v_{dq}\|$, a standard procedure in measurable disturbance decoupling. In the next subsection, we will discuss two extensions to this control strategy following PBC and droop control specifications.

> COROLLARY 6—DISTURBANCE DECOUPLING CONTROL
>   Consider system (25) with $\mathcal{Y} = 0$. Assume that the load disturbance $i_{l,dq} = s_{l,dq}$ is a constant and measurable signal and that ψ defined in (27) is positive. Given a reference AC voltage $r_{ref} > 0$, assign the modulation amplitude
>
> $$\mu = \mu_+(s_{l,dq}),$$
>
> where μ_+ is as in (30). Further assume that the passivity condition (17) holds. Then, the unique equilibrium is characterized by $v_{dc}^* = v_{dc,ref}$ and $\|v_{dq}^*\| = r_{ref}$, and is globally asymptotically stable for the closed loop.

Proof. For any constant $\mu > 0$ the desired closed-loop equilibrium is described in (28). The existence of such equilibrium is guaranteed under the condition $\psi > 0$ and for $\mu_\pm$ as in (30). By assigning the positive solution in (30), the amplitude $\mu = \mu_+(s_{l,dq})$ is constant for a given constant load $s_{l,dq}$. The stability claim now follows from the same reasoning as in the proof of Theorem 4. □

4.2.3   Compatibility with existing control techniques.
While very effective in achieving the prescribed steady-state specification, notice that the disturbance feedback control in Corollary (6) requires exact knowledge of the plant as well as load measurement. To assess the robustness of this framework, we investigate two additional extensions which could provide some insight into the practicality of the implementation.

PI-PBC   Inspired by [Zonetti et al., 2014], we now derive a PI-PBC feedback by identifying the passive output corresponding to the new considered input. In this regard, with pick input $\mu = \tilde{\mu} + \mu^*$, with $\mu^* = \mu_+$ from (30) and $\tilde{\mu}$ yet to be designed. We rewrite (25) with $\mathcal{Y}_l = 0$ as

$$
\begin{aligned}
\dot{\tilde{\xi}} &= \tilde{v}_{dc} \\
(C_{dc}+K_p)\dot{\tilde{v}}_{dc} &= -(G_{dc} + K_p)\tilde{v}_{dc} - K_i\tilde{\xi} - \frac{\tilde{\mu}+\mu_+}{2}\mathbf{e}_2^\top \tilde{i}_{dq} - \frac{\tilde{\mu}}{2}\mathbf{e}_2^\top i_{dq}^* \\
L\dot{\tilde{i}}_{dq} &= -\left(\mathcal{Z} + \tilde{v}_{dc}\eta L\boldsymbol{J}\right)\tilde{i}_{dq} - \tilde{v}_{dc}\eta L\boldsymbol{J}i_{dq}^* \\
&\quad + \frac{\tilde{\mu}+\mu_+}{2}\mathbf{e}_2^\top \tilde{v}_{dc} + \frac{\tilde{\mu}}{2}\mathbf{e}_2 v_{dc}^* - \tilde{v}_{dq} \\
C\dot{\tilde{v}}_{dq} &= -\left(\mathcal{Y} + \tilde{v}_{dc}\eta\,C\boldsymbol{J}\right)\tilde{v}_{dq} - \tilde{v}_{dc}\eta\,C\boldsymbol{J}v_{dq}^* + \tilde{i}_{dq}.
\end{aligned}
\tag{31}
$$

For the computation of μ_+ in (30) we also assume a constant measurable load current $i_{l,dq}$, such that the prescribed equilibrium of (31) satisfies (28), or equivalently $\psi > 0$. Observe that system (31) is passive with respect to input $\tilde{\mu}$, output $y = \tilde{i}_q v_{dc}^* - i_q^* \tilde{v}_{dc}$, and storage function $\mathcal{V}_2$ from before, since

$$
\dot{\mathcal{V}}_2 = -\begin{bmatrix} \tilde{v}_{dc} & \tilde{i}_{dq}^\top & \tilde{v}_{dq}^\top \end{bmatrix} \mathcal{Q} \begin{bmatrix} \tilde{v}_{dc} & \tilde{i}_{dq}^\top & \tilde{v}_{dq}^\top \end{bmatrix}^\top + \tilde{\mu}^\top y.
$$

This last observation motivates the PI-PBC feedback

$$\dot{\nu} = y \tag{32a}$$

$$\tilde{\mu} = -\kappa_p y - \kappa_i \tilde{\nu} \,, \quad \dot{\tilde{\nu}} = y \,, \tag{32b}$$

where $y = \tilde{i}_q v_{dc}^* - i_q^* \tilde{v}_{dc}$ and $\kappa_p, \kappa_i > 0$. Finally, the resulting error feedback becomes

$$y = i_q v_{dc,ref} - i_q^* v_{dc},$$

with $i_q^* = \mathbf{e}_2^\top (\mathcal{Z} + \mathcal{Y}^{-1})^{-1} (\frac{\mu}{2} \mathbf{e}_2 v_{dc,ref} + \mathcal{Y}^{-1})^{-1} s_{l,dq}$. This is the same type of output to be regulated to zero as identified in [Zonetti et al., 2014] indicating a power imbalance across the inverter.

> PROPOSITION 7—PI-PBC
> Consider system (31) with the PI-PBC feedback (32b). Assume that the load disturbance $s_{l,dq}$ is a constant measurable signal and that ψ defined in (27) is positive. Further assume that the passivity condition (11) holds. Then the unique equilibrium is characterized by $v_{dc}^* = v_{dc,ref}$ and $\|v_{dq}^*\| = r_{ref}$, and is globally asymptotically stable for the closed loop.

Proof. Consider the radially unbounded Lyapunov function $\mathcal{V}_3 = \mathcal{V}_2 + \frac{\kappa_i}{2} \tilde{\nu}^2$ and its derivative along trajectories of (31), (32b)

$$\dot{\mathcal{V}}_3 = - \begin{bmatrix} \tilde{v}_{dc} & \tilde{i}_{dq}^\top & \tilde{v}_{dq}^\top \end{bmatrix} \mathcal{Q} \begin{bmatrix} \tilde{v}_{dc} & \tilde{i}_{dq}^\top & \tilde{v}_{dq}^\top \end{bmatrix}^\top - \kappa_p y^2 \leq 0 \,,$$

where $\mathcal{Q}$ is as in (14) with G_{dc} replaced by $G_{dc} + K_p$. Assuming condition (17) is met, a LaSalle argument accounting for the evolution of $\tilde{\xi}$ and $\tilde{\nu}$ guarantees global asymptotic stability. □

Observe that the PI-PBC law (32b) requires that the load current $i_{l,dq} = s_{l,dq}$ is measurable, as it is used in the computation of the steady-state inducing terms μ_+ and i_q^* is the feedback law. In this way, the feed forward control (30), as well as PI-PBC (32b), endow the closed-loop with the ability of rejecting the disturbance $i_{l,dq}$ as long as it is constant or, due to global asymptotic stability, provided it eventually settles to a value which is state-independent.

Voltage droop control   We have seen that, without an integral term, the matching control has the inherent droop properties of the SM. However, by introducing controller (24) for exact frequency regulation, this droop effect has been removed in both the amplitude and the frequency of the AC-side voltage. In the remainder of this subsection, we propose a control strategy that implements, instead, a voltage-power droop behavior. The droop dependency will be based on active power measurement. Nevertheless, the same reasoning applies to the case of reactive power. We start by choosing

$$\mu = \mu_{ref} + d \, (P_l - P_{ref}), \tag{33}$$

105

where $\mu_{ref} = \frac{2r_{ref}}{vdc,ref}$. Here r_{ref} and P_{ref} are set-points for the modulation amplitude and load power, respectively, $d_v > 0$ is the droop coefficient, and $P_l = i_{l,dq}^\top v_{dq}$ denotes the entire load power measurement. The droop factor d_v represents a linear trade-off between the modulation amplitude μ and the active power P_l, and induces a steady-state amplitude $\|v_{dq}^*\|$ that is not necessarily equal to the prescribed reference r_{ref}. The aim of the following result is to show that this particular droop strategy is also compatible with our framework.

> PROPOSITION 8—VOLTAGE DROOP CONTROL
>   Consider system (25) with input μ given by (33) and $\mathcal{Y}_l = 0$. Further assume that the closed loop (25), (33) admits a steady state $(\tilde{\xi}, \tilde{v}_{dc}, \tilde{i}_{dq}^\top, \tilde{v}_{dq}^\top)^\top = 0$. Assuming that condition (11) holds, then for a sufficiently small droop coefficient $d_v > 0$, this steady state is globally asymptotically stable for the closed loop.

Proof. We rewrite the closed-loop DC/AC converter in error coordinates with $\mu = \mu_{ref} + d_v(P_l - P_{ref})$ as

$$\dot{\tilde{\xi}} = \tilde{v}_{dc}$$

$$(C_{dc} + K_p)\dot{\tilde{v}}_{dc} = -(G_{dc} + K_p)\tilde{v}_{dc} - K_i\tilde{\xi} - \frac{\mu_{ref}}{2}\mathbf{e}_2^\top \tilde{i}_{dq}$$

$$- \frac{d_v(P_l - P_{ref})}{2}\mathbf{e}_2^\top \tilde{i}_{dq} - \frac{d_v\tilde{P}_l}{2}\mathbf{e}_2^\top i_{dq}^*$$

$$L\dot{\tilde{i}}_{dq} = -(\mathcal{Z} + \tilde{v}_{dc}\eta L\boldsymbol{J})\,\tilde{i}_{dq} - \tilde{v}_{dc}\eta L\boldsymbol{J}i_{dq}^*$$

$$+ \frac{\mu_{ref} + d(P_l - P_{ref})}{2}\mathbf{e}_2\tilde{v}_{dc} + \frac{d\tilde{P}_l}{2}\mathbf{e}_2 v_{dc}^* - \tilde{v}_{dq}$$

$$C\dot{\tilde{v}}_{dq} = -(\mathcal{Y} + \tilde{v}_{dc}\eta C\boldsymbol{J})\,\tilde{v}_{dq} - \tilde{v}_{dc}\eta C\boldsymbol{J}v_{dq}^* + \tilde{i}_{dq},$$

with $\tilde{P}_l = P_l - P_l^*$ and P_l^* as the value of the load power at steady-state. The derivative of $\mathcal{V}_2$ can be obtained analogously to the proof of Theorem 4, as $\dot{\mathcal{V}}_2 = -\begin{bmatrix} \tilde{v}_{dc} & \tilde{i}_{dq}^\top & \tilde{v}_{dq}^\top \end{bmatrix}(\mathcal{Q} + d_v\mathcal{M})\begin{bmatrix} \tilde{v}_{dc} & \tilde{i}_{dq}^\top & \tilde{v}_{dq}^\top \end{bmatrix}^\top \leq 0$, where $\mathcal{Q}$ is as in (14) and $\mathcal{M}$ is a constant matrix, i.e., its entries do not depend on the droop coefficient d_v. Since $\mathcal{Q}$ is positive definite under condition (17), there exists $d_v > 0$ sufficiently small such that $\mathcal{P} + d_v\mathcal{M}$ is positive definite. A LaSalle argument accounting for the evolution of $\tilde{\xi}$ then asserts global asymptotic stability of the load-induced equilibrium. □

5. Numerical case study

We validate and test the proposed controllers in a numerical case study. We consider for this purpose an inverter designed for 10^4 W power output with the

following parameters [3]: $G_{dc} = 0.1, C_{dc} = 0.001, R = 0.1, L = 5 \cdot 10^{-4}, C = 10^{-5}$, and nominal DC voltage of $v_{dc,ref} = v_{dc}(0) = 1000$. In order to obtain the desired open-circuit (no load) values $r_{x,ref} = r_{ref} = 165$ and $\omega^* = \omega_0 = 2\pi 50$, we choose the constant gains $\eta = \frac{\omega_0}{v_{dc,ref}} = 0.3142$, $\mu = \frac{2r_{ref}}{v_{dc,ref}} = 0.33$.

5.1   Voltage and frequency regulation – single inverter

To validate our results for frequency and amplitude regulation, we present three scenarios implementing the matching control (6) and the frequency regulation (24), together with the three different amplitude controllers. We consider a load step of 55% at $t = 0.5s$. The resulting amplitudes and power waveforms are shown in Fig. 3, whereas Fig. 5 shows a time-domain electromagnetic transient (EMT) simulation of the output capacitor voltage.

The parameters of the frequency controller (24) were selected as $i_{dc,ref} = 100, K_p = 1, K_i = 10, K_d = 0$ and $\xi(0) = 0$. For voltage control we consider the feedforward control (30), PI-PBC (32b) with (in S.I. $\kappa_p = 0.1, \kappa_i = 10, \nu(0) = 0$), as well as droop control (33) (in S.I. $\mu_{ref} = 0.33, d_v = 10^{-5}$ and $P_{ref} = 10^4$) plotted as red, green and blue signals, respectively. For all considered controllers, the DC voltage exactly tracks the reference voltage $v_{dc,ref} = 1000V$. The feedforward and PI-PBC designs indeed also track the desired amplitude $r_{ref} = 165V$. Observe that the constant amplitude objective of these controllers requires higher steady-state current amplitudes after the load step. The droop controller on the other hand ensures a trade-off between the power load and AC voltage amplitude. We observe that all controllers yield well-behaved transient response to the step in disturbance.

5.2   Multi-Converter Case Study

Next, we consider a network of two inverters connected in parallel to a conductance load via a $\Pi-$transmission line model; see Fig.6. The $\Pi-$line parameters are $R_{net} = 0.5, L_{net} = 2.5 \cdot 10^{-5}$ and $C_{net} = 2 \cdot 10^{-7}$, where the capacitors account for the filter and line charge capacitance. The interconnection dynamics are considered for $k \in \{1, 2\}$:

$$C\dot{v}_{\alpha\beta,k} = -Gv_{\alpha\beta,k} + i_{\alpha\beta,k} - i_{net,k}$$
$$L_{net}\dot{i}_{net,k} = -R_{net}i_{net,k} + v_{\alpha\beta,i} - v_l$$
$$C_{net}\dot{v}_{net} = -G_{net}v_{net} + i_{net,1} + i_{net,2}.$$

We implemented the matching control (6) with gains according to (19) to demonstrate the proportional power sharing with ratio $\rho = 3$. We chose the current control parameters for the inverters as $i_{dc,ref,1} = 100, K_{p1} = 2$ in (S.I.), neglected internal losses $G_{dc,1} = G_{dc,2} = 0$, fixed the modulation

---

[3] All units are in S.I.
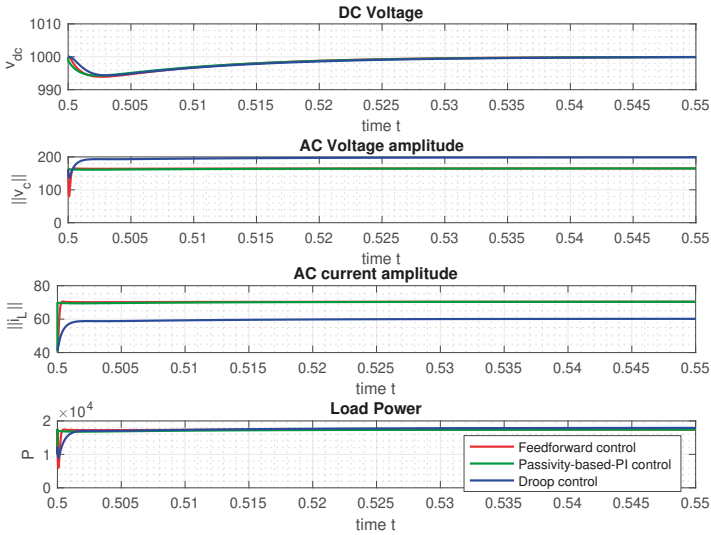
Figure 3. The response id the system under the three controller from Section 4 after a step in load conductance at $t = 0.5$
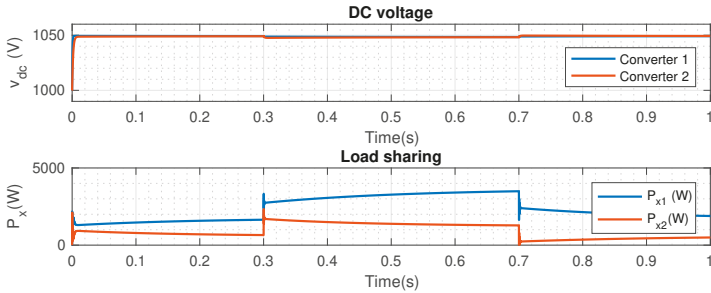
Figure 4. The response of the parallel converter scenario in Fig. (6) during two steps in the load conductance G_{net}.
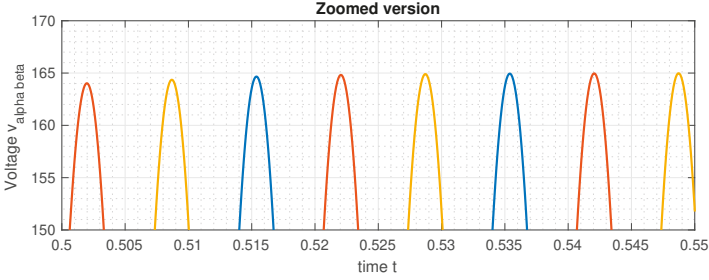
Figure 5.   Magnified plot of the three-phase AC bus voltage.
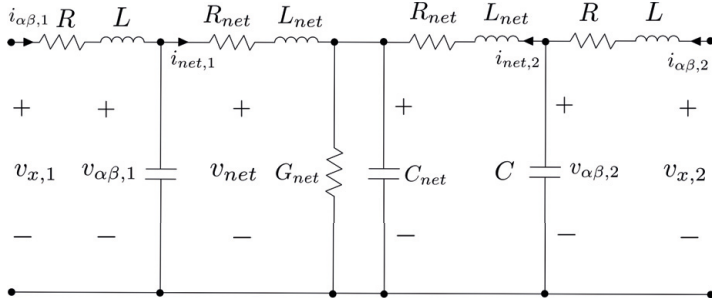
Figure 6.   Two inverters connected in parallel to a conductance load $G_l > 0$ via a $\Pi-$line model.

amplitude at $\mu_1 = \mu_2 = 0.33$, removed the integral action $K_{i,1} = K_{i,2} = 0$, and set all other parameters as before. Our simulation in Fig. 4 displays a prescribed power sharing ratio of 3:1 under resistive load steps at times $t = 0.3$ and $t = 0.7$.

6.   Conclusions

This paper addresses the problem of designing grid-forming inverter control strategies for weak-grid scenarios, those in which no other unit is able to regulate the AC grid frequency. Based on the idea of matching the dynamics of a SM, we enable by feedback the crucial coupling between the inverter DC-side voltage and its AC-side frequency. As a result, the AC grid frequency measurement is replaced by that of the DC-link voltage, further obviating the conventional time-scale separation approach. The seamless compatibility with synchronous machines, set up by the matching control, yields droop and proportional power sharing characteristics, while preserving passivity properties for the inverter. Moreover, the addition of synthetic damping and inertia

109

is straightforward. By pairing the proposed controller with additional outer loops, we also study output voltage regulation in the presence of measurable disturbances. These outer controllers are designed based on passivity-based and disturbance decoupling methods and achieve exact tracking for two quantities if interest: output voltage frequency and its amplitude. In the light of our analysis, a natural counterpart is to investigate the compatibility of networked objectives and to design suitable controllers that encompass multiple converters.

References

Aghir, C., D. Gross, and F. Dörfler (2016). "On the steady state behavior of a nonlinear power grid model". In: *6th IFAC Workshop on Distributed Estimation and Control in Networked Systems*. Submitted. DOI: `10.1016/j.automatica.2017.12.057`.

Akagi, H., Y. Kanazawa, and A. Nabae (1983). "Generalized theory of the instantaneous reactive power in three-phase circuits". In: *IPEC*. Vol. 83. Tokyo, pp. 1375–1386. DOI: `10.1002/eej.4391030409`.

Bevrani, H., T. Ise, and Y. Miura (2014). "Virtual synchronous generators: a survey and new perspectives". *International Journal of Electrical Power & Energy Systems* **54**, pp. 244–254. DOI: `10.1016/j.ijepes.2013.07.009`.

Caliskan, S. Y. and P. Tabuada (2014). "Compositional transient stability analysis of multimachine power networks". *IEEE Transactions on Control of Network systems* **1**:1, pp. 4–14. DOI: `10.1109/TCNS.2014.2304868`.

Chen, Y., R. Hesse, D. Turschner, and H.-P. Beck (2011). "Improving the grid power quality using virtual synchronous machines". In: *2011 international conference on power engineering, energy and electrical drives*. IEEE, pp. 1–6. DOI: `10.1109/PowerEng.2011.6036498`.

Colombino, M., D. Groß, and F. Dörfler (2017). "Global phase and voltage synchronization for power inverters: a decentralized consensus-inspired approach". In: *IEEE 56th Annual Conference on Decision and Control (CDC)*. IEEE, pp. 5690–5695. DOI: `10.1109/CDC.2017.8264518`.

D'Arco, S. and J. A. Suul (2013). "Virtual synchronous machines—classification of implementations and analysis of equivalence to droop controllers for microgrids". In: *2013 IEEE Grenoble Conference*. IEEE, pp. 1–7. DOI: `10.1109/PTC.2013.6652456`.

De Persis, C. and N. Monshizadeh (2017). "Bregman storage functions for microgrid control". *IEEE Transactions on Automatic Control* **63**:1, pp. 53–68. DOI: `10.1109/TAC.2017.2709246`.

Denis, G., T. Prevost, P. Panciatici, X. Kestelyn, F. Colas, and X. Guillaud (2015). "Review on potential strategies for transmission grid operations based on power electronics interfaced voltage sources". In: *2015 IEEE Power & Energy Society General Meeting*. IEEE, pp. 1–5. DOI: 10.1109/PESGM.2015.7286111.

Dörfler, F. and S. Grammatico (2017). "Gather-and-broadcast frequency control in power systems". *Automatica* **79**, pp. 296–305. DOI: 10.1016/j.automatica.2017.02.003.

Dörfler, F., J. W. Simpson-Porco, and F. Bullo (2015). "Breaking the hierarchy: distributed control and economic optimality in microgrids". *IEEE Transactions on Control of Network Systems* **3**:3, pp. 241–253. DOI: 10.1109/TCNS.2015.2459391.

ENTSO-E (2016). *Frequency Stability Evaluation Criteria for the Synchronous Zone of Continental Europe*. Tech. rep. RG-CE System Protection & Dynamics Sub Group.

Escobar, G., A. J. van der Schaft, and R. Ortega (1999). "A hamiltonian viewpoint in the modeling of switching power converters". *Automatica* **35**:3, pp. 445–452. DOI: 10.1016/S0005-1098(98)00196-4.

Fiaz, S., D. Zonetti, R. Ortega, J. Scherpen, and A. van der Schaft (2013). "A port-hamiltonian approach to power network modeling and analysis". *European Journal of Control* **19**:6, pp. 477–485. ISSN: 0947-3580. DOI: 10.1016/j.ejcon.2013.09.002.

Groß, D., C. Arghir, and F. Dörfler (2016). "On the steady-state behavior of a nonlinear power system model". *Automatica*. . Submitted. Available at https://arxiv.org/abs/1607.01575. DOI: 10.1016/j.automatica.2017.12.057.

Groß, D. and F. Dörfler (2017). "On the steady-state behavior of low-inertia power systems". In: *IFAC World Congress*. To appear. DOI: 10.1016/j.ifacol.2017.08.2264.

Guerrero, J. M., M. Chandorkar, T.-L. Lee, and P. C. Loh (2012). "Advanced control architectures for intelligent microgrids—part i: decentralized and hierarchical control". *IEEE Transactions on Industrial Electronics* **60**:4, pp. 1254–1262. DOI: 10.1109/TIE.2012.2194969.

Johnson, B. B., S. V. Dhople, A. O. Hamadeh, and P. T. Krein (2014). "Synchronization of nonlinear oscillators in an lti electrical power network". *IEEE Transactions on Circuits and Systems I: Regular Papers* **61**:3, pp. 834–844. DOI: 10.1109/TCSI.2013.2284180.

Jouini, T., C. Arghir, and F. Dörfler (2016). "Grid-friendly matching of synchronous machines by tapping into the DC storage". *IFAC-PapersOnLine* **49**:22, pp. 192–197. DOI: 10.1016/j.ifacol.2016.10.395.

Karapanos, V., S. de Haan, and K. Zwetsloot (2011). "Real time simulation of a power system with vsg hardware in the loop". In: *IECON 2011-37th Annual Conference of the IEEE Industrial Electronics Society*. IEEE, pp. 3748–3754. DOI: 10.1109/IECON.2011.6119919.

Kroposki, B., B. Johnson, Y. Zhang, V. Gevorgian, P. Denholm, B.-M. Hodge, and B. Hannegan (2017). "Achieving a 100% renewable grid: operating electric power systems with extremely high levels of variable renewable energy". *IEEE Power and Energy Magazine* **15**:2, pp. 61–73. DOI: 10.1109/MPE.2016.2637122.

Ortega, R. and E. Garcia-Canseco (2004). "Interconnection and damping assignment passivity-based control: a survey". *European Journal of control* **10**:5, pp. 432–450. DOI: 10.3166/ejc.10.432-450.

Perez, M., R. Ortega, and J. R. Espinoza (2004). "Passivity-based PI control of switched power converters". *IEEE Transactions on Control Systems Technology* **12**:6, pp. 881–890. DOI: 10.1109/TCST.2004.833628.

Schaft, A. J. van der (2000). *L2-gain and passivity techniques in nonlinear control*. Vol. 2. Springer, New York City, USA.

Sinha, M., F. Dörfler, B. Johnson, and S. Dhople (2015a). "Uncovering droop control laws embedded within the nonlinear dynamics of Van der Pol oscillators". *IEEE Transactions on Control of Network Systems*. DOI: 10.1109/TCNS.2015.2503558.

Sinha, M., F. Dörfler, B. B. Johnson, and S. V. Dhople (2015b). "Uncovering droop control laws embedded within the nonlinear dynamics of van der pol oscillators". *IEEE Transactions on Control of Network Systems* **4**:2, pp. 347–358. DOI: 10.1109/TCNS.2015.2503558.

Tabesh, A. and R. Iravani (2008). "Multivariable dynamic model and robust control of a voltage-source converter for power system applications". *IEEE Transactions on Power Delivery* **24**:1, pp. 462–471. DOI: 10.1109/TPWRD.2008.923531.

Taylor, J. A., S. V. Dhople, and D. S. Callaway (2016). "Power systems without fuel". *Renewable and Sustainable Energy Reviews* **57**, pp. 1322–1336. DOI: 10.1016/j.rser.2015.12.083.

Teodorescu, R., F. Blaabjerg, M. Liserre, and P. C. Loh (2006). "Proportional-resonant controllers and filters for grid-connected voltage-source converters". *IEE Proceedings Electric Power Applications* **153**:5, pp. 750–762.

Torres, M. and L. A. Lopes (2013). "Virtual synchronous generator: a control strategy to improve dynamic frequency control in autonomous power systems". *Energy and Power Engineering* **5**:2A, pp. 32–38.

Trip, S., M. Cucuzzella, C. De Persis, A. van der Schaft, and A. Ferrara (2018). "Passivity-based design of sliding modes for optimal load frequency control". *IEEE Transactions on control systems technology* **27**:5, pp. 1893–1906. DOI: 10.1109/TCST.2018.2841844.

Van Wesenbeeck, M., S. De Haan, P. Varela, and K. Visscher (2009). "Grid tied converter with virtual kinetic storage". In: *2009 IEEE Bucharest PowerTech*. IEEE, pp. 1–7. DOI: 10.1109/PTC.2009.5282048.

Zhong, Q.-C. and G. Weiss (2010). "Synchronverters: inverters that mimic synchronous generators". *IEEE Transactions on Industrial Electronics* **58**:4, pp. 1259–1267. DOI: 10.1109/TIE.2010.2048839.

Zonetti, D., R. Ortega, and A. Benchaib (2014). "A globally asymptotically stable decentralized PI controller for multi-terminal high-voltage DC transmission systems". In: *European Control Conference (ECC), 2014 European*. IEEE, pp. 1397–1403. DOI: 10.1109/ECC.2014.6862419.

Paper II

Frequency synchronization of a high-order multi-converter system

Taouba Jouini   **Zhiyong Sun**

Abstract

We investigate the frequency stability of a high-order multi-converter system. For this, we identify its symmetry (i.e., rotational invariance) generated by a static angle shift and rotation of AC signals. We characterize the synchronous steady state set, primarily determined by the steady state angles and DC power input. Based on eigenvalue conditions of its Jacobian matrix, we show asymptotic stability of the multi-converter system in a neighborhood of the frequency synchronous steady state set by applying the center manifold theory. We guarantee the Jacobian's eigenvalue condition via an explicit approach that requires sufficient damping on DC- and AC-side. Finally, we demonstrate our results based on a numerical example involving a network of DC/AC converters.

1.   Introduction

Electricity production is one of the largest sources of greenhouse gas emissions in the world. Carbon-free electricity will be critical for keeping the average global temperature within the United Nation's target and avoiding the worst effects of climate change [Prachi, 2019]. Prompted by these environmental concerns, the electrical grid has witnessed a major shift in power generation from conventional (coal, oil) into renewable (wind, solar) resources. The massive deployment of distributed, renewable generation had an elementary effect on its operation via power electronics converters interfacing the grid, deemed as game changers of the conventional analysis methods of power system stability and control.

Literature review: Modeling and stability analysis in power system networks is conducted as a matter of perspective from two different angles. First, network perspective suggests an *up to bottom* approach, where DC/AC converter dynamics are regarded as controllable voltage sources and voltage control is directly accessible. The most prominent example is droop control that leads to the study of second-order pendulum dynamics, emulating the swing equation of synchronous machines [Kundur et al., 1994], which resembles the celebrated Kuramoto-oscillator [Dörfler and Bullo, 2012]. The analogy drawn between the two models has motivated a vast body of literature that harness the results available for synchronization via Kuramoto oscillators to analyze frequency stability in power systems. Second, a *bottom to up* approach derives DC/AC converter models from first-order principles, where their governing dynamics are inferred from the circuitry of DC- and AC-side and the intermediate switching block, which can structurally match that of synchronous machines. Recently, the matching control has been proposed in [Arghir et al., 2018] as a promising control strategy, which achieves a structural equivalence of the two models and endows the closed-loop system with advantageous features (droop properties, power sharing, etc.). By augmenting the system dynamics with a virtual angle, the frequency is set to be proportional to DC capacitor voltage deviations, constituting a measure of power imbalance in the grid. This leads to the derivation of higher-order models that describe a network of coupled DC/AC converters on high-order nonlinear manifolds.

Similar to the physical world, where the laws governing interactions in a set of particles are invariant with respect to static translations and rotations of the whole rigid body [Sarlette, 2009], power system trajectories are invariant under a static shift in their angles, or said to possess a *rotational invariance*. The symmetry of the vector field describing the power system dynamics, indicates the existence of a continuum of steady states for the multi-converter (with suitable control that induces/preserves angle symmetry) or multi-machine dynamics. In particular, the rotational invariance is

the topological consequence of the absence of a reference frame or absolute angle in power systems and regarded thus far as a fundamental obstacle for defining suitable error coordinates for the stability analysis. To alleviate this, a common approach is to perform transformations either resulting from projecting into the orthogonal complement, if the steady state set is a linear subspace [Schiffer et al., 2019], or grounding a node [Tegling et al., 2015], where classical stability tools such as Lyapunov direct method can be deployed.

To analyze power system stability, different conditions have been proposed. In [Arghir et al., 2018] and [Caliskan and Tabuada, 2014], sufficient stability conditions are obtained for a single-machine/converter connected to a load. In [Dörfler and Bullo, 2012], a sufficient algebraic stability condition connects the synchronization of power systems with network connectivity and power system parameters. Although these conditions give qualitative insights into the sensitivities influencing stability, they usually require strong and often unrealistic assumptions. For example, the underlying models are of reduced order (mostly first or second order) [Johnson et al., 2013; Dörfler and Bullo, 2012]. Reduced-order systems, where one infers stability of the whole system from looking at only a subset of variables, are not a truthful representation of the full-order dynamics if important assumptions are not met [Khalil, 2002]. Some stability conditions are valid only in radial networks [Schiffer et al., 2019]. Moreover, implicit conditions e.g., based on semi-definite programming are not very insightful [Vu and Turitsyn, 2015].

Contributions: In this work, we ask in essence two fundamental questions: i) Under mild assumptions on input feasibility, how can we describe the behavior of the steady state trajectories of the nonlinear power system in closed-loop with a suitable control that induces/preserves the symmetry, e.g., the matching control [Arghir et al., 2018; Jouini and Sun, 2020]? ii) Based on the properties of the steady state manifold, can we ensure local stability, i.e., local synchronization?

To answer the first question, we study the behavior of the steady state set. For this, we derive a steady state map, which embeds known steady state angles into the DC power inputs to the converters as a function of the network topology and converter parameters. We show that the steady state angles fully describe the steady state behavior and determine all the other states. The steady state map depends on network topology, which is known to play a crucial role in the synchronization of power systems [Sarlette, 2009; Schiffer et al., 2019]. Since the vector field exhibits symmetry with respect to translation and rotation actions, i.e., under a shift in all angles and a rotation in all AC signals, the steady state manifold inherits the same property and every steady state trajectory is invariant under the same actions. This allows us to define a frequency synchronous steady state set generated under these actions.

117

   We address the second question by showing asymptotic stability of the nonlinear trajectories confined to a neighborhood of the frequency synchronous steady state set. For this, we study the stability of the nonlinear dynamics as a direct application of the center manifold theory to the multi-converter power system. We assume that the eigenvalues of the Jacobian evaluated at a frequency synchronous steady state can be split into one mode at zero and the rest in the open-left half-plane. Then, we can decompose the nonlinear system into two interconnected subsystems, whose dynamics are dictated by zero and Hurwitz matrices, respectively. This allows to define a center manifold upon modal transformation, where we use the reduction principle [Wiggins, 1990, p.195] to deduce the stability of the trajectories of the multi-converter system from the dynamics evolving on the center manifold. The point-wise application of the center manifold theory allows to construct a neighborhood of the frequency synchronous steady state set and thereby shows its local asymptotic stability.

   To satisfy the Jacobian eigenvalue condition in an explicit way, we study the linearized system trajectories and pursue a parametric linear stability analysis approach at a frequency synchronous steady state. Towards this, we develop a novel stability analysis for a class of partitioned linear systems characterized by a stable subsystem and one-dimensional invariant subspace. We propose a new class of Lyapunov functions characterized by an oblique projection onto the complement of the Jacobian zero eigenspace, where the inner product is taken with respect to a matrix to be chosen as solution to Lyapunov and $\mathcal{H}_\infty-$algebraic Riccati equations (ARE). For the multi-source power system model, we arrive at explicit stability conditions that depend only on the converter's parameters and steady-state values. In accordance with other works, our conditions require sufficient DC- and AC-side damping.

   Paper organization The paper unfurls as follows: Section 2 presents the model setup based on a high-order power system model. Section 3 characterizes the frequency synchronous steady state set and feasible inputs. Section 4 studies local asymptotic stability of the nonlinear power system using center manifold theory. Section 5 proposes one approach to satisfy the Jacobian's eigenvalue condition. Finally, Section 6 exemplifies our theory via simulations in two test cases and Section 7 concludes the paper.

   Notation: Define an undirected graph $\mathbb{G} = (\mathcal{V}, \mathcal{E})$, where $\mathcal{V}$ is the set of nodes with $|\mathcal{V}| = n$ and $\mathcal{E} \subseteq \mathcal{V} \times \mathcal{V}$ is the set of interconnected edges with $|\mathcal{E}| = m$. We assume that the topology specified by $\mathcal{E}$ is arbitrary and define the map $\mathcal{E} \to \mathcal{V}$, which associates each oriented edge $e_{ij} = (i, j) \in \mathcal{E}$ to an element from the subset $\mathcal{I} = \{-1, 0, 1\}^{|\mathcal{V}|}$ resulting in the incidence matrix $\mathcal{B} \in \mathbb{R}^{n \times m}$. We denote the identity matrix by

$$I = \begin{bmatrix} 1 & 0 \\ 0 & 1 \end{bmatrix},$$
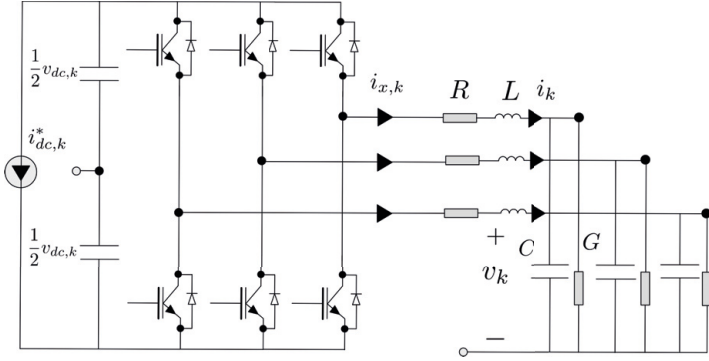
Figure 1.   Circuit diagram of a balanced and averaged three-phase DC/AC converter with $i_{x,k} = \frac{\mu}{2} r^\top (\gamma_k)\, i_k$ and $v_{x,k} = \frac{\mu}{2} r(\gamma_k)\, v_{dc,k}$, see, e.g., [Wittig et al., 2009]. Note that DC conductance is not represented in this diagram.

and $\mathbf{I}$ the identity matrix of suitable dimension $p \in \mathbb{N}$ and $\mathbf{J} = \mathbf{I} \otimes J_2$ with

$$J_2 = \begin{bmatrix} 0 & -1 \\ 1 & 0 \end{bmatrix}.$$

We define the rotation matrix

$$R(\gamma) = \begin{bmatrix} \cos(\gamma) & -\sin(\gamma) \\ \sin(\gamma) & \cos(\gamma) \end{bmatrix},$$

and $\mathbf{R}(\gamma) = \mathbf{I} \otimes R(\gamma)$. Let $\mathrm{diag}(v)$ denote a diagonal matrix, whose diagonals are elements of the vector v and $\mathrm{Rot}(\gamma) = \mathrm{diag}(r(\gamma_k))$, $k = 1 \ldots n$, with $r(\gamma_k) = \begin{bmatrix} -\sin(\gamma_k) & \cos(\gamma_k) \end{bmatrix}^\top$. Let $\mathbb{1}_n$ be the $n-$dimensional vector with all entries being one and $\mathbb{T}^n = \mathbb{S}^1 \times \cdots \times \mathbb{S}^1$ the $n-$dimensional torus. We denote by $d(\cdot, \cdot)$ a distance metric. Given a set $\mathcal{A} \subseteq \mathbb{R}^n$, then $d(z, \mathcal{A}) = \inf_{x \in \mathcal{A}} d(z, x)$ and $T_z \mathcal{A}$ is the tangent space of $\mathcal{A}$ at z. Given a vector $v \in \mathbb{R}^n$, we denote by $v^\perp$ its orthogonal complement, v_k its $k-$th entry. For a matrix A, let $\|A\|_2 = \overline{\sigma}(A)$ denote its induced 2-norm and $\overline{\sigma}(A)$ denote its maximum singular value. Given dynamical system $\dot{x} = f(x)$, $x(0) = x_0$, let $J_f(x^*) = \left. \frac{\partial f(x)}{\partial x} \right|_{x=x^*}$ be the system Jacobian evaluated at some point $x = x^*$.

2.   Modeling and setup

2.1   Multi-source power system dynamics

We start from the following high-order model describing the evolution of the dynamics of $n-$identical three-phase balanced and averaged DC/AC converters interconnected through $m-$identical resistive and inductive lines. An

example of converter circuit diagram is depicted in Figure 1. Each converter is assumed to be in closed-loop with the matching control, a control strategy that renders its dynamics structurally equivalent to a synchronous machine [Arghir et al., 2018]. At the $k-$th converter input u_k, we assign a sinusoid with constant magnitude $\mu \in]0,1[$ and frequency $\dot{\gamma}_k \in \mathbb{R}$ given by,

$$\dot{\gamma}_k = \eta(v_{dc,k} - v_{dc}^*),\tag{1a}$$

$$u_k = \mu \begin{bmatrix} -\sin(\gamma_k) \\ \cos(\gamma_k) \end{bmatrix}, \quad k = 1, \dots, n.\tag{1b}$$

Here $\gamma_k \in \mathbb{S}^1$ is the virtual converter angle in $dq-$frame, after Park transformation, see, e.g., [Kundur et al., 1994], whose angle $\theta_{dq}(t) = \int_0^t \omega^* d\tau$ is chosen to rotate at the nominal steady state frequency $\omega^* > 0$. Moreover, $\eta > 0$ is a control gain defining the slope of the linear map from DC voltage deviation to the oscillator frequency.

The closed-loop converter dynamics are given by the following set of first-order differential equations in $dq-$frame. For simplicity of notation, we will drop the subscript $dq-$from all AC signals.

$$\begin{bmatrix} \dot{\gamma}_k \\ C_{dc}\dot{v}_{dc,k} \\ L\dot{i}_k \\ C\dot{v}_k \end{bmatrix} = \begin{bmatrix} \eta(v_{dc,k} - v_{dc}^*) \\ -K_p(v_{dc,k} - v_{dc}^*) - \frac{\mu}{2}r(\gamma_k)^\top i_k \\ -(R\,I + L\,\omega^* J)\,i_k + \frac{\mu}{2}r(\gamma_k)v_{dc,k} - v_k \\ -(G\,I + C\,\omega^* J)\,v_k + i_k - i_{net,k} \end{bmatrix} + \begin{bmatrix} 0 \\ i_{dc,k}^* \\ 0 \\ 0 \end{bmatrix}.\tag{2}$$

Let $v_{dc,k} \in \mathbb{R}$ denote the voltage across the DC capacitor $C_{dc} > 0$ with nominal value v_{dc}^*. The conductance $G_{dc} > 0$, together with the proportional control gain $\hat{K}_p > 0$ are described by $K_p = G_{dc} + \hat{K}_p > 0$. This results from designing the controllable current source $i_{dc,k} = -\hat{K}_p(v_{dc,k} - v_{dc}^*) + i_{dc,k}^*$, where we denote by $i_{dc,k}^* \in \mathbb{R}$ a constant representing DC-side input to the converter. The modulation amplitude μ, feed-forward current $i_{dc,k}^*$ and the control gain $\hat{K}_p$ are regarded as constants usually determined offline or in outer control loops. See [Arghir et al., 2018] for more details. On the AC-side, let $i_k \in \mathbb{R}^2$ be the inductance current and $v_k \in \mathbb{R}^2$ the output voltage. The filter resistance and inductance are specified by $R > 0$ and $L > 0$, respectively. The capacitor $C > 0$ is set in parallel with the load conductance $G > 0$ to ground and connected to the network via the output current $i_{net,k} \in \mathbb{R}^2$.

Observe that the closed-loop DC/AC converter dynamics (2) match one-to-one those of a synchronous machine with single-pole pair, non-salient rotor under constant excitation [Arghir et al., 2018]. Thus, all the results derived ahead can conceptually also be applied to synchronous machines.

By lumping the states of $n-$converters and $m-$transmission lines and defining the shunt impedance matrices $Z_R = R\,\mathbf{I} + L\,\omega^*\,\mathbf{J}$, $Z_\ell = R_\ell\,\mathbf{I} + L_\ell\omega^*\,\mathbf{J}$ and shunt admittance matrix $Y_C = G\,\mathbf{I} + C\,\omega^*\,\mathbf{J}$, we obtain the following power system model,

$$
\begin{bmatrix} \dot{\gamma} \\ \dot{v}_{dc} \\ \dot{i} \\ \dot{v} \\ \dot{i}_\ell \end{bmatrix} = K^{-1} \begin{bmatrix} \eta(v_{dc} - v_{dc}^*\mathbb{1}_n) \\ -K_p(v_{dc} - v_{dc}^*\mathbb{1}_n) - \frac{1}{2}\mu\mathrm{Rot}(\gamma)^\top i \\ -Z_R\,i + \frac{1}{2}\mu\mathrm{Rot}(\gamma)\,v_{dc} - v \\ -Y_C\,v + i - \mathbf{B}\,i_\ell \\ -Z_\ell\,i_\ell + \mathbf{B}^\top v \end{bmatrix} + K^{-1} \begin{bmatrix} 0 \\ \mathbf{u} \\ 0 \\ 0 \\ 0 \end{bmatrix} , \quad (3)
$$

where we define the angle vector $\gamma = \begin{bmatrix} \gamma_1, \ldots, \gamma_n \end{bmatrix}^\top \in \mathbb{T}^n$, with DC voltage vector $v_{dc} = \begin{bmatrix} v_{dc,1}, \ldots, v_{dc,n} \end{bmatrix}^\top \in \mathbb{R}^n$, the inductance current $i = \begin{bmatrix} i_1^\top, \ldots, i_n^\top \end{bmatrix}^\top \in \mathbb{R}^{2n}$ and AC capacitor voltage $v = \begin{bmatrix} v_1^\top, \ldots, v_n^\top \end{bmatrix}^\top \in \mathbb{R}^{2n}$. The last equation in (3) describes the line dynamics and in particular, the evolution of the line current $i_\ell := \begin{bmatrix} i_{\ell_1}^\top, \ldots, i_{\ell_m}^\top \end{bmatrix}^\top \in \mathbb{R}^{2m}$, where $R_\ell > 0$ is the line resistance, $L_\ell > 0$ is the line inductance and $i_{net} = \mathbf{B}\,i_\ell$. Here $\mathbf{B} = \mathcal{B} \otimes I$ denotes the extended incidence matrix and $K = \mathrm{diag}\,(\mathbf{I}, C_{dc}\,\mathbf{I}, L\,\mathbf{I}, C\,\mathbf{I}, L_\ell\,\mathbf{I})$. The multi-converter inputs are collected in $\mathbf{u} = \begin{bmatrix} i_{dc,1}^*, \ldots, i_{dc,n}^* \end{bmatrix}^\top \in \mathbb{R}^n$.

Let N be the dimension of the state vector $z = \begin{bmatrix} \gamma^\top & \tilde{v}_{dc}^\top & x_{ac}^\top \end{bmatrix}^\top$, whereby we define the vectors of relative DC voltage $\tilde{v}_{dc} = v_{dc} - v_{dc}^*\mathbb{1}_n$, AC quantities $x_{ac} = \begin{bmatrix} i^\top & v^\top & i_\ell^\top \end{bmatrix}^\top$ and the input $u = \begin{bmatrix} 0^\top, \mathbf{u}^\top, \ldots, 0^\top \end{bmatrix}^\top$. By putting it all together, we arrive at the nonlinear power system dynamics compactly described by,

$$
\dot{z} = f(z, u), \quad z(0) = z_0. \quad (4)
$$

Here $z, z_0 \in \mathbb{R}^N$ and $f(z, u)$ denotes the vector field given by (3).

REMARK 1
Without loss of generality, we assume that all DC/AC converters are identical and connected via identical RL lines, that is a common assumption in the analysis of power system stability, see e.g., [Johnson et al., 2013; Simpson-Porco et al., 2013]. Nonetheless, our analysis carries over to more general heterogeneous settings, where converters and lines differ in their parameter values. ■

3. Characterization of the steady state set

In this section, we characterize the steady state set resulting from the rotational invariance of the vector field (4) and feasible DC inputs to the con-

verters as a mapping from known steady state angles.

3.1 Steady state set

Let $\mathcal{M} \subset \mathbb{R}^N$ be a non-empty steady-state manifold resulting from setting (4) to zero and given by,

$$\mathcal{M} = \{z^* \in \mathbb{R}^N \mid f(z^*, u) = 0\}. \tag{5}$$

We are particularly interested in a synchronous steady-state in rotating $dq-$frame with the following properties:

- The converters' frequencies are synchronized at the nominal value ω^* mapped into a nominal DC voltage $v_{dc}^* \geq 1$,

$$[\omega] = \{\omega \in \mathbb{R}_{\geq 0}^n \mid \omega = \omega^* \mathbb{1}_n\},$$
$$[v_{dc}] = \{v_{dc} \in \mathbb{R}_{\geq 0}^n \mid v_{dc} = v_{dc}^* \mathbb{1}_n\}.$$

- The converters' angles are stationary,

$$[\gamma] = \{\gamma \in \mathbb{T}^n \mid \dot{\gamma}^* = 0\}.$$

- The AC quantities, namely the inductor currents, capacitor voltages and line currents are constant at steady state,

$$[x_{ac}] = \{x_{ac} \in \mathbb{R}^{4n+2m} \mid \dot{x}_{ac}^* = 0\}.$$

3.2 Symmetry of the vector field

Consider the nonlinear power system model (4). For all $\theta \in \mathbb{S}^1$, it holds that,

$$f(\theta\, s_0 + S(\theta)\, z, u) = S(\theta)\, f(z, u), \tag{6}$$

where we define the translation vector $s_0 = \begin{bmatrix} \mathbb{1}_n^\top & 0^\top & 0^\top \end{bmatrix}^\top$, the matrix

$$S(\theta) = \begin{bmatrix} \mathbf{I} & 0 & 0 \\ 0 & \mathbf{I} & 0 \\ 0 & 0 & \mathbf{R}(\theta) \end{bmatrix},$$

and the set,

$$\mathcal{S}(z) = \left\{ \begin{bmatrix} (\gamma + \theta\mathbb{1}_n)^\top & \tilde{v}_{dc}^\top & (\mathbf{R}(\theta)\, x)^\top \end{bmatrix}^\top, \theta \in \mathbb{S}^1 \right\}. \tag{7}$$

The symmetry (6) follows from observing that the rotation matrix $\mathbf{R}(\theta)$ commutes with the impedance and admittance matrices Z_R, Z_ℓ, Y_C, the skew-symmetric matrix $\mathbf{J}$ and the incidence matrix $\mathbf{B}$. The symmetry (6) arises

from knowing that the nonlinear power system model (4) has no absolute angle. In fact, the vector field remains invariant with respect to a shift in all angles $\gamma \in \mathbb{T}^n$, corresponding to a translation by s_0 and a rotation in the angles of AC signals by $\mathbf{R}(\theta)$ (up to re-defining the dq−transformation angle to $\theta'_{dq}(t) = \theta_{dq}(t) + \theta$). Notice that for $\theta = 0$, we deduce that $\mathcal{S}(z) = \{z\}$ and hence $z \in \mathcal{S}(z)$.

Consider the steady state manifold $\mathcal{M}$ described by (5). Observe that $z^* \in \mathcal{M}$ pertains to a continuum of steady states, as a consequence of the rotational symmetry (6). Thus, the steady state set is given by,

$$\mathcal{S}(z^*) = \left\{ \left[(\gamma^* + \theta \mathbb{1}_n)^\top \quad 0^\top \quad (\mathbf{R}(\theta)\, x_{ac}^*)^\top \right]^\top , \, \theta \in \mathbb{S}^1 \right\}, \tag{8}$$

that is for all $z^* \in \mathcal{M}$, it holds that $\mathcal{S}(z^*) \subset \mathcal{M}$.

3.3 Steady state map

LEMMA 1—STEADY STATE MAP
Consider the nonlinear power system model (4). Given the steady state angle vector γ^* satisfying $\dot{\gamma}^* = 0$. Then, a feasible input $\mathbf{u}$ is given by,

$$\mathbf{u} = \nu \operatorname{Rot}(\gamma^*)^\top \mathcal{Y} \operatorname{Rot}(\gamma^*) \, \mathbb{1}_n, \tag{9}$$

where $\nu = \frac{1}{4}\mu^2 v_{dc}^* > 0$ and $\mathcal{Y} = (Z_R + (Y_C + \mathbf{B}\, Z_\ell^{-1}\, \mathbf{B}^\top)^{-1})^{-1} \in \mathbb{R}^{2n \times 2n}$.

Proof. We solve for the frequency synchronous steady state z^* by setting (4) to zero. Note that $Y_C + \mathbf{B}\, Z_\ell^{-1}\mathbf{B}^\top$ and $Z_R + (Y_C + \mathbf{B}\, Z_\ell^{-1}\, \mathbf{B}^\top)^{-1}$ are non-singular matrices due to the presence of the load conductance $G > 0$ and the resistance $R > 0$, where $\mathbf{B}\, Z_\ell^{-1}\mathbf{B}^\top$ is a weighted Laplacian matrix. The lines' current vector is described by $i_\ell^* = Z_\ell^{-1}\, \mathbf{B}^\top v^*$, from which follows that $v^* = (Y_C + \mathbf{B}Z_\ell^{-1}\, \mathbf{B}^\top)^{-1}i^*$ for the AC capacitor voltage. The inductance current reads as $i^* = \frac{1}{2}v_{dc}^*\, \mu\, \mathcal{Y} \operatorname{Rot}(\gamma^*) \mathbb{1}_n$. Finally from $\frac{1}{2}\mu \operatorname{Rot}^\top(\gamma^*)i^* = \mathbf{u}$, we deduce (9). $\qquad \square$

Notice that the matrix $\mathcal{Y}$ in (9) has an *admittance-like* structure which is customary in the analysis of power system models and encodes in particular the parameters of the transmission lines and the network topology given by the weighted Laplacian $\mathbf{B}\, Z_\ell^{-1}\, \mathbf{B}^\top$, as well as the converters' parameters (their AC filters, namely given by the impedance and admittance matrices Z_R and Y_C). Once $\gamma^* \in \mathbb{T}^n$ is given, we recover the full vector $z^* \in \mathcal{M}$ associated with a frequency synchronous steady state set $\mathcal{S}(z^*)$ as described in (8).

Equation (9) can be comprehended as a map (in the sense of [Isidori and Byrnes, 1990]),

$$\mathcal{P} : \mathbb{T}^n \to \mathbb{R}^n, \, \gamma^* \mapsto \nu \operatorname{Rot}(\gamma^*)^\top \mathcal{Y} \operatorname{Rot}(\gamma^*) \mathbb{1}_n,$$

that takes as argument γ^* and returns a feasible input $\mathbf{u}$. The angles γ^* can be obtained, e.g., from solving an AC optimal power flow problem. Equation (9) indicates a power balance between the electrical power $P_e^* = \nu \, v_{dc}^* \, \mathrm{Rot}^\top(\gamma^*) \, i^*$ and the DC power given by $P_{dc}^* = v_{dc}^* \mathbf{u}$ at steady state.

4. Local synchronization of multi-converter power system

In this section, we study local asymptotic stability of the steady state set $\mathcal{S}(z^*)$ in (8), as an application of center manifold theory [Wiggins, 1990; Carr, 2012, p.195].

4.1 Preliminaries

We provide some background and review key concepts from center manifold theory [Carr, 2012] that serve as our main tool for proving local asymptotic stability. For this, consider a dynamical system given in normal form,

$$\dot{y} = A_y y + f_1(y, \rho), \tag{10a}$$
$$\dot{\rho} = B_\rho \rho + f_2(y, \rho), \tag{10b}$$

where $A_y \in \mathbb{R}^{c \times c}$ has eigenvalues with zero real part and $B_\rho \in \mathbb{R}^{(n-c) \times (n-c)}$ has eigenvalues with negative real part (or Hurwitz), and f_1 and f_2 are nonlinear functions with the following properties,

$$f_1(0,0) = 0, \quad J_{f_1}(0,0) = 0, \tag{11}$$
$$f_2(0,0) = 0, \quad J_{f_2}(0,0) = 0. \tag{12}$$

An invariant manifold $\mathcal{W}^c$ is a center manifold of (10), if it can be locally expressed as,

$$\mathcal{W}^c = \{(y, \rho) \in \mathcal{W}^0 \,|\, \rho = h(y)\}, \tag{13}$$

where $\mathcal{W}^0$ is a sufficiently small neighbourhood of the origin, $h(0) = 0$ and,

$$J_h(0) = \left. \frac{\mathrm{d}\,h}{\mathrm{d}y} \right|_{y=0} = 0 \,.$$

It has been shown in [Khalil, 2002, Thm. 8.1] that a center manifold always exists and the dynamics of (10) restricted to the center manifold are described by,

$$\dot{\xi} = A_y \, \xi + f_1(\xi, h(\xi)), \tag{14}$$

for a sufficiently small $\xi \in \mathbb{R}^c$. Note that ξ is a parametric representation of the dynamics along points on the center manifold $\mathcal{W}^c$ in (13).

The stability of the system dynamics (10) is analyzed from the dynamics on the center manifold (13) using the reduction principle described in the following theorem.

> THEOREM 2—[WIGGINS, 1990], P.195
> If the origin is stable under (14), then the origin of (10) is also stable. Moreover there exists a neighborhood $\mathcal{W}^0$ of the origin, such that for every $(y(0), \rho(0)) \in \mathcal{W}^0$, there exists a solution $\xi(t)$ of (14) and constants $c_1, c_2 > 0$ and $\gamma_1, \gamma_2 > 0$ such that,
>
> $$y(t) = \xi(t) + r_1(t),$$
> $$\rho(t) = h(\xi(t)) + r_2(t),$$
>
> where $\|r_i(t)\| < c_i\, e^{-\gamma_i t}$, $i = 1, 2$.

Next, we provide background on set stability in the following definition.

DEFINITION 1—SET STABILITY [ANGELI, 2004]
A set $\mathcal{K}$ is called stable with respect to the dynamical system (4), if for all $\epsilon > 0$, there exists $\delta > 0$, so that,

$$d(z_0, \mathcal{K}) \leq \delta \implies d(z(t, z_0), \mathcal{K}) < \epsilon, \quad \forall t \geq 0 \tag{15}$$

■

A set $\mathcal{K}$ is called *asymptotically stable* with respect to a dynamical system (4), if (15) holds and,

$$\lim_{t \to \infty} d(z(t, z_0), \mathcal{K}) = 0.$$

4.2   Local asymptotic stability

Next, we present our main result concerning local asymptotic stability of the set $\mathcal{S}(z^*)$ with respect to the power system dynamics (4). The following assumption on the eigenvalues of the Jacobian of (4) is crucial for our result.

ASSUMPTION 1
Consider the multi-converter system (4) linearized at $z^* \in \mathcal{M}$ and given by,

$$\delta\dot{z} = J_f(z^*)\,\delta z, \tag{16}$$

with $\delta z = z - z^* \in T_{z^*}\mathcal{M}$, $J_f(z^*) = \frac{\mathrm{d}f}{\mathrm{d}z}\big|_{z=z^*}$ its Jacobian matrix. Assume that $J_f(z^*)$ has only one eigenvalue at zero and all other eigenvalues are in the open-left half-plane.

REMARK 2
In Section 5, we suggest one possible approach to satisfy the Jacobian eigen-values' condition in Assumption 1 that leads to sufficient and explicit stability conditions. ∎

We now present our main result in the following theorem.

THEOREM 3—LOCAL ASYMPTOTIC STABILITY
Consider the power system dynamics in (4) under Assumption 1 with a feasible input **u** as in (9). Then, $\mathcal{S}(z^*)$ is locally asymptotically stable. Moreover, there exists a neighborhood $\mathcal{N}$ of $\mathcal{S}(z^*)$ such that for every $z(0) \in \mathcal{N}$, there exists a point $s \in \mathcal{S}(z^*)$, where

$$\lim_{t \to \infty} z(t, z_0) = s.$$

Proof. To prove that $\mathcal{S}(z^*)$ is stable, we consider the system dynamics (4) under Assumption 1. Without loss of generality, assume $z^* = 0$. From Assumption 1, we know there exists a transformation $T \in \mathbb{R}^{N \times N}$, such that $T J_f(0) T^{-1}$ is block diagonal, where $J_f(0)$ is given in (16), with zero for the first vector component and a block diagonal matrix B that is Hurwitz. We rewrite the dynamics of (4) as,

$$\dot{z} = J_f(0) z + (f(z, u) - J_f(0) z),$$

where z is near the origin. Next, by defining $(y, \rho) = T z$, we arrive at the following system dynamics in normal form,

$$\dot{y} = f_1(y, \rho), \tag{17a}$$
$$\dot{\rho} = B \rho + f_2(y, \rho), \tag{17b}$$

where $f_1(0, 0) = 0$, $f_2(0, 0) = 0$ and $J_{f_1}(0, 0) = J_{f_2}(0, 0) = 0$. Now, we show that,

$$\mathcal{W}^c := \{(y, \rho) | (\exists z \in \mathcal{S}(0)) \times ((y, \rho) = T z)\},$$

is a center manifold for the system dynamics (17). First, $\mathcal{W}^c$ is invariant because it consists of steady states of (17). Second, $\mathcal{W}^c$ is tangent to the $y-$axis at $y = 0$. To see this, define

$$\tilde{f}(y, \rho) := f\left(T^{-1} \begin{bmatrix} y \\ \rho \end{bmatrix}\right) = f(z).$$

Then $\mathcal{W}^c = \{(y, \rho) | \tilde{f}(y, \rho) = 0\}$. The row vectors of the Jacobian given by

$$J_{\tilde{f}}(0, 0) = \begin{bmatrix} \frac{\partial \tilde{f}_1(0,0)}{\partial y} & \frac{\partial \tilde{f}_1(0,0)}{\partial \rho} \\ \vdots & \vdots \\ \frac{\partial \tilde{f}_N(0,0)}{\partial y} & \frac{\partial \tilde{f}_N(0,0)}{\partial \rho} \end{bmatrix} = \left.\frac{\mathrm{d}f}{\mathrm{d}z}\right|_{z=0} T^{-1} = J_f(0) T^{-1},$$

span the normal space of $\mathcal{W}^c$ at 0. Since the columns of $T^{-1} = (v(0), \dots)$ consist of the right eigenvectors of $J_f(0)$, by means of $J_f(0) \, v(0) = 0$, $J_f(0) \, T^{-1}$ has a zero first column. This shows that $J_{\tilde{f}}(0,0)$ has its first entry (corresponding to $y-$component) equal to zero. As a consequence, there exists a function $h(y)$ such that $h(0) = 0$ and $\frac{\mathrm{d}h}{\mathrm{d}y}|_{y=0} = 0$ in a neighborhood $\mathcal{W}^0$ of 0, where $\mathcal{W}^c \cap \mathcal{W}^0 = \{(y, \rho) | \rho = h(y)\}$. It follows that the dynamics restricted to $\mathcal{W}^0$ are given by $\dot{\xi} = 0$ because $\mathcal{W}^c$ is a steady state manifold to (17) and thus $f_1(\xi, h(\xi)) = 0$. This shows that $\xi(t) = \xi(0)$. By applying Theorem 2, the solutions for (y, ρ) starting in $\mathcal{W}^0$ are described by,

$$y(t) = \xi(t) + r_1(t),$$
$$\rho(t) = h(\xi(t)) + r_2(t),$$

where $\|r_i(t)\| < c_i e^{-\gamma_i t}$, $i = 1, 2$, for some constants $c_i, \gamma_i > 0$. This implies that,

$$\lim_{t \to \infty} \big(y(t), \rho(t)\big) = \big(\xi(0), h(\xi(0))\big),$$

and thus,

$$\lim_{t \to \infty} z(t) = T^{-1}\big(\xi(0), h(\xi(0))\big) \in \mathcal{S}(0).$$

This argument can be repeated for each point on $\mathcal{S}(0)$ to obtain a cover $\{\mathcal{W}^k\}$ of $\mathcal{S}(0)$. Since $\mathcal{S}(0)$ is compact, we can construct a finite sub-cover to form a neighborhood $\mathcal{N} = \bigcup_k \mathcal{W}^k$ of $\mathcal{S}(0)$. Local asymptotic stability of $\mathcal{S}(0)$ follows directly. $\qquad\square$

Note that our results conceptually apply to prove local asymptotic stability of a synchronous steady state set with respect to trajectories of high-order dynamics of synchronous machines and find an estimate of their region of attraction. Even though our analysis dwells upon a local statement, it can pave the way for a global analysis of the stability of high-order multi-machine or multi-converter system connected through non-trivial lines' conductance, which has been an open problem within the power system community for a long time [Willems, 1976; Chiang, 1989].

5. Sufficient conditions for stability of the linearized system

This section suggests one possible approach to satisfy the eigenvalue condition imposed by Assumption 1 in a sufficient and explicit way for a class of linear systems, that applies later to the stability of the linearized multi-converter system.

5.1 Lyapunov stability of vector fields with symmetries

We develop a stability theory for a general class of linear systems enjoying some of the structural properties featured by the Jacobian matrix (16). For this, we consider a class of partitioned linear systems of the form,

$$\dot{x} = \underbrace{\left[\begin{array}{c|c} A_{11} & A_{12} \\ \hline A_{21} & A_{22} \end{array}\right]}_{A} x, \tag{18}$$

where $x = [x_1^\top \ x_2^\top]^\top$ denotes the partitioned state vector and the block matrices $A_{11}, A_{12}, A_{21}, A_{22}$ are of appropriate dimensions.

In the following, we assume stability of the subsystem characterized by A_{11} and the existence of a symmetry, i.e., an invariant zero eigenspace of A.

ASSUMPTION 2
The block diagonal matrix A_{11} given in (18) is Hurwitz.

ASSUMPTION 3
There exists a vector $p = [p_1^\top \ p_2^\top]^\top$, so that

$$A \cdot \text{span}\{p\} = 0.$$

We are interested in asymptotic stability of the zero subspace $\text{span}\{p\}$. This is equivalent to showing that, all eigenvalues of A have their real part in the open-left half-plane, except for only one at zero, whose eigenspace is $\text{span}\{p\}$. In this manner, we later satisfy Assumption 1. Recall that the standard stability definitions and Lyapunov methods extend from stability of the origin to stability of closed and invariant sets when using the point-to-set-distance rather than merely the norm in the comparison functions; see e.g., [Lin et al., 1996, Theorem 2.8]. In our case, we seek a quadratic Lyapunov function that vanishes on $\text{span}\{p\}$, is positive elsewhere and whose derivative is decreasing everywhere outside $\text{span}\{v\}$. We start by defining a Lyapunov function candidate,

$$V(x) = x^\top \left(P - \frac{P p p^\top P}{p^\top P p} \right) x, \tag{19}$$

where P is *a positive definite* matrix. The Lyapunov function candidate constructed in (19) is based on *two* key observations:

- First, the function $V(x)$ is defined via an oblique projection of the vector $x \in \mathbb{R}^n$ parallel to $\text{span}\{p\}$ onto $\{x \in \mathbb{R}^n | p^\top P x = 0\}$. If $P = \mathbf{I}$, then V is the *orthogonal projection onto* $\text{span}\{p\}^\perp$. Hence, $V(x)$ vanishes on $\text{span}\{p\}$ and is strictly positive definite elsewhere.

- Second, the positive definite matrix P is *a degree of freedom* that can be specified later to provide sufficient and explicit stability conditions.

In standard Lyapunov analysis, one seeks a pair of matrices $(P, \mathcal{Q})$ with suitable positive (semi-) definiteness properties so that the Lyapunov equation $P A + A^\top P = -\mathcal{Q}$ is met. In the following, we apply a helpful twist and parameterize the $\mathcal{Q}$ matrix as a quadratic function $\mathcal{Q}(P)$ of P, which renders the Lyapunov equation, in part, an $\mathcal{H}_\infty$−ARE. We choose the following structure for the matrix $\mathcal{Q}(P)$,

$$\mathcal{Q}(P) = \begin{bmatrix} \mathcal{Q}_1 & H^\top(P) \\ H(P) & H(P)\mathcal{Q}_1^{-1}H(P)^\top + \mathcal{Q}_2 \end{bmatrix}, \tag{20}$$

where $\mathcal{Q}_1$ is a positive definite matrix, $\mathcal{Q}_2$ is a positive semi-definite matrix with respect to span$\{p_2\}$, P is block-diagonal,

$$P = \begin{bmatrix} P_1 & 0 \\ 0 & P_2 \end{bmatrix}, \tag{21}$$

with $P_1 = P_1^\top > 0$ and $P_2 = P_2^\top > 0$, i.e., the Lyapunov function is *separable*, and finally $H(P) = A_{12}^\top P_1 + P_2 A_{21}$ is a shorthand.

We need to introduce a third and final assumption.

ASSUMPTION 4
Consider the matrix $F = A_{22} + A_{21}\mathcal{Q}_1^{-1}P_1 A_{12}$ and the transfer function,

$$\mathcal{G} = \mathcal{C}\,(s\,\mathbf{I} - F)^{-1}\,B,$$

with $B = A_{21}\mathcal{Q}_1^{-1/2}$, $\mathcal{C} = (A_{12}^\top P_1\mathcal{Q}_1^{-1}P_1 A_{12} + \mathcal{Q}_2)^{1/2}$. Assume that F is Hurwitz and $\|\mathcal{G}\|_\infty < 1$.

Assumption 4 will guarantee suitable definiteness and decay properties of the Lyapunov function (21) under sufficient and explicit stability conditions discussed in Section 5.3. Assumptions 2, 3 and 4 recover our requirement for positive definiteness of the matrix P in (21) and semi-definitness (with respect to span$\{p\}$) of $\mathcal{Q}(P)$ in (20) as shown in the following.

COROLLARY 4
Under Assumptions 2, 3 and 4, the matrix P in (21) exists, is unique and positive definite.

Proof. By calculating $P A + A^\top P = -\mathcal{Q}(P)$, where $A, Q(P)$ and P are given respectively by (18), (20) and (21), we obtain

$$\begin{bmatrix} P_1 A_{11} + A_{11}^\top P_1 & H(P)^\top \\ H(P) & P_2 A_{22} + A_{22}^\top P_2 \end{bmatrix} = - \begin{bmatrix} \mathcal{Q}_1 & H(P)^\top \\ H(P) & H(P)\mathcal{Q}_1^{-1}H(P)^\top + \mathcal{Q}_2 \end{bmatrix},$$

the block-diagonal terms of which are

① $P_1 A_{11} + A_{11}^\top P_1 = -\mathcal{Q}_1,$

② $P_2 A_{22} + A_{22}^\top P_2 = -H(P)\mathcal{Q}_1^{-1}H(P)^\top - \mathcal{Q}_2,$

where $H(P) = A_{12}^\top P_1 + P_2 A_{21}$.

Since A_{11} is Hurwitz, there is a unique and positive definite matrix P_1 solving ①. Moreover, ② is equivalent to solving for P_2 the following $\mathcal{H}_\infty-$ARE:

$$P_2 A_{21}\mathcal{Q}_1^{-1}A_{21}^\top P_2 + P_2 F + F^\top P_2 + A_{12}^\top P_1 \mathcal{Q}_1^{-1}P_1 A_{12} + \mathcal{Q}_2 = 0,$$

where $F = A_{22} + A_{21}\mathcal{Q}_1^{-1}P_1 A_{12}$. Under Assumption 4, the pair (F, B) is stabilizable with $B = A_{21}\mathcal{Q}_1^{-1/2}$ and for $\|\mathcal{G}\|_\infty < 1$, Theorem 7.4 in [Scherer, 2001] implies that no eigenvalues of the Hamiltonian matrix

$$\mathcal{H} = \begin{bmatrix} F & B\,B^\top \\ -\mathcal{C}^\top \mathcal{C} & -F^\top \end{bmatrix},$$

are on the imaginary axis with,

$$\mathcal{C} = (A_{12}^\top P_1 \mathcal{Q}_1^{-1}P_1 A_{12} + \mathcal{Q}_2)^{1/2}.$$

By Theorem 7.2 in [Scherer, 2001], there exists a unique stabilizing solution P_2 to ②. Define $E = A_{12}^\top P_1 \mathcal{Q}_1^{-1}P_1 A_{12} + \mathcal{Q}_2 + P_2 A_{21}\mathcal{Q}_1^{-1}A_{21}^\top P_2 \geq 0$. From $Ap = 0$, follows that $A_{12}p_2 = -A_{11}p_1 \neq 0$ (by Hurwitzness of A_{11} under Assumption 2) and since $\mathcal{Q}_2 p_2 = 0$, this implies that $\ker \mathcal{Q}_2 \cap \ker A_{12} = \{0\}$. Therefore, E is a non-singular and positive definite matrix. Since F is Hurwitz, by standard Lyapunov theory [Khalil, 2002], the Lyapunov equation $P_2 F + F^\top P_2 + E = 0$ admits a positive definite solution P_2. □

> COROLLARY 5
> Under Assumptions 2, 3 and 4, the matrix $\mathcal{Q}(P)$ in (20) is positive semi-definite. Additionally, $\ker(A) = \ker(\mathcal{Q}(P)) = \text{span}\{p\}$.

Proof. First, note that by Proposition 4, the matrix $P = P^\top > 0$ and observe that the matrix $\mathcal{Q}(P)$ in (20) is symmetric and the upper left block $\mathcal{Q}_1 > 0$ is positive definite. By using the Schur complement and positive semi-definiteness of $\mathcal{Q}_2$, we obtain that $\mathcal{Q}(P)$ is positive semi-definite. Second, by virtue of $p^\top \mathcal{Q}(P)p = p^\top (P A + A^\top P)p = 0$ due to Assumption 3, it follows that $\text{span}\{p\} \subseteq \ker(\mathcal{Q}(P))$. Third, consider a general vector $s = \begin{bmatrix} s_1^\top s_2^\top \end{bmatrix}^\top$, so that $\mathcal{Q}(P)s = 0$. Given $H(P) = A_{12}^\top P_1 + P_2 A_{21}$, we obtain the algebraic equations $\mathcal{Q}_1 s_1 + H(P)^\top s_2 = 0$, $H(P)s_1 + \left(H(P)\mathcal{Q}_1^{-1}H(P)^\top + \mathcal{Q}_2\right) s_2 = 0$.

One deduces that $\mathcal{Q}_2 s_2 = 0$ and thus $s_2 \in \text{span}\{p_2\}$. The latter implies $s_1 \in -\mathcal{Q}_1^{-1} H(P)^\top \text{span}\{p_2\} \in \text{span}\{p_1\}$ because $\mathcal{Q}(P)\text{span}\{p\} = 0$. Thus, it follows that $s \in \text{span}\{\begin{bmatrix} s_1^\top & s_2^\top \end{bmatrix}^\top\} = \text{span}\{p\}$ and we deduce that $\ker(\mathcal{Q}(P)) = \text{span}\{p\}$. Fourth and finally, for the sake of contradiction, take a vector $\tilde{v} \notin \text{span}\{p\}$, so that $\tilde{v} \in \ker(A) \Rightarrow \tilde{v}^\top \left(A^\top P + P A\right) \tilde{v} = 0 \Rightarrow \tilde{v}^\top \mathcal{Q}(P)\tilde{v} = 0 \Rightarrow \tilde{v} \in \ker(\mathcal{Q}(P))$. This is a contradiction to $\ker(\mathcal{Q}(P)) = \text{span}\{p\}$. Hence, we conclude that $\ker(A) = \ker(\mathcal{Q}(P)) = \text{span}\{p\}$. $\square$

The main result of this section is given by the following lemma.

LEMMA 6
Consider the linear system (18). Under Assumptions 2, 3 and 4, $\text{span}\{p\}$ is an asymptotically stable subspace of A.

Proof. Consider the function $V(x)$ in (19). The matrix P in (21) is positive definite by Proposition 4. By taking $y = P^{1/2}x$ and $w = P^{1/2}p$, the function $V(x)$ can be rewritten as $V(y) = y^\top \left(\mathbf{I} - \frac{ww^\top}{w^\top w}\right) y = y^\top \Pi_w y$. The matrix $\Pi_w = \mathbf{I} - \frac{ww^\top}{w^\top w}$ is a projection matrix onto the orthogonal complement of $\text{span}(w)$ and is hence positive semi-definite with one-dimensional nullspace corresponding to $P^{1/2}\text{span}\{p\}$. It follows that the function $V(x)$ is positive definite for all $x \in \text{span}\{p\}^\perp$. By means of $Ap = \mathcal{Q}(P)p = 0$, it holds that $p^\top P A = p^\top (\mathcal{Q}(P) - A^\top P) = 0$ and we obtain $\dot{V}(x) = -x^\top \mathcal{Q}(P) x$. By Lemma 5, $\dot{V}(x)$ is negative definite for all $x \in \text{span}\{p\}^\perp$. We apply Lyapunov's method and Theorem 2.8 in [Lin et al., 1996] to conclude that $\text{span}\{p\}$ is asymptotically stable. $\square$

5.2 Stability of the linearized multi-DC/AC converter

Our next analysis seeks to find sufficient and explicit conditions, so that the Jacobian of the multi-converter system given in (16) satisfies Assumption 1. For this, consider the linearized system (16) given by the following equations,

$$
\delta \dot{z} = K^{-1}
\begin{bmatrix}
0 & \eta\mathbf{I} & 0 & 0 & 0 \\
-\nabla^2 U(\gamma^*) & -K_p\mathbf{I} & -\Lambda(\gamma^*)^\top & 0 & 0 \\
\Xi(\gamma^*) & \Lambda(\gamma^*) & -Z_R & -\mathbf{I} & 0 \\
0 & 0 & \mathbf{I} & -Y_C & -\mathbf{B} \\
0 & 0 & 0 & \mathbf{B}^\top & -Z_\ell
\end{bmatrix}
\delta z
$$

$$
= \begin{bmatrix} A_{11} & A_{12} \\ \hline A_{21} & A_{22} \end{bmatrix} \delta z. \tag{22}
$$

In (22), the system matrix is the Jacobian $J_f(z^*) = \frac{\mathrm{d}f}{\mathrm{d}z}\big|_{z=z^*}$, $\delta z = \begin{bmatrix} \delta z_1^\top & \delta z_2^\top \end{bmatrix}^\top \in T_{z^*}\mathcal{M}$, corresponding to the partition $\delta z_1 = \begin{bmatrix} \delta\gamma^\top & \delta v_{dc}^\top \end{bmatrix}^\top \in$

$\mathbb{R}^{2n}$, $\delta z_2 \in \mathbb{R}^{6n}$. Moreover, the matrices are given by,

$$\nabla^2 U(\gamma^*) = \frac{1}{4}\mu^2 v_{dc}^* \text{diag}(\text{Rot}^\top(\gamma^*) \, \mathbf{J}^\top \mathcal{Y} \, \text{Rot}(\gamma^*) \, \mathbb{1}_n),$$

$$= \frac{1}{2}\mu \text{diag}((\mathbf{J}\text{Rot}(\gamma^*))^\top i^*),$$

$$\Xi(\gamma^*) = \frac{1}{2}\mu \mathbf{J} \, \text{Rot}(\gamma^*),$$

$$\Lambda(\gamma^*) = \frac{1}{2}\mu v_{dc}^* \, \text{Rot}(\gamma^*),$$

where we consider the smooth potential function,

$$U : \mathbb{T}^n \to \mathbb{R}, \; \gamma \mapsto -\xi \, \mathbb{1}_n^\top \, \text{Rot}^\top(\gamma) \, \mathbf{J}^\top \mathcal{Y} \, \text{Rot}(\gamma^*) \, \mathbb{1}_n.$$

Note that the Jacobian $J_f(z^*)$ has one-dimensional zero eigenspace denoted by,

$$\text{span}\{v(z^*)\} = \text{span}\{\begin{bmatrix} \mathbb{1}_n^\top & 0^\top & (\mathbf{J}\,x^*)^\top \end{bmatrix}^\top\} \subset T_{z^*}\mathcal{M},$$

with $\mathbf{J}\,x^* = \begin{bmatrix} (\mathbf{J}\,i^*)^\top & (\mathbf{J}v^*)^\top & (\mathbf{J}\,i_\ell^*)^\top \end{bmatrix}^\top$. In fact, we can establish a formal link between the linear subspace $\text{span}\{v(z^*)\}$ and the steady state set $\mathcal{S}(z^*)$ in (8) as follows. For all $\theta \in \mathbb{S}^1$,

$$\mathcal{S}(z^*) = z^* + \int_0^\theta v(z^*) \, \mathrm{d}s, = z^* + \int_0^\theta \begin{bmatrix} \mathbb{1}_n \\ 0 \\ \mathbf{J}\,\mathbf{R}(s)\,x^* \end{bmatrix} \mathrm{d}s.$$

In fact, $v(z^*)$ is the tangent vector of $\mathcal{S}(z^*)$ in the $\theta-$direction and lies on the tangent space $T_{z^*}\mathcal{M}$ and $\mathcal{S}(z^*)$ is the angle integral curve of $\text{span}\{v(z^*)\}$.

REMARK 3
We can retrieve the relationship $\text{span}\{v(z^*)\} \subseteq \ker(J_f(z^*))$ from (6) as follows. We set $z = z^* \in \mathcal{M}$ and expand the first-order Taylor polynomial around $\theta' \in \mathbb{S}^1$ of the left hand-side in (6). The right hand-side amounts to zero since $f(z^*, u) = 0$ and we obtain,

$$\left.\frac{\mathrm{d}f}{\mathrm{d}z}\right|_{z=z^*} \left(s_0 + \left.\frac{\mathrm{d}S(\theta)}{\mathrm{d}\theta}\right|_{\theta=\theta'} z^*\right) (\theta - \theta') = 0, \qquad \blacksquare$$

where $\frac{\mathrm{d}f}{\mathrm{d}z}\big|_{z=z^*} = J_f(z^*)$, $s_0 + \frac{\mathrm{d}S}{\mathrm{d}\theta}\big|_{\theta=\theta'} z^* = v(z^*)$. Thus, we recover,

$$J_f(z^*) \, v(z^*) = 0.$$

Next, we consider the linearized model (22) and identify the matrices,

$$A_{11} = \begin{bmatrix} 0 & \eta\mathbf{I} \\ -C_{dc}^{-1}\nabla^2 U(\gamma^*) & -C_{dc}^{-1}K_p\mathbf{I} \end{bmatrix}, \quad A_{12} = \begin{bmatrix} 0 & 0 & 0 \\ -C_{dc}^{-1}\Lambda(\gamma^*)^\top & 0 & 0 \end{bmatrix},$$

$$A_{21} = \begin{bmatrix} L^{-1}\Xi(\gamma^*) & L^{-1}\Lambda(\gamma^*) \\ 0 & 0 \\ 0 & 0 \end{bmatrix}, \quad A_{22} = \begin{bmatrix} -L^{-1}\mathbf{Z}_R & -L^{-1}\mathbf{I} & 0 \\ C^{-1}\mathbf{I} & -C^{-1}\mathbf{Z}_V & -C^{-1}\mathbf{B} \\ 0 & L_\ell^{-1}\mathbf{B}^\top & -L_\ell^{-1}\mathbf{Z}_\ell \end{bmatrix}.$$

Define the Lyapunov function $V(z)$ as in (19) with $v(z^*) := p$ and $v(z^*) = [v_1^{*\top}, v_2^{*\top}]^\top$. Hence, $V(z)$ is positive semi-definite with respect to span$\{v(z^*)\}$. Next, we select the matrix $\mathcal{Q}(P)$ given by (20), set $\mathcal{Q}_1 = \mathbf{I}$, $\mathcal{Q}_2 = \mathbf{I} - v_2^* v_2^{*\top}/v_2^{*\top} v_2^*$ and search for the positive definite matrix P so that,

$$P J_f(z^*) + J_f(z^*)^\top P = -\mathcal{Q}(P).$$

Similar to (21), we choose the block diagonal matrix as,

$$P = \left[\begin{array}{cc|c} P_{11} & P_{12} & 0 \\ P_{12} & P_{22} & 0 \\ \hline 0 & 0 & P_{33} \end{array} \right] = \left[\begin{array}{c|c} P_1 & 0 \\ \hline 0 & P_2 \end{array} \right]. \tag{23}$$

Here, P_{11}, P_{12} and P_{22} are matrices of appropriate dimensions. Notice that the chosen structure of P_1 and the zeros in the off-diagonals in P originate from the physical intuition of the tight coupling between the angle of the converter and its corresponding DC voltage (proportional to the AC frequency), as enabled by the matching control (1). The same type of coupling comes into play in synchronous machines between the rotor angle and its frequency, due to the presence of the electrical power in the swing equation [Kundur et al., 1994]. The matrix P_2 is dense with off-diagonals coupling at each phase, the inductance current of one converter with the others. In the sequel, we show that this structure allows to derive sufficient and explicit conditions that satisfy Assumption 1.

CONDITION 7—PARAMETRIC SYNCHRONIZATION CONDITIONS
Consider $P_{x,k} = \frac{1}{2}v_{dc}^*\mu r^\top(\gamma_k^*)i_k^* > 0$, $Q_{x,k} = \frac{1}{2}v_{dc}^*\mu r^\top(\gamma_k^*)J^\top i_k^* > 0$ and the matrix F in Assumption 4. Assume the following condition is satisfied,

$$\cos(\phi_k) < \sqrt{1 - \frac{\alpha^2}{P_{x,k}^2 + \alpha^2}}, \quad k = 1, \dots, n, \tag{24}$$

133

where,

$$\cos(\phi_k) = \frac{P_{x,k}}{\sqrt{Q_{x,k}^2 + P_{x,k}^2}} \in [0, 1[,$$

is the power factor of k-th converter, $\alpha = \max\left\{\frac{\mu^2 v_{dc}^{*2}}{16\,R}, \frac{\mu\, v_{dc}^{*2}}{4\,\sqrt{Y^{-2}-1}}\right\}$, $Y = \frac{1}{2}\mu v_{dc}^* L^{-1} \sup_\zeta \|(j\zeta\mathbf{I} - F)^{-1}\|_2$, where $Y < 1$. Additionally, assume that,

$$\frac{\frac{\mu}{2}\left(1 + \eta\, C_{dc} v_{dc}^* Q_{x,k}^{-1}\right)}{\sqrt{\frac{4}{v_{dc}^{*2}}\left(Y^{-2} - 1\right) - \frac{1}{4}\mu^2 v_{dc}^{*2}\, Q_{x,k}^{-2}}} < K_p, \quad k = 1, \dots, n. \tag{25}$$

Next, we provide the main result of this section.

LEMMA 8

Consider the linearized closed-loop multi-converter model (22). Under Condition 7, the subspace $\mathrm{span}\{v(z^*)\}$ is asymptotically stable.

Proof. Since $v(z^*) \in \ker(J_f(z^*))$, Assumption 3 is satisfied. If (24) is true, then $r^\top(\gamma_k^*) J^\top i_k^* > 0$, for all $k = 1, \dots n$, the sub-matrix A_{11} is Hurwitz and hence Assumption 2 is also valid.

Next, we verify Assumption 4. First, the matrix P_1 can be identified from specification ① with $\mathcal{Q}_1 = \mathbf{I}$ by the following expressions,

$$P_{11} = \frac{1}{\eta}\left[\frac{1}{2}K_p(\nabla^2 U(\gamma^*))^{-1} + \frac{\nabla^2 U(\gamma^*)}{2K_p}(\mathbf{I} + \eta C_{dc}(\nabla^2 U(\gamma^*))^{-1})\right],$$

$$P_{12} = P_{12}^\top = \frac{1}{2}(\nabla^2 U(\gamma^*))^{-1} C_{dc},$$

$$P_{22} = \frac{C_{dc}}{2K_p}\left(\mathbf{I} + \eta C_{dc}\left(\nabla^2 U(\gamma^*)\right)^{-1}\right).$$

The feasibility of specification ② with the positive semi-definite matrix $\mathcal{Q}_2 = \mathbf{I} - \frac{v_2^* v_2^{*\top}}{v_2^{*\top} v_2^*}$ is given by

$$P_2 A_{21} A_{21}^\top P_2 + P_2 F + F^\top P_2 + N N^\top + \mathcal{Q}_2 = 0, \tag{27}$$

where $F = A_{22} + A_{21} P_1 A_{12}$ and $N = A_{12}^\top P_1$. If Assumption 4 is satisfied, then there exists a positive definite matrix P_2 that satisfies $\mathcal{H}_\infty$−ARE in (27).

Next, we find sufficient conditions, for which F satisfies the Lyapunov equation $P_F F + F^\top P_F = -\mathcal{Q}_F$. We choose P_F and $\mathcal{Q}_F$ to be block-diagonal matrices

$$P_F = \begin{bmatrix} L & 0 & 0 \\ 0 & C & 0 \\ 0 & 0 & L_\ell \end{bmatrix}, \quad \mathcal{Q}_F = \begin{bmatrix} \Gamma & 0 & 0 \\ 0 & 2G\,\mathbf{I} & 0 \\ 0 & 0 & 2R_\ell\mathbf{I} \end{bmatrix},$$

with,

$$\Gamma = 2R\,\mathbf{I} + C_{dc}^{-1}\left(\Xi(\gamma^*)P_{12}\Lambda(\gamma^*)^\top + \Lambda(\gamma^*)P_{12}\Xi(\gamma^*)^\top\right)$$
$$+ 2C_{dc}^{-1}\left(\Lambda(\gamma^*)P_{22}\Lambda(\gamma^*)^\top\right),$$

being itself block-diagonal. Aside from Γ, all diagonal blocks of P_F and $\mathcal{Q}_F$ are positive definite. We evaluate the block-diagonal matrix Γ for positive definiteness by exploring its two-by-two block diagonals, where trace and determinant of each block are positive under,

$$Q_{x,k}^* = \frac{1}{2}v_{dc}^*\mu(r(\gamma_k^*))^\top J^\top i_k^* > \frac{\mu^2 v_{dc}^{*2}}{16\,R}.$$

Furthermore, we impose $\|\mathcal{G}\|_\infty < 1$, by equivalently setting $\sup\limits_{\zeta\in\mathbb{R}}\|\mathcal{C}\,(j\zeta\mathbf{I} - F)^{-1}B\|_2 < 1$, where

$$\mathcal{C} = \left(A_{12}^\top P_1^\top P_1 A_{12} + \mathbf{I} - \frac{(\mathbf{J}x^*)(\mathbf{J}x^*)^\top}{(\mathbf{J}x^*)^\top(\mathbf{J}x^*)}\right)^{1/2}, \quad B = A_{21}.$$

It is sufficient to consider $\|\mathcal{C}\|_2^2 < (\sup\limits_{\zeta\in\mathbb{R}}\|(j\zeta\mathbf{I} - F)^{-1}\|_2\|B\|_2)^{-2}$. Using the triangle inequality for the induced 2-norm, we arrive at $\|\mathcal{C}\|_2^2 \leq \|A_{12}^\top P_1^\top P_1 A_{12}\|_2 + \|\mathcal{Q}_2\|_2$. Since $\|\mathcal{Q}_2\|_2 = 1$, we consider instead,

$$\|A_{12}^\top P_1^\top P_1 A_{12}\|_2 \leq (\sup\limits_{\zeta}\|(j\zeta I - F)^{-1}\|_2\|B\|_2)^{-2} - 1.$$

Additionally, it holds that,

$$\|B\|_2^2 = \|A_{21}\|_2^2 = L^{-2}\|\begin{bmatrix}\Xi^\top\Xi & \Xi^\top\Lambda \\ \Lambda^\top\Xi & \Lambda^\top\Lambda\end{bmatrix}\|_2$$

$$= L^{-2}\|\begin{bmatrix}\Xi^\top\Xi & 0 \\ 0 & \Lambda^\top\Lambda\end{bmatrix}\|_2 = (\frac{1}{2}\mu v_{dc}^*)^2 L^{-2},$$

where the last equality follows from $v_{dc}^* \geq 1$. Define $Y = \frac{1}{2}\mu v_{dc}^*\sup\limits_{\zeta}\|(j\,\zeta\mathbf{I} - F)^{-1}\|_2 L^{-1}$. For $Y < 1$, straightforward calculations show that,

$$\|A_{12}^\top P_1^\top P_1 A_{12}\|_2 = \overline{\sigma}(C_{dc}^{-2}\Lambda(\gamma^*)(P_{12}^2 + P_{22}^2)\Lambda(\gamma^*)^\top) =$$

$$\max_{k=1,\ldots,n} d_k\,\overline{\sigma}(r(\gamma_k^*)r^\top(\gamma_k^*)) < \frac{4}{v_{dc}^{*2}}(Y^{-2} - 1),$$

with,

$$d_k = (r_k^\top(\gamma_k^*)J^\top i_k^*)^{-2} + \frac{1}{4K_p^2}\left(1 + \eta C_{dc}(\frac{1}{2}\mu r^\top(\gamma_k^*)J^\top i_k^*)^{-1}\right)^2.$$

Under
$$4/v_{dc}^{*2}\left(Y^{-2}-1\right)-\max_{k=1,\dots,n}\left(r_k^\top(\gamma_k^*)J^\top i_k^*\right)^{-2}>0,$$

we solve for the gain K_p with $\overline{\sigma}(r(\gamma_k^*)r^\top(\gamma_k^*))=1,\ k=1,\dots,n$, to find,

$$\sqrt{\frac{\max\limits_{k=1,\dots,n}\frac{\mu^2}{4}\left(1+\eta C_{dc}\left(\frac{1}{2}\mu\,r^\top(\gamma_k^*)\,J^\top i_k^*\right)^{-1}\right)^2}{\frac{4}{v_{dc}^{*2}}\left(Y^{-2}-1\right)-\max\limits_{k=1,\dots,n}\left(r^\top(\gamma_k^*)\,J^\top i_k^*\right)^{-2}}}<K_p.$$

This can be simplified into (25). The condition

$$4/v_{dc}^{*2}\left(Y^{-2}-1\right)-\max_{k=1,\dots,n}\left(r_k^\top(\gamma_k^*)J^\top i_k^*\right)^{-2}>0$$

can be written as $Q_{x,k}^2>\frac{\mu^2 v_{dc}^{*4}}{16(Y^{-2}-1)}$ under the assumption that $Y<1$ and we deduce that,

$$\max\left\{\frac{\mu^2 v_{dc}^{*2}}{16\,R},\frac{\mu\,v_{dc}^{*2}}{4\sqrt{Y^{-2}-1}}\right\}<Q_{x,k}.$$

From the definition of the power factor $\cos(\phi_k)=\frac{P_{x,k}}{\sqrt{Q_{x,k}^2+P_{x,k}^2}}$, we arrive at (24). In summary, we arrive at (25) and (24). By applying Theorem 3, we deduce that $\mathrm{span}\{v(x^*)\}$ is asymptotically stable for the linearized system (22). $\qquad\square$

5.3 Results contextualization

Generally speaking, (24) and (25) can be regarded as a requirements on the AC- and DC-side, respectively. Both of them are explicit and sufficient for asymptotic stability.

Condition (24) connects the efficiency of the converter given by the power factor that defines the amount of current producing useful work to the lower bound $\alpha>0$. From (24), the power factor approaches 1, as $\alpha\to0$.

If
$$\max\left\{\frac{\mu^2 v_{dc}^{*2}}{16\,R},\frac{\mu v_{dc}^{*2}}{4\sqrt{Y^{-2}-1}}\right\}=\frac{\mu^2 v_{dc}^{*2}}{16\,R},$$

then (24) depends on the converter's resistance R, modulation amplitude μ, nominal DC voltage v_{dc}^*, and the steady state current i^*. This is a known practical stability condition [Wang et al., 2014]. In fact from (24), sufficient resistive damping is often enforced by *virtual impedance control* which makes $\alpha\to0$.

If
$$\max\left\{\frac{\mu^2 v_{dc}^{*2}}{16\,R},\frac{\mu v_{dc}^{*2}}{4\sqrt{Y^{-2}-1}}\right\}=\frac{\mu v_{dc}^{*2}}{4\sqrt{Y^{-2}-1}},$$

then we can again deploy $\mathcal{H}_\infty$ control to make $\|G_{ac}\|_\infty$ arbitrarily small and thus $\alpha \to 0$. We note that, the AC-side feedback control is crucial to achieve desired steady states for our power system model (4). This can be implemented e.g., via outer loops that take AC measurements and use the classical vector control architecture for the regulation of the inductance current and the output capacitor voltage; see e.g., [D'Arco et al., 2015].

That $Y < 1$ translates into the requirement,

$$\|G_{ac}\|_\infty < \beta, \ \beta = \frac{2\,L}{\mu v_{dc}^*},$$

where $G_{ac}(j\zeta) = (j\zeta \mathbf{I} - F)^{-1}$ asks for $\mathcal{L}_2$ gain from the disturbances on the AC-side to AC signals to be less than β. This can be achieved via $\mathcal{H}_\infty$ control; see [Zhou et al., 1996].

Condition (25) depends on the steady state angles γ^* and the converter and network parameters and asks for damping as for other stability conditions obtained in the literature on the study of synchronous machines [Arghir et al., 2018; Dörfler and Bullo, 2012]. Note that the smaller is the *synchronization gain* $\eta > 0$, the larger is the operating range of the DC damping gain $\widehat{K}_p$.

For more general settings with heterogeneous converters and transmission lines parameters, our stability analysis can be applied and analogous sufficient and explicit conditions to (24) and (25) can be derived.

6. Simulations

The goal of this section is to assess the asymptotic stability of the trajectories of the nonlinear power system (4) in Theorem 3 locally, i.e., by numerically finding an estimate of the region of attraction $\mathcal{N}$ for a given $z^* = [\gamma^{*\top}, 0^\top, v_c^{*\top}, i_\ell^{*\top}]^\top$. Let us consider three identical DC/AC converters in closed-loop with the matching control depicted in Figure 2 and connected via three identical resistive and inductive lines, as in (4) and connected to an inductive and resistive load to ground. Table 1 summaries the converter parameters and their controls (in S.I.).

First, we start by verifying the parametric conditions established in Condition 7 via (24) and (25). We tune the filter resistance $R > 0$ (e.g., using virtual impedance control) and choose the DC-side gain $K_p > 0$ so that (24) and (25) are satisfied, respectively.

Second, we numerically estimate of the region of attraction $\mathcal{N}$ in $\gamma-$space by initializing sample trajectories of the angles depicted in Figure 2 at various locations and illustrate the evolution of the angle trajectories of (4) to estimate a projection of $\mathcal{N}$ into the angle space. As predicted by Theorem 3, we observe that the set $\mathcal{S}(z^*)$ restricted to the angles (relative to their steady
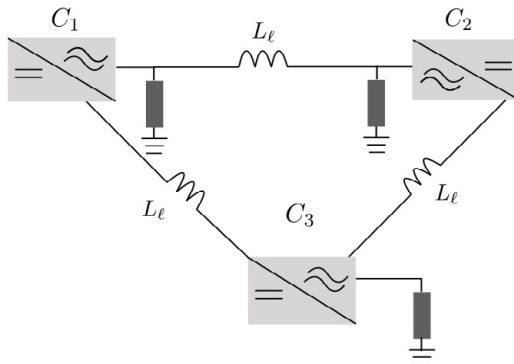
Figure 2.   Three-converter setup with dynamics described by (4), consisting of identical three-phase converters C_1, C_2 and C_3 in closed-loop with the matching control and connected via identical RL lines. The internal dynamics of each converter are modeled as in Figure 1.

state) space, and represented by span$\{\mathbb{1}_3\}$ is asymptotically stable for the sampled angle trajectories of (4).

Figure 3 depicts a projection onto $(\gamma_1, \gamma_2, \gamma_3)-$space of the estimate of $\mathcal{N}$ (in rad and relative to their respective steady state values). The convergence of angle trajectories to the subspace $\mathbb{1}_3$ is guaranteed for initial conditions at distance $d(\gamma(0), \text{span}\{\mathbb{1}_3\}) = \left\| \left(\mathbf{I} - \frac{\mathbb{1}_3 \mathbb{1}_3^\top}{\mathbb{1}_3^\top \mathbb{1}_3} \right) \gamma(0) \right\|_2 = 3.1$ (in rad) resulting from varying the initial angles $\gamma(0)$, while keeping the remaining initial states fixed. In particular, DC voltages and AC currents are also initialized close to their steady state values, as shown in Figure 4. Our simulations show that the DC capacitor voltage v_{dc} in Figure 4 and the AC output capacitor voltage v_c in $abc-$frame (resulting from transforming v into $abc-$frame using inverse Park transformation followed by inverse Clarke transformation) converge to their respective steady state values. This validates our theoretical results from Section 4.

For completeness, we also illustrate a projection of the level sets of the Lyapunov function (19) of an example network consisting of *two* DC/AC converters connected via one RL line (for more details see [Jouini and Dörfler, 2019]) with system dynamics (4) into $(\gamma_1, \gamma_2)-$space (in rad and relative to their respective steady state values) in Figure 5. The parameter values can be
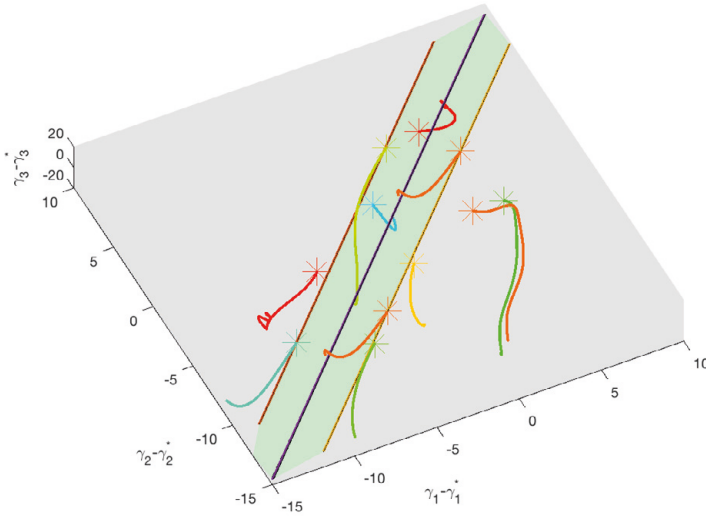
Figure 3. A representation of the region of attraction $\mathcal{N}$ and the frequency synchronous steady state set $\mathcal{S}(z^*)$ restricted to $(\gamma_1 - \gamma_1^*, \gamma_2 - \gamma_2^*, \gamma_3 - \gamma_3^*)$−space of the three DC/AC converter angles and convergence of the sample angle trajectories of (4) to the subspace $\mathbb{1}_3$. The depicted region is obtained from varying the initial angles, while keeping the remaining initial states fixed. A sample of angles deviations initialized within the green area and denoted by stars converge towards the stable set, while some angle trajectories initialized outside the estimated region are divergent. The green area is defined by $d(\gamma(0), \operatorname{span}\{\mathbb{1}_3\}) = \|\left(\mathbf{I} - \frac{\mathbb{1}_3 \mathbb{1}_3^\top}{\mathbb{1}_3^\top \mathbb{1}_3}\right) \gamma(0)\|_2 = 3.1$ (in rad), where $\gamma(0)$ is the angle vector initialized on the boundary of $\mathcal{N}$. All the angles are represented in rad.

taken from Table 1. The vector $v(z^*) = \begin{bmatrix} v_1^\top(z^*) & v_2^\top(z^*) \end{bmatrix}^\top \in \ker(J_f(z^*))$, is given by,

$$v_1(z^*) = \begin{bmatrix} 0.043, & 0.043, & 0, & 0 \end{bmatrix}^\top,$$

and,

$$v_2(z^*) = [-0.0033 \quad -0.0023 \quad -0.0033 \quad -0.0023$$
$$-0.7034 \quad -0.0108 \quad -0.7034 \quad -0.0108 \quad 0 \quad 0].$$

For a positive definite matrix P given by (23), the function $V(x)$ takes positive values everywhere and is zero on the subspace spanned by $v(z^*)$ and given by Figure 5.

139
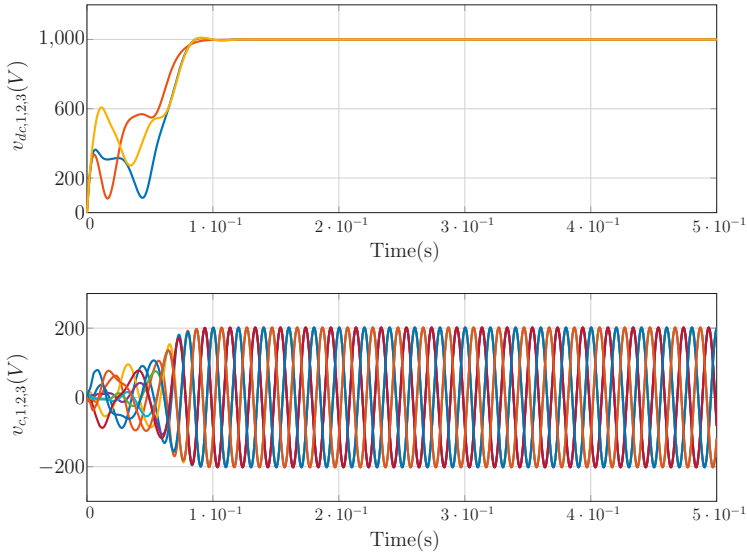
Figure 4. Synchronization of DC capacitor voltages corresponds to frequency synchronization at the desired value. Hereby the angles are initialized at $(-6, -2, -13.15)$ (in rad) and belong to the region estimated in Figure 3. The AC capacitor voltage v_c (resulting from transforming v into $abc-$frame using inverse Park followed by inverse Clarke transformation) converges to a sinusoidal steady state v_c^*.

7.   Conclusions

We investigated the characteristics of a high-order steady state manifold of a multi-converter power system by exploiting the symmetry of the vector field. We studied local asymptotic stability of the steady state set as a direct application of the center manifold theory and provided an operating range for the control gains and converter parameters. Future directions include finding better estimates of the region of attraction using advanced numerical methods and large-scale simulations of the power system dynamics.

Acknowledgment

Table 1. Parameter values of the converters and the RL lines (in S.I).

	C_i, $i = \{1, 2, 3\}$	Lines
i_{dc}^*	16.5	–
v_{dc}^*	1000	–
C_{dc}	10^{-3}	–
G_{dc}	10^{-5}	–
K_P	0.099	–
η	0.0003142	–
μ	0.33	–
L	$5 \cdot 10^{-4}$	–
C	10^{-5}	–
G	0.1	–
R	0.2	–
R_ℓ	–	0.2
L_ℓ	–	$5 \cdot 10^{-5}$
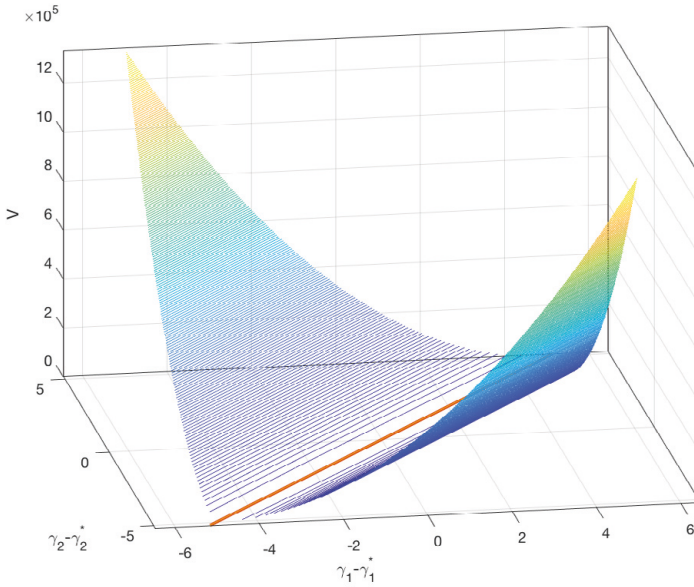
Figure 5. $3D-$representation of the Lyapunov function $V(x)$ in (19) for *two* DC/AC converters in closed-loop with the matching control and connected via an RL line in (3) after a projection into $(\gamma_1 - \gamma_1^*, \gamma_2 - \gamma_2^*)$ space for $P > 0$ as in (23) and the subspace spanning $v(x^*)$. The parameter values can be found in Table 1.

References

Angeli, D. (2004). "An almost global notion of input-to-state stability". *IEEE Transactions on Automatic Control* **49**:6, pp. 866–874. DOI: 10.1109/TAC.2004.829594.

Arghir, C., T. Jouini, and F. Dörfler (2018). "Grid-forming control for power converters based on matching of synchronous machines". *Automatica* **95**, pp. 273–282. DOI: 10.1016/j.automatica.2018.05.037.

Caliskan, S. Y. and P. Tabuada (2014). "Compositional transient stability analysis of multimachine power networks". *IEEE Transactions on Control of Network systems* **1**:1, pp. 4–14. DOI: 10.1109/TCNS.2014.2304868.

Carr, J. (2012). *Applications of centre manifold theory.* Vol. 35. Springer Science & Business Media, Berlin/Heidelberg, Germany.

Chiang, H.-D. (1989). "Study of the existence of energy functions for power systems with losses". *IEEE Transactions on Circuits and Systems* **36**:11, pp. 1423–1429. DOI: 10.1109/31.41298.

D'Arco, S., J. A. Suul, and O. B. Fosso (2015). "A virtual synchronous machine implementation for distributed control of power converters in smartgrids". *Electric Power Systems Research* **122**, pp. 180–197. DOI: 10.1016/j.epsr.2015.01.001.

Dörfler, F. and F. Bullo (2012). "Synchronization and transient stability in power networks and nonuniform Kuramoto oscillators". *SIAM Journal on Control and Optimization* **50**:3, pp. 1616–1642. DOI: 10.1137/110851584.

Isidori, A. and C. Byrnes (1990). "Output regulation of nonlinear systems". *IEEE Transactions on Automatic Control* **35**:2, pp. 131–140. DOI: 10.1109/9.45168.

Johnson, B. B., S. V. Dhople, A. O. Hamadeh, and P. T. Krein (2013). "Synchronization of parallel single-phase inverters with virtual oscillator control". *IEEE Transactions on Power Electronics* **29**:11, pp. 6124–6138. DOI: 10.1109/TPEL.2013.2296292.

Jouini, T. and F. Dörfler (2019). "Local synchronization of two DC/AC converters via matching control". In: *2019 18th European Control Conference (ECC).* IEEE, pp. 2996–3001. DOI: 10.23919/ECC.2019.8795908.

Jouini, T. and Z. Sun (2020). "Fully decentralized conditions for local convergence of DC/AC converter network based on matching control". In: *2020 59th IEEE Conference on Decision and Control (CDC)*, pp. 836–841. DOI: 10.1109/CDC42340.2020.9304344.

Khalil, H. K. (2002). *Nonlinear systems.* Vol. 3. Prentice Hall, Upper Saddle River, NJ.

Kundur, P., N. J. Balu, and M. G. Lauby (1994). *Power system stability and control.* Vol. 7. McGraw-Hill, New York.

Lin, Y., E. D. Sontag, and Y. Wang (1996). "A smooth converse Lyapunov theorem for robust stability". *SIAM Journal on Control and Optimization* **34**:1, pp. 124–160. DOI: 10.1137/S0363012993259981.

Prachi, P. (2019). *How inexpensive must energy storage be for utilities to switch to 100 percent renewables?*

Sarlette, A. (2009). *Geometry and symmetries in coordination control*. PhD thesis. Université de Liège, Belgium. URL: https://hdl.handle.net/2268/9544.

Scherer, C. (2001). "Theory of robust control". *Delft University of Technology*, pp. 1–160.

Schiffer, J., D. Efimov, and R. Ortega (2019). "Global synchronization analysis of droop-controlled microgrids—a multivariable cell structure approach". *Automatica* **109**, p. 108550. DOI: 10.1016/j.automatica.2019.108550.

Simpson-Porco, J. W., F. Dörfler, and F. Bullo (2013). "Synchronization and power sharing for droop-controlled inverters in islanded microgrids". *Automatica* **49**:9, pp. 2603–2611. DOI: 10.1016/j.automatica.2013.05.018.

Tegling, E., B. Bamieh, and D. F. Gayme (2015). "The price of synchrony: evaluating the resistive losses in synchronizing power networks". *IEEE Transactions on Control of Network Systems* **2**:3, pp. 254–266. DOI: 10.1109/TCNS.2015.2399193.

Vu, T. L. and K. Turitsyn (2015). "Lyapunov functions family approach to transient stability assessment". *IEEE Transactions on Power Systems* **31**:2, pp. 1269–1277. DOI: 10.1109/TPWRS.2015.2425885.

Wang, X., Y. W. Li, F. Blaabjerg, and P. C. Loh (2014). "Virtual-impedance-based control for voltage-source and current-source converters". *IEEE Transactions on Power Electronics* **30**:12, pp. 7019–7037. DOI: 10.1109/TPEL.2014.2382565.

Wiggins, S. (1990). *Introduction to applied nonlinear dynamical systems and chaos*. Vol. 2. Springer, New York City, USA.

Willems, J. (1976). "Comments on 'a general Liapunov function for multimachine power systems with transfer conductances'". *International Journal of Control* **23**:1, pp. 147–148. DOI: 10.1080/00207177608922148.

Wittig, B., W.-T. Franke, and F. Fuchs (2009). "Design and analysis of a DC/DC/AC three phase solar converter with minimized dc link capacitance". In: *2009 13th European Conference on Power Electronics and Applications*. IEEE, pp. 1–9.

Zhou, K., J. C. Doyle, K. Glover, et al. (1996). *Robust and optimal control*. Vol. 40. Prentice hall New Jersey.

Paper III

On cost design in applications of optimal control

Taouba Jouini   **Anders Rantzer**

Abstract

A new approach to feedback control design based on optimal control is proposed. Instead of expensive computations of the value function for different penalties on the states and inputs, we use a control Lyapunov function that amounts to be a value function of an optimal control problem with suitable cost design and then study combinations of input and state penalty that are compatible with this value function. This drastically simplifies the role of the Hamilton-Jacobi-Bellman equation, since it is no longer a partial differential equation to be solved, but an algebraic relationship between different terms of the cost. This letter illustrates this idea in different examples, including $\mathcal{H}_\infty$ control and optimal control of coupled oscillators.

1. Introduction

The objective in optimal control problems is to transfer the state of a dynamical system with minimum cost from one point to another. The advent of modern control theory, particularly the formulation of the famous Maximum Principle of Pontryagin [Sassano and Astolfi, 2020] has had a considerable impact on the treatment of optimization theory. Dynamic programming gives necessary and sufficient conditions for optimality and optimal control laws in feedback form, which are very satisfactory but suffer from several drawbacks [Bertsekas, 2011; Liberzon, 2011]. First, analytic solutions can only be obtained in few cases (in particular linear quadratic problems). Second, the Hamilton-Jacobi-Bellman (HJB) partial differential equation (PDE) is in general very hard to solve numerically. The main problem is that the full state space must be discretized and a huge number of samples are needed to get reasonable solutions. This is *the curse of dimensionality*. For this, many efforts have been dedicated to find solutions of value function for HJB-PDE, either numerically [Lukes, 1969] or by relaxing the equality to inequality using approximate dynamic programming [Powell, 2007].

The traditional way to use optimal control is to view the cost function as a set of tuning knobs that can be used to influence the trade-off between control effort and error decay rates. This works well in idealized settings such as linear quadratic control, but for nonlinear problems the map from cost function to the optimal controller could be overwhelmingly complicated. The purpose of this paper is to show that by carefully restricting the choice of the cost function, a simple map from parameters in the cost function to an explicit expression for the optimal controller can be obtained also for nonlinear systems. In fact, our analysis provides a novel perspective for the application of optimal control in engineering systems and makes a significant twist compared to the classical approach. The idea is that, once a stabilizing feedback controller with a (control) Lyapunov function is found, then by appropriate choice of the cost function, involving state and input penalties, the control Lyapunov function satisfies the HJB equation and is a value function of the optimal control problem. As a consequence, a whole family of other cost functions will fit as well for different penalties on the states and inputs. This makes it possible to design stabilizing controllers that are uniquely optimal for nonlinear systems in a manner comparable to linear quadratic control for linear systems. Our approach keeps a simple structure of the cost for nonlinear systems, while adding suitable parametrization and thus circumvents the computational complexity related to solving for a value function by suggesting a fixed (control) Lyapunov function a priori. For this, we showcase the role the cost design plays in two typical settings of optimal control problems: first for nominal or disturbance-free and second for disturbance attenuation or robust $\mathcal{H}_\infty$ optimal control [Scherer, 2001; Zhou

and Doyle, 1998; Ba sar and Bernhard, 2008]. Finally, we clarify our results with examples related to classical equations in linear and nonlinear control theory. As a continuation of ideas from [Jouini et al., 2021], we opt for an application to coupled oscillators that can represent e.g., controlled inverters in power systems.

The paper unfurls as follows: Section 2 motivates and provides the main result on cost design for the nominal and disturbance attenuation case. Section 3 applies our theory to coupled oscillators with numerical simulations.

Notation: Let $\mathbb{1}_n$ denote the column vector of all ones and I_n the $n-$th dimensional identity matrix. We denote by $P > 0$ a symmetric and positive definite matrix and $\mathbb{R}_{>0}$ be the set of positive real numbers. Let $\|\cdot\|_P = \sqrt{(\cdot)^\top P (\cdot)}$. Given a vector v, let $\|v\|_\infty = \sup_{i=1...n} |v_i|$, $\underline{\sin}(v)$ and $\underline{\cos}(v)$ be the vector-valued sine and cosine functions. Given a differentiable function $V(x)$, let $\nabla_x V = \frac{\partial V}{\partial x}$ be the gradient of V at x and $\nabla_x^2 V$ is the Hessian of V at x. Given a matrix A, let $\text{Im}(A)$ denote its image space. Consider a connected undirected graph $G = (\mathcal{V}, \mathcal{E})$ consisting of $|\mathcal{V}| = n$ nodes and $|\mathcal{E}| = m$ edges. By assigning an arbitrary orientation to the m edges, the incidence matrix $\mathcal{B} \in \mathbb{R}^{n \times m}$ is defined element-wise as $\mathcal{B}_{il} = 1$, if node i is the sink of the $l-$th edge, $\mathcal{B}_{il} = -1$ if i is the source of the $l-$th edge, and $\mathcal{B}_{il} = 0$ otherwise. We denote by $\mathcal{N}_i$ the neighbor set of node $i \in \mathcal{V}$.

2.   Main result

We start our analysis with the following motivating example.

EXAMPLE 1
Example 1: For the matrices $R = R^\top > 0$, consider the following nonlinear optimal control problem

$$V(x_0) := \underset{u}{\text{minimize}} \quad \int_0^\infty \left(q(x(s)) + \|u(s)\|_R^2 \right) \mathrm{d}s,$$
$$\text{subject to} \quad \dot{x} = -\underline{\sin}(x) + u, \quad x(0) = x_0,$$
$$x \in \mathcal{X} = \{x \in \mathbb{R}^n : \{\|x\|_\infty < \pi/2 : \mathbb{1}^\top \underline{\cos}(x) \geq c\},$$

for some $0 < c < n$, for two different cases,

Case 1:	$q(x) = \|x\|^2,$
Case 2:	$q(x) = \|\underline{\sin}(x)\|_{I_n + R^{-1}/4}^2.$

The first case may look simpler on the surface, since the cost function is quadratic in x. However, a closer look at Case 1 leads to a HJB partial differential equation, that is difficult to solve. At the same time, as we will

see in the remainder, Case 2 is a special case of a rich class of problems that have a simple explicit solution. In fact, the optimal control law is given by

$$u^*(x) = -\frac{1}{2}R^{-1}\underline{\sin}(x),$$

and the value function amounts to

$$V(x) = -\mathbb{1}_n^\top \underline{\cos}(x) + n,$$

To see that V is positive definite, note that $V(0) = 0$ and $V(x)$ is strictly convex and thus positive definite ($\nabla_x^2 V(x) > 0$ for all $x \in \mathcal{X}$). Notice that the matrix R appears in the expression for q, but not in the value function V. Hence, when the penalty on the input is increased, the penalty on the corresponding state is decreased. This makes it convenient to use R for tuning with appropriate trade-offs between control effort and error decay. ∎

Motivated by the previous example, we consider the following nonlinear optimal control problem

$$\underset{u}{\text{minimize}} \quad \underset{w}{\text{maximize}} \quad \int_0^\infty q(x, R, S) + \|u\|_R^2 - \xi\|w\|_S^2 \, ds, \qquad (1\text{a})$$

$$\text{subject to} \quad \dot{x} = f(x) + G^\top(x)\,u + \overline{G}^\top(x)\,w, \qquad (1\text{b})$$

$$x(0) = x_0.$$

Here, $x \in \mathbb{R}^n$ denotes the state vector, $x(0) = x_0$ is the initial state and $f(x)$ is a nonlinear vector field representing a mapping from $\mathbb{R}^n$ to $\mathbb{R}^n$. We assume that $f(x)$ is continuous and locally Lipschitz with $f(0) = 0$, that is the zero state is a steady state when no inputs are applied. The input matrix $G(x) = [g_1^\top(x), \ldots, g_m^\top(x)]^\top \in \mathbb{R}^{m \times n}$ is given by the nonlinear functions $g_i(x)$, $i = 1, \ldots m$ that are mappings from $\mathbb{R}^n$ to $\mathbb{R}^n$ and continuous over $\mathbb{R}^n$. The disturbance input matrix $\overline{G}(x) = [\overline{g}_1^\top(x), \ldots, \overline{g}_{n_w}^\top(x)]^\top \in \mathbb{R}^{n_w \times n}$ and given by the nonlinear functions $\overline{g}_i(x)$, $i = 1, \ldots n_w$, that are mappings from $\mathbb{R}^n$ to $\mathbb{R}^n$ and continuous over $\mathbb{R}^n$. We denote by $w \in \mathbb{R}^{n_w}$ an unknown disturbance, ξ is a positive constant, $R = R^\top > 0$, $S = S^\top > 0$ are design matrices. Moreover, the mapping $q : \mathbb{R}^n \to \mathbb{R}_{>0}$ vanishes only at the origin, that is $q(0) = 0$ and will be determined in the remainder.

Our goal is to find a state feedback controller $u^*(x) \in \mathbb{R}^m$ that solves the following Hamiltonian-Jacobi-Isaacs-Equation (HJIE) to optimality.

$$\min_u \max_w \left\{ L(x, u, w, R, S) + \nabla_x^\top V \left(f(x) + G^\top(x)\,u \right) \right\} = 0, \qquad (2)$$

where $L(x, u, w, R, S) = q(x, R, S) + \|u\|_R^2 - \xi\|w\|_S^2$, and $V : \mathbb{R}^n \mapsto \mathbb{R}_{>0}$ is the value function of the optimal control problem, defined as [Ba sar and

Bernhard, 2008, Ch.2],

$$V(x_0) := \inf_u \sup_w \int_0^\infty \left(q(x, R, S) + \|u\|_R^2 - \xi \|w\|_S^2 \right) \mathrm{d}s.$$

Throughout this work, we illustrate feedback control synthesis via cost design and using a *control Lyapunov* function [Sontag, 1999], i.e., a Lyapunov function for the closed-loop system associated with some choice of the control law.

2.1 Cost design for optimal control

We start our analysis with the nominal optimal control problem (1) and set $w = 0$. In the subsequent analysis, we propose an approach to solve the nonlinear control problem (1) to optimality with an appropriate choice of the function $q(x, R)$ in the following theorem.

THEOREM 1

Consider the nominal optimal control problem (1), i.e., when $w = 0$. Let $V : \mathbb{R}^n \mapsto \mathbb{R}_{>0}$ be a continuously differentiable function associated with a stabilizing feedback control law

$$u^*(x, R) = -\frac{1}{2} R^{-1} G(x) \nabla_x V, \tag{3}$$

where,

$$\nabla_x V^\top \left(f(x) + G^\top(x) u^*(x, R) \right) < -\|u^*(x, R)\|_R^2. \tag{4}$$

Define

$$q(x, R) = -\nabla_x V^\top \left(f(x) + G^\top(x) u^*(x, R) \right) - \|u^*(x, R)\|_R^2. \tag{5}$$

Then, the following statements hold:

1. The unique optimal control is given by u^* in (3).

2. The optimal control problem (1) has the optimal value $V(x_0)$.

Proof. Consider the Hamiltonian function

$$H(x, u, \lambda) = L(x, u) + \lambda^\top (f(x) + G^\top(x) u),$$

where $\lambda \in \mathbb{R}^n$ is the vector of co-state variables. We minimize $H(x, \lambda)$ by calculating,

$$\frac{\partial H(x, u, \lambda)}{\partial u} = 2 R u^*(x) + G(x) \lambda.$$

The optimal controller reads as,

$$u^*(x) = -\frac{1}{2}R^{-1}G(x)\,\lambda = -\frac{1}{2}R^{-1}G(x)\nabla_x V,$$

where we set $\lambda = \nabla_x V$, following [Vinter, 2010, Ch.1.4]. This coincides with the stabilizing controller (3).

For the sufficiency for optimality of (3), we plug-in the controller (3) into (2) and obtain,

$$q(x, R) - \|G(x)\nabla_x V\|_{R^{-1}}^2 + \nabla_x^\top V f(x) = 0. \qquad \square$$

By choice of the function $q(x, R)$ in (5), the HJBE is satisfied. The positive definiteness of $q(x, R)$ follows from the inequality (4). We conclude that V is a value function and the control law (3) is sufficient for optimality. The optimal value is given by $V(x_0)$ and the proof is standard. See e.g., [Liberzon, 2011, Ch 5.]

REMARK 1
We make the following observations:

- The inequality (4) is equivalent to,

$$\dot{V}(x) < -\|u^*(x)\|_R^2.$$

  This implies by Lyapunov's second method that the origin is asymptotically stable for all system trajectories in closed-loop with (3).

- Our approach relies on feedback design via a control Lyapunov function $V(x)$ to find a stabilizing controller $u^*(x)$ of the form (3). By cost design of $q(x, R)$ as defined in (5), $V(x)$ is a value function of (1) and we recover the optimal controller (3).

- Given a control Lyapunov function V, the matrix $R > 0$ represents a tuning knob that can be used to improve the error decay or minimize the control effort. Note that V is a value function of the optimal control problem (1) with any positive definite matrix R', where $R' \leq R$ and associated with the cost function $L(\cdot, R')$ given in (1).

- The cost design in (5) exploits the intrinsic properties of the origin of the open-loop or unforced system (1b) (i.e., when $u = 0$) to achieve optimality. In particular, if $\nabla_x^\top V f(x) < 0$, then the inequality (4) is always satisfied (for any positive definite R) and the origin of the unforced system is asymptotically stable with the Lyapunov function $V(x)$. In this case, the matrix $R > 0$ can be tuned *arbitrarily* with the same fixed $V(x)$. ∎

Example 2 (Linear systems) Consider the following LTI system together with $q(x, R) = x^\top Q(R)\, x$, where $Q(R) \in \mathbb{R}^{n \times n}$ is a matrix to be determined with $R = R^\top > 0$.

$$\dot{x} = A\, x + B\, u, \; x(0) = x_0, \tag{6}$$

where $A \in \mathbb{R}^{n \times n}$, $B \in \mathbb{R}^{n \times m}$, $u \in \mathbb{R}^m$ and $x_0 \in \mathbb{R}^n$. Given the Lyapunov function defined by

$$V(x) = \frac{1}{2}\, x^\top P\, x, \; P = P^\top > 0,$$

we apply Theorem 1 and the optimal controller is given by,

$$u^*(x, R) = -\frac{1}{2} R^{-1} B^\top P\, x. \tag{7}$$

We demonstrate in the sequel, that the application of optimal control theory is simplified, if we keep P fixed and only tune the matrices R and consequently $Q(R)$ given as in (5) by,

$$Q(R) = \frac{1}{4} P\, B\, R^{-1} B^\top P - A^\top P - P\, A. \tag{8}$$

Given a positive definite Q defined in (8), the matrix R can be tuned by choice of any positive definite matrices $R' \le R$ with $Q(R')$ in (8). Thus, we do not need to resolve the algebraic Riccati equation (8) for every value of the input matrix R, while fixing the positive definite matrix P.

Special case: Under the assumption that A is asymptotically stable, let $P > 0$ satisfy,

$$P\, A + A^\top P = -Q^*, \; Q^* = Q^{*\top} > 0. \tag{9}$$

Then, the matrix $Q(R')$ in (8) is a positive definite matrix for any other positive definite matrix $R' > 0$. The resulting control law (7) is optimal using the matrix P in (9).

The following illustrative example is taken from [Jouini et al., 2021].

Example 3 (no dynamics): Consider the optimal control problem described by,

$$\underset{u}{\text{minimize}} \quad \int_0^\infty q(x(s)) + \|u(s)\|_R^2 \, \mathrm{d}s, \; R = R^\top > 0,$$

$$\text{subject to} \quad \dot{x} = u, \quad x(0) = x_0,$$

where $x \in \mathbb{R}^n$ is the state vector, $u \in \mathbb{R}^n$ is the control input and the mapping $q(x, R)$ is to be determined. Given a continuously differentiable function $V(x) > 0$ with $V(0) = 0$, we arrive at the optimal feedback controller,

$$u^*(x, R) = -\frac{1}{2} R^{-1} \nabla_x V, \tag{10}$$

151

associated with the cost function given by Theorem 1 as

$$q(x, R) = \frac{1}{4} \|\nabla_x V\|_{R^{-1}}^2.$$

Observe that, due to the trivial system dynamics, i.e., $f(x) = 0$, we can select any other control input matrix $R' > 0$ with $L(x, R')$, while assuring optimality of $u^*(x, R')$ in (10).

2.2 Cost design for $\mathcal{H}_\infty-$control

We now turn our attention to the disturbed/robust optimal control problem (1) by setting $w \neq 0$. We arrive to the following result.

> PROPOSITION 2
> Consider the robust optimal control problem (1) together with continuously differentiable function $V : \mathbb{R}^n \mapsto \mathbb{R}_{>0}$ associated with a controller u^* in (3). Let $w^*(x) = \frac{1}{2\xi} S^{-1}\overline{G}(x)\nabla_x V$. Assume that,
>
> $$\nabla_x V^\top \left(f(x) + G^\top(x) u^*(x) + \overline{G}^\top(x) w^*(x) \right) < -\|u^*(x)\|_R^2 + \xi \|w^*(x)\|_S^2, \tag{11}$$
>
> and define
>
> $$q(x, R, S) = -\nabla_x V^\top \left(f(x) + G^\top(x) u^*(x) + \overline{G}^\top(x) w^*(x) \right)$$
> $$- \|u^*(x)\|_R^2 + \xi \|w^*(x)\|_S^2. \tag{12}$$
>
> Then,
>
> 1. The optimal control u^* is given by (3).
>
> 2. The robust optimal control problem (1) has the optimal value $V(x_0)$.

Proof. For $w = 0$, the optimal controller is given by (3). For $u = 0$, we determine the worst case disturbance $w = w^*$, i.e., that maximizes the Hamiltonian function,

$$H(x, u, \nabla_x V) = \max_w \{L(x, u, w) + \nabla_x^\top V(f(x) + G_w^\top(x) w)\}.$$

This is achieved at $w = w^*$, where

$$-2\xi S w^* + \overline{G}(x)\nabla_x V = 0,$$

which in turn implies that,

$$w^*(x) = \frac{1}{2\xi} S^{-1}\overline{G}(x)\nabla_x V. \tag{13}$$

Next, we plug in (3) into HJIE (2) and obtain,

$$q(x, R, S) + \nabla_x^\top V \left(f(x) - \frac{1}{4} G^\top(x) R^{-1} G(x) \nabla_x V \right)$$
$$+ \nabla_x^\top V \overline{G}^\top(x) \, w^*(x) - \xi \|w^*(x)\|_S^2 = 0. \qquad \square$$

By letting $w^*(x)$ as in (13), we arrive at the function $q(x, R, S)$ in (12) and the HJIE in (2) is satisfied. The positive definiteness of $q(x, R, S)$ is guaranteed by (11). This shows that V is a value function of the robust optimal control problem (1). The optimal value is given by $V(x_0)$ and the proof is standard. See e.g., [Ba sar and Bernhard, 2008, Thm 4.15].

REMARK 2
We have the following observations:

- The system in closed-loop with (3) is finite-gain $\mathcal{L}_2-$ stable with $\mathcal{L}_2$ gain less than or equal to $2\sqrt{\xi}$.

- For a given value function $V(x)$, the design matrices $R > 0$ and $S > 0$ are tuning knobs that can be exploited to penalize the control input and disturbance deviations with the same V and any positive definite matrices R' and S' with $R' \leq R$, $S' \geq S$ and $L(\cdot, R', S')$ in (1).

- If it holds that,

$$\nabla_x^\top V(f(x) + \overline{G}^\top(x) \, w^*(x)) < 0,$$

then, the origin is asymptotically stable for the worst case disturbance $w^*(x)$ and $V(x)$ is a Lyapunov function of the unforced system. Thus, condition (11) is always satisfied and $q(x, R', S')$ in (16) is positive definite independently of the choice of R' and S' and we can tune these design matrices arbitrarily using the same fixed V. ∎

We illustrate our approach using the following example.
Example 4 (Linear systems) Given the LTI system,

$$\dot{x} = A\,x + B\,u + \overline{B}\,w, \quad x(0) = x_0 \qquad (14)$$

where $\overline{B} \in \mathbb{R}^{n \times n_w}$ is disturbance input matrix and $w \in \mathbb{R}^{n_w}$ is unknown additive disturbance. We define the cost function,

$$L(x, u, w, R, S) = \|x\|_Q^2 + \|u\|_R^2 - \xi \|w\|_S^2, \ \xi > 0. \qquad (15)$$

Following Proposition 2, we select

$$Q(R,S) = \frac{1}{4}PBR^{-1}B^\top P - \frac{1}{4\xi}P\overline{B}S^{-1}\overline{B}^\top P - PA - A^\top P. \qquad (16)$$

Given a positive definite matrix P, so that $Q > 0$, where Q is given in (16). Then we can tune the design matrices S and R by choice of positive definite matrices R' and S' with $R' \le R$ and $S' \ge S$ using the same matrix P with $L(\cdot, R', S')$ in (15).

Special case: Under the assumption that A is asymptotically stable, given a positive definite solution $P = K^{-1}$ where,

$$A K + K A^\top + \frac{1}{4\xi}\overline{B}^\top S^{-1}\overline{B} < 0,$$

then $Q(R', S') > 0$ as given in (16) and for any other positive definite matrices R' and S', the control law (7) is optimal using the same matrix P with $L(\cdot, R', S')$ in (15).

3.   Application

3.1   Optimal control of coupled oscillators

Consider a network of $n-$coupled oscillators whose $i-$th oscillator dynamics are described by the following differential equations.

$$\dot{\theta}_i = \omega_i, \qquad i = 1 \ldots n, \qquad (17)$$

$$M_i\dot{\omega}_i = -D_i\,\omega_i - \sum_{j \in \mathcal{N}_i} b_{ij}\left(\sin(\theta_{ij}) - \sin(\theta_{ij}^*)\right),$$

with $M_i > 0$ and $D_i > 0$ and $b_{ij} > 0$ denotes the coupling strength between the oscillators i and j. Each oscillator is represented by its phase angle $\theta_i \in \mathbb{R}$ and frequency $\omega_i \in \mathbb{R}$. Let $\omega = [\omega_1, \ldots, \omega_n]^\top$, $\theta = [\theta_1, \ldots, \theta_n]^\top$ and $\theta^* = [\theta_1^*, \ldots, \theta_n^*]^\top$ be the vector of the relative (to a nominal) oscillator frequencies, oscillator angles and nominal steady state angles respectively. Define $\theta_{ij} = \theta_i - \theta_j$ and $\theta_{ij}^* = \theta_i^* - \theta_j^*$. Let $\mathcal{B}$ be the incidence matrix of the underlying graph G.

Given a trajectory $[\theta(t)^\top, \omega(t)^\top]^\top$ of (17), then $[(\theta(t) + \alpha\mathbb{1}_n)^\top, \omega(t)^\top]^\top$, $\alpha \in \mathbb{R}$ is also a trajectory of the system (17). To eliminate this rotational invariance, we consider the following coordinate transformation,

$$\delta(t) = \mathcal{B}^\top\theta(t) \in \mathbb{R}^m. \qquad (18)$$

Let θ^s be an induced steady state angle of (19) with steady state frequency $\omega^* = 0$, $\delta^s = \mathcal{B}^\top\theta^s$ and $\delta^* = \mathcal{B}^\top\theta^* \in \mathbb{R}^m$ be the nominal angle differences.

Observe that local asymptotic stability of $[\delta^{s\top}, 0^\top]^\top$ is equivalent to local asymptotic convergence of the solutions of (17) to $[\theta^{s\top}, 0^\top]^\top$. See e.g., [Monshizadeh et al., 2017]. Next, we make the following assumption.

ASSUMPTION 1—[MONSHIZADEH ET AL., 2017]
  Assume that the steady state vector $\delta^s \in \mathbb{R}^m$ satisfies,

$$\mathcal{B}\,\Xi\,\sin(\delta^s) = \mathcal{B}\,\Xi\,\sin(\delta^*),$$

for all $\delta^s \in \mathrm{Im}(\mathcal{B}^\top) \cap (-\frac{\pi}{2}, \frac{\pi}{2})^m$.

Next, consider the following optimization problem,

$$\begin{aligned}
\underset{u}{\text{minimize}} \quad & \int_0^\infty q(\delta(s), \omega(s)) + \|u(s)\|_R^2 - \xi\,\|w(s)\|_S^2 \,ds \\
\text{subject to} \quad & \dot{\delta} = \mathcal{B}^\top \omega + u, \\
& M\dot{\omega} = -D\,\omega - \mathcal{B}\,\Xi\,(\underline{\sin}(\delta) - \underline{\sin}(\delta^*)) + w, \qquad (19) \\
& (\delta(0), \omega(0)) = (\delta_0, \omega_0),
\end{aligned}$$

where $M > 0$ and $D > 0$ are diagonal matrices of inertia and damping coefficients and the coupling strengths $b_{ij} > 0$ are collected in the diagonal matrix $\Xi = \mathrm{diag}(b_{ij})$. Let ξ be a positive constant and $R = R^\top$ and $S = S^\top$ be positive definite matrices, $u = [u_1, \ldots, u_m]^\top \in \mathbb{R}^m$ be the input and $w = [w_1, \ldots, w_n]^\top \in \mathbb{R}^n$ the disturbance vector. Furthermore, consider the following function (see e.g., [Monshizadeh et al., 2017; Dörfler and Bullo, 2012]) given by,

$$\begin{aligned}
V(\delta - \delta^s, \omega) = &\frac{1}{2}\|\omega\|_M^2 - \mathbb{1}_n^\top\,\Xi\,(\underline{\cos}(\delta) - \underline{\cos}(\delta^s)) \\
&- (\delta - \delta^s)^\top\,\Xi\,\underline{\sin}(\delta^s). \qquad (20)
\end{aligned}$$

It is noteworthy that under Assumption 1, $V(\delta - \delta^s, \omega)$ in (20) is locally (i.e., in a neighborhood Ω of $(\delta^s, 0)$) positive definite.
    Next, we have the following corollary.

COROLLARY 3
Consider the optimal control problem (19) under Assumption 1. The value function $V(\delta - \delta^s, \omega)$ given by (20) satisfies the HJBE (2) together with the following formulas for the cost functions.

  1. For $w = 0$, then

$$q(\delta, \omega, R) = \frac{1}{4}\|\underline{\sin}(\delta) - \underline{\sin}(\delta^s)\|_{\Xi\,R^{-1}\,\Xi}^2 + \|\omega\|_D^2. \qquad (21)$$

2. For $w \neq 0$, if $D - \frac{1}{4\xi}S^{-1} > 0$, then

$$q(\delta, \omega, R, S) = \frac{1}{4}\|\underline{\sin}(\delta) - \underline{\sin}(\delta^s)\|^2_{\Xi\, R^{-1}\, \Xi} + \|\omega\|^2_{D - \frac{1}{4\xi}S^{-1}}. \quad (22)$$

Moreover, the optimal controller is uniquely given by

$$u^*(\delta, R) = -\frac{1}{2}\, R^{-1}\, \Xi\, (\underline{\sin}(\delta) - \underline{\sin}(\delta^s)). \quad (23)$$

Proof. The two statements follow directly from Theorem 1 and Proposition 2 with the Lyapunov function (20). To see this, Lie derivative of V is given by

$$\dot{V}(\delta - \delta^s, \omega) = -\|\omega\|^2_D \leq 0.$$

Under Assumption 1, the sub-level sets of V are bounded in a neighborhood Ω of $[\delta^{s\top}, 0^\top]^\top$. By applying Lasalle's invariance principle [Khalil, 2002], the trajectories of the dynamical system (19) starting at Ω converge to the set where $\omega = 0$, which in turn implies that $\delta = \delta^s$, where $\delta^s - \delta^*$ is a constant angle vector. This establishes that $[\delta^{s\top}, 0^\top]^\top$ is locally asymptotically stable and V in (20) is a Lyapunov function for the system dynamics (19), for all $x \in \Omega$. For the second statement, the condition $D > \frac{1}{4\xi}S^{-1}$ ensures that $q(\cdot, R, S) > 0$ as in Proposition 2. □

Note that the controller $u^*(\delta, R)$ in (23) is locally optimal, i.e., valid in a neighborhood Ω of $[\delta^{s\top}, 0^\top]^\top$ and distributed, i.e., depends on the angle differences of the neighboring oscillator angles and the functions $q(\cdot, R')$ and $q(\cdot, R', S')$ remain positive for any other positive definite matrices $R', S' > 0$.

3.2 Simulations

We adopt the same setup as in [Jouini et al., 2021] and consider a network of three inverters with system dynamics (17). The parameters M_i and D_i represent inertia and damping coefficients. The inverters are connected by purely inductive transmission lines with line susceptance $b_{ij} > 0$ as shown in Figure 1. We test numerically the derived optimal controller (23) for nominal ($w = 0$) and disturbance attenuation ($w \neq 0$) settings. The disturbance $w = [w_1, \ldots, w_n]^\top \in \mathbb{R}^n$ models e.g., DC-side generation and AC side fluctuations [Kundur et al., 2004]. For simplicity, we set all line susceptances b_{ij} to one per unit (p.u.). The parameters in (17) are chosen uniformly with $M_1 = M_2 = M_3 = 0.01[\text{s}^2/\text{rad}]$ and $D_1 = D_2 = D_3 = 0.1[\text{s/rad}]$.

Time-domain simulations of the open-loop angle differences and frequencies with the unforced inverter system (i.e., $u = 0$) in (17) and the desired steady state angle differences $\delta^* = [0, 0, 0]^\top$, starting at $\delta(0) = [0.02, 0.015, 0]^\top$ show that $\delta^s = [0.0113, 0.0113, -0.0113]^\top$ and thus satisfy Assumption 1. Moreover, the inverters' frequencies synchronize at $\omega^* = 0$.
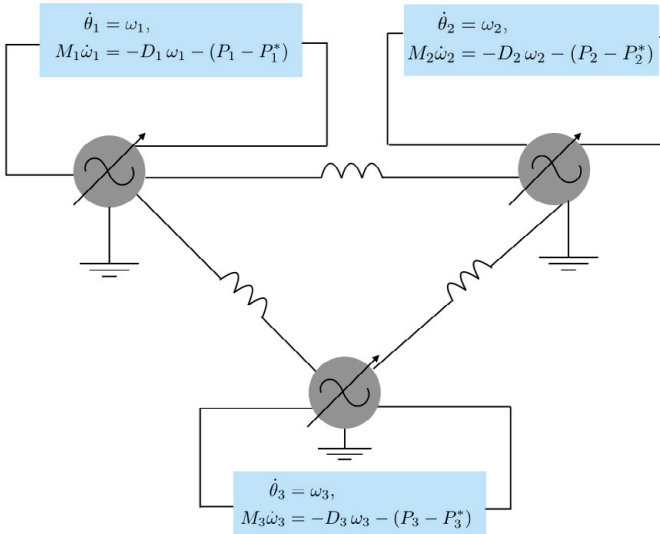
Figure 1. Three inverter system with dynamics given in (17), where $P_i = \sum_{j \in \mathcal{N}_i} b_{ij} \sin(\theta_{ij})$ and $P_i^* = \sum_{j \in \mathcal{N}_i} b_{ij} \sin(\theta_{ij}^*)$ for $i = 1, 2, 3$.

Next, we consider the optimal control problem (19) and implement the control law (23) both for nominal ($w = 0$) and disturbance attenuation ($w \neq 0$). We additionally verify the optimal controller for two examples of the design matrix R_1 and R_2. Once in closed-loop with the optimal controller (23), all frequencies synchronize at the nominal value with a decay towards zero and improved transient behavior both for $R_1 = 0.1 \cdot I_3$ and $R_2 = 0.01 \cdot I_3$ in Figures 2 and 3 respectively. Compared to the input matrix R_1, the matrix R_2 penalizes less the input variations and thus allows for more control input effort leading to faster error decay rate. In the presence of non-zero, additive and randomly generated disturbances $w = [w_3, w_2, w_1]^\top$, Figure 4 shows that the frequencies remain bounded, albeit non-synchronized, which is in accordance with our theory. The nominal and disturbed cost functions are decreasing towards a value that is nearby zero.

4. Conclusion

We studied the role of cost design for optimal feedback control in satisfying HJBE or HJIE in theory and via examples and an application to control of oscillatory systems. The optimal control problem reduces to a decision on how to tune the control gains, while the value function remains unchanged. The optimal controller is thus comparable to a linear quadratic regulator. It is
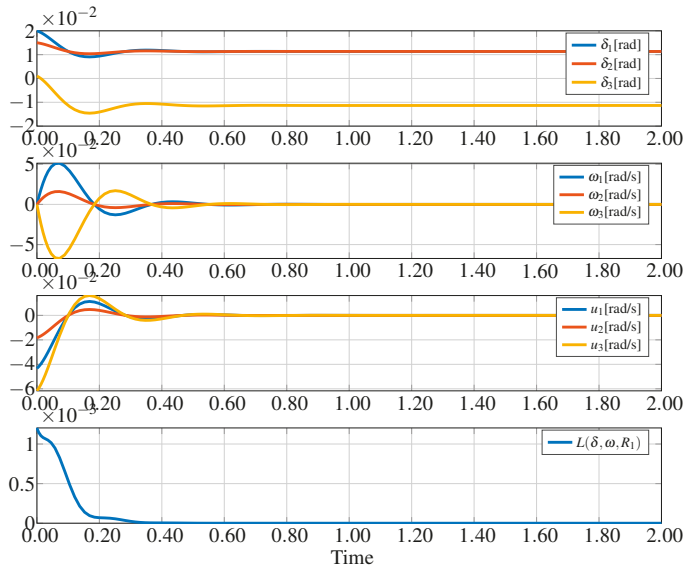
Figure 2. Simulations for $w = 0$ of angle differences, frequencies, inputs and the cost function of the three inverter system described in Figure 1 for $w = 0$ after closing the loop with the optimal control (23) with $R_1 = 0.1 \cdot I_3$. The angles are stabilized at the specified steady state and the frequencies synchronize and decay towards zero. The cost function $L(\delta, \omega, R_1)$ strictly decreases towards a nearby zero value.

in our future interest to investigate the ramifications of the proposed design method on the study of passive systems and constrained optimal control problems.

References

Başar, T. and P. Bernhard (2008). *H-infinity optimal control and related minimax design problems: a dynamic game approach.* Springer Science & Business Media, Berlin/Heidelberg, Germany.

Bertsekas, D. P. (2011). *Dynamic programming and optimal control 3rd edition, volume II.*

Dörfler, F. and F. Bullo (2012). "Synchronization and transient stability in power networks and nonuniform Kuramoto oscillators". *SIAM Journal on Control and Optimization* **50**:3, pp. 1616–1642. DOI: 10.1137/110851584.
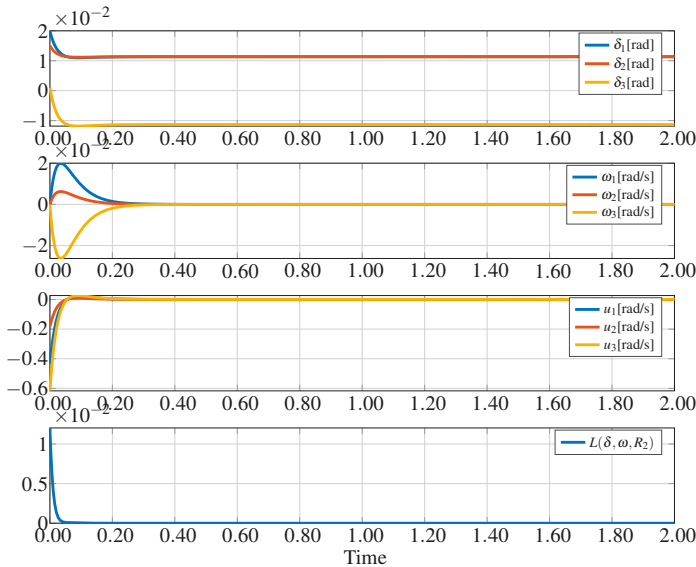
Figure 3. Simulations for $w = 0$ of angle differences, frequencies, inputs and the cost function after closing the loop with the optimal control (23) for $R_2 = 0.1 \cdot R_1$. The error decay transients of the angles and frequencies improve significantly with more control effort (compared to Figure 2). The nominal cost function $L(\delta, \omega, R_2)$ decays towards a nearby zero value.

Jouini, T. and A. Rantzer (2021). "On cost design in applications of optimal control". *IEEE Control Systems Letters*, pp. 1–1. DOI: `10.1109/LCSYS.2021.3079642`.

Jouini, T., A. Rantzer, and E. Tegling (2021). "Inverse optimal control for angle stabilization in converter-based generation". *ArXiv:2101.11141, submitted to American Control Conference (ACC)*.

Khalil, H. K. (2002). *Nonlinear systems*. 3rd ed. Prentice hall New Jersey.

Kundur, P., J. Paserba, V. Ajjarapu, G. Andersson, A. Bose, C. Canizares, N. Hatziargyriou, D. Hill, A. Stankovic, C. Taylor, et al. (2004). "Definition and classification of power system stability". *IEEE Transactions on Power Systems* **19**:2, pp. 1387–1401. DOI: `10.1109/TPWRS.2004.825981`.

Liberzon, D. (2011). *Calculus of variations and optimal control theory: a concise introduction*. Princeton University Press, Princeton, New Jersey.

Lukes, D. L. (1969). "Optimal regulation of nonlinear dynamical systems". *SIAM Journal on Control* **7**:1, pp. 75–100. DOI: `10.1137/0307007`.

Monshizadeh, P., C. De Persis, T. Stegink, N. Monshizadeh, and A. van der Schaft (2017). "Stability and frequency regulation of inverters with

159
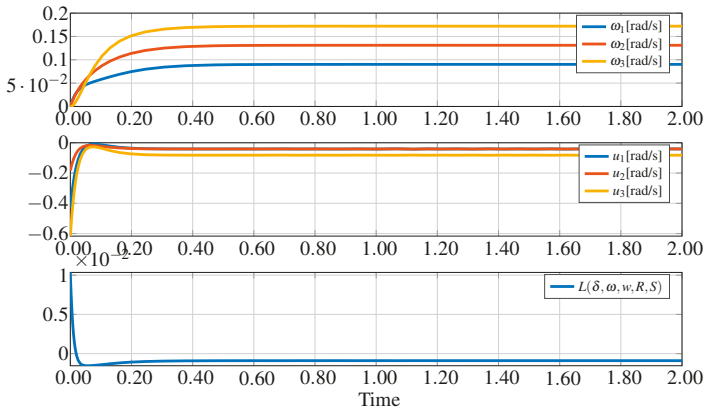
Figure 4. Simulations of the frequencies, input and cost function of the three-inverter system for constant non-zero disturbance w in closed-loop with (23) for $R = 0.01 \cdot I_3$, $S = I_3$ and $\xi = 2.8 > \frac{1}{4D}$. The frequencies remain bounded and the cost function $L(\delta, \omega, w, R, S)$ in (1) takes negative values with a randomly generated disturbance $w \neq w^*(x)$.

capacitive inertia". In: *2017 IEEE 56th Annual Conference on Decision and Control (CDC)*. IEEE, pp. 5696–5701. DOI: 10.1109/CDC.2017.8264519.

Powell, W. B. (2007). *Approximate Dynamic Programming: Solving the curses of dimensionality*. Vol. 703. John Wiley & Sons, Hoboken, New Jersey, USA.

Sassano, M. and A. Astolfi (2020). "Combining Pontryagin's Principle and dynamic programming for linear and nonlinear systems". *IEEE Transactions on Automatic Control* **65**:12, pp. 5312–5327. DOI: 10.1109/TAC.2020.3021385.

Scherer, C. (2001). "Theory of robust control". *Delft University of Technology*, pp. 1–160.

Sontag, E. D. (1999). "Control-Lyapunov functions". In: Blondel, V. et al. (Eds.). *Open Problems in Mathematical Systems and Control Theory*. Springer London, London, pp. 211–216. ISBN: 978-1-4471-0807-8. DOI: 10.1007/978-1-4471-0807-8.

Vinter, R. (2010). *Optimal control*. Springer Science & Business Media, Berlin/Heidelberg, Germany.

Zhou, K. and J. C. Doyle (1998). *Essentials of robust control*. Vol. 104. Prentice hall Upper Saddle River, NJ.
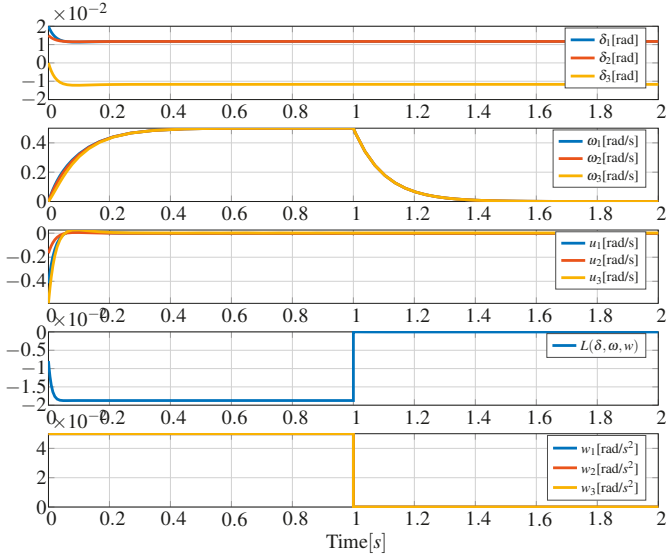
Addendum to Paper III, post print

We have the following observations and errata in regards of Paper III.

1. At the time of submission, the authors were not aware of the literature on inverse optimal control theory, which already exploits the powerful idea of cost design to derive optimal controllers. The results were derived independently.

2. The aspect of showcasing the application of inverse optimal control in networked systems by deriving controllers with structure (i.e., distributed) is a novelty in our work. This can be spotted through the derivation of an inverse optimal robust stabilizing control for the angles of the network of second-order coupled oscillators. In the context of power systems, these can be droop-controlled inverters.

3. In Example 1, the sub-level c, where $0 < c < n$, describes the set $\mathcal{X} = \{x \in \mathbb{R}^n | : \|x\|_\infty < \pi/2, \mathbb{1}_n^\top \underline{\cos}(x) \geq c\}$ and must be chosen sufficiently close to n to guarantee forward invariance of $\mathcal{X}$.

4. Under many operational conditions, the induced steady state angles δ^s given in Assumption 1, might not be given or accessible. This impedes the implementation of the control law (23) along with the functions (21) and (22). We propose a solution for radial or *acyclic* graphs, i.e., when the graph with associated incidence matrix $\mathcal{B} \in \mathbb{R}^{n \times m}$ contains no cycles and hence $\ker(\mathcal{B}) = 0$. The steady state of (19) results from setting the frequency error $\dot{\omega} = \omega = 0$ and we obtain,

$$\underline{\sin}(\delta^s) = \underline{\sin}(\delta^*).$$
(A.1)

In this case, the gradient of V an be written as,

$$\nabla_\delta V(\delta) = \frac{1}{2} \Xi \left(\underline{\sin}(\delta) - \underline{\sin}(\delta^s) \right) = \frac{1}{2} \Xi \left(\underline{\sin}(\delta) - \underline{\sin}(\delta^*) \right),$$

Figure A.1. Simulations of the three oscillators' angles, frequencies, inputs and the integrand of the disturbed cost functional as a correction to Figure 4 with $\xi = 2.501$.

where we had recourse to (A.1). In this way, the controller (23) and the cost functions (21) and (22) depend on the nominal steady state angle δ^*, readily obtained from dispatched values resulting from solving the optimal power flow at steady state.

5. We note that θ^s is the induced steady state of the transformed system angle (17), instead of the power system in original coordinates (19) and $\delta(0) = [0.02, 0.015, 0] \in \mathbb{R}^3$.

6. Note that the disturbance $w(t)$ in (1) is assumed to have a finite $\mathcal{L}_2$−norm, i.e., it holds that $\sqrt{\int_0^\infty w(s)^\top w(s)\mathrm{d}s} < \infty$.

7. In Figure 2, the cost function $L(\delta, \omega, R_1)$ strictly decreases towards *a zero* value, instead of a nearby zero value.

8. In Figure A.1, we provide , *new* simulations for the inverse optimal robust control problem depicted in Figure 4, where the cost function is seen to be strictly decreasing towards -0.01873. We simulate the closed-loop behavior in the disturbed case. For non-zero disturbance $w \in \mathbb{R}^3$, the oscillator frequencies *synchronize* at an induced steady state frequency 0.3 [rad/s].

Paper IV

Inverse optimal control for angle stabilization in converter-based generation

Taouba Jouini   Anders Rantzer   Emma Tegling

Abstract

In inverse optimal control, an optimal controller is synthesized with respect to a meaningful, a posteriori defined, cost functional. Our work illustrates the usefulness of this approach in the control of converter-based power systems and networked systems in general, and thereby in finding controllers with topological structure and known optimality properties. In particular, we design an inverse optimal feedback controller that stabilizes the phase angles of voltage source-controlled DC/AC converters at an induced steady state with *zero* frequency error. The distributed angular droop controller yields active power to angle droop behavior at steady state. Moreover, we suggest a practical implementation of the controller and corroborate our results through simulations on a three-converter system and a numerical comparison with standard frequency droop control.

1.   INTRODUCTION

A diagnosis of the event of September 28, 2016 in Australia shows anomalous power systems dynamics caused by a series of voltage dips [Australian Energy Market Operator (AEMO), 2017]. This was originated by the growing angle difference between the respective voltage phase angles, resulting in a loss of synchronism between South Australia and the remainder of the Australian grid. Following separation, sudden phase angle changes accompanied by a rapid change in the load have resulted in inaccuracies in short-term frequency measurements [Paolone et al., 2020]. A lesson that can be drawn from the event in Australia is the importance of phase angles in monitoring the stability of converter-based generation and, in particular, in providing useful information that can be exploited for a better design of control schemes for converters [Paolone et al., 2020]. Recently, different DC/AC converter control strategies have been proposed to stabilize the output voltage angles at a desired steady state, for example, based on gradient systems and Kuramoto-like oscillator dynamics [Arghir and Dörfler, 2019; Tayyebi et al., 2020]. Similarly, our work aims to control the angles of DC/AC converters.

Optimal control theory remains an important theoretical tool for stability and control in power systems [Molzahn et al., 2017] and is the backbone of a plethora of strategies for an improved operation of the electrical grid. In [Hauswirth et al., 2016], dynamic online feedback optimization is used to synthesize controllers, while accounting for input and output constraints and allowing for non-smooth feasible sets based on projected gradient descent algorithms. Furthermore, the online feedback optimization discussed in [Colombino et al., 2019] enables the study of time-varying convex optimization problems, while allowing for disturbance rejection and exact tracking, and is showcased for power transmission systems to compress the time scales between secondary and tertiary control. Feedback optimization based on dynamic programming is deployed in [Guo et al., 2018] for power scheduling of converters and the associated operational cost in a data-driven stochastic framework.

In optimal control, it is well-known that every meaningful value function is a Lyapunov function. This constitutes an important link between stability and optimality and allows for the systematic analysis of optimal feedback controllers. In *inverse* optimal control, the converse link is established. Namely, it is shown that every Lyapunov function is a meaningful value function. This allows for a systematic design of feedback controllers associated with control Lyapunov functions, that are optimal with respect to an a *posteriori* specified cost functional, satisfying the Hamilton-Jacobi-Bellman (HJB) equation. This was first spotted by R.E. Kalman [Kalman, 1964] for linear systems with quadratic cost and later extended to nonlinear systems by Moylan and Anderson in [Moylan and Anderson, 1973], Casti et al. [Casti, 1980]

for a class of cost functionals that are, e.g., strictly convex in the input for a fixed state, subject to general nonlinear systems. Afterwards, Freeman and Kokotovic incremented the system dynamics with a disturbance in [Freeman and Kokotovic, 1996] and studied the inverse robust stabilization problem leading to the analysis of the Hamilton-Jacobi-Isaacs (HJI) equation. Our previous work in [Jouini and Rantzer, 2021] exploits the same theory to design a distributed controller in coupled second-order oscillators.

In this work, we consider a network of voltage-source controlled converters, each of which is equipped with the capability of actuating the voltage phase angle, using synchrophasors. Synchrophasors are time-synchronized electrical measurements that represent both the magnitude and phase angle of the electrical sinusoids, measured by fast time-stamped devices, or phasor measurement units (PMUs), and constitute the basis of real-time monitoring and control actions in the electric grid [Usman and Faruque, 2019]. In particular, we formulate an inverse optimal control problem, where a *distributed* solution to the HJB equation can be tuned without expensive computations. From a theoretical point of view, the proposed controller demonstrates the usefulness of inverse optimal control theory in networked settings via synthesis of an optimal and stabilizing controller, namely *the angular droop control* with topological structure, a feat that is otherwise challenging.

The angular droop controller, designed for the multi-converter system, coincides with that proposed in [Zhang and Xie, 2015; Zhang and Xie, 2016]. In these works, only a linear stability analysis is conducted and optimality is not established. Here, we prove local asymptotic stability of the induced steady state angle with respect to nonlinear system dynamics. The angular droop controller turns out to be the inverse optimal locally stabilizing control law for the multi-converter system with respect to a meaningful cost functional. As such, our control design bridges a gap between control theorists and power system experts , by demonstrating optimality for the intuitively appealing controller of power converters. The optimal controller has desired gradient descent form and possesses grid-forming capabilities contributing to angle stabilization and thus achieves both primary and secondary frequency control, i.e., zero frequency error. Finally, we validate our results on a high-order model of three DC/AC converter system in closed-loop with the angular droop control, give nuts and bolts on how a practical implementation can be achieved and provide a numerical comparison to standard frequency droop control analyzed in [Jouini et al., 2021] demonstrating, in particular, improved scalability properties to large networks.

Notation: For a matrix $P \in \mathbb{R}^{n \times n}$, $P = P^\top > 0$ and a vector $v \in \mathbb{R}^n$, let $\|v\|_P = \sqrt{v^\top P v}$. Let $\mathrm{diag}(v)$ be the diagonal matrix with elements v_i, $\|v\|_\infty = \sup_{i=1\ldots n} |v_i|$ be the maximum norm of v, and $\underline{\sin}(v)$ and $\underline{\cos}(v)$ be the vector-valued sine and cosine functions. Given a continuously differentiable function $V(x)$, let $\nabla_x V = \frac{\partial V}{\partial x}$ be the the gradient of V with respect

to x and $\nabla_x^2 V = \frac{\partial^2 V}{\partial^2 x}$ its Hessian matrix. For $p \in \mathbb{N}$, let I_p be the $p \times p$ identity matrix and $\mathbb{1}_p$ be the $p \times 1$ vector of all ones. Given a dynamical system, $\dot{x}(t) = f(x(t))$, $x(0) = x_0$, we consider the system to be time-invariant throughout and mostly drop the time-dependence of the state variables in the notation.

Furthermore, consider a network described by a connected graph $\mathcal{G} = (\mathcal{V}, \mathcal{E}, \Xi)$, consisting of $|\mathcal{V}| = n$ nodes representing DC/AC converter buses and $|\mathcal{E}| = m$ edges modeling purely inductive transmission lines (i.e., with zero conductances) with susceptance $b_{kj} > 0$, $(k, j) \in \mathcal{E}$ collected in the diagonal matrix $\Xi = \mathrm{diag}(b_{kj})$, $(k, j) \in \mathcal{E}$. The topology of the graph $\mathcal{G}$ is described by the incidence matrix $\mathcal{B} \in \mathbb{R}^{n \times m}$. Let $\mathcal{N}_k$ be the neighbor set of converter k. We denote by $\mathcal{L} = \mathcal{B} \Xi \mathcal{B}^\top$ the bus admittance matrix of $\mathcal{G}$, which is a weighted Laplacian with eigenvalues $0 = \lambda_1 < \lambda_2 \leq \cdots \leq \lambda_n$.

2. Problem formulation

In this section, we start by presenting the multi-converter model following [Kundur et al., 1994; Dörfler et al., 2016] and then formulate the corresponding optimal control problem. This underlies the analysis of the angular feedback control that is at the core of our main result.

2.1 Modeling and setup

Consider a network of DC/AC power converters (e.g., islanded microgrid), each represented by a voltage phasor and interconnected via inductive transmission lines. We make the common assumption that the system is in quasi-stationary state, i.e., around a nominal steady state frequency ω^*, see [Kundur et al., 1994; Dörfler et al., 2016], meaning that all phasors are modeled with constant magnitude (1 per unit), and assume that the angle dynamics are controllable. For this, the converter dynamics are reduced to the following integrator dynamics,

$$\dot{\theta} = u\left(\theta\right) + \omega^* \mathbb{1}_n, \quad \theta(0) = \theta_0. \tag{1}$$

Here, $u(\theta) = [u_1(\theta), \ldots, u_n(\theta)]^\top \in \mathbb{R}^n$ is the control input, $\theta = [\theta_1, \ldots, \theta_n]^\top \in \mathbb{R}^n$ is the vector of phase angles of the DC/AC converters and $\theta_0 \in \mathbb{R}^n$ is the initial angle vector. While the modeling choice in this section ignores the internal dynamics of the converter, it enables the design of the optimal controller in a concise, closed-form due to its simplicity and mathematical tractability. Later, Section 4 considers a network of detailed internal converter dynamics, descendent from first-order principles as in [Jouini and Sun, 2021], and discusses a practical implementation of the control scheme.

For the control design (1), we consider a scenario where synchrophasor measurements, with respect to a global frame of reference, are available to each converter. This is a reasonable scenario for a future power grid, as PMU installation is becoming increasingly widespread [Usman and Faruque, 2019]. We define the set of nominal phase angles, rotating at a synchronous frequency ω^*, as $\theta^*(t) = \omega^* \mathbb{1}_n t + \theta_0^* \in \mathbb{R}^n$, where $\theta_0^* = [\theta_{01}^*, \ldots, \theta_{0n}^*]^\top \in \mathbb{R}^n$ is the nominal initial angle vector. Let $\theta_{kj}^* = \theta_k^* - \theta_j^*$ define the nominal phase angle difference between neighboring converters $(k, j) \in \mathcal{E}$. Assuming inductive (i.e. lossless) transmission lines, the active power deviation from the nominal is given by,

$$P_{e,k}(\theta) - P_{e,k}^* = \sum_{j \in \mathcal{N}_k} b_{kj} \left(\sin(\theta_{kj}) - \sin(\theta_{kj}^*) \right),$$

where $P_{e,k}(\theta)$ is the electrical power injected into the network at the $k-$th converter and $P_{e,k}^*$ is the nominal power drawn from a DC source behind the $k-$th converter.

REMARK 1
Recall that the control law,

$$u_k(\theta) = -1/d_k \left(P_{e,k}(\theta) - P_{e,k}^* \right), \quad d_k > 0, \ k = 1, \ldots, n, \tag{2}$$

results in the first-order frequency-droop control, that represents a prevalent approach for primary control in islanded microgrids. This, however, results in stationary frequency errors, which requires (2) to be augmented with a secondary control architecture, namely the automated generation control [Dörfler et al., 2016]. ∎

Following Remark 1, our goal in this work is to use measurements obtained from PMUs to synthesize a feedback controller with optimality guarantees. This will be shown to coincide with *the angular droop control* proposed in [Zhang and Xie, 2015; Zhang and Xie, 2016]. This controller stabilizes the phase angle error (with respect to a nominal steady state angle) and is characterized by zero frequency deviation at stationarity.

2.2   Optimal control problem formulation

Consider the following optimization problem,

$$\min_{u \in \mathbb{R}^n} \int_0^\infty \sum_{k=1}^n \left(\alpha_k u_k^2(\theta) + \right. \tag{3}$$

$$\left. \frac{1}{4\alpha_k} \left(\gamma_k(\theta_k - \theta_k^*) + P_{e,k}(\theta) - P_{e,k}^* \right)^2 \right) \mathrm{d}t,$$

$$\text{s.t. } \dot{\theta} = u(\theta) + \omega^* \mathbb{1}_n, \quad \theta(0) = \theta_0.$$

In (3), the first term in the running cost (the integrand) penalizes the control effort through the positive gains $\alpha_k > 0$, $k = 1,\ldots,n$ by minimizing the scaled total power generation. The second term is designed to accommodate a desired steady state behavior: power to angle droop, or $P-\theta$ droop, where $\gamma_k > 0$, $k = 1,\ldots,n$, is a droop gain. This droop behavior leads to zero stationary frequency error and can be seen as follows: under the optimal control $u^*(\theta)$ that solves (3), the running cost goes asymptotically to zero and it holds that,

$$\lim_{t\to\infty} \left(\gamma_k(\theta_k(t) - \theta_k^*(t)) + P_{e,k}(\theta) - P_{e,k}^*\right) = 0.$$

More precisely, let $\theta_k^s := \lim_{t\to\infty} \theta_k(t)$ be an induced steady state angle at the $k-$th converter. Then,

$$\gamma_k(\theta_k^s - \theta_k^*) = P_{e,k}^* - P_{e,k}(\theta^s), \quad k = 1,\ldots,n. \tag{4}$$

Equation (4) describes the steady state as a power balance between the active power and angle deviation from the nominal value, where $\theta^s = \{\theta_k^s\}_{k=1}^n$ given by (4) is the induced steady state angle vector. By taking the time derivative of (4), we arrive at $\dot{\theta}_k^s = \omega^*$. It is evident that the steady state frequency error is zero. Intuitively, (4) is able to guarantee primary and secondary frequency control at once, i.e., resulting in a power system steady state with zero frequency error. In what follows, we synthesize an angle feedback control law $u^*(\theta)$ that uniquely solves (3).

3. Inverse optimal control design

An innovative approach to optimal control synthesis was introduced in [Kalman, 1964; Freeman and Kokotovic, 1996; Haddad and Chellaboina, 2011; Sepulchre et al., 2012; Jouini and Rantzer, 2021] and relies on the following idea: a stabilizing feedback control law associated with a control Lyapunov function for a dynamical system is *first* determined and *then* a suitably chosen cost functional is found that satisfies the HJB equation. This constitutes the so-called *inverse* optimal control problem, where the running cost and the control parameters, representing a tuning knob, are determined *a posteriori*. This circumvents the need for an extensive search for a *good* cost functional and gives a value function from a suggested control Lyapunov function *for free* (without analytically and computationally expensive calculations). It also allows an easy control tuning with stability guarantees and is applicable to a wide range of optimal control problems.

For our power network application, inverse optimal control allows us to design a *distributed* controller with feasible implementation. In this section, we show that the optimization problem (3) obeys the systematic optimal

control synthesis presented in [Freeman and Kokotovic, 1996; Haddad and Chellaboina, 2011; Sepulchre et al., 2012; Jouini and Rantzer, 2021]. For convenience, we cite the following Theorem from our previous work [Jouini and Rantzer, 2021]. The same results are also found in [Freeman and Kokotovic, 1996, Theorem 8.1], [Sepulchre et al., 2012, Section 3.5].

THEOREM 1

Consider the optimal control problem,

$$\min_{u \in \mathbb{R}^n} \int_0^\infty \|u(s)\|_{\overline{R}}^2 + q(x(s)) \, \mathrm{d}s, \tag{5a}$$

$$\text{s.t.} \quad \dot{x} = H^\top(x)\, u, \quad x(0) = x_0, \tag{5b}$$

where x, $x_0 \in \mathbb{R}^n$, $u \in \mathbb{R}^n$, $\overline{R} = \overline{R}^\top > 0$, $q(x)$ is a function satisfying $q(x) > 0$, $q(0) = 0$ and $H(x) \in \mathbb{R}^{m \times n}$ is the input matrix. Furthermore, let $V : \mathbb{R}^n \mapsto \mathbb{R}_{>0}$, be a continuously differentiable function associated with a stabilizing feedback control law,

$$u^*(x) = -\frac{1}{2}\, \overline{R}^{-1} H(x) \nabla_x V, \tag{6}$$

where, $\nabla_x V^\top H^\top(x)\, u^*(x) < -\|u^*(x)\|_{\overline{R}}^2$. Define

$$q(x) = -\nabla_x V^\top H^\top(x) u^*(x) - \|u^*(x)\|_{\overline{R}}^2. \tag{7}$$

Then, the following statements hold:

1. The unique optimal control is given by $u^*(x)$ in (6).

2. The optimal control problem (5) has the optimal value $V(x_0) := \inf_{u \in \mathbb{R}^n} \int_0^\infty \|u(s)\|_{\overline{R}}^2 + q(x(s)) \, \mathrm{d}s$ with $q(x)$ in (7).

We make the following assumption.

ASSUMPTION 1

The induced steady state angle vector $\theta^s = \{\theta_k^s\}_{k=1}^n$ satisfies, $\mathcal{B}^\top \theta^s \in \left(-\frac{\pi}{2}, \frac{\pi}{2}\right)^m$, where $\mathcal{B} \in \mathbb{R}^{n \times m}$ is the incidence matrix of the underlying graph $\mathcal{G}$.

Assumption 1 states that the difference in steady state voltage angles between neighboring nodes is not larger than $\pi/2$. This is commonly referred to as a *security constraint*, see e.g., [Monshizadeh et al., 2017]. For ease of

presentation, we introduce,

$$R = \text{diag}\{\alpha_1, \ldots, \alpha_n\}, \quad \Gamma = \text{diag}\{\gamma_1, \ldots, \gamma_n\}.$$

Let the induced steady state angle θ^s be given by (4) and define the following function, that is used in deriving our main result,

$$V(\theta) = \frac{1}{2}\|\theta - \theta^s\|_\Gamma^2 \tag{8}$$

$$+ \sum_{k=1}^n \sum_{j \in \mathcal{N}_k} b_{kj} \left(\cos(\theta_{kj}) - \cos(\theta_{kj}^s) - (\theta_{kj} - \theta_{kj}^s)\sin(\theta_{kj}^s)\right).$$

Our main result is summarized in the following proposition.

PROPOSITION 2
Consider the optimal control problem (3) under Assumption 1. Then, the following statements hold:

  i) The optimal solution of (3) at the $k-$th converter in a neighborhood of $\theta^s = \{\theta_k^s\}_{k=1}^n$ is the angular droop control defined as,

$$u_k^*(\theta) = -\frac{1}{2\alpha_k}\left(\gamma_k(\theta_k - \theta_k^*) + P_{e,k}(\theta) - P_{e,k}^*\right). \tag{9}$$

  ii) The steady state angle $\theta^s = \{\theta_k^s\}_{k=1}^n$ is locally asymptotically stable for the closed-loop system (i.e., (1) together with (9)).

Proof. The proof relies on the observation that the optimal control problem (3) satisfies the conditions of Theorem 1 *locally*, i.e., in the vicinity of the induced steady state angle θ^s.

First, we establish the positive definiteness of the function V around θ^s. That is, we establish that $V(\theta^s) = 0$ and $V(\theta) > 0$ for $\theta \neq \theta^s$ with θ being in a neighborhood of θ^s. For this, we follow a similar approach to [Monshizadeh et al., 2017] and define $V_1(\theta) = \frac{1}{2}\|\theta - \theta^s\|_\Gamma^2$ and $V_2(\theta) = W_2(\theta) - W_2(\theta^s) - (\theta - \theta^s)^\top \nabla_\theta W_2(\theta^s)$ with,

$$W_2(\theta) = -\mathbb{1}_n^\top \Xi \underline{\cos}(\mathcal{B}^\top \theta),$$

to rewrite the function $V(\theta)$ in (8) as, $V(\theta) = V_1(\theta) + V_2(\theta)$.

Note that V_1 is clearly positive definite around θ^s. V_2 is positive definite around θ^s if W_2 is strictly convex around θ^s. To show that W_2 is strictly convex around θ^s, we introduce the coordinate change $\eta := \mathcal{B}^\top \theta$ and calculate $\nabla_\eta^2 W_2(\eta) = \Xi \underline{\cos}(\eta)$. Under Assumption 1, it holds that $\eta^s := \mathcal{B}^\top \theta^s \in (-\frac{\pi}{2}, \frac{\pi}{2})^m$ and hence $\nabla_\eta^2 W_2(\eta) > 0$, for η in the neighborhood of η^s. This shows that $W_2(\eta)$ is strictly convex around η^s. Since strict

convexity is invariant under affine maps, $W_2(\theta)$ is strictly convex around θ^s. From the argumentation above, we deduce that V_2 and therefore V is positive definite around θ^s.

Second, we seek to apply Theorem 1. The gradient of $V(\theta)$ can be equivalently expressed as,

$$\nabla_\theta V = \Gamma(\theta - \theta^s) + P_e(\theta) - P_e(\theta^s), \tag{10}$$

$$= \Gamma(\theta - \theta^*) + P_e(\theta) - P_e^* + \overbrace{\Gamma(\theta^* - \theta^s) + P_e^* - P_e(\theta^s)}^{=0},$$

$$= \Gamma(\theta - \theta^*) + P_e(\theta) - P_e^*,$$

where $P_e(\theta) = [P_{e,1}(\theta), \ldots, P_{e,n}(\theta)]^\top$, $P_e^* = [P_{e,1}^*, \ldots, P_{e,n}^*]^\top$ and the last term in the second step is zero by the induced steady state equation (4). This means that the control law (9) takes the form, $u^*(\theta) = -\frac{1}{2}R^{-1}\nabla_\theta V$. By left-multiplying with the gradient of V, it can be deduced that,

$$\dot{V}(\theta) = \nabla_\theta^\top V \, u^*(\theta) = -\frac{1}{2}\nabla_\theta^\top V \, R^{-1} \, \nabla_\theta V.$$

Denote by Ω a neighborhood of θ^s. Note that V is positive definite on Ω and $\dot{V}(\theta) \leq 0$ for all $\theta \in \Omega$. Let $S = \{\theta \in \Omega, \dot{V}(\theta) = 0\}$. The only trajectory that can stay in S is where the gradient of V given in (10) vanishes, that is, only at $\theta = \theta^s$. By the Barbashin-Krasovskii theorem [Khalil, 2002, Corollary 4.1], the steady state angle θ^s is locally asymptotically stable. Now, we write,

$$\|u^*(\theta)\|_R^2 = \frac{1}{4}\nabla_\theta^\top V \, R^{-1} \, \nabla_\theta V.$$

Hence, for all $\theta \in \Omega$, $\nabla_\theta^\top V \, u^*(\theta) < -\|u^*(\theta)\|_R^2$. The cost functional (3) can be compactly expressed as, $\int_0^\infty \|u(\theta)\|_R^2 + q(\theta)\,\mathrm{d}s$, with

$$q(\theta) = -\nabla_\theta V^\top u^*(\theta) - \|u^*(\theta)\|_R^2 = \frac{1}{4}\nabla_\theta V^\top R^{-1}\nabla_\theta V,$$

as given in (7) and explicitly written in (3).

All in all, the control problem (3) satisfies the conditions of Theorem 1 *locally*, in a neighborhood of θ^s. It follows that (9) is an inverse optimal locally stabilizing control law for the system dynamics in (3) and $V(\theta_0)$ in (8) is the value function of (3). □

The angular droop control (9) is *distributed*, i.e., it requires only knowledge of the neighboring angles $\theta_j, j \in \mathcal{N}_k, k \in \mathcal{V}$. Nonetheless, it can be implemented in a fully *decentralized* fashion by measuring the active power $P_{e,k}$ using PMUs. It is grid-forming according to definitions in [Denis, 2017] and its tuning is easily understood: If the control gain α_k is larger, more control

effort is allowed at the $k-$th converter, and the rate of convergence towards an induced steady state angle θ^s is faster. In this sense, the input matrix $R > 0$ is a tuning knob that allows us to study combinations of the input penalty, while keeping the same value function.

REMARK 2—LQR CONTROL
By linearizing around $\theta = \theta^*$, the cost functional in (3) can be written as,

$$\int_0^\infty u(s)^\top R\, u(s) + (\theta(s) - \theta^*)^\top \overline{Q}\, (\theta(s) - \theta^*)\, \mathrm{d}s, \tag{11}$$

where $\Gamma = \mathrm{diag}\{\gamma_1, \ldots, \gamma_n\}$, $R = \mathrm{diag}\{\alpha_1, \ldots, \alpha_n\}$, $\overline{Q} = \frac{1}{4}(\Gamma + \mathcal{L})^\top R^{-1}(\Gamma + \mathcal{L})$ and $\mathcal{L} = \mathcal{B}\,\Xi\,\mathcal{B}^\top$. Hence, the optimal control problem (3) becomes an LQR problem [Khalil, 2002]. As delineated in [Jouini and Rantzer, 2021], after linearization around $\theta = \theta^*$, the control law (9) becomes,

$$u_{\mathrm{LQR}}^*(\theta) = -\frac{1}{2}R^{-1}(\Gamma + \mathcal{L})\,(\theta - \theta^*), \tag{12}$$

and represents the $\mathcal{H}_2-$optimal controller of (11). ∎

## 4.   Implementation and numerical simulations

Even though the converter dynamics are not taken into consideration in our optimal control synthesis, we propose a practical design of the angular droop control (9) for a network of high-order DC/AC converters. We also remark that, even though our previous analysis neglects the internal dynamics of each converter, we numerically demonstrate in the next section that high-order converter models can be accounted for.

4.1   Test case 1: Angular droop control

For this, we consider the following three-phase averaged and balanced DC/AC converter dynamics after transformation into $\alpha\beta-$frame, adapted from [Jouini and Sun, 2021],

$$\begin{aligned}
C_{dc}\dot{v}_{dc} &= -K_p\,(v_{dc} - v_{dc}^*\mathbb{1}_n) - \frac{1}{2}U^\top i + i_{dc}^*, \\
L\dot{i} &= -R\,i + \frac{1}{2}U\,v_{dc} - v, \\
C\dot{v} &= -G\,v + i - \mathbf{B}\,i_\ell, \\
L_\ell\dot{i}_\ell &= -R_\ell\,i_\ell + \mathbf{B}^\top v,
\end{aligned} \tag{13}$$

where the system parameters are summarized in Table 1. Note that the modulation signal $\overline{u}_k \in \mathbb{R}^2$, collected in the matrix U, represents the main input to the $k-$th DC/AC converter.
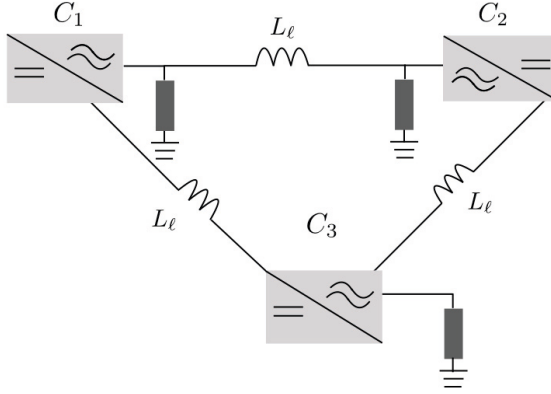
Figure 1. Three high-order DC/AC converter system described by the dynamics (13) in closed-loop with angular droop (14).

Table 1. Parameters of the multi converter system in Fig. 1 and 2.

Symbol	Definition	Range	Numerical value
$\overline{u}_k$	modulation signal	$\mathbb{R}^2$	–
A	modulation amplitude	$[0,1]$	0.33
$U = \mathrm{diag}(\overline{u}_1,\dots,\overline{u}_n)$	matrix of input signals	$\mathbb{R}^{2n\times n}$	–
v_{dc}^*	nominal DC voltage	$\mathbb{R}_{>0}$	1000
i_{dc}^*	nominal DC current source	$\mathbb{R}^n$	$500 \cdot \mathbb{1}_3$
C_{dc}	DC capacitance	$\mathbb{R}_{>0}$	10^{-3}
K_p	DC side control gain	$\mathbb{R}_{>0}$	0.5
R	AC filter resistance	$\mathbb{R}_{>0}$	0.2
L	AC filter inductance	$\mathbb{R}_{>0}$	$5 \cdot 10^{-4}$
C	AC filter capacitance	$\mathbb{R}_{>0}$	10^{-5}
G	AC filter conductance	$\mathbb{R}_{>0}$	0.1
L_ℓ	line inductance	$\mathbb{R}_{>0}$	$5 \cdot 10^{-5}$
$\alpha_k = \alpha, k = 1\dots n$	control gain	$\mathbb{R}_{>0}$	0.5
$\gamma_k = \gamma, k = 1\dots n$	droop gain	$\mathbb{R}_{>0}$	10^6
$\mathbf{B} = I_2 \otimes \mathcal{B}$	extended incidence matrix	$\mathbb{R}^{2n\times 2m}$	–
$v_{dc} = [v_{dc,1},\dots,v_{dc,n}]^\top$	DC capacitor voltage	$\mathbb{R}^n$	–
$v = [v_1^\top,\dots,v_n^\top]^\top$	AC capacitor voltage	$\mathbb{R}^{2n}$	–
$i = [i_1^\top,\dots,i_n^\top]^\top$	AC inductance current	$\mathbb{R}^{2n}$	–
$i_\ell = [i_{\ell,1}^\top,\dots,i_{\ell,m}^\top]^\top$	AC line current	$\mathbb{R}^{2m}$	–

After introducing $i_{net} = \mathbf{B}i_\ell$ and defining the active power $\widehat{P}_{e,k} = v_k^\top i_{net,k}$, as well as the nominal steady state active power $\widehat{P}_{e,k}^* = v_k^{*\top} i_{net,k}^*$ at the $k-$th converter, we propose to implement the angular droop controller as follows,

$$\dot{\theta}_k = -\frac{1}{2\alpha_k}\left(\gamma_k(\theta_k - \theta_k^*) + (\widehat{P}_{e,k} - \widehat{P}_{e,k}^*)\right) + \omega^*, \tag{14}$$

$$\overline{u}_k = A\begin{bmatrix}\cos(\theta_k)\\ \sin(\theta_k)\end{bmatrix},$$

where $0 < A < 1$ is the amplitude of the control input. In Figure 2, we

depict a summarizing block diagram of a single DC/AC converter whose system dynamics are given by (13), set in closed loop with the angular droop control (14). Note that in this setup, the angular droop control (14) increments the converter internal dynamics with a virtual angle dynamics $\dot{\theta}_k$ that represents the phase angle of the modulation signal $\overline{u}_k$.

Next, we consider three DC/AC converters with open-loop dynamics described in (13) in closed-loop with the angular droop control (14) as depicted in Figure 1. The desired steady state angles are given (in rad) by $\theta_1^*(0) = 0.951, \theta_2^*(0) = 0.92, \theta_3^*(0) = 0.967$, and thus satisfy Assumption 1. We select the control gains uniformly for all three converters with parameter values in Table 1.
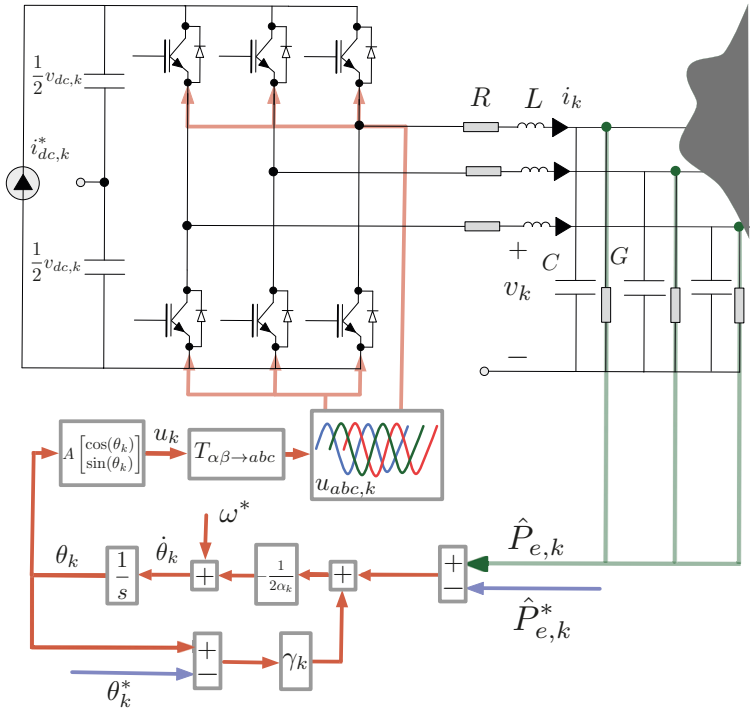
Figure 2. Block diagram of the interconnection of a single three-phase balanced and averaged DC/AC converter with (13) and (14). The green arrows represent PMUs measurements. $T_{\alpha\beta\rightarrow abc}$ is the inverse of the Clark transformation, see [Kundur et al., 1994].

We demonstrate the effectiveness of the proposed optimal controller both for angle stability and frequency synchonization via time-domain simulations before (under nominal conditions) and after an event corresponding to an
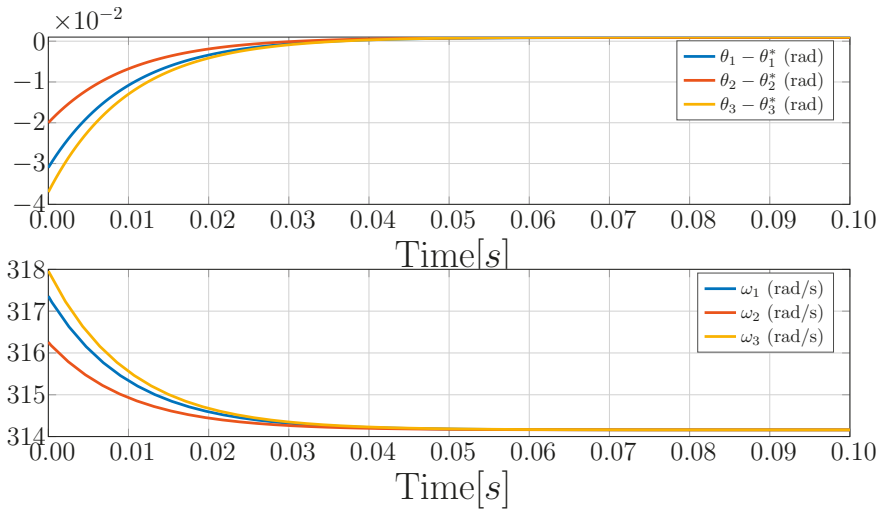
**Figure 3.** Time evolution of the converters' angle errors (in rad) with respect to the steady state θ^* initialized at $\theta_1(0) = 0.92, \theta_2(0) = 0.90, \theta_3(0) = 0.93$ and frequency synchronization at $\omega^* = 2\pi 50\,\text{rad/s}$, for the setup in Fig. 1.

increase in the load consumption at one of the converters. Fig. 3 illustrates the angle stability for the control gains in Table 1 of the angular droop control for the initial angle values $\theta_1(0) = 0.92, \theta_2(0) = 0.90, \theta_3(0) = 0.93$. We observe in simulations that a decrease in the gain α improves the angle transients, i.e., it results in faster convergence of the angles towards the induced steady state angle. We also note that the gain γ defines the droop behavior between a sudden power change and the angle deviation at steady state. Notice the first-order behavior of the phase angle trajectories dictated by (14), while converging to their respective steady state values depicted in Fig. 3. Similarly, the frequencies synchronize at the nominal steady value $\omega^* = 2\pi 50\,\text{rad/s}$. Fig. 4 illustrates the droop behavior in the phase angle after a sudden change in the load consumption and the corresponding effect on the frequency at the affected converter (C_1). The angle drops correspond to peaks in the frequency time evolution, while the frequency error remains zero, also during the event.

Finally, we note that angular droop (9) has been numerically tested in [Zhang and Xie, 2015; Zhang and Xie, 2016] on different setups involving radial and loopy distribution systems.
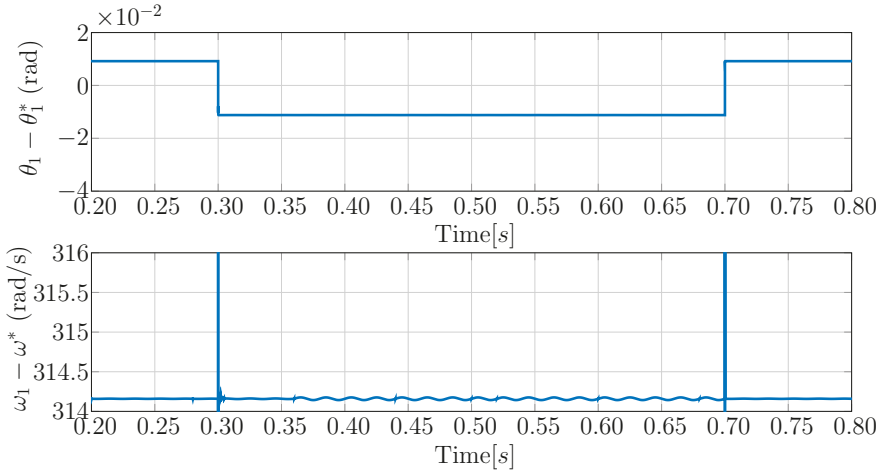
Figure 4. $P - \theta$ droop illustrated at the converter 1 (C1) angle and frequency after a sudden increase in the load consumption from $t = 0.3$s to $t = 0.7$s. The converter angle converges to the induced steady state angle θ_1^s during the load disturbance.

4.2 Test case 2: Comparison with frequency droop control

For the second test case, we compare qualitatively the transient performance tr(see Definition 1 in [Jouini et al., 2021]) of angular and frequency droop after linearization, in a scalability analysis that is analogous to [Andreasson et al., 2017]. For this, consider the angular control (12) and frequency droop given by [Andreasson et al., 2017] with the same droop coefficients. We model two example path graph networks, first with 10 nodes and later with 100 nodes interconnected via inductive lines of unit susceptance (in p.u). We then subject the closed-loop dynamics to arbitrary initial angular perturbations. The deviation of the angle error trajectories $\theta - \theta^*$ is depicted in Figure 5. We observe that the convergence to a steady state is faster with the angular droop for both networks, i.e., a better transient performance (compare a) to c) and b) to d)). More importantly, however, we note that, as the network size grows from 10 to 100 nodes, the frequency droop shows a significantly degraded transient performance (compare d) to c)), while the angular droop shows similar transient performance for the larger network (in b)) as for the smaller one (in a)), and thus a better scalability.
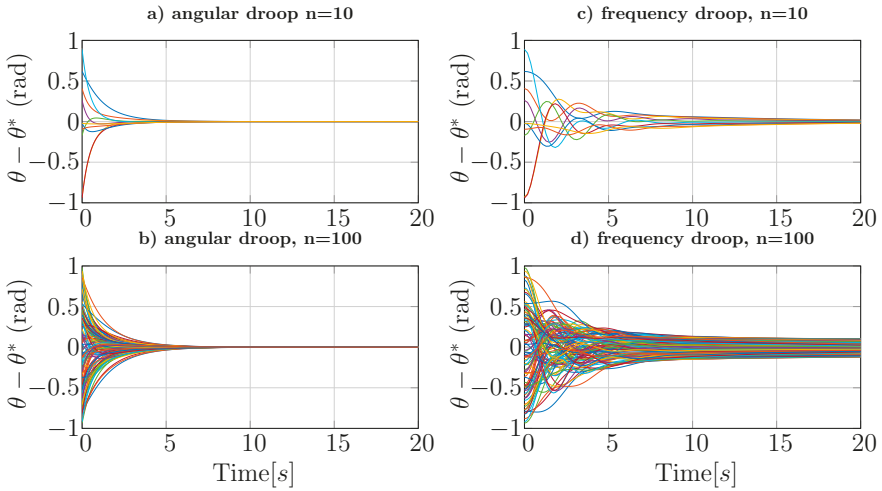
Figure 5. A comparison of the transient performance between the linearized angular droop (12) displayed in a) and b) and the frequency droop [Andreasson et al., 2017] in c) and d) for a path network, where the network size increases from $n = 10$ in a) and c) to $n = 100$ nodes in b) and d).

5.   Conclusion

In this work, we proposed novel insights into the design of the angular droop control, that establishes its optimality, while accounting for phase angle stability with zero stationary frequency error. The angular droop control is distributed and thus showcases the utility of inverse optimal control theory in networked settings, and is numerically tested on power system simulations. It is of our future interest to study the stability of the angular droop control, while including internal DC/AC converter dynamics.

References

Andreasson, M., E. Tegling, H. Sandberg, and K. H. Johansson (2017). "Coherence in synchronizing power networks with distributed integral control". In: *2017 IEEE 56th Annual Conference on Decision and Control (CDC)*. IEEE, pp. 6327–6333. DOI: 10.1109/CDC.2017.8264613.

Arghir, C. and F. Dörfler (2019). "The electronic realization of synchronous machines: model matching, angle tracking, and energy shaping techniques". *IEEE Transactions on Power Electronics* **35**:4, pp. 4398–4410. DOI: 10.1109/TPEL.2019.2939710.

177

Australian Energy Market Operator (AEMO) (2017). *Black system South Australia, 28 September 2016*. Tech. rep. Available: `http://www.aemo.com.au/Electricity/National-Electricity-Market-NEM/Market-notices-and-events/Power-System-Operating-Incident-Reports`.

Casti, J. (1980). "On the general inverse problem of optimal control theory". *Journal of Optimization Theory and Applications* **32**:4, pp. 491–497. DOI: `10.1007/BF00934036`.

Colombino, M., E. Dall'Anese, and A. Bernstein (2019). "Online optimization as a feedback controller: stability and tracking". *IEEE Transactions on Control of Network Systems* **7**:1, pp. 422–432.

Denis, G. (2017). *From grid-following to grid-forming: The new strategy to build 100% power-electronics interfaced transmission system with enhanced transient behavior*. PhD thesis. Centrale Lille, Lille, France.

Dörfler, F., J. W. Simpson-Porco, and F. Bullo (2016). "Breaking the hierarchy: distributed control and economic optimality in microgrids". *IEEE Transactions on Control of Network Systems* **3**:3, pp. 241–253. DOI: `10.1109/TCNS.2015.2459391`.

Freeman, R. A. and P. V. Kokotovic (1996). "Inverse optimality in robust stabilization". *SIAM Journal on Control and Optimization* **34**:4, pp. 1365–1391. DOI: `10.1137/S0363012993258732`.

Guo, Y., K. Baker, E. Dall'Anese, Z. Hu, and T. Summers (2018). "Stochastic optimal power flow based on data-driven distributionally robust optimization". In: *2018 Annual American Control Conference (ACC)*. IEEE, pp. 3840–3846. DOI: `10.23919/ACC.2018.8431542`.

Haddad, W. M. and V. Chellaboina (2011). *Nonlinear dynamical systems and control*. Princeton university press, Princeton, New Jersey.

Hauswirth, A., S. Bolognani, G. Hug, and F. Dörfler (2016). "Projected gradient descent on riemannian manifolds with applications to online power system optimization". In: *2016 54th Annual Allerton Conference on Communication, Control, and Computing (Allerton)*, pp. 225–232. DOI: `10.1109/ALLERTON.2016.7852234`.

Jouini, T. and A. Rantzer (2021). "On cost design in applications of optimal control". *IEEE Control Systems Letters*, pp. 1–1. DOI: `10.1109/LCSYS.2021.3079642`.

Jouini, T., A. Rantzer, and E. Tegling (2021). "Inverse optimal control for angle stabilization in converter-based generation". *arXiv preprint arXiv:2101.11141*.

Jouini, T. and Z. Sun (2021). "Frequency synchronization of a high-order multi-converter system". *ArXiv:2007.14064, to appear in IEEE Transactions on Control of Network Systems*. DOI: `10.1109/TCNS.2021.3128493`.

Kalman, R. E. (1964). "When is a linear control system optimal?" *Journal of Basic Engineering* **86**:1, pp. 51–60. DOI: 10.1115/1.3653115.

Khalil, H. K. (2002). *Nonlinear systems.* 3rd ed. Prentice hall New Jersey.

Kundur, P., N. J. Balu, and M. G. Lauby (1994). *Power system stability and control.* Vol. 7. McGraw-Hill, New York.

Molzahn, D. K., F. Dörfler, H. Sandberg, S. H. Low, S. Chakrabarti, R. Baldick, and J. Lavaei (2017). "A survey of distributed optimization and control algorithms for electric power systems". *IEEE Transactions on Smart Grid* **8**:6, pp. 2941–2962. DOI: 10.1109/TSG.2017.2720471.

Monshizadeh, P., C. De Persis, T. Stegink, N. Monshizadeh, and A. van der Schaft (2017). "Stability and frequency regulation of inverters with capacitive inertia". In: *2017 IEEE 56th Annual Conference on Decision and Control (CDC)*. IEEE, pp. 5696–5701. DOI: 10.1109/CDC.2017.8264519.

Moylan, P. and B. Anderson (1973). "Nonlinear regulator theory and an inverse optimal control problem". *IEEE Transactions on Automatic Control* **18**:5, pp. 460–465. DOI: 10.1109/TAC.1973.1100365.

Paolone, M., T. Gaunt, X. Guillaud, M. Liserre, S. Meliopoulos, A. Monti, T. Van Cutsem, V. Vittal, and C. Vournas (2020). "Fundamentals of power systems modelling in the presence of converter-interfaced generation". *Electric Power Systems Research* **189**, p. 106811. DOI: 10.1016/j.epsr.2020.106811.

Sepulchre, R., M. Jankovic, and P. V. Kokotovic (2012). *Constructive nonlinear control.* Springer Science & Business Media, Berlin/Heidelberg, Germany.

Tayyebi, A., A. Anta, and F. Dörfler (2020). "Hybrid angle control and almost global stability of grid-forming power converters". *ArXiv preprint ArXiv:2008.07661.*

Usman, M. U. and M. O. Faruque (2019). "Applications of synchrophasor technologies in power systems". *Journal of Modern Power Systems and Clean Energy* **7**:2, pp. 211–226. DOI: 10.1007/s40565-018-0455-8.

Zhang, Y. and L. Xie (2015). "Online dynamic security assessment of microgrid interconnections in smart distribution systems". *IEEE Transactions on Power Systems* **30**:6, pp. 3246–3254. DOI: 10.1109/TPWRS.2014.2374876.

Zhang, Y. and L. Xie (2016). "A transient stability assessment framework in power electronic-interfaced distribution systems". *IEEE Transactions on Power Systems* **31**:6, pp. 5106–5114. DOI: 10.1109/TPWRS.2016.2531745.

5

Conclusions

In this thesis, we studied frequency synchronization of coupled high-order oscillators and synthesized inverse optimal (robust) stabilizing controllers in networked settings, exemplified through the study of inverter-based power generation.
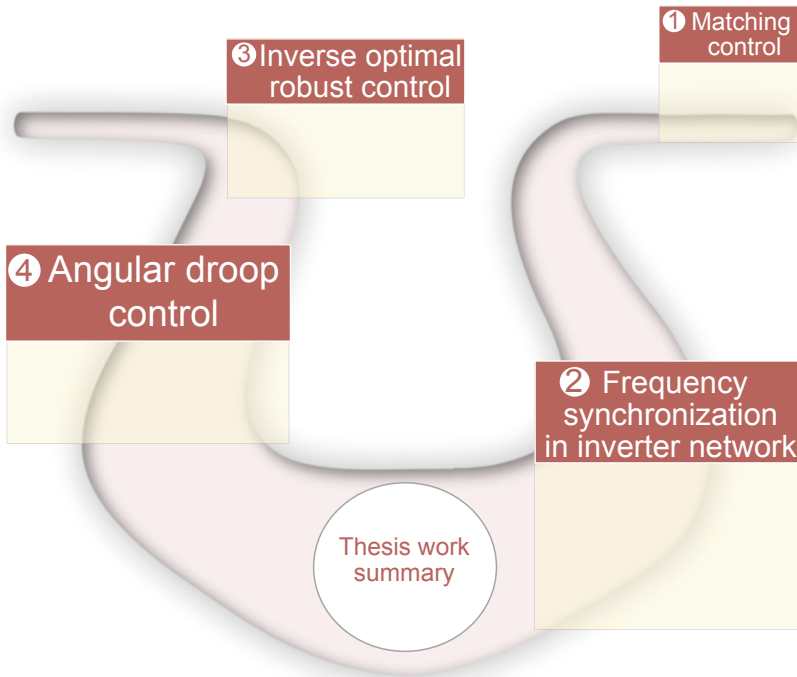
5.1 Concluding discussion

In the following, we summarize four takeaways presented in each paper of this thesis and then answer the research questions posed in Chapter 1. A summary of all the papers presented in this thesis is given in Fig. IV.1.

5.1.1 Takeaways

Next, we discuss the implications of our work for control designers and power engineers. We summarize how we should think of our results and use them.

The matching control draws the attention to the DC circuit The matching control demonstrates the relevance of DC-side measurements, namely the DC capacitor's voltage, to achieve transient stability with global frequency synchronization with the remainder of the grid. This draws the attention to the key role that DC circuit plays in control of converters. We corroborated the intuition that AC power must come from somewhere, namely the DC-side of the converter. Bringing the attention to the DC-side control in the example of the matching control, is provably crucial to provide resilience to the power grid through different services (stable operation, droop behavior at steady state, power support, power sharing).

A high-order converter-system achieves local frequency synchronization, provided sufficient damping For a network of high-order DC/AC converter system, characterized by their symmetry that results from a static shift in all angles, we have seen how local asymptotic (or small-signal) stability of

❸ Inverse optimal robust control

❶ Matching control

❹ Angular droop control

❷ Frequency synchronization in inverter network

Thesis work summary

Figure IV.1 A summary of all papers presented in this thesis.

their steady state set can be deduced from center manifold theory. This is achieved under the eigenvalue conditions on the system Jacobian (upon linearization of the converter system dynamics around a steady state) that leads to physically meaningful and explicit conditions. The damping on the DC-side, achieved via proportional control, and a high resistance of the output filter or H_∞ control on AC-side, are sufficient for the local frequency synchronization among the DC/AC converters.

This (re-)affirms that damping in converter control is sufficient for local frequency stability in power systems.

The choice of the cost to minimize is key to design optimal stabilizing controllers Starting from a given stabilizing controller, we have seen how the cost functional can be used as a design tool for the controller be optimal. This is achieved at a zero analytical and computational effort. We illustrated this important observation through the study of inverse optimal robust control

problems, where the disturbance affects both the cost and system dynamics. For power networks, inverse optimal control improves the error decay rate of the angle transients in droop-controlled inverters.

From a practical point of view, associating optimality with an existing stabilizing controller provides engineers and practitioners with an intuition, on when and how to deploy a given controller and make an appropriate selection of its parameters. This is measured by a performance index represented by the cost to minimize. Additionally, optimality endows the closed-loop system with inherent robustness guarantees of the controller against uncertainties, analogous in the linear case, to an LQR controller known (for a diagonal input matrix R) to have an *infinite* gain and 60° phase margin.

Angular droop is an inverse optimal stabilizing controller   This work examines, theoretically and numerically, inverse optimal control, when embedded in a networked system, in the example of inverter-based power systems. We highlight the possibility of deploying inverse optimal control to specifically design nonlinear controllers with topological structure. Indeed, the angular droop controller is a *distributed* solution of the optimization problem, as a function of neighboring converters' angles, and thus admits a feasible implementation.

The angular droop controller exploits the idea of power-to-angle droop in achieving exact frequency synchronization and thus merging primary with secondary frequency control. This suggests to rethink the classical scheme of time-scale separation, associated with the presence of synchronous machines in the grid. The angular droop control was suggested in the literature of power systems. From a methodological point of view and given the large number of controllers already suggested for DC/AC converter-based generation, reverse engineering optimality for an *existing* controller, in our case, the angular droop control, sheds light into the role optimization theory can play in making a decision between possibly different controllers and which one to deploy in a given setup and for a well-defined purpose.

5.1.2   Revisiting the research questions

In the following, we revisit the research questions posed in Chapter 1.

Question ①   *From a system-theoretical perspective, how can we understand and predict frequency synchronization in a network of coupled oscillators, where each oscillator is represented by high-order dynamics, and provide control strategies with provable stability guarantees that achieve desired waveforms?*

In Papers I and II, we have investigated the dynamical behavior of a (network of) nonlinear oscillator(s), (each) described by a sixth-order model,

whose frequency follows the matching control, an adaptive feedback control law. The power system has a rotational invariance resulting from a static shift of all angles and thus possesses a continuum of equilibria. To study network stability, we have employed the center manifold theorem to predict the behavior of nonlinear trajectories in the vicinity of the steady state set and arrived at sufficient conditions for local frequency synchronization. Moreover, we have deployed a set of theoretical tools based on passivity theory, direct and indirect Lyapunov methods and the center manifold theorem.

Question ②   *How can we exploit cost design for the setting, where the cost, in addition to the system dynamics, is affected by bounded disturbances, to circumvent numerical and computational complexity, resulting from solving partial differential equations? In networks, how can we derive optimal control laws that inherit topological structure, i.e., that are feasible for implementation, in an explicit and closed-form?*

In Papers III and IV, we have developed a systematic approach to design (robust) feedback stabilizing controllers that are optimal with respect to an *a posteriori* chosen cost functional following inverse optimal control theory. Their tuning is comparable, intuitively, to that of linear quadratic regulators. We provided extensions to existing robust settings by including a term accounting for the disturbance in the cost functional, and also in the system dynamics. We have demonstrated the benefits of inverse optimal control through different examples to derive optimal (robust) stabilizing distributed controllers for networked systems.

Question ③   *Bearing the two previous questions in mind and given a power system network dominated by inverter-based generation interconnected via transmission lines, how can we derive primary (and possibly secondary) frequency controllers with a feasible structure, i.e., whose implementation is possible, while also guaranteeing transient or small-signal stability? Under which mild physical conditions can this be achieved? Can we also guarantee plug and play properties and improve upon existing control schemes?*

In the light of our analysis of the matching control in Paper I, we have investigated the behavior of a single converter in closed-loop with the matching control connected to a resistive load. We proposed different approaches to increment the matching control with frequency and amplitude regulation schemes based on passivity-based and energy shaping techniques, as well as droop and feedforward control methods. We studied the steady state properties of this control scheme leading to linear mapping between power and frequency and to power sharing among converters. Moreover, we extended our setup in Paper II to a power network consisting of identical inverters, in closed-loop with matching control, interconnected via identical inductive and

resistive lines. We guarantee frequency synchronization (global for a single converter connected to a load, local in a high-dimensional multi-converter system) under mild conditions, asking for sufficient damping on the DC- and AC-side of (each) inverter.

In Papers III and IV, we have demonstrated the usefulness of inverse optimal control in networked settings to design controllers with network topological structure, i.e., distributed controllers at different occasions. For frequency droop-controlled inverters, we have shown how we can increment these with a distributed controller that improves the error decay rate of the angle transients despite recurrent, yet unpredictable load or generation fluctuations. This leads to an overall better response of the multi-converter system with respect to common disturbances and to avoid stress situations during transients, where many devices can saturate. For voltage-source controlled inverters, the angular droop control has been shown to be inverse optimal stabilizing and guarantees zero frequency error at steady state. The tuning of these inverse optimal controllers is intuitive. Droop behavior and therefore, power sharing among inverters are guaranteed.

5.2   Future research directions

This thesis work leaves the door open for many research directions that are inspired by our findings. We indicate future research directions.

5.2.1   Conservativeness of local synchronization analysis

We conjecture that local asymptotic stability results presented in this thesis are conservative and can be extended to an almost-global stability result, where global convergence to a steady state set is guaranteed, up to a set of initial conditions of zero Lebesgue measure. For second-order oscillators in the example of droop-controlled inverters, an almost global analysis has been conducted in [Schiffer et al., 2019]. Similarly, first-order nonlinear oscillators in the light of virtual oscillator controlled inverters are known to be globally synchronizing [Colombino et al., 2019]. We leverage the interpretation of the matching control as a nonlinear oscillator established in [Jouini et al., 2016] and the multiple numerical studies that tested the matching control [Jouini et al., 2018]. It has been observed, at many occasions, that this controller is stabilizing for a network of high-order converter model, even under large disturbances, e.g., line faults and resilient to abrupt load changes. These numerical and intuitive interpretations guide and motivate the consideration of almost global frequency synchronization analysis of a network of high-order oscillators.

5.2.2 Constrained inverse optimal control

The important limitation that, for long, has challenged control theorists in dealing with direct optimal control using dynamic programming, is the analytical and numerical difficulty associated with solving partial differential equations for optimal solutions. Incorporating input and state constraints makes the problem even harder to solve. Inverse optimal control flips the order of optimal control synthesis. It starts with a stabilizing controller, whose optimality is a byproduct of reverse engineering the cost functional. This motivates the exploration of the potential of inverse optimal control in the study of optimization problems with input, state and output constraints. Despite recent efforts in the direction of incorporating input [Nakamura et al., 2007] and state [Deniz et al., 2020] constraints, inverse optimal control problems with general set constraints that account for input, state and output states, simultaneously, have not been studied in the literature. Additionally, we aim to integrate our approach into the big picture with other important classical methods that are known to handle constraints well, such as Model Predictive Control (MPC) [Morari and Lee, 1999] and emerging new approaches, such as online feedback optimization [Colombino et al., 2020; Hauswirth et al., 2020]. For the ease of comparison, it is more convenient to embed our control law in a discrete-time formulation (as in [Haddad and Chellaboina, 2011; Sanchez and Ornelas-Tellez, 2017]) and suggest suitable implementations under input and state constraints. Power systems remain a direct application of this future work, where input limitations represent, for example, lower and upper limits on power generation set-points or modulation amplitude limits in converter-based generation and the output/state constraints consist in upper and lower bounds on line congestion [Menta et al., 2018].

5.2.3 Study of inverter-interfaced generation

Despite the large and growing number of papers on inverter-based control, the power system community is still facing a myriad of theoretical and practical challenges hindering a full integration of inverter-based generation. In this thesis, we have put our primary emphasis on frequency synchronization and control, since system frequency is a global quantity, quintessential for primary control. Voltage regulation came into the picture only as ad-hoc to the matching control in Paper I through outer layers via the control of the modulation amplitude. It is known that the modulation signal, is constrained to the interval $[-1, 1]$, which makes the controllability margin limited and some control solutions might not be practically implementable. This suggests to think of an alternative, more systematic approach for voltage control. Motivated by the interpretation of the matching control as a nonlinear virtual oscillator as delineated in [Jouini et al., 2016], we can increment the matching controller with an adaptive amplitude function, similar to the dynamics

of $(\lambda - \omega)$ oscillations in biological systems [Murray, 2007]. The adaptive voltage and frequency functions suggested in these oscillations serve as degrees of freedom to regulate important DC and AC voltages and currents. This constitutes a future research direction that we aim to investigate in our future work.

Bibliography

Ab Azar, N., A. Shahmansoorian, and M. Davoudi (2020). "From inverse optimal control to inverse reinforcement learning: a historical review". *Annual Reviews in Control* **50**, pp. 119–138. DOI: `10.1016/j.arcontrol.2020.06.001`.

Acebrón, J. A., L. L. Bonilla, C. J. P. Vicente, F. Ritort, and R. Spigler (2005). "The Kuramoto model: a simple paradigm for synchronization phenomena". *Reviews of Modern Physics* **77**:1, p. 137. DOI: `10.1103/RevModPhys.77.137`.

Aeyels, D. and J. A. Rogge (2004). "Existence of partial entrainment and stability of phase locking behavior of coupled oscillators". *Progress of Theoretical Physics* **112**:6, pp. 921–942. DOI: `10.1143/PTP.112.921`.

Anderson, P. M. and A. A. Fouad (2008). *Power system control and stability*. John Wiley & Sons, Hoboken, New Jersey, USA.

Angeli, D. (2004). "An almost global notion of input-to-state stability". *IEEE Transactions on Automatic Control* **49**:6, pp. 866–874. DOI: `10.1109/TAC.2004.829594`.

Arghir, C. and F. Dörfler (2019). "The electronic realization of synchronous machines: model matching, angle tracking, and energy shaping techniques". *IEEE Transactions on Power Electronics* **35**:4, pp. 4398–4410. DOI: `10.1109/TPEL.2019.2939710`.

Arghir, C., T. Jouini, and F. Dörfler (2018). "Grid-forming control for power converters based on matching of synchronous machines". *Automatica* **95**, pp. 273–282. DOI: `10.1016/j.automatica.2018.05.037`.

Barabanov, N., J. Schiffer, R. Ortega, and D. Efimov (2016). "Almost global attractivity of a synchronous generator connected to an infinite bus". In: *2016 IEEE 55th Conference on Decision and Control (CDC)*. IEEE, pp. 4130–4135. DOI: `10.1109/CDC.2016.7798895`.

Başar, T. and P. Bernhard (2008). *H-infinity optimal control and related minimax design problems: a dynamic game approach.* Springer Science & Business Media, Berlin/Heidelberg, Germany.

Bennett, M., M. F. Schatz, H. Rockwood, and K. Wiesenfeld (2002). "Huygens's clocks". *Proceedings of the Royal Society of London. Series A: Mathematical, Physical and Engineering Sciences* **458**:2019, pp. 563–579. DOI: 10.1098/rspa.2001.0888.

Berret, B. and F. Jean (2016). "Why don't we move slower? The value of time in the neural control of action". *Journal of neuroscience* **36**:4, pp. 1056–1070. DOI: 10.1523/JNEUROSCI.1921-15.2016.

Bevrani, H., T. Ise, and Y. Miura (2014). "Virtual synchronous generators: a survey and new perspectives". *International Journal of Electrical Power & Energy Systems* **54**, pp. 244–254. DOI: 10.1016/j.ijepes.2013.07.009.

Bick, C., M. Goodfellow, C. R. Laing, and E. A. Martens (2020). "Understanding the dynamics of biological and neural oscillator networks through exact mean-field reductions: a review". *The Journal of Mathematical Neuroscience* **10**, pp. 1–43. DOI: 10.1186/s13408-020-00086-9.

Boltyanskiy, V., R. Gamkrelidze, Y. Mishchecnko, and L. Pontryagin (1962). *Mathematical theory of optimal processes.* Interscience, New York, USA.

Bullo, F. (2021). *Lectures on Network Systems.* Kindle Direct Publishing. ISBN: 978-1986425643. URL: http://motion.me.ucsb.edu/book-lns.

Busby, J. W., K. Baker, M. D. Bazilian, A. Q. Gilbert, E. Grubert, V. Rai, J. D. Rhodes, S. Shidore, C. A. Smith, and M. E. Webber (2021). "Cascading risks: understanding the 2021 winter blackout in Texas". *Energy Research & Social Science* **77**, p. 102106.

Caliskan, S. Y. and P. Tabuada (2014). "Compositional transient stability analysis of multimachine power networks". *IEEE Transactions on Control of Network systems* **1**:1, pp. 4–14. DOI: 10.1109/TCNS.2014.2304868.

Cao, F., T. Yang, Y. Li, and S. Tong (2019). "Adaptive neural inverse optimal control for a class of strict feedback stochastic nonlinear systems". In: *2019 IEEE 8th Data Driven Control and Learning Systems Conference (DDCLS).* IEEE, pp. 432–436. DOI: 10.1109/DDCLS.2019.8908901.

Casti, J. (1974). *A Note on the General Inverse Problem of Optimal Control Theory.* IIASA Research Memorandum. IIASA, Laxenburg, Austria. URL: http://pure.iiasa.ac.at/id/eprint/196/.

Chandorkar, M. C., D. M. Divan, and R. Adapa (1993). "Control of parallel connected inverters in standalone AC supply systems". *IEEE Transactions on Industry Applications* **29**:1, pp. 136–143. DOI: 10.1109/28.195899.

Chang, H.-D., C.-C. Chu, and G. Cauley (1995). "Direct stability analysis of electric power systems using energy functions: theory, applications, and perspective". *Proceedings of the IEEE* **83**:11, pp. 1497–1529. DOI: 10.1109/5.481632.

Chiang, H.-D. (1989). "Study of the existence of energy functions for power systems with losses". *IEEE Transactions on Circuits and Systems* **36**:11, pp. 1423–1429. DOI: 10.1109/31.41298.

Chopra, N. and M. W. Spong (2009). "On exponential synchronization of Kuramoto oscillators". *IEEE Transactions on Automatic Control* **54**:2, pp. 353–357. DOI: 10.1109/TAC.2008.2007884.

Colombino, M., E. Dall'Anese, and A. Bernstein (2020). "Online optimization as a feedback controller: stability and tracking". *IEEE Transactions on Control of Network Systems* **7**:1, pp. 422–432. DOI: 10.1109/TCNS.2019.2906916.

Colombino, M., D. Groß, J.-S. Brouillon, and F. Dörfler (2019). "Global phase and magnitude synchronization of coupled oscillators with application to the control of grid-forming power inverters". *IEEE Transactions on Automatic Control* **64**:11, pp. 4496–4511. DOI: 10.1109/TAC.2019.2898549.

Como, G. and F. Fagnani (2021). *Lecture notes on Network Dynamics*. URL: https://www.control.lth.se/education/engineering-program/frtn30-network-dynamics/.

De Persis, C. and N. Monshizadeh (2017). "Bregman storage functions for microgrid control". *IEEE Transactions on Automatic Control* **63**:1, pp. 53–68. DOI: 10.1109/TAC.2017.2709246.

Delavari, A., I. Kamwa, and P. Brunelle (2018). "Simscape power systems benchmarks for education and research in power grid dynamics and control". In: *2018 IEEE Canadian Conference on Electrical Computer Engineering (CCECE)*, pp. 1–5. DOI: 10.1109/CCECE.2018.8447645.

Denis, G. (2017). *From grid-following to grid-forming: The new strategy to build 100% power-electronics interfaced transmission system with enhanced transient behavior*. PhD thesis. Centrale Lille, Lille, France.

Deniz, M., P. Devi, and S. N. Balakrishnan (2020). "Inverse Optimal Control with Set-Theoretic Barrier Lyapunov Function for Handling State Constraints". In: *2020 American Control Conference (ACC)*, pp. 981–986. DOI: 10.23919/ACC45564.2020.9147707.

Di Benedetto, M. D. and A. Isidori (1986). "The matching of nonlinear models via dynamic state feedback". *SIAM journal on control and optimization* **24**:5, pp. 1063–1075. DOI: 10.1137/0324063.

Dörfler, F. and F. Bullo (2012a). "Kron reduction of graphs with applications to electrical networks". *IEEE Transactions on Circuits and Systems I: Regular Papers* **60**:1, pp. 150–163. DOI: 10.1109/TCSI.2012.2215780.

Dörfler, F. and F. Bullo (2012b). "Synchronization and transient stability in power networks and nonuniform Kuramoto oscillators". *SIAM Journal on Control and Optimization* **50**:3, pp. 1616–1642. DOI: 10.1137/110851584.

Dörfler, F. and F. Bullo (2014). "Synchronization in complex networks of phase oscillators: a survey". *Automatica* **50**:6, pp. 1539–1564. DOI: 10.1016/j.automatica.2014.04.012.

Dörfler, F., M. Chertkov, and F. Bullo (2013). "Synchronization in complex oscillator networks and smart grids". *Proceedings of the National Academy of Sciences* **110**:6, pp. 2005–2010. DOI: 10.1073/pnas.1212134110.

Dörfler, F., J. W. Simpson-Porco, and F. Bullo (2015). "Breaking the hierarchy: distributed control and economic optimality in microgrids". *IEEE Transactions on Control of Network Systems* **3**:3, pp. 241–253. DOI: 10.1109/TCNS.2015.2459391.

European Commission (2012). "Energy roadmap 2050". URL: https://ec.europa.eu/energy/sites/ener/files/documents/2012_energy_roadmap_2050_en_0.pdf.

Finn, C., S. Levine, and P. Abbeel (2016). "Guided cost learning: deep inverse optimal control via policy optimization". In: *International conference on machine learning.* PMLR, pp. 49–58. DOI: 10.5555/3045390.3045397.

Forni, F. and R. Sepulchre (2013). "A differential Lyapunov framework for contraction analysis". *IEEE Transactions on Automatic Control* **59**:3, pp. 614–628. DOI: 10.1109/TAC.2013.2285771.

Franci, A., A. Chaillet, and W. Pasillas-Lépine (2010). "Phase-locking between Kuramoto oscillators: robustness to time-varying natural frequencies". In: *49th IEEE Conference on Decision and Control (CDC).* IEEE, pp. 1587–1592. DOI: 10.1109/CDC.2010.5717876.

Freeman, R. A. and P. V. Kokotovic (1996). "Inverse optimality in robust stabilization". *SIAM Journal on Control and Optimization* **34**:4, pp. 1365–1391. DOI: 10.1137/S0363012993258732.

Gazzola, F. and E. M. Marchini (2021). "The moon lander optimal control problem revisited". *Mathematics in Engineering* **3**, pp. 1–14. DOI: 10.3934/mine.2021040.

Geng, Y., D. Song, and R. Sun (2016). "Inverse optimal stabilization of an underactuated spacecraft using two wheels". In: *2016 8th International Conference on Intelligent Human-Machine Systems and Cybernetics (IHMSC).* Vol. 1. IEEE, pp. 279–282. DOI: 10.1109/IHMSC.2016.270.

Glad, S. T. (1987). "Robustness of nonlinear state feedback—a survey". *Automatica* **23**:4, pp. 425–435. DOI: 10.1016/0005-1098(87)90072-0.

Godsil, C. and G. F. Royle (2001). *Algebraic graph theory.* Vol. 207. Springer Science & Business Media, Berlin/Heidelberg, Germany.

Gülen, S. C. (2019). "The alternating current generator". In: *Gas Turbines for Electric Power Generation*. Cambridge University Press, pp. 425–452. DOI: 10.1017/9781108241625.016.

Ha, T.-J., J. Lee, and J. H. Park (2007). "Robust control by inverse optimal PID approach for flexible joint robot manipulator". In: *2007 IEEE International Conference on Robotics and Biomimetics (ROBIO)*. IEEE, pp. 336–341. DOI: 10.1109/ROBIO.2007.4522184.

Haddad, W. M. and V. Chellaboina (2011). *Nonlinear dynamical systems and control*. Princeton university press, Princeton, New Jersey.

Hauswirth, A., S. Bolognani, G. Hug, and F. Dörfler (2020). "Timescale separation in autonomous optimization". *IEEE Transactions on Automatic Control* **66**:2, pp. 611–624. DOI: 10.1109/TAC.2020.2989274.

Izhikevich, E. M., Y. Kuramoto, et al. (2006). "Weakly coupled oscillators". *Encyclopedia of Mathematical Physics* **5**, p. 448. DOI: 10.1016/B0-12-512666-2/00106-1.

Jadbabaie, A., N. Motee, and M. Barahona (2004). "On the stability of the Kuramoto model of coupled nonlinear oscillators". In: *Proceedings of the 2004 American Control Conference*. Vol. 5. IEEE, pp. 4296–4301. DOI: 10.23919/ACC.2004.1383983.

Jafarpour, S. and F. Bullo (2018). "Synchronization of Kuramoto oscillators via cutset projections". *IEEE Transactions on Automatic Control* **64**:7, pp. 2830–2844. DOI: 10.1109/TAC.2018.2876786.

Jin, W. and S. Mou (2021). "Distributed inverse optimal control". *Automatica* **129**, p. 109658. DOI: 10.1109/LCSYS.2021.3050093.

Johnson, B. B., S. V. Dhople, A. O. Hamadeh, and P. T. Krein (2013). "Synchronization of parallel single-phase inverters with virtual oscillator control". *IEEE Transactions on Power Electronics* **29**:11, pp. 6124–6138. DOI: 10.1109/TPEL.2013.2296292.

Jouini, T. (2016). *Grid-friendly Matching Control of Synchronous Machines by DC/AC converters in Bulk Power Networks*. Master thesis, Institute for Systems Theory and Control (IST), University of Stuttgart.

Jouini, T., C. Arghir, and F. Dörfler (2016). "Grid-friendly matching of synchronous machines by tapping into the DC storage". *IFAC-PapersOnLine* **49**:22, pp. 192–197. DOI: 10.1016/j.ifacol.2016.10.395.

Jouini, T., U. Markovic, and D. Gross (2018). "WP3-Control and Operation of a Grid with 100% converter-based devices". *Final deliverables of Migrate project*. URL: https://www.h2020-migrate.eu.

Kalman, R. E. (1964). "When is a linear control system optimal?" *Journal of Basic Engineering* **86**:1, pp. 51–60. DOI: 10.1115/1.3653115.

Bibliography

Kalman, R. E. (1960). "Contributions to the theory of optimal control". *Bol. soc. mat. mexicana* **5**:2, pp. 102–119. DOI: 10.1109/9780470544334.ch8.

Kamel, N. and J. Glotfelty (2003). "Interim report: causes of the August 14th blackout in the United States and Canada". URL: https://digital.library.unt.edu/ark:/67531/metadc26005/.

Khalil, H. K. (2002). *Nonlinear systems*. Vol. 3. Prentice Hall, Upper Saddle River, NJ.

Kot, M. (2014). *A first course in the calculus of variations*. Vol. 72. American Mathematical Society.

Krick, L., M. E. Broucke, and B. A. Francis (2009). "Stabilisation of infinitesimally rigid formations of multi-robot networks". *International Journal of control* **82**:3, pp. 423–439. DOI: 10.1080/00207170802108441.

Krstic, M. and P. Tsiotras (1999). "Inverse optimal stabilization of a rigid spacecraft". *IEEE Transactions on Automatic Control* **44**:5, pp. 1042–1049. DOI: 10.1109/9.763225.

Kundur, P., N. J. Balu, and M. G. Lauby (1994). *Power system stability and control*. Vol. 7. McGraw-Hill, New York.

Kundur, P., J. Paserba, V. Ajjarapu, G. Andersson, A. Bose, C. Canizares, N. Hatziargyriou, D. Hill, A. Stankovic, C. Taylor, et al. (2004). "Definition and classification of power system stability". *IEEE Transactions on Power Systems* **19**:2, pp. 1387–1401. DOI: 10.1109/TPWRS.2004.825981.

Kuramoto, Y. (1975). "Self-entrainment of a population of coupled non-linear oscillators". In: *International symposium on mathematical problems in theoretical physics*. Springer, New York City, USA, pp. 420–422. DOI: 10.1007/BFb0013365.

"Land-Based Wind Market Report: 2021 Edition" (2021). DOI: 10.2172/1818841. URL: https://www.osti.gov/biblio/1818841.

Lehtomaki, N., N. Sandell, and M. Athans (1981). "Robustness results in linear-quadratic Gaussian based multivariable control designs". *IEEE Transactions on Automatic Control* **26**:1, pp. 75–93. DOI: 10.1109/TAC.1981.1102565.

Leonov, G. A. (2006). "Phase synchronization: theory and applications". *Automation and Remote Control* **67**:10, pp. 1573–1609. DOI: 10.1134/S0005117906100031.

Liberzon, D. (2011). *Calculus of variations and optimal control theory: a concise introduction*. Princeton University Press, Princeton, New Jersey.

Lin, Y., J. H. Eto, B. B. Johnson, J. D. Flicker, R. H. Lasseter, H. N. Villegas Pico, G.-S. Seo, B. J. Pierre, and A. Ellis (2020). *Research roadmap on grid-forming inverters*. Tech. rep. National Renewable Energy Lab.(NREL), Golden, CO (United States). DOI: 10.2172/1721727.

Lin, Y., E. D. Sontag, and Y. Wang (1996). "A smooth converse Lyapunov theorem for robust stability". *SIAM Journal on Control and Optimization* **34**:1, pp. 124–160. DOI: 10.1137/S0363012993259981.

Lincoln, B. and A. Rantzer (2006). "Relaxing dynamic programming". *IEEE Transactions on Automatic Control* **51**:8, pp. 1249–1260. DOI: 10.1109/TAC.2006.878720.

Liu, X., G. Zhang, D. Yang, T. Shi, and X. He (2014). "Discrete-time optimal control of photovoltaic grid-connected inverter based on particle swarm optimization". *Mathematical Problems in Engineering* **2014**. DOI: 10.1155/2014/249312.

Lu, C., J. Si, and X. Xie (2008). "Direct heuristic dynamic programming for damping oscillations in a large power system". *IEEE Transactions on Systems, Man, and Cybernetics, Part B (Cybernetics)* **38**:4, pp. 1008–1013. DOI: 10.1109/TSMCB.2008.923157.

Meditch, J. (1964). "On the problem of optimal thrust programming for a lunar soft landing". *IEEE Transactions on Automatic Control* **9**:4, pp. 477–484. DOI: 10.1109/TAC.1964.1105758.

Menner, M., P. Worsnop, and M. N. Zeilinger (2021). "Constrained inverse optimal control with application to a human manipulation task". *IEEE Transactions on Control Systems Technology* **29**:2, pp. 826–834. DOI: 10.1109/TCST.2019.2955663.

Menta, S., A. Hauswirth, S. Bolognani, G. Hug, and F. Dörfler (2018). "Stability of dynamic feedback optimization with applications to power systems". In: *2018 56th Annual Allerton Conference on Communication, Control, and Computing (Allerton)*, pp. 136–143. DOI: 10.1109/ALLERTON.2018.8635640.

Miele, A. (1962). "The calculus of variations in applied aerodynamics and flight mechanics". In: *Mathematics in Science and Engineering*. Vol. 5. Elsevier, pp. 99–170.

Mirollo, R. E. and S. H. Strogatz (2005). "The spectrum of the locked state for the Kuramoto model of coupled oscillators". *Physica D: Nonlinear Phenomena* **205**:1-4, pp. 249–266.

Molloy, T. L., J. Inga, M. Flad, J. J. Ford, T. Perez, and S. Hohmann (2019). "Inverse open-loop non-cooperative differential games and inverse optimal control". *IEEE Transactions on Automatic Control* **65**:2, pp. 897–904. DOI: 10.1109/TAC.2019.2921835.

Mombaur, K., A. Truong, and J.-P. Laumond (2010). "From human to humanoid locomotion—an inverse optimal control approach". *Autonomous robots* **28**:3, pp. 369–383. DOI: 10.1007/s10514-009-9170-7.

Morari, M. and J. H. Lee (1999). "Model predictive control: past, present and future". *Computers & Chemical Engineering* **23**:4-5, pp. 667–682. DOI: 10.1016/S0098-1354(98)00301-9.

Moreno, Y. and A. F. Pacheco (2004). "Synchronization of Kuramoto oscillators in scale-free networks". *EPL (Europhysics Letters)* **68**:4, p. 603. DOI: 10.1209/epl/i2004-10238-x.

Moylan, P. and B. Anderson (1973). "Nonlinear regulator theory and an inverse optimal control problem". *IEEE Transactions on Automatic Control* **18**:5, pp. 460–465. DOI: 10.1109/TAC.1973.1100365.

Murray, J. D. (2007). *Mathematical biology: I. An introduction*. Vol. 17. Springer Science & Business Media, Berlin/Heidelberg, Germany.

Murray, R. M. (2009). *Optimization-based control*. Tech. rep., pp. 111–128. URL: http://www.cds.caltech.edu/~murray/amwiki/OBC.

Nabae, A., I. Takahashi, and H. Akagi (1981). "A new neutral-point-clamped pwm inverter". *IEEE Transactions on industry applications* 5, pp. 518–523.

Najmabadi, S. and M. Martinez (2021). *''We're in it alone": Power outages leave millions of Texans desperate for heat and safety*. URL: https://www.tARGHIR2018273exastribune.org/2021/02/16/texans-weather-power-outage/.

Nakamura, N., H. Nakamura, Y. Yamashita, and H. Nishitani (2007). "Inverse optimal control for nonlinear systems with input constraints". In: *2007 European Control Conference (ECC)*, pp. 5376–5382. DOI: 10.23919/ECC.2007.7068412.

Nishikawa, T., A. E. Motter, Y.-C. Lai, and F. C. Hoppensteadt (2003). "Heterogeneity in oscillator networks: Are smaller worlds easier to synchronize?" *Physical Review Letters* **91**:1, p. 014101. DOI: 10.1103/PhysRevLett.91.014101.

O'Keeffe, K. P., H. Hong, and S. H. Strogatz (2017). "Oscillators that sync and swarm". *Nature Communications* **8**:1, pp. 1–13. DOI: 10.1038/s41467-017-01190-3.

Ornelas-Tellez, F., J. Rico, G. Zunig, and G. Casarrubias (2012). "Inverse optimal trajectory tracking for discrete–time nonlinear systems: application to the boost converter". *Proceedings of the 2012 ROPEC INTERNACIONAL, Colima, México*, pp. 7–9.

Ornelas, F., E. N. Sanchez, and A. G. Loukianov (2010). "Discrete-time inverse optimal control for nonlinear systems trajectory tracking". In: *49th IEEE Conference on Decision and Control (CDC)*. IEEE, pp. 4813–4818. DOI: 10.1109/CDC.2010.5716974.

Ortega, R., M. Galaz, A. Astolfi, Y. Sun, and T. Shen (2005). "Transient stabilization of multimachine power systems with nontrivial transfer conductances". *IEEE Transactions on Automatic Control* **50**:1, pp. 60–75. DOI: `10.1109/TAC.2004.840477`.

Ortega, R., A. van der Schaft, B. Maschke, and G. Escobar (2002). "Interconnection and damping assignment passivity-based control of port-controlled Hamiltonian systems". *Automatica* **38**:4, pp. 585–596. DOI: `10.1109/CDC.2004.1429236`.

Pahlevaninezhad, M., P. Das, J. Drobnik, G. Moschopoulos, P. K. Jain, and A. Bakhshai (2012). "A nonlinear optimal control approach based on the control-Lyapunov function for an AC/DC converter used in electric vehicles". *IEEE Transactions on Industrial Informatics* **8**:3, pp. 596–614. DOI: `10.1109/TII.2012.2193894`.

Pai, M. and P. Murthy (1973). "On Lyapunov functions for power systems with transfer conductances". *IEEE Transactions on Automatic Control* **18**:2, pp. 181–183. DOI: `10.1109/TPWRS.2003.811207`.

Pai, M. (1981). *Power system stability: analysis by the direct method of Lyapunov*. Vol. 3. North-Holland Publishing Company, Amsterdam, Netherlands.

Papachristodoulou, A., A. Jadbabaie, and U. Münz (2010). "Effects of delay in multi-agent consensus and oscillator synchronization". *IEEE Transactions on Automatic Control* **55**:6, pp. 1471–1477. DOI: `10.1109/TAC.2010.2044274`.

Poolla, B. K., S. Bolognani, and F. Dörfler (2017). "Optimal placement of virtual inertia in power grids". *IEEE Transactions on Automatic Control* **62**:12, pp. 6209–6220. DOI: `10.1109/TAC.2017.2703302`.

Rantzer, A. and M. E. Valcher (2018). "A tutorial on positive systems and large scale control". In: *2018 IEEE Conference on Decision and Control (CDC)*. IEEE, pp. 3686–3697. DOI: `10.1109/CDC.2018.8618689`.

Rocabert, J., A. Luna, F. Blaabjerg, and P. Rodriguez (2012). "Control of power converters in AC microgrids". *IEEE Transactions on Power Electronics* **27**:11, pp. 4734–4749. DOI: `10.1109/TPEL.2012.2199334`.

Ruiz-Cruz, R., E. N. Sanchez, A. G. Loukianov, and J. A. Ruz-Hernandez (2018). "Real-time neural inverse optimal control for a wind generator". *IEEE Transactions on Sustainable Energy* **10**:3, pp. 1172–1183. DOI: `10.1109/TSTE.2018.2862628`.

Sanchez-Sanchez, E., D. Gross, E. Prieto-Araujo, F. Dörfler, and O. Gomis-Bellmunt (2019). "Optimal multivariable MMC energy-based control for DC voltage regulation in HVDC applications". *IEEE Transactions on Power Delivery* **35**:2, pp. 999–1009. DOI: `10.1109/TPWRD.2019.2933771`.

Sanchez, E. N. and F. Ornelas-Tellez (2017). *Discrete-time inverse optimal control for nonlinear systems*. CRC Press, Boca Raton, Florida, USA.

Sarlette, A. (2009). *Geometry and symmetries in coordination control*. PhD thesis. Université de Liège, Belgium. URL: https://hdl.handle.net/2268/9544.

Sauer, P. W., M. A. Pai, and J. H. Chow (2017). *Power system dynamics and stability: with synchrophasor measurement and power system toolbox*. John Wiley & Sons, Hoboken, New Jersey, USA.

Schaft, A. J. van der (2000). *L2-gain and passivity techniques in nonlinear control*. Vol. 2. Springer, New York City, USA.

Schaft, A. van der and D. Jeltsema (2014). "Port-Hamiltonian systems theory: an introductory overview". *Foundations and Trends in Systems and Control* **1**:2-3, pp. 173–378. DOI: 10.1561/2600000002.

Schiffer, J., D. Efimov, and R. Ortega (2019). "Global synchronization analysis of droop-controlled microgrids—a multivariable cell structure approach". *Automatica* **109**, p. 108550. DOI: 10.1016/j.automatica.2019.108550.

Schiffer, J., D. Zonetti, R. Ortega, A. M. Stanković, T. Sezi, and J. Raisch (2016). "A survey on modeling of microgrids—from fundamental physics to phasors and voltage sources". *Automatica* **74**, pp. 135–150. DOI: 10.1016/j.automatica.2016.07.036.

Schmidt, G. S., A. Papachristodoulou, U. Münz, and F. Allgöwer (2012). "Frequency synchronization and phase agreement in Kuramoto oscillator networks with delays". *Automatica* **48**:12, pp. 3008–3017. DOI: 10.1016/j.automatica.2012.08.013.

Self, R., S. N. Mahmud, K. Hareland, and R. Kamalapurkar (2020). "Online inverse reinforcement learning with limited data". In: *2020 59th IEEE Conference on Decision and Control (CDC)*. IEEE, pp. 603–608. DOI: 10.1109/CDC42340.2020.9303883.

Sepulchre, R., M. Jankovic, and P. V. Kokotovic (2012). *Constructive nonlinear control*. Springer Science & Business Media, Berlin/Heidelberg, Germany.

Sepulchre, R., D. A. Paley, and N. E. Leonard (2007). "Stabilization of planar collective motion: all-to-all communication". *IEEE Transactions on Automatic Control* **52**:5, pp. 811–824. DOI: 10.1109/TAC.2007.898077.

Shaik, F., D. Zonetti, R. Ortega, J. Scherpen, and A. van der Schaft (2012). "Port hamiltonian modeling of power networks". In: *20th International Symposium on Mathematical Theory of Networks and Systems*. DOI: 10.1016/j.ejcon.2013.09.002.

Shklyaev, O. E., V. V. Yashin, S. I. Stupp, and A. C. Balazs (2020). "Enhancement of chemical oscillations by self-generated convective flows". *Communications Physics* **3**:1, pp. 1–9. DOI: 10.1038/s42005-020-0341-3.

Simpson-Porco, J. W. (2020). "A dynamic stability and performance analysis of automatic generation control". *arXiv preprint arXiv:2007.01832*.

Simpson-Porco, J. W., F. Dörfler, and F. Bullo (2013). "Synchronization and power sharing for droop-controlled inverters in islanded microgrids". *Automatica* **49**:9, pp. 2603–2611. DOI: `10.1016/j.automatica.2013.05.018`.

Sinha, M., F. Dörfler, B. B. Johnson, and S. V. Dhople (2015). "Uncovering droop control laws embedded within the nonlinear dynamics of van der pol oscillators". *IEEE Transactions on Control of Network Systems* **4**:2, pp. 347–358. DOI: `10.1109/TCNS.2015.2503558`.

Skar, S. J. (1980). "Stability of multi-machine power systems with nontrivial transfer conductances". *SIAM Journal on Applied Mathematics* **39**:3, pp. 475–491. DOI: `10.1137/0139040`.

Svenska Kraftnät (2020). URL: `https://www.svk.se/en/national-grid/map-of-the-national-grid`.

Tayyebi, A., A. Anta, and F. Dörfler (2020). "Hybrid angle control and almost global stability of grid-forming power converters". *ArXiv preprint ArXiv:2008.07661*.

Tegling, E., B. Bamieh, and D. F. Gayme (2015). "The price of synchrony: evaluating the resistive losses in synchronizing power networks". *IEEE Transactions on Control of Network Systems* **2**:3, pp. 254–266. DOI: `10.1109/TCNS.2015.2399193`.

Tsolas, N., A. Arapostathis, and P. Varaiya (1985). "A structure preserving energy function for power system transient stability analysis". *IEEE Transactions on Circuits and Systems* **32**:10, pp. 1041–1049. DOI: `10.1109/TCS.1985.1085625`.

Vega, C. and R. Alzate (2014). "Inverse optimal control on electric power conversion". In: *2014 IEEE International Autumn Meeting on Power, Electronics and Computing (ROPEC)*. IEEE, pp. 1–5. DOI: `10.1109/ROPEC.2014.7036320`.

Verwoerd, M. and O. Mason (2008). "Global phase-locking in finite populations of phase-coupled oscillators". *SIAM Journal on Applied Dynamical Systems* **7**:1, pp. 134–160. DOI: `10.1016/j.physd.2005.01.017`.

Verwoerd, M. and O. Mason (2009). "On computing the critical coupling coefficient for the Kuramoto model on a complete bipartite graph". *SIAM Journal on Applied Dynamical Systems* **8**:1, pp. 417–453. DOI: `10.1137/080725726`.

Vinter, R. (2010). *Optimal control*. Springer Science & Business Media, Berlin/Heidelberg, Germany.

Vu, T. L. and K. Turitsyn (2015). "Lyapunov functions family approach to transient stability assessment". *IEEE Transactions on Power Systems* **31**:2, pp. 1269–1277. DOI: `10.1109/TPWRS.2015.2425885`.

Weerasinghe, G., B. Duchet, H. Cagnan, P. Brown, C. Bick, and R. Bogacz (2019). "Predicting the effects of deep brain stimulation using a reduced coupled oscillator model". *PLoS Computational Biology* **15**:8, e1006575. DOI: 10.1371/journal.pcbi.1006575.

Wieland, P. (2010). *From static to dynamic couplings in consensus and synchronization among identical and non-identical systems.* Logos Verlag Berlin GmbH.

Wiggins, S. (1990). *Introduction to applied nonlinear dynamical systems and chaos.* Vol. 2. Springer, New York City, USA.

Willems, J. (1971). "Least squares stationary optimal control and the algebraic Riccati equation". *IEEE Transactions on Automatic Control* **16**:6, pp. 621–634. DOI: 10.1109/TAC.1971.1099831.

Willems, J. C. (2007). "Dissipative dynamical systems". *European Journal of Control* **13**:2-3, pp. 134–151. DOI: 10.3166/ejc.13.134-151.

Willems, J. C. (1972a). "Dissipative dynamical systems part I: General theory". *Archive for Rational Mechanics and Analysis* **45**:5, pp. 321–351. DOI: 10.1007/BF00276493.

Willems, J. C. (1972b). "Dissipative dynamical systems Part II: Linear systems with quadratic supply rates". *Archive for Rational Mechanics and Analysis* **45**:5, pp. 352–393. DOI: 10.1007/BF00276494.

Witthaut, D., S. Wimberger, R. Burioni, and M. Timme (2017). "Classical synchronization indicates persistent entanglement in isolated quantum systems". *Nature Communications* **8**:1, pp. 1–7. DOI: 10.1038/ncomms14829.

Yazdani, A. and R. Iravani (2010). *Voltage-sourced converters in power systems: modeling, control, and applications.* John Wiley & Sons, Hoboken, New Jersey, USA.

Zampieri, S. (2008). "Trends in networked control systems". In: *IFAC World Congress.* DOI: 10.3182/20080706-5-KR-1001.00486.

Zhang, C. and M. Fu (1996). "A revisit to the gain and phase margins of linear quadratic regulators". *IEEE Transactions on Automatic Control* **41**:10, pp. 1527–1530. DOI: 10.1109/9.539438.

Zhang, G. R., D. S. Yang, T. Liu, J. Y. Zeng, and Y. K. Xu (2013). "Grid-connected of photovoltaic module using inverse optimal control". In: *Advanced Materials Research.* Vol. 765. Trans Tech Publ, pp. 1834–1839. DOI: 10.4028/www.scientific.net/AMR.765-767.1834.

Zhang, H. (2019). *Optimizing Networked Systems and Inverse Optimal Control.* PhD thesis. KTH Royal Institute of Technology, Sweden. ISBN: 978-91-7873-085-8. URL: http://urn.kb.se/resolve?urn=urn:nbn:se:kth:diva-241424.

Zhang, H., J. Umenberger, and X. Hu (2019). "Inverse optimal control for discrete-time finite-horizon linear quadratic regulators". *Automatica* **110**, p. 108593. DOI: 10.1016/j.automatica.2019.108593.

Zhang, Y. and L. Xie (2015). "Online dynamic security assessment of microgrid interconnections in smart distribution systems". *IEEE Transactions on Power Systems* **30**:6, pp. 3246–3254. DOI: 10.1109/TPWRS.2014.2374876.

Zhang, Y. and L. Xie (2016). "A transient stability assessment framework in power electronic-interfaced distribution systems". *IEEE Transactions on Power Systems* **31**:6, pp. 5106–5114. DOI: 10.1109/TPWRS.2016.2531745.

Zhong, Q.-C. and G. Weiss (2010). "Synchronverters: inverters that mimic synchronous generators". *IEEE Transactions on Industrial Electronics* **58**:4, pp. 1259–1267. DOI: 10.1109/TIE.2010.2048839.

Zonetti, D. (2016). *Energy-based modelling and control of electric power systems with guaranteed stability properties*. Theses no. 2016SACLS118. Université Paris-Saclay. URL: https://tel.archives-ouvertes.fr/tel-01321857.

Zonetti, D., G. Bergna-Diaz, R. Ortega, and N. Monshizadeh (2021). "PID passivity-based control of power converters: large-signal stability, robustness and performance". *arXiv preprint arXiv:2101.05047*.

Zonetti, D., R. Ortega, and A. Benchaib (2014). "A globally asymptotically stable decentralized PI controller for multi-terminal high-voltage DC transmission systems". In: *European Control Conference (ECC), 2014 European*. IEEE, pp. 1397–1403. DOI: 10.1109/ECC.2014.6862419.

Get to Know Your Power

Taouba Jouini

Department of Automatic Control at LTH

Unless you have been hibernating in a remote cave, you have heard of the clean energy transition that will radically transform the generation and distribution of today's electricity around the world and in particular in Sweden. Swedish energy decision-makers and operators (e.g., Svenska Kraftnät) target carbon neutrality by the year 2040 [1]. In reality, the large rotating machines responsible for regulating the response of power generators to consumers' demand, will soon be replaced by, much smaller in size, fast-actuated, power electronics devices or inverters. They function by drawing power from a renewable energy source; e.g., solar, to provide consumers with electricity, and will be thereby responsible for maintaining waveforms at desired 50 Hz frequency and 230 V magnitude. This thesis is concerned with deriving methods to achieve the successful integration of inverters into power generation.

Sweden's transmission grid is a part of the Nordic power system.

Now, imagine that on an extremely windy morning in southern Sweden, you have just finished your shower, picked up your hairdryer, and introduced it into the wall socket. You press the 'on' button, but the device does not seem to work. Don't wonder for a long time about the cause because the answer is in front of your eyes. It is the storm that pressures the electrical system at that moment, which in turn failed to provide power. This scenario is inspired by real-life events of the blackout that spread over southern Sweden and

---

[1] [**https://www.svk.se/siteassets/om-oss/rapporter/2018**]

Denmark in September 2003, in the aftermath of a storm that hit a power line [2]. This shows how disturbances such as weather conditions can disrupt or even shut down the operation of power systems. In this thesis, we aim to develop tools to understand and counteract the effect of disturbances in power systems largely dominated by inverters.

The inverters left alone, will fail to provide any service, unless they are equipped with a *suitable* controller. Control theory is a field concerned with the mathematical explanation of dynamical systems and the adequate intervention to change their behavior to a desirable one. Our research aims to exactly find such control solutions that help accelerate the energy transition in Sweden and build resilience against disturbances such as unpredictable weather conditions. In short, the goal of our work can be summarized as follows:

Find control algorithms for inverters that are robust with respect to perturbations in power systems. They should also be responsible for maintaining frequency synchronization, i.e., all inverters' output voltages oscillate at a common frequency around nominal (50 Hz) with provable guarantees, while providing reliable power supply.

Our work lies at the intersection of topics in control theory, the backbone of our results. To reach our goal, we first propose the *matching control*, a controller that is inspired by the classical operation of power systems with rotating machines. Second, we use optimization tools, a branch of mathematics that deals with finding the best solutions that minimize a given cost, to derive *angle controllers.* All the above-mentioned controllers allow for synchronization at desired frequency and respond quickly to changes, e.g., when power demand fluctuates. We show the usefulness of these controllers in theory and simulations to help experts gain insights into control strategies for tomorrow's Nordic power system.
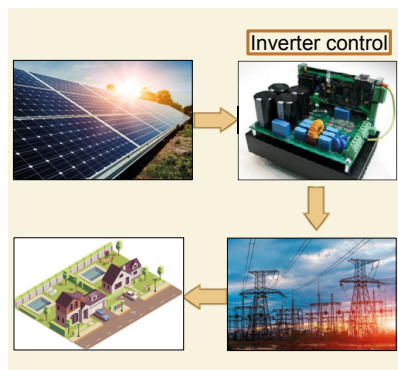
From renewables to consumers: the power supply goes primarily through inverter control.

---

[2] [**http://news.bbc.co.uk/2/hi/europe/3132332.stm**]